IEA Annex 41 whole building heat, air, moisture response

Closing seminar, Nordic Building Physics Conference

Rode, Carsten; Hens, Hugo; Janssen, Hans

Publication date:
2008

Document Version
Publisher's PDF, also known as Version of record

International Energy Agency
Executive committee on Energy Conservation in Buildings and Community Systems

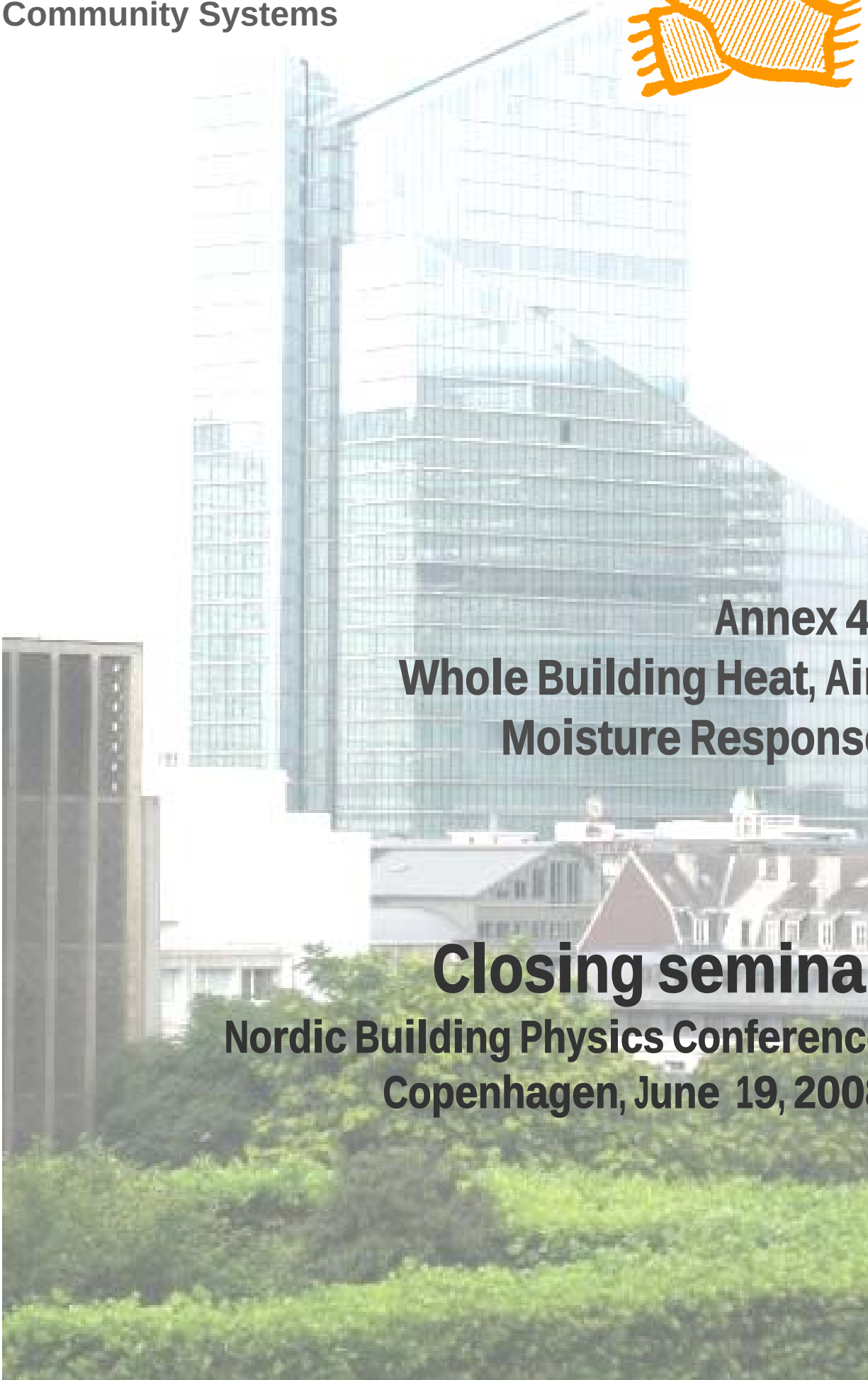

Annex 41
Whole Building Heat, Air, Moisture Response

Closing seminar

Nordic Building Physics Conference
Copenhagen, June 19, 2008

Proceedings of the

IEA ECBCS Annex 41
Closing Seminar, Copenhagen, June 19, 2008

Editing Committee:
Carsten Rode, Technical University of Denmark (chairman)
Hugo Hens, Katholieke Universiteit, Leuven, Belgium
Hans Janssen, Technical University of Denmark

Contact Address

IEA Annex 41 Closing Seminar, secretariat
Department of Civil Engineering
Brovej, Building 118
Technical University of Denmark
DK-2800 Kgs. Lyngby, Denmark

Phone: +45 45 25 17 00
Fax: +45 45 88 32 82
E-mail: byg@byg.dtu.dk
Web: www.byg.dtu.dk

Reference to papers

Author. Title. Proceedings of the IEA ECBCS Annex 41 Closing Seminar, Copenhagen, June 19, 2008 (C. Rode, editor), Dept. of Civil Engineering, BYG R-191, Technical University of Denmark, Kgs. Lyngby, Denmark, 2008

DTU Byg Report R-191

ISBN 9788778772671

Number of copies printed: 75
Printed by the Danish Society of Engineers, IDA
Copenhagen, Denmark, June, 2008

Acknowledgement:
Printing of the proceedings has been supported by Rockwool International A/S.
The support is gratefully acknowledged!

Preface

The need for a whole building HAM approach became clear during previous IEA implementing agreement on Energy Conservation in Buildings and Community Systems annexes. Annex 14 showed that fungal defacement in buildings is directly linked to the heat, air and moisture balances at building level. In annex 24, the indoor climate had to be imposed as boundary condition, although measurements revealed whole building air balances and moisture buffering effects had a large influence on the instantaneous humidity conditions indoors. Annex 32 convinced all participants that envelope and whole building performance continuously interact. So, an annex on whole building heat, air, moisture response was a logic next step on the way to better assess indoor climate, energy efficiency and durability of buildings.

The new annex called 'Whole building Heat Air Moisture Response', who got the number 41 and the nickname 'Moisteng', started in autumn 2003 with a preparatory meeting. During that meeting four subtasks were defined, focussing on fundamentals (ST1), measurements (ST2), boundary conditions (ST3) and application (ST4) with Carsten Rode and Monika Woloszyn (ST1), Staf Roels (ST2), Chris Sanders and Kumar Kumaran (ST3) and Andreas Holm (ST4) as subtask leaders and Hans Janssen as Annex secretary.

The working phase ran from January 1, 2004 till December 31, 2007. During that period, eight working meetings were organised. In total, over 100 individuals, belonging to more than 18 institutes participated in one, some or all of these meetings. All together, they produced over 250 papers, which were presented and discussed at these meetings, while the common work done ranged from a series of exercises (CE's) over round robin testing to data collection, model refinement and model validation. All was performed with a lot of enthusiasm and produced results which in turn activated discussion on why remarkable differences in the outcomes were sometimes seen.

All that common work resulted in the four reports and three CD's that are made public on this Annex 41 closing seminar, June 19, 2008, just after the 8th Nordic Building Physics Conference in Copenhagen. Though quite impressive in the number of pages and the quality of their content, reports always remain a condensed reflection of what really happened during an annex. Those who participated will remember the many instructive hours spent together with coffee breaks in between, the common dinners at the end of each second meeting day and the beach visits in Florianopolis, while those who did not participate hopefully pick-up a flavour of what was annex 41 when reading the papers presented today and using the four annex books and CD's later-on.

Hugo HENS

Annex 41 Operating Agent

Table of Contents

IEA-ECBCS Annex 41
Whole building heat, air and moisture response

Hugo Hens
Operating agent
Department of Civil Engineering, Laboratory of Building Physics
hugo.hens@bwk.kuleuven.be/ http://www.kuleuven.be/bwf/eng/index.htm

KEYWORDS: Combined heat, air and moisture transport, moisture buffering, air leakage, energy, durability, perceived indoor environmental quality

SUMMARY:
Combined heat, air and moisture (HAM) simulation at the envelope's part level and building simulation have been separate activities for many decades. In HAM-models, the indoor conditions are handled as known boundary values, while all building simulation tools predict inside temperatures and net energy demand without much consideration for relative humidity and air pressure gradients.

Things started to change with airflow modeling. That step not only allowed a better quantification of ventilation related energy consumption but also permitted a refinement of the humidity balances in the building. However, at least two facts remained poorly exploited: (1) the fact that many air flows enter and leave the building across the envelope causing a complex pattern of indoor air washing, wind washing and air looping; (2), the fact that moisture buffering in indoor finishes, furniture and furnishings delays and dampens the inside water vapor pressure compared to the exterior. Both phenomena may have an impact on energy consumed for heating, cooling and air conditioning and influence indoor environmental quality, while humidity transported by adventitious air flows in and across the envelope may accelerate degradation. Analyzing both facts through whole building heat, air and moisture modeling and studying the impact on energy consumption, durability and indoor environmental quality were at the core of the annex 41 activity.

1. Introduction

Although it is well known that the heat, air and moisture flows (called HAM) generated by building use and entering from outside, that the HAM flows traversing the enclosure and that the HAM flows injected by the HVAC system are in permanent and mutual balance, simulation tools and designers hardly consider that reality. Building designs are scrutinized on energy needed for heating and cooling, while HVAC-systems are dimensioned to deliver the power needed to keep the indoor temperature at comfort level even under extreme outdoor weather conditions. Indoor relative humidity however is mostly kept free floating, as it is perceived to be less important except when the building's function imposes full air conditioning,. Few designers detail the envelope taking into account the full hygrothermal load from inside and outside, while hardly anyone considers the whole heat, air and moisture balance that develops between the building's interior, its envelope and the outside environment. This is a pity as air pressure gradients inside the building and between the building and the outside generate airflows that change the heat, air and moisture response of the envelope and the building drastically, while buffering effects dampen indoor water vapor pressure fluctuations significantly compared to outdoors. Resulting air ingress, possible rain penetration and moisture deposits in the envelope could not only negatively affect energy consumption but also trigger the envelope's durability. Simultaneously, inside relative humidity, if not well managed, may affect perceived indoor environmental quality and become a driving force for mold and dust mite infection.

Clearly, whole building heat, air moisture response has impact on human comfort, indoor environmental quality, energy consumption and envelope durability, reasons why in 2003 a IEA-ECBCS Annex, termed Annex 41, Moist-En was initiated (Hens, 2003).

2. State of the art

Building modeling started in the fifties. From the beginning, the objectives were quantifying the net energy demand, analyzing the ways that demand could be reduced by building related measures and getting information on the temperature without heating and cooling as this allowed evaluating overheating. Later-on, HVAC-models were added and energy consumption became the quantity quantified. Hardly any model, however, was able to quantify the air and humidity balances in the building. Instead rough estimates on infiltration and ventilation were used and humidity remained untouched (ASHRAE, 2001)

During the same period, the research effort on heat, air and moisture transport focused on the envelope. In the sixties, a few simple evaluation tools became popular. They scaled the moisture response reality down to one

main problem – interstitial condensation - two steady state transport modes - heat flow by conduction and water vapor flow by diffusion (Glaser, 1958, Glaser 1958, ASHRAE, 2001). Today highly sophisticated one- and two-dimensional full heat and moisture models are available that allow modeling vapor and liquid flow, that are transient in nature, that consider moisture sources such as wind-driven rain, rising damp, initial moisture, sorption and desorption, interstitial condensation and surface condensation. Some even allow quantifying some of the consequences of unfit moisture tolerance, such as hygrothermal stress and strain, mold infection, corrosion, salt transport, and frost damage (Pedersen 1990) (Carmeliet 1992) (Künzel 1994) (Grünewald 1997) (Sedlbauer et al. 2003) (Nicolai 2007). Examples of such models are: Match, Wufi, Latenite, Delphin and HygIRC. In Europe, the one-dimensional full models even became subject of a standard (CEN, 2003). All envelope models, however, take the indoor conditions (temperature, relative humidity, air pressures) as known boundary values. This of course is fiction, except in case of full air conditioning, when the indoor environment is completely decoupled from outdoors. Also a correct implementation of wind driven rain and its impact on the building envelope remained a weakness. In fact, although wind and wind driven rain have been a research topic for many decades, one had to wait until CFD became a commonly used tool before a turn was made from experiment and simple calculation to full simulation of rain loads on envelopes (Lacy et al., 1962)(Blocken et al., 2004)

As said, the analysis of airflow patterns within a building was an important step on the road to whole building HAM analysis. Basic work on inter-zonal flow has been done by the Comis group and Annex 23 (Allard et al., 1990). The last decade, large numbers of researchers use CFD to analyze intra-zone flow (Baker et al., 1994). The linkage between the flows in the building and those in the envelope, however, is hardly established, although the study of air flows in and through envelope parts has underlined their importance for a correct evaluation of the hygrothermal response (Kronvall, 1982) (Trechsel ed., 1994) (Janssens 1998).

Finally, the last years, we saw a renewed interest in indoor moisture buffering by finishing layers and furniture (see figure 1) (Svennberg et al., 2004). A few software packages have been developed, which allow evaluating the effect. Measurements on buffering capacity of finishing materials and furniture were performed in several laboratories. Nordtest initiated a research program on the subject, included a round robin on buffering (Rode, 2003).

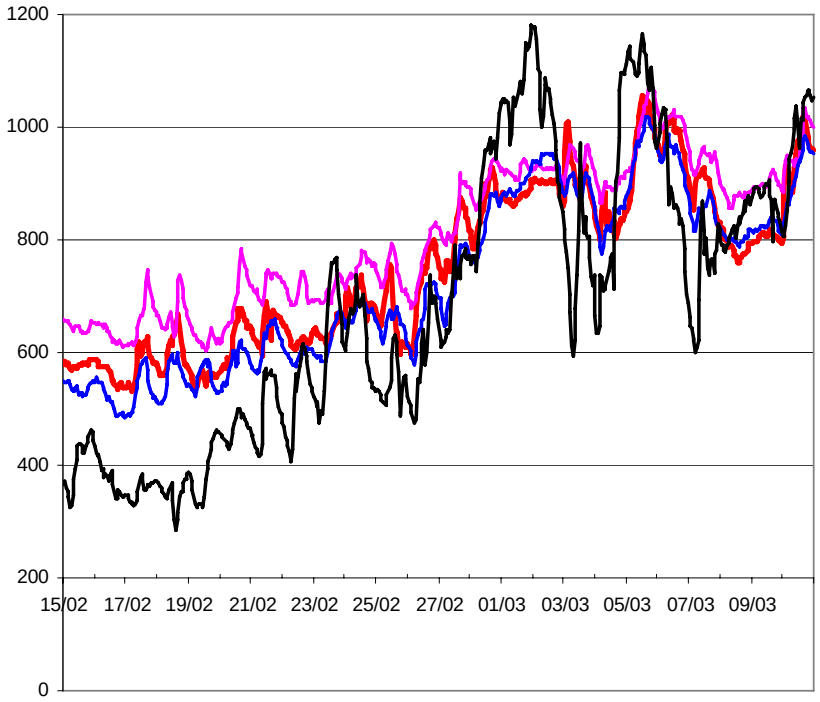

FIG 1: Inside water vapor pressure in an office, comparison with the water vapor pressure outside. Without buffering, the value inside should never pass the one outside. It does, proving that buffering is a fact

3. Annex objectives

The annex was meant to develop a holistic view on the overall HAM transfer between the buildings interior, the enclosure and outside. The two specific objectives were:

1. Exploring the physics involved in whole building HAM response. That included basic research, a further development of models, measuring moisture storage in finishing materials, substrates, furniture and furnishings, mock up testing and field testing. Test results were used to verify and validate models by inter-comparison and confrontation with measured data.
2. Analyzing the effects of whole building HAM on comfort, indoor environmental quality, energy consumption and enclosure durability.

The first objective focused on a better understanding of the overall HAM-flows that come from inside and outdoors under different weather conditions and their effect on the building's overall hygrothermal response. The annex had no intention to develop an own, so-called reference whole building HAM model. Instead, all participants were motivated to develop their own full or simplified models and to use the annex activity for refining the tools. Within that context, simplified modeling was seen as quite important as full tools are very demanding in terms of input and time consumed.

Good comfort and good indoor environmental quality being an important part of the building user's satisfaction was a strong drive behind the second objective. In many climates, people spend 80% and more of their lifetime inside buildings, which means that a whole society is benefiting when comfort and indoor environmental quality are optimal. At the same time, avoided energy consumption is of great help in establishing the goals of the Kyoto and future post-Kyoto protocol. From that point of view, air humidity changes, which are termed as latent energy, play a significant in warm and moist regions, where latent heat often represents 50% and more of the annual cooling load. Well balanced moisture storage in finishing layers, substrates, furniture and furnishings could reduce that percentage. On the long run, the result should be a net saving in energy resources, less CO_2 produced and added sustainability. A better durability also increases sustainability. Longer service live of buildings in fact economizes on material use, embodied energy and embodied pollution. Hence, damage statistics learn that bad moisture management is the most important cause of to short service lives, especially when the envelope is considered.

Objective 1 was translated in a set of original research tasks with a round robin on vapor permeability and sorption of painted and unpainted dry wall and model simplification, verification and validation as kernel activities. Under objective 2 measures were studied as to moderate possible negative effects of combined HAM transfer with correct moisture management, humidity storage, humidity controlled ventilation and better energy efficiency as some of the tracks followed.

4. Annex organisation

The work was structured in four subtasks:

1. Modeling principles and common exercises
2. Experimental investigation
3. Boundary conditions
4. Applications

Each subtask got one or two subtask leaders: Carsten Rode of DTU, Denmark, and Monika Woloszyn of Cethil, France, for subtask 1, Staf Roels of K.U.Leuven, Belgium, for subtask 2, Kumar Kumaran of NRC, Canada, and Chris Sanders of GCU, UK, for subtask 3 and Andreas Holm of FiB, Germany, for subtask 4. They were responsible for the activity within their subtask and acted as editors for the final report on their subtask.

5. Annex activity

5.1 Working meetings

One three day's kick-off meeting and eight three day's working meetings were organized:

Meeting	Date, place
Kick off meeting	Leuven, (B) November 26-28, 2003
First working meeting	Zürich (Ch), May 12-14, 2004
Second working meeting	Glasgow (UK), October 27-29, 2004
Third working meeting	Montreal (C), May 16-18, 2005
Fourth working meeting	Trondheim (N), October 26-28, 2005
Fifth working meeting	Kyoto (J), April 3-5, 2006
Sixth working meeting	Lyon (F), October 25-27, 2006
Seventh working meeting	Florianopolis (B), April 2-4, 2007
Eighth working meeting	Porto (P), October 22-24, 2007

During the kick-off meeting, the Annex structure was created and all participants got the opportunity to present their experiences in the field of whole building heat, air, moisture modeling. Each working meeting had an identical outline: discussing the results of the common activity in each of the subtasks, presenting free papers with new idea's, research results and deepened knowledge and planning for the next six months. From the sixth meeting on, more time was devoted to discussing the final report outlines and reviewing the text of the reports. In all meetings, except the one in Montreal, all participants followed the activity going on in each of the subtasks. That way, a kind of common knowledge basis was created, which facilitated the discussions and the review process of the final reports.

5.2 Participation

In total, 113 people participated in all or part of the working meetings. They introduced 269 free papers and worked on in total 11 common exercises.

6. Annex results

6.1 Subtask 1: modeling principles and common exercises

That subtask concentrated on whole building HAM modeling with special emphasis on HAM-transfer between the outdoor and the exterior surface of the building envelope, HAM transfer in the envelope, HAM transfer between the interior surface of the envelope and indoors, HAM transfer from outdoors to indoors and vice versa through leakages, purpose designed ventilation grids and air in- and outlets, HAM transfer between the indoor air, furniture and furnishing plus HAM transfer between the different zones in a building. The models that were verified and validated using common exercises took into account parameters such as location and orientation of the building, the HVAC-system, adventitious and user defined air flows, moisture response by hygroscopic finishes, furniture and furnishings, the type of room (bathroom, living room, etc.) and user's behavior (number of people, activities that released moisture and heat, frequency and duration of window ventilation).. The schedule of common exercises looked as follows:

Exercise 0	Dry BESTEST. Verification of the thermal part of the models by inter-model comparison
Exercise 1	Wet BESTEST. Generating vapor in the BESTEST building, predicting of the inside relative humidity in isothermal and transient conditions. Verification by inter-model comparison
Exercise 2	Validating models by simulating experimental results at room level under isothermal conditions
Exercise 3	Validating models by simulating experimental results at room level under non-isothermal conditions
Exercise 4	Energy consumption in the room used for the non-isothermal measurements, assuming a humidity controlled ventilation system is applied. Verification by inter-model comparison
Exercise 5	Real world case, evaluating the impact of adventitious infiltration flows that traverse the envelope on durability and energy consumption. Looking to the ability of the participants to handle a typical moisture damage case by using simplified models
Exercise 6	Experimental work on a coupled room configuration under isothermal conditions

Exercises 0 and 1 had as objective to verify models. The results were to some extend disappointing, especially when humidity was added. But even without, the variance between the many solutions was not less than noted fifteen years ago, when the same exercise ran under Annex 10. Exercises 2 and 3 were conceived to validate the models. The results learned that common assumptions, such as ideal air mixing, could produce predictions that deviated substantially from the measured data. Of course, also measured data show a bias of uncertainty, which must be taken into account. Exercise 4 looked to the ability of whole building HAM-models to predict net energy demand. Exercise 5 offered the participants the possibility to explain a real life problem and to propose solution, while exercise 6 produced a set of very interesting measurement data that may be useful for future validation of new models, included CFD-based tools. Thanks to these exercises, the participants got the opportunity to refine their models.

6.2 Subtask 2: experimental investigation

Here, moisture buffering in finishing materials, furniture and furnishings was the main objective. For that purpose a round robin on vapor permeability and hygroscopic adsorption/desorption of painted and unpainted drywall samples was organized. The data produced created confusion, as large differences in measured vapor permeability were noted between the many participating laboratories, which could not be explained otherwise than by measuring errors. One of the conclusions was that future standards on vapor permeability measuring techniques should include more precise and restrictive information on how to prepare the samples, how to vapor tighten the joint between the sample and the cup and how to perform the tests (duration, number of measuring

moments, time interval between measurements, etc). Also the adsorption/desorption data showed quite some dispersion. From that point of view, gypsum is a difficult material, as chemical bound water molecules are easily released when dried at too high temperatures.

Two additional tests and exercises were organized, one looking to buffering by the same drywall used in the round robin in response to a stepwise and sinusoidal change in relative humidity in the air and the other looking to the humidity built-up in a pile of drywall boards in response to a sudden change in relative humidity in the air. Simulation of the first test by several participants gave again rather disappointing results, with large spreads between the different solutions. The second test instead was quite well reproduced by the different models used by the participants. Some also tried to use CFD as simulation vehicle, in combination with a material model. The first trials showed large differences between the measured data and the CFD data. Follow-up trials, however, did quite well

Apart of that testing and validating activity, a new track in simplified modeling was explored, using a short term (1 h) and mid-term (8 hrs) moisture buffering value (MBV). The concept was developed by the Nordic countries (DTU-Denmark, VTT-Finland, NTNU-Norway and LTH-Sweden). It gives the humidity uptake per percentage of change in relative humidity when 1 m² of a surface is exposed to a succession of 1 (short) or 8 hours (mid) at 75% relative humidity, followed by 23 (short) or 16 hours (mid) at 33% humidity. The MBV-value is quite easily measurable for all types of substrate, finishes, furniture and furnishings (figure 2). The annex extended the concept from the 1 m^2 and one object level to room level, among others based on experimental work done at the Universidade do Porto and on modeling work done at DTU and K.U.Leuven.

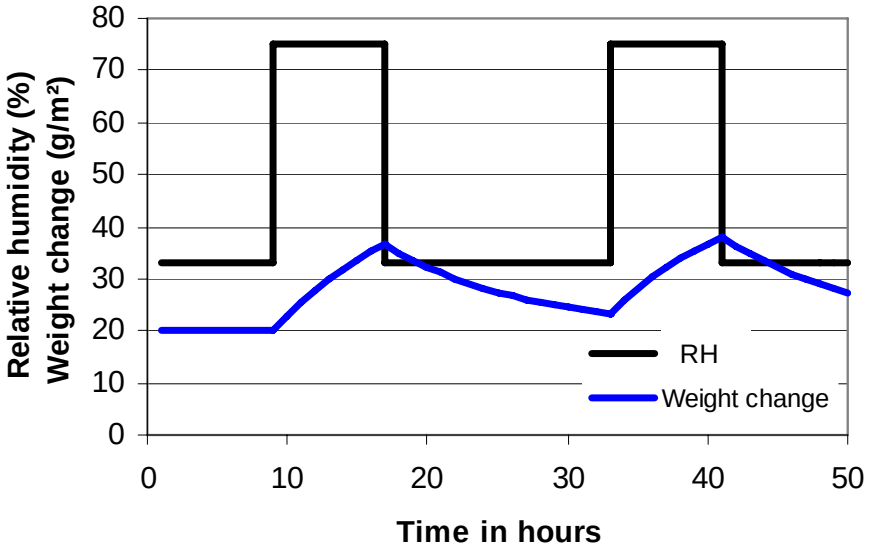

FIG 2: Measuring the moisture buffering value

6.3 Subtask 3: boundary conditions

The indoor conditions part was mainly devoted to measuring the indoor conditions in residential buildings, student homes and schools by participants of the UK, Finland, Estonia, Germany, Belgium and Canada, (2) a literature review of moisture production and building usage schedules, (3) an evaluation of simple indoor humidity calculation tools. Included were the EN climate classes model with inside water vapor pressure excess being a function of the monthly mean outside temperature (figure 3), the ASHRAE SPC 160P—Design Criteria for Moisture Control in Buildings – 2003 proposals and the Jones model, which accounts for buffering. The EN climate class model was also tested by using the indoor data, measured in the countries mentioned. The results deviated quite substantially from the EN class curves. Especially a water vapor excess zero at 20°C outside and an excess slope zero below 0°C were questionable.

Special attention also went to the convective surface film coefficient for heat and mass and the air pressure gradients between in- and outdoors. In both cases literature reviews were complemented with experimental work and CFD-work performed within and outside the frame of the Annex.

The study of outdoor conditions was restricted to wind-driven rain, under-cooling and climate change. The wind-driven rain activity had as main focus two exercises. In a first exercise, participants were asked to simulate the rain impact on a series of building configurations, tested beforehand in a wind tunnel, by using simplified me-

thods and CFD plus rain drop trajectory calculations. The second exercise had as objective to validate CFD and rain drop trajectory codes by simulating the rain load on a Norwegian test building and comparing the results with the wind-driven rain load data and local climate data as monitored on site. While the simplified models gave rain load results that deviated quite substantially from the wind tunnel and CFD/ rain drop trajectory calculation results for the building configurations proposed, the CFD/rain drop trajectory-validation exercise did quite well.

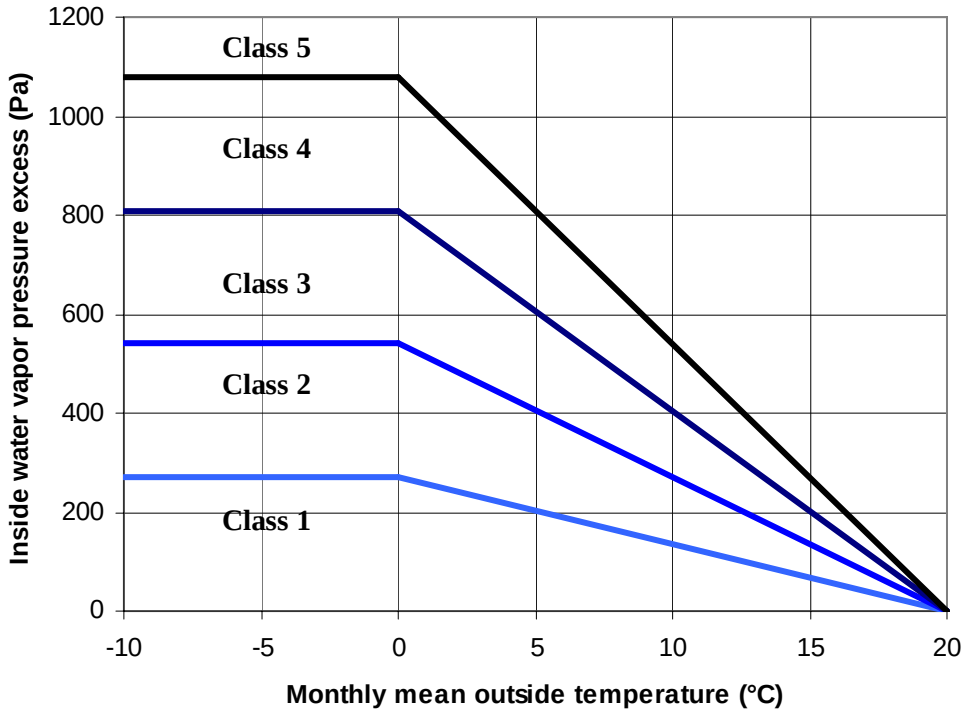

FIG 3: The EN climate classes

6.4 Subtask 4: long term performance and technology transfer

Subtask 4 devoted quite some time studying the impact of low and high relative humidity on human health and comfort. Also the indoor conditions in museums, monumental buildings and landmark buildings were a topic of concern.. The annex further-on looked to recent advances in mold and mildew research, with isopleth interpretation, sensitivity of substrates for mould infestation and mold growth modeling as specific topics. A question of importance was what energy benefit demand controlled ventilation could have in combination with indoor moisture buffering. The results presented looked somewhat dispersed, ranging from hardly any difference in net energy demand to measurable net energy demand gains in winter and summer.

Also the effect of air permeability on interstitial condensation deposit in roofs was tackled as was the discussion about attic ventilation. Here, two different answers were given. The UK seemed quite sure that correct ventilation, in combination with best achievable ceiling air tightness, diminished condensation risk to an acceptable level. Sweden instead introduced the concept of fan-controlled attic ventilation. The basis for their proposal were simulations on a reference attic volume, which showed that even a perfectly air-tight ceiling did not prevent nighttime underlay wetting by under-cooling. When happening, fan driven attic ventilation came out as a best choice for providing daytime drying as long as the outdoor conditions were favorable for that.

7. Annex products

The annex products include

In general	An internet site containing all meeting proceedings, most annex free papers and the common exercise results (http://www.kuleuven.ac.be/bwf/projects/annex41/).
Subtask 1	Final report on whole building HAM modeling and common exercises (Rode et al 2008)
Subtask 2	Final report on experimental investigations (Roels et al 2008)
Subtask 3	Final report on boundary conditions for whole building HAM simulation (Kumaran et al 2008)
Subtask 4	Final report on applications (Holm et al 2008)

All final reports are available in hard copy form. Three CD's are added, one with the annex free papers, a second with the measured data used as validation basis in the common exercise 2, 3 and the measured data of exercise 6 and one with indoor climate data files foe dwellings, student rooms and classes..

8. Conclusion

Annex 41 had a huge program to cover. The initiative motivated 18 countries and more than 100 experts to participate. That underlines the interest in the topic and the expectation people had that the activity will not only generate a better understanding of the whole building heat, air and moisture response but also establish ways how to benefit from that knowledge in terms of better comfort, better indoor air quality, better durability and less energy consumed. The work started 18 months ago and will proceed for another 30 months.

9. Ackowledgement

The success of Annex 41 was due to the enthusiasm of the subtask leaders and all participants. Their contributions are gratefully acknowledged

10. References

Alard F., Dorer V.B., Feustel H.E. (1990), Fundamentals of the multi-zone air flow model-COMIS, Technical Note 29, AIVC

ASHRAE (2001), Handbook of Fundamentals, chapters 23 and 31, Atlanta, Georgia

Baker A. J., Williams P.T., Kelso R.M. (1994), Development of a robust finite element CFD procedure for predicting indoor room air motion, Building and Environment, Vol.29, No 3, pp 261-273

Blocken B., Roels S., Carmeliet J. (2003), A numerical study of wind nuisance for a high-rise building group, Research in Building Physics, Balkema, 981-990

Carmeliet J. (1992), Durability of fiber-reinforced renderings for exterior insulation systems, Doctoraal Proefschrift (in Dutch)

CEN/TC89 WG10 (2003). Hygrothermal performance of building components and building elements – Assessment of moisture transfer by numerical simulation (pre-normative text).

Glaser H. (1958), Temperatur und Dampfdruckverlauf in einer homogene Wand bei Feuchteausscheidung, Kältetechnik 6, pp 174-181

Glaser H. (1958), Vereinfachte Berechnung der Dampfdiffusion durch geschichtete Wand bei Ausscheiden von Wasser und Eis, Kältetechnik 11, 12, pp 358, pp 386-390

Grünewald J. (1997), Konvektiver und diffusiver Stoff- und Energietransport in kapillarporösen Baustoffen, Dissertation an der TU Dresden, Fakultät Bauingenieurswesen

Hens H. (2003), Proposal for a New Annex, 17 p (accepted by the EXCO as Annex 41 in the fall meeting of 2003)

Holm A. (2008), Whole building heat, air, moisture response: applications, Final Report IEA, EXCO ECBCS Annex 41, subtask 4, ACCO, Leuven

Janssens A. (1998), Reliable control of interstitial condensation in lightweight roof systems, PhD-thesis, K.U.Leuven, 217 p

Kronvall J. (1982), Air flows in building components, Report TVBH-1002, Division of Building Technology, Lund University of Technology

Künzel H.M. (1994), Verfahren zur ein- und zweidimensionalen Berechnung des gekoppelten Wärme und Feuchtetransport in Bauteilen mit Einfachen Kenwerten, Abhandlung zur Erlangung der Würde eines Doktor-Ingenieurs, Stuttgart

Kumaran K., Sanders C. (2008), Boundary conditions and whole building HAM-analysis, Final Report IEA, EXCO ECBCS Annex 41, subtask 3, ACCO, Leuven, 235 p

Lacy R., Shellard H. (1962), An index for driving rain, The Meteorological Magazine 91, no 1080, pp 177-184

Nicolai A, Grunewald J., Zhang J.S. (2007), Salt transport and phase transitions, modeling and numerical solution in the simulation code Delphin 5/CHAMPS-BES, Proceedings of the 12 th Bauklimatisches Symposium, Dresden, 29-31 Mrach 2007, p 877-884

Pedersen C. R. (1990), Combined heat and moisture transfer in building constructions, Report no 214, TUD

Rode C. editor (2003) Nordtest, Workshop on Moisture Buffer Capacity, DTU, 33 p.

Rode C., Woloszyn M. (2008), Modelling principles and common exercises, Final Report IEA, EXCO ECBCS Annex 41, subtask 1, ACCO, Leuven, 234 p

Roels S (2008), Experimental analysis of moisture buffering, Final Report IEA, EXCO ECBCS Annex 41, ACCO, Leuven, subtask 2, 173 p

Sedlbauer K., Krus M. (2003), A new model for mold prediction and its application in practice, Research in Building Physics, Balkema, 921-928

Trechsel H, editor (1994) Moisture Control in Buildings, ASTM Manual Series: MNL 18, 485 p.

Svennberg K., Hedegaard L, Rode C. (2004), moisture Buffer performance of a fully furnished room, Proceeding of the Performance of Exterior Envelopes of Whole Buildings IX International Conference (CD-ROM)

From EMPD to CFD – overview of different approaches for Heat Air and Moisture modeling in IEA Annex 41

Arnold Janssens, A.Prof.
Department of Architecture and Urban Planning,
Ghent University, Belgium
arnold.janssens@ugent.be

Monica Woloszyn, A.Prof.
Thermal sciences centre,
Université de Lyon, France
monika.woloszyn@insa-lyon.fr

Carsten Rode, A.Prof.
Department of Civil Engineering,
Technical University of Denmark
car@byg.dtu.dk

Angela Sasic-Kalagasidis, A.Prof.
Department of Building Technology,
Chalmers University of Technology, Sweden
angela.sasic@chalmers.se

Michel De Paepe, A.Prof.
Department of Flow, Heat and Combustion Mechanics,
Ghent University, Belgium
michel.depaepe@ugent.be

KEYWORDS: HAM, simulation, CFD, indoor environment.

SUMMARY
This paper provides an overview of the recent developments of Heat, Air and Moisture modeling of Whole Buildings, which were carried out within a collaborative project of the International Energy Agency. The project has strived to advance the possibilities to calculate the integrated phenomena of heat, air and moisture flows while including the important interactions that take place in buildings between the various building materials, components, and room air, and how those conditions are influenced by occupants and HVAC systems. Principles and some applications of different levels of modeling are presented: simplified modeling of moisture buffering, whole building coupled models as well as more detailed contributions for airflow modeling, including CFD models.

1. Scope of IEA-Annex 41, subtask 1

Modeling of different physical aspects of buildings (Heat, Air and Moisture) has been a key element of Annex 41, involving most of the participants. Annex 41 of the International Energy Agency's (IEA) Energy Conservation in Buildings and Community Systems program (ECBCS) was a four-year cooperative project on "Whole Building Heat, Air and Moisture Response" (2004-2007). The project sought to deepen the knowledge about the integrated heat, air and moisture transport processes when the whole building is considered. Altogether researchers from some 39 institutions representing 19 different countries participated in the project.

The objective of one of the subtasks: *Subtask 1 - Modelling and Common Exercises* was to encourage the development and testing of new models that:

- integrate several physical aspects of buildings (Heat, Air and Moisture),
- operate on the various scales of a building: from porous materials, over composite building constructions to whole buildings with their furnishing, systems and users,
- consider indoor as well as outdoor climatic conditions, and
- adopt 1-, 2- and 3-dimensional aspects, or combinations, as appropriate.

The purpose of Subtask 1 has been to advance development in modeling the integral heat, air and moisture transfer processes that take place in "whole buildings". It is believed that a full understanding of these processes for the whole building is absolutely crucial for future energy optimization of buildings, as this cannot take place without a coherent and complete description of all hygrothermal processes. This paper presents an overview of different simulation tools and approaches that have been discussed and improved within the project.

2. Hygrothermal modelling approaches

2.1 Classification based on spatial discretization

Heat and mass transfer in buildings can be described by energy and mass conservation equations. Energy balances consider the flows of heat by conduction, convection and radiation. Mass balances for moisture include moisture flows by vapor diffusion, convection and liquid transport, and mass balances for air comprise air flows driven by natural, external or mechanical forces. The interactions between these phenomena are essential for the whole building (WB) Heat Air and Moisture (HAM) response. Figure 1 shows the main interactions between different transport phenomena to be considered in coupled HAM analysis.

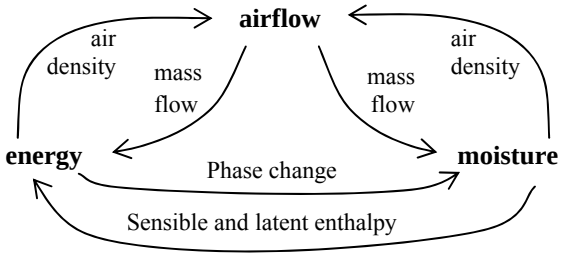

FIG. 1: Main interactions between heat and mass flows

Balance and interface equations may be implemented in simulation tools and solved using numerical methods for space and time discretization. Spatial discretization requires the division of the whole building into small computational cells. While some important transfer processes take place in narrow layers of air or building material, other processes in the same building do not require as finely discretized analyses. It is important to consider both heat and mass transfer processes with the most appropriate accuracy and computational efficiency when the hygrothermal conditions in rooms and building assemblies are to be predicted. The computational procedures may therefore need to work on different levels of spatial resolution. Whole building HAM-models may be categorized on the basis of the spatial discretization (further called granularity) of the room air volume, on the one hand, and the building envelope on the other.

Four principal levels of granularity can be distinguished for the air volume:

- *Very fine*-grained models: Computational fluid dynamic (*CFD*) modelling of room air, enabling detailed calculations of temperature, velocity and concentration fields in a room. Typically a room is divided into thousands to millions of control volumes and the conservation equations are solved for each control volume e.g. by using control volume or finite element techniques.
- *Fine*-grained models. In fine-grained models, the air in each room is subdivided into several control volumes (typically between ten and a few hundred). These *zonal* models can also be used to represent several adjacent rooms connected by openings.
- *Intermediate*-grained models: m*ulti-zone* models for a combination of well-mixed air volumes, that allow several rooms or groups of rooms, each with different characteristics, to be simulated. Therefore heat and mass transfer must be modelled not only between the indoor and outdoor environments but also between different zones inside one building. This includes transfer in walls and also air flows, that can be computed using for example pressure network modelling.
- *Coarse-grained* models: *mono-zone* models for air volumes, where the whole building is represented as one perfectly mixed zone and the same temperature and humidity are assumed for all rooms.

For the building envelope the main difference in HAM-transfer modeling is made by the dimension of represented phenomena. Therefore, granularity refers here to the dimension of spatial discretization used:

- *Very fine*-grained models: *3D models* for the envelope, using control volume or finite element techniques to calculate the heat and mass fluxes, as well as the temperature and concentration fields in the envelope parts, including 3D thermal bridges or similar singular geometries.
- *Fine*-grained models: *2D models* for the envelope.

- *Intermediate*-grained models: *1D models* for the envelope.
- *Coarse-grained* models: *transfer function* models for the envelope, where the dynamic heat and possibly mass fluxes are determined without investigating conditions within the envelope

2.2 Models used within IEA-Annex 41

Table 1. WB HAM simulation tools used in Annex 41

Name	Web site / reference	Availability	Origin	Granularity	
				Air	Envelope
BSim	www.bsim.dk Rode & Grau, 2003	Commercial	Energy	Intermediate	Intermediate Heat-Moisture
BUILDOPT-VIE	www.bph.tuwien.ac.at Sofic, Bednar 2007	No	Energy	Intermediate	Intermediate Heat-Moisture
Clim2000	Plathner and Woloszyn, 2002	No	Energy	Intermediate	Intermediate Heat, Coarse Moisture
DELPHIN 4.5	www.bauklimatik.-dresden.de Funk & Grunewald, 2002	Commercial	Envelope	Coarse	Fine Heat-Air - Moisture
EnergyPlus v1.2.1	www.energy-plus.org Crawley et al., 2004	Freeware	Energy	Intermediate	Intermediate Heat, Coarse Moisture
ESP-r	www.esru.strath.ac.uk Koronthályová et al., 2004	Freeware	Energy	Intermediate	Intermediate Heat, (Moisture: see NPI)
NPI	ICA SAS (Slovakia)	No	Envelope	Coarse	Intermediate Heat-Moisture
IDA-ICE	http://www.equa.se Sahlin et al., 2004	Commercial	Energy	Intermediate	Intermediate Heat-Air-Moisture
HAMFitPlus	Tariku, 2007	No (Personal program)	WB HAM	Intermediate	Intermediate/Fine Heat-Air-Moisture
HAMLab	http://sts.bwk.tue.nl/hamlab van Schijndel, 2007	Freeware	Energy	Intermediate /able of very fine	Coarse Heat-Moisture, able of very fine Heat-Air-Moisture
HAM-Tools	www.ibpt.org Sasic Kalagasidis, 2004	Freeware	WB HAM	Intermediate	Intermediate Heat-Air-Moisture
PowerDomus	www.pucpr.br/LST Mendes et al., 2003	No	Envelope	Intermediate	Intermediate Heat-Moisture
SPARK 2.01	http://gundog.lbl.gov/ Wurtz et al., 2006	Freeware	Energy	Intermediate / fine	Intermediate Heat-Moisture
TRNSYS 16.00	sel.me.wisc.edu/trnsys/ Klein et al., 2004	Commercial	Energy	Intermediate	Intermediate Heat, Coarse Moisture
TRNSYS ITT	www.tu-dresden.de Perschk, 2000	No	Energy	Intermediate	Intermediate Heat-Moisture
WUFI-Plus	www.wufi.de Holm et al, 2003	Commercial	Envelope	Coarse	Intermediate Heat-Moisture
Xam	Iwamae et al., 1999	No (Personal program)	Energy	Coarse	Intermediate Heat-Moisture

Altogether 17 tools were used to provide solutions for different applications and common exercises. All of them are able to represent dynamic evolution of indoor temperature and relative humidity influenced by variable outdoor climate and hygrothermal loads including the effect of moisture buffering by indoor materials. Table 1 shows the 17 simulation tools that have been used in IEA-Annex 41.

The simulation tools include existing multi-zone models for building energy simulation, such as TRNSYS and EnergyPlus. The main focus of these models is to predict the temperature fluctuations and energy demands of individual rooms. As a result the moisture transfer models for the envelope have a coarse granularity in these tools. Also in some cases the granularity is different for heat (intermediate) and moisture (coarse). This excludes the coupling of transfer phenomena in the envelope.

Other tools also originate from building energy simulation but have implemented building enevelope models with a higher level of granularity (eg BSim, IDA-ICE, …). Most of these models are therefore situated at intermediate level of granularity for both air and envelope. Finally a smaller group of Whole Building HAM-models are the ones originating from detailed models for heat-, air and moisture transfer in building envelopes (eg Delphin, WUFI,…). Since HAM-models are capable of describing heat and mass transfer within the layers of the building envelope in a very precise way, the exchange of water vapour between the room air and the surrounding walls may be accurately defined. However in some of these tools the fine granularity for the building envelope model is associated with a coarse representation of the air volume. A more detailed comparison can be found in Woloszyn and Rode (2008).

2.3 Simulation problems studied in IEA-Annex 41, Subtask 1

The WB-HAM-models were used to study various problems. This was organised by means of several common exercises. They all involved simulations of the indoor hygrothermal response in a room or simple building exposed to variable indoor loads and outdoor conditions. Some of them were based on Bestest procedures, others on experimental data collected in climatic chambers and test rooms. Most of the exercises aimed to analyse the interaction between the moisture storage in walls and the room and envelope performance, like energy demand for heating and cooling, indoor temperature and humidity variations, critical moisture conditions in the envelope… In one exercise also the performance of humidity controlled ventilation systems was analysed and optimized. The exercises thus allowed for extensive testing of simulation tools, by inter-code comparison, comparison to experimental data and various sensitivity studies.

The 17 tools from table 4 proved their suitability for whole building hygrothermal simulation and to simultaneously predict indoor climate, as well as energy consumption. Tools situated at intermediate level of granularity for envelopes could also predict local hygrothermal conditions within the building elements. Clearly when the moisture level in constructions is of interest, the investigations require use of coupled heat and mass transfer models, of at least intermediate granularity, to describe the complex physics in walls. However when only the impact of moisture on whole building energy response is of interest, this can be done by using simplified course-grained models for moisture transfer and storage, such as the Effective Moisture Penetration Depth (EMPD) model.

Since airborn moisture transfer has an important influence on the whole building HAM-response, specific attention was given in IEA-Annex 41 to an improved modelling of convective flow fields both between zones (network models) and within zones (CFD-models). These models were applied to study the relation between convective heat and moisture transfer and whole building HAM-performance. Typical applications studied with multi-zone WB-HAM-models were dynamic insulation (Sasic 2007), ventilation drying of cavity walls (Stovall and Karagiozis 2004, Grau and Rode 2006), moisture problems due to air leakage or attic ventilation (Hens 2004, Sasic and Mattson 2005) and humidity controlled ventilation (Woloszyn et al. 2005).

In some applications the detailed knowledge of local conditions in air and envelope is important for evaluating local thermal comfort and for the assessment of the risk of moisture related damage to materials. This analysis is not possible with a coarse or intermediate level of granularity for the air volume. When a detailed field of moisture in the air or in the constructions is needed, Computational Fluid Dynamics (CFD) can help to get a precise prediction of the conditions.

All these approaches, from EMPD to CFD, are complementary, and are of interest in HAM simulations of buildings. In the following two examples are given of work performed within Subtask 1 of IEA-Annex 41. The first example deals with the choice of model parameter values in simplified coarse-grained models. The second example deals with CFD-studies of indoor humidity variations in a room.

3. Model parameters for simplified models

3.1 Governing equations

A full and coupled calculation of the impact of water vapor storage on the indoor climate is complicated. The detailed knowledge of geometry and properties of many indoor materials is needed, such as building materials, wall and floor finishing, furniture and even books and other hygroscopic objects. This information is often not available. Therefore the moisture exchange between the air and surrounding materials may be modeled in a simplified way.

Equation 1 gives the non-steady-state moisture balance for the indoor air in a room, in terms of the partial pressure of water vapor. This equation assumes that the air in a room is well mixed, such that the room conditions (temperature, humidity, air pressure) are equal in the whole zone.

$$\dot{m}_p + \dot{m}_{sys} + \frac{\dot{V}}{R_v T_i}(p_e - p_i) = \frac{V}{R_v T_i}\frac{dp_i}{dt} + \sum_j A_j \beta_j (p_i - p_{s,j}) \qquad (1)$$

The left-hand side contains all moisture sources/sinks: indoor vapor production ($\dot{m}_p$, kg/s), vapor addition/removal by the HVAC-system ($\dot{m}_{sys}$, kg/s) and vapor gains/losses by ventilation and infiltration. The right-hand side contains the terms describing the vapor storage in the air and the convective vapor transfer from the air to the interior surfaces of the enclosure walls. The balance may also include interzonal airflow from adjacent rooms but is not taken into account here. Other symbols are: p_i and p_e for the partial water vapor pressures of the indoor and outside air (Pa), R_v the gas constant for water vapor (462 J/kg/K), T_i the indoor air temperature (K), $\dot{V}$ the volume flow rate of outside air (m³/s), V the room volume, m^3, A_j the area of the interior surface of wall j, m², β_j the convective surface film coefficient for vapor transfer (s/m) and $p_{s,j}$ the vapor pressure at the interior surface of wall j (Pa).

This latter variable couples the enclosure moisture balance to the moisture conservation equations of materials surrounding the enclosure. Equation 2 describes the mass balance equation for 1D-transfer and storage of water vapor in a wall with porous building materials, the typical basis of HAM-models for the envelope:

$$\frac{\partial}{\partial x}\left(\delta(\varphi)\frac{\partial p}{\partial x}\right) = \frac{\partial w}{\partial t} = \rho\xi(\varphi)\frac{\partial}{\partial t}\left(\frac{p}{p_{sat}(T)}\right) \qquad (2)$$

where δ is the vapor permeability (s), φ is the relative humidity (-), w is the moisture content by volume (kg/m³), $\rho\xi$ is the moisture capacity in terms of relative humidity, derived from the material sorption isotherm (kg/m³) and $p_{sat}(T)$ is the saturation water vapor pressure at temperature T (Pa). Vapor transfer and storage properties are typically a function of ambient humidity.

Finally the boundary condition at the interior material surface is:

$$\beta_i (p_i - p_s) = -\delta(\varphi)\left.\frac{\partial p}{\partial x}\right|_s \qquad (3)$$

3.2 Classification of simplified models

3.2.1 Effective Moisture Penetration Depth Model.

The EMPD model is a simplified lumped approach to simulate surface moisture adsorption and desorption (Keresteciogl u et al. 1989). In the EMPD approach, Equation 2and 3 are solved by assuming that only a thin layer near the interior surface interacts with the indoor air (the so-called sorption-active layer or humidity buffer). This implies that water vapor diffusion between the indoors and outdoors through exterior walls is neglected. The thin layer absorbs and releases moisture to the room air when exposed to cyclic air humidity variations. Temperature and vapor pressure are assumed to vary linearly in that layer.

The depth d_p of the sorption-active layer is related to the effective moisture penetration depth EMPD associated with the period of typical fluctuations in the vapor pressure at the wall surface:

$$\mathrm{EMPD} = \sqrt{\frac{\delta \cdot p_{sat}(T) \cdot t_p}{\rho \cdot \xi \cdot \pi}} \qquad (4)$$

In Equation 4 t_p is the period of the cyclic variation (s). For porous building materials the effective penetration depth for moisture exchange is typically in the order of millimeters for daily variations and in the order of centimeters for yearly fluctuations. It can be shown that at the depth of three times EMPD, the moisture variation is less than 5% of the variation at the surface.

With the assumption that the wall-air interaction occurs in a humidity buffering layer with thickness d_p, Equations 2 and 3 are reduced to a single equation:

$$\frac{p_i - p_b}{\frac{1}{\beta_j} + Z_b} = \rho \cdot \xi(\varphi_b) \cdot d_b \frac{d}{dt}\left(\frac{p_b}{p_{sat}(T_b)}\right) \qquad (5)$$

where p_b is the average vapor pressure in the humidity buffering layer (Pa) and Z_b is the vapour diffusion resistance between the surface and the moisture storage centre of the layer (m/s).

The calculation of indoor humidity as a function of time now requires the numerical solution of the set of ordinary differential Equations 1 and 5. In a more complete approach, Equation 5 is applied to all wall surfaces. The number of equations to be solved per room is *j*+1, where *j* is the number of humidity buffering surfaces. Non-isothermal conditions are assumed: the temperature used in Equation 5 comes from the solution of the energy conservation equations for the individual walls. The moisture capacity of the intervening layer is a function of the relative humidity of the layer. This more complete approach is used in the computer code EnergyPlus (Crawley et al. 2004).

In a more simple approach, Equation 5 is applied to a single humidity buffering layer with properties representative of the average moisture storage properties of all room surrounding surfaces. Isothermal conditions are assumed when solving the buffering layer mass balance: the temperature of the humidity buffering layer is constant in time. Also, the moisture capacity is constant and independent of the layer humidity. This approach is used in the computer code TRNSYS. Isothermal, but time-varying conditions are assumed in the computer code Clim2000. With the assumption of isothermal conditions, the interaction between the heat transfer in the walls and the moisture balance in the enclosure is neglected. For some applications, however, this interaction has an important impact on the humidity variations in a room (Janssens et al., 2005).

It is clear that representing moisture adsorption by a single sorption active layer means that only moisture variations with a single well-defined cycle, e.g. daily fluctuations, can be modeled. To overcome this limitation, the EMPD-approach has been elaborated further in the TRNSYS and Clim2000 codes by dividing the humidity buffer into a surface layer and a deep layer (Abadie et al, 2005, Plathner and Woloszyn, 2002). With this representation, both short-term exchanges (between the air and the surface buffer) and mid-term exchanges (using the deep buffer) can be modeled.

3.2.2 Effective capacitance model.

The previous approach is further simplified by assuming that the thermal and humidity conditions in the humidity buffering layer are the same as in the room air, and so the moisture capacities of walls, furniture and room air are combined into a single room moisture capacity (the so-called effective capacitance or air mass multiplier). Hence the vapor pressure of the wall layer is eliminated from Equation 1, and the set of 2 equations reduces to a single differential equation, Equation 6. This simplest approach is also incorporated in most building simulation codes (effective capacitance humidity model). The factor C on the right-hand side is then treated as a constant capacitance, independent of temperature. It aggregates the influence of room air and of different materials and objects present in a room, each characterized by a buffering layer thickness and volumetric moisture capacity.

$$\dot{m}_p + \dot{m}_{sys} + \frac{\dot{V}}{R_v T_i}(p_e - p_i) = C\frac{dp_i}{dt} \qquad (6)$$

3.3 Definition of model parameters

One of the problems with simplified models is that it is difficult to correctly evaluate the model parameters based on the materials that compose the envelope and are in contact with the room air. Janssens et al. (2005) and Abadie et al. (2005) give some guidance on the choice of the buffering layer thickness (d_p) to be used in simplified humidity models. They compare simulations of the humidity variation in a room with homogeneous walls of aerated concrete. The comparison shows a good agreement between predictions with the simplified EMPD-model and a WB-HAM-model when the buffering layer thickness is taken equal to the effective moisture penetration depth defined in Equation 4. The diffusion resistance Z_b in Equation 5 is taken equal to half the diffusion resistance of the buffering layer. This is based on the assumption of a linearly varying vapor pressure in the layer.

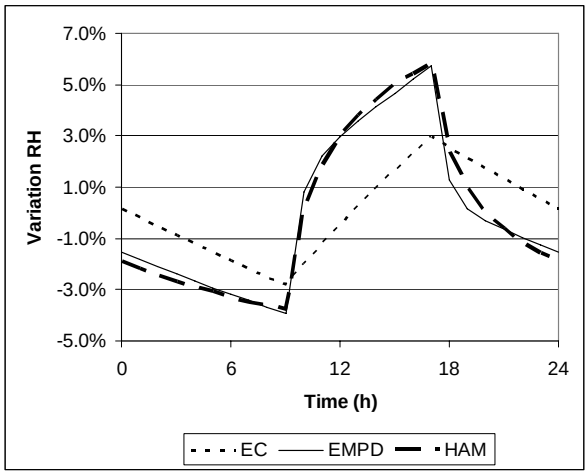

FIG. 2: Periodic state solution of three models: relative humidity variation around the daily average for effective capacitance model (EC), effective penetration depth model (EMPD) and HAM-model.

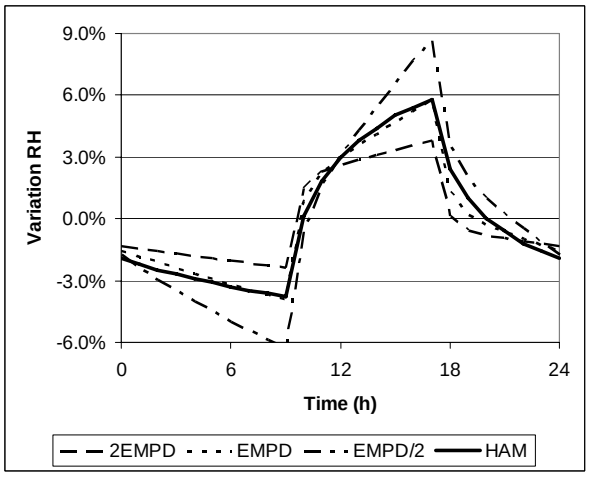

FIG. 3: Periodic state solution of two models: relative humidity variation around the daily average. The figure shows the sensitivity of the EMPD-model to the choice of the buffering layer thickness d_p

Figure 2 makes this more clear: it shows a comparison between periodic state solutions of the indoor humidity variation predicted with the simplified models described above, and a state-of-the-art HAM-model (Janssens et al., 2005). For the model comparison, room geometry was adopted from a hypothetical base case building used in the Annex 41 Common exercise 1 (Woloszyn and Rode, 2008b). The building walls, roof and floor are made of monolithic aerated concrete with thickness 15 cm and a vapor tight exterior finishing. The analysis is performed for constant boundary conditions: indoor and outdoor temperature 20°C, outdoor relative humidity 50% and air exchange rate 0.5 ach. Only the release of water vapor is variable: it is released in the room from 9.00h until 17.00h at a constant rate of 0.5 kg/h.

The simplified models are the EMPD-model and the EC-model (effective capacitance). In these two models, the diffusion resistance and moisture capacity of the humidity buffer are taken constant and evaluated at average indoor humidity conditions. The HAM-model takes the dependency of moisture properties with relative humidity into account. The material properties used in the analysis may be found in the references given above. As Figure 2 shows, the effective capacitance model gives a reasonable estimate of indoor humidity variations. However, this simple model is not able to predict the initial fast response of indoor humidity to changes in moisture production, compared to the HAM- and EMPD-model.

The humidity variation predicted by the EMPD-model is very sensitive to the choice of the buffering layer thickness. Figure 3 shows this by comparing the previous simulation results to calculations where the buffering layer thickness is taken double and half the value of the EMPD of the wall material. Clearly the humidity variation is underestimated and overestimated, respectively, when the model parameters are not properly defined.

In case where the humidity absorbing walls are not homogeneous but multi-layered, the model parameters should be calculated from the properties of the finishing layers and one or more of the layers behind. If the thickness of a wall finishing (d_1) is larger than its effective moisture penetration depth ($EMPD_1$), then the

influence of the other layers is not taken into account. If its thickness is smaller (for instance a wall paper), then the whole finishing layer is considered sorption active and the effective moisture penetration depth of the layer behind is added (Hens, 2005). The model parameters in Equation 5 are calculated as follows (suffix 1 refers to the wall finishing, 2 to the layer behind):

$EMPD_1 > d_1$: *(7)*

$$\rho\xi d_p = \rho\xi_1 d_1 + \rho\xi_2 EMPD_2$$

$$Z_b = 0.5\left(Z_1 + \frac{EMPD_2}{\delta_2}\right)$$

4. Modelling humidity distribution within a room

4.1 Developments within IEA-Annex 41

The assumption of well-mixed air in a zone or in an air cavity is typiclly used in building simulations with a coarse or intermediate level of granularity of the air volume. The air volume is treated as homogeneous and air circulation, caused by temperature and concentration gradients within it or by mechanical devices, is neglected.

In reality, the air in a zone is never perfectly mixed. HAM models based on the well-mixed air assumption may lead to erroneous results in situations where there exist regions with low air circulation, such as in corners or spaces behind furniture. This is because the wall partitions, which are well-flushed with air, experience at least one order of magnitude larger surface transfer coefficients and different heat and moisture transfer driving potentials than those in a hidden position. As a result, only a part of the wall appears active in the HAM transfer investigated, while the other part is practically inactive. Models based on very-fine spatial discretization of an air volume and on the detailed conservation equations of mass, momentum and energy in the air are needed for such problems.

The difficulties associated with modeling convective flow fields have led to the development of specialized Computational Fluid Dynamics (CFD) tools. In the past few years CFD has been playing an increasingly important role in building design, following its continuing development for over a quarter of a century. The areas in building design where CFD has been used are widespread: HVAC-design, ventilation design, fire and smoke control, draft comfort, etc… A good overview of recent developments is given by Zhai (2006). It is interesting to note that whole building heat, air and moisture modeling does not appear in this overview. Most of the existing CFD-tools can represent water vapor diffusion and transport in air, however they do not take into account mass transfer at the interface of the air and the building envelope. Some extended modeling was needed in order to include both heat and moisture transfer in CFD codes. During Annex 41 several approaches were formulated in order to solve coupled mass transfer in air and building envelopes in very fine-grained models for the air volume.

Hedegaard et al. (2004) proposed a method using the existing diffusion equations in a CFD code mainly because it is a method were no programming of user defined functions is needed. As diffusion is computed only in fluid domains, the walls need to be defined as fluids. The building envelope was therefore modeled as immobile fluids with ordinary building material characteristics as material properties. This enables the modeling of moisture diffusion within the walls.

Steeman et al. (2005, 2008) programmed a user defined function using the EMPD-model in order to describe moisture transfer in the building envelope. The main advantage of this approach is a better flexibility of the model. This model was further expanded by using user defined scalars in Fluent containing the mass transfer equations in the solid porous material. This way the solver of the CFD code can be used to solve the mass transfer in the material. This model was successfully validated with experimental data.

Neale et al. (2006) programmed a moisture transfer model in Matlab and made an external coupling with Fluent in order to solve heat and mass transfer in air and porous materials. This approach was also compared to the experimental data.

In IEA-Annex 41 CFD has proven to be a promising tool to get detailed information of the air flows in buildings and over building components. It also may provide the users with local values of heat and mass transfer coefficients which can be used in whole building simulation programs. Additional possibilities for applying CFD simulations in practice are envisioned through the further integration with building simulation tools.

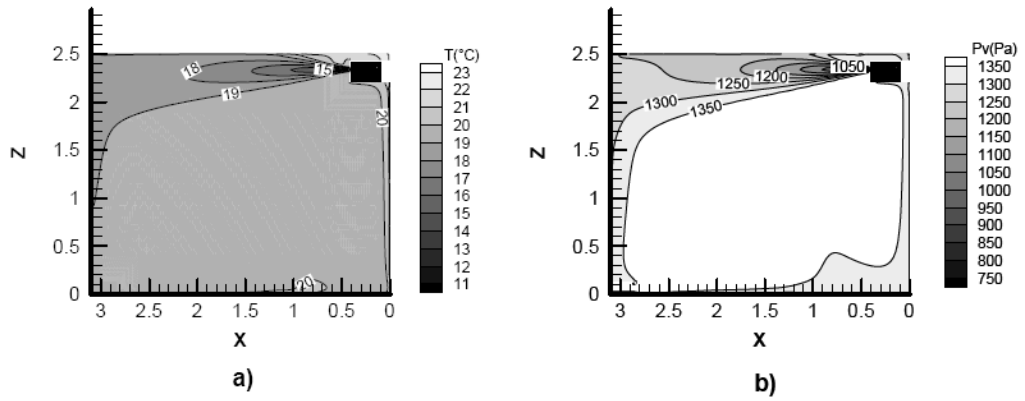

FIG. 4: Air temperature (a) and water vapour pressure (b) distribution in the symmetry plane after 8 hours.

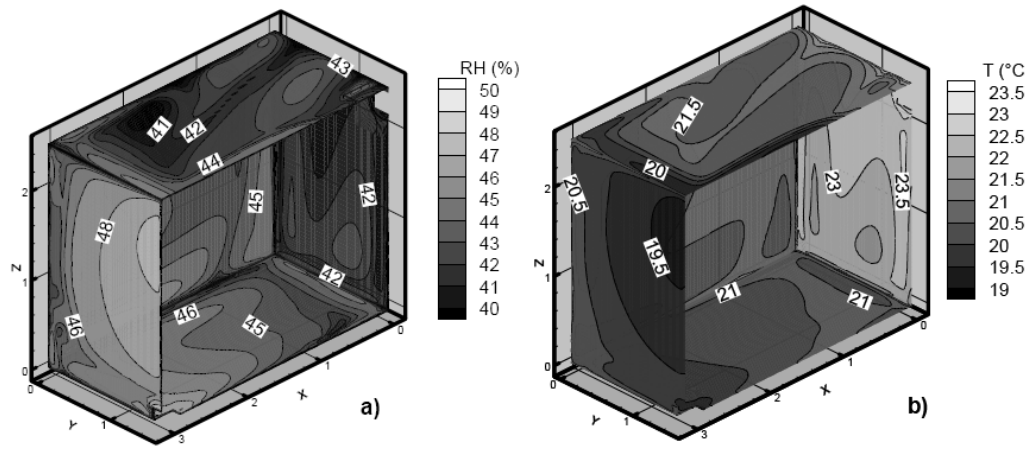

FIG. 5: Distributions after 8 hours: a) Relative humidity inside the walls, b) Temperatures at the wall surface

In spite of the important advances in this field, two major limits are still imposed for such a detailed approach. One is the computational time: even though computing power has risen and is rising significantly every year, annual simulations of whole building using CFD are still far beyond the capabilities of current computers. The second and very important limit consists in the problem of validation. Such detailed tools require very detailed description of the room (geometry and material properties) and a very experienced user in order to provide realistic results.

4.2 Example of a coupled HAM-CFD approach (Steeman et al. 2008)

In this example, the standard CFD model Fluent® is used to solve the heat and mass balance for a room. Therefore, the room is descretized in a number of 'air' control volume elements. The heat conduction in the wall is solved by the CFD solid model. Therefore, the wall is discretized in a number of 'heat' control volume elements. For moisture transport in the porous material, the EMPD-model is used, which only requires a discretization of the surface layer of the wall into one layer of 'hygric' control volume elements (Equation 5). The dimensions of the 'hygric' control volume element are defined by the corresponding air control volume element and the penetration depth. For the moisture balance of the air control volume adjacent to the sorption active surface, all the terms in Equation 1 are considered. The EMPD-model is implemented in the CFD code by means of user defined functions.

The coupling between the CFD and the EMPD numerical model is explicit in time. Hence small time steps have to be used in the CFD-EMPD model. It is noted that the transport processes in the walls are much slower than in the air. Hence by choosing a time step of the same order of magnitude as the time constant of the air transport the accuracy of the coupling is guaranteed. In this example a time step of 5s is chosen.

The coupled model is used to study the temperature and water vapour pressure distribution in a room with hygrothermal wall interaction. The geometry of the rectangular room considered in the example is based on an experimental setup for the validation of CFD models for indoor air flow (Hohota 2003). The room is ventilated through an air inlet located at the top of one wall, and an air outlet at the bottom of the opposite wall. The walls consist of cellular concrete, with a thickness of 0.1 m. The room response is studied after a period of 8h moisture production with a uniformly distributed moisture source of 0.5 kg/h, starting from a steady state situation without moisture source. All the time a cold and dry air flow is supplied to the room at a flow rate of 55 m³/h, temperature of 11°C and water vapour content of 4.3 g/kg. The temperature at the outside of the inlet wall is 27°C, and at the outside of the other walls 22°C. This leads to a non-uniform temperature distribution.

Figure 4 shows the predicted temperature and water vapour pressure distributions in the symmetry plane of the room after 8 hours. The figures clearly show that the jet hits the opposite wall (called outlet wall) forming a distinct zone of air with lower temperature and water vapour pressure sticking to the ceiling and outlet wall. The jet does not penetrate into the occupied zone of the room. Figure 5 shows the RH distribution in the walls and the distribution of the wall surface temperature corresponding to the air conditions in Figure 4. The higher surface temperatures at the inlet wall are related to the higher temperature (27°C) as boundary condition at the outside surface of this wall. For the outlet wall, the surface temperatures are lower compared to the temperatures in the occupied zone, as aresult of the cold jet hitting the outlet wall. The locally higher RH values in the outlet wall are explained by the colder surface temperatures of the wall, resulting in lower water vapour saturation pressures and thus higher RH values and moisture contents.

The predicted variation of temperature and humidity conditions over a wall surface shows that, when an accurate prediction of the local relative humidity in the wall is required, the use of a fine-grained model which can take into account local temperature and humidity distributions in the indoor air, is necessary.

5. Conclusions

5.1 HAM-modelling in IEA-Annex 41

Many models and simulation tools are available to represent the HAM behavior of buildings at different levels of granularity and complexity. The models are ranged from simplified (coarse-grained) approaches where analytical solutions can be found, to detailed CFD simulations (very finely-grained). According to the objectives of Annex 41, all of them are complementary and help to understand better how a whole building works in terms of its hygrothermal conditions. All tools involve modeling of several physical processes pertaining to coupled flow of heat, air, and moisture. They represent different building elements at various levels: its spaces, the building envelope with its materials, the interior building structures and furnishing, the system for heating, ventilating and air conditioning, occupants and equipment, and finally the exposure to the exterior environment.

Simplified modeling for moisture buffering showed its usefulness in many situations, especially when detailed calculations of coupled heat and mass transfer through the envelope are not needed, but rather correct estimations of indoor air relative humidity are of interest. The main problem pointed out was how to correctly evaluate the model parameters based on the materials that compose the envelope and that are in contact with the room air.

Whole building models, mainly situated at intermediate level of granularity, demonstrated that they can correctly predict indoor climate, energy performance, together with hygrothermal conditions within the envelope.

Fine and very-fine-grained models have proven to be a useful tool to get detailed information of the air flows in buildings and over building components, and on local hygro-thermal fields within multi dimensional building elements. They also provide the users with local values of heat and mass transfer coefficients, or hygrothermal bridges, which can be used in whole building simulation programs at intermediate and coarse levels of granularity.

5.2 Future development of HAM tools for buildings

The actual challenge in whole building HAM modeling is to ensure a good balance between many different physical phenomena which interact with each other, rather than to develop models that focus too much on mainly one phenomenon. For example, in most of the existing programs, if moisture is well modeled, then the energy model is rather simple; or if energy is rather well calculated, then moisture behavior is treated in a

simplified way – if not neglected. In this field a lot of progress has been made and encouraging outcomes resulted from this collaborative project. For example, some interesting modeling approaches of air flows through envelopes were proposed.

Also a correct balance should be ensured between different granularities for air volume and for the envelope. Multi-dimensional effects, both in air spaces and in construction elements, need more analysis. The challenge is to have a fully coupled multi-dimensional model of both: the building element and the indoor space, in order to better capture the interactions. Mainly due to modeling and computational difficulties, relatively little attention has been given until now to the problems of air which is not well mixed, and to specification of the cases when it is acceptable to treat the air in a zone as one bulk. Also the influence of possible 2D or 3D HAM transfer through the envelope parts, and the possible variability in space and time of the surface film coefficients, have not been greatly investigated.

To link different levels of modeling, whole building performance with problems of mould behind furniture for example, some adapted approach should be employed – such as multi-scale, reduced order or zonal models. It is not possible to calculate the whole space in the building by a grid whose size is in the order of millimeters, such as those which may be used for calculation of the transport in building materials. Rather than having one tool that calculates everything, a suite of separate, specialized tools should be developed which are able to work together synchronously (distributed calculations).

6. References

Abadie, M., Deblois, J.P., Mendes, N. 2005. A comparison exercise for calculation heat and moisture transfers using TRNSYS and PowerDomus. IEA Annex 41 report A41-T1-Br-05-2.

Crawley D.B., L. K. Lawrie, C. O. Pedersen, F.C. Winkelmann. 2004. EnergyPlus: An Update. In Proc. SimBuild, Boulder, CO (USA) LBNL-55518

Funk, M, J. Grunewald. 2002. Die thermodynamischen Grundlagen des numerischen Simulationsprogramms DELPHIN4 Tagungsband zum 11. Bauklimatisches Symposium an der TU Dresden (Germany).

Grau K., Rode C. 2006. A model for air flow in ventilated cavities implemented in a program for whole-building hygrothermal simulation. IEA Annex 41 report A41-T1-Dk-06-1.

Hedegaard, L., M. Woloszyn and G. Rusaouen. 2004. Moisture interactions between air and constructions modelled with CFD. IEA Annex 41 report A41-T1-DK-04-4.

Hens H. 2004. Impact of adventitious ventilation on the moisture performance of roofs in moderate climates. IEA Annex 41 report A41-T1-B-04-1.

Hens, H. 2005. Impact of hygric inertia on indoor climate: simple models. IEA Annex 41 report A41-T1-B-05.

Hohota R. 2003. Moisture modeling in a CFD code (low velocity in large enclosure). Comparison with experiments. (in French) PhD thesis, Laboratoire CETHIL INSA de Lyon, (France)

Holm. A., Künzel H.M., Sedlbauer, K. 2003. The Hygrothermal Behaviour of Rooms: Combining Thermal Building Simulation and Hygrothermal Envelope Calculation. Proceedings of the Eighth International IBPSA Conference, Eindhoven, Netherlands, August 11-14, 2003.

Iwamae, A., H. Hanibuchi, T. Chikada. 1999. A Windows-based PC-software to design thermal environment in residential houses, Proceedings of Building Simulation'99, Volume 3: 1325-1330.

Janssens, A. and M, De Paepe. 2005. Effect of moisture inertia models on the predicted indoor humidity in a room. In: Proceedings of the 26th AIVC-Conference ‘Ventilation in Relation to the Energy Performance of Buildings’, Brussels, ISBN 2-9600355-8-5, INIVE EEIG.

Keresteciogl u, A., M. Swami and A. Kamel, 1989, "Theoretical and Computational Investigation of Simultaneous Heat and Moisture Transfer in Buildings: Effective Penetration Depth Theory." ASHRAE Winter Meeting, Atlanta, GA.

Klein, S.A., Beckman, W.A., Mitchell, J.W. et al. 2004. TRNSYS 16 – A TRaNsient System Simulation program, User manual. Solar Energy Laboratory. Madison: University of Wisconsin-Madison.

Koronthalyova O., P. Mihalka, P. Matiasovsky. 2004. Model for Whole HAM-Transfer Simulation in Room. IEA Annex 41 report A41-T1-Sl-04-1.

Mendes, N., Oliveira, R.C.L.F. and Santos, G.H.dos. 2003. Domus 2.0: A Whole-Building Hygrothermal Simulation Program. Proceedings of the 8th International Building Performance Simulation Association (IBPSA), 1, Eindhoven – Netherlands.

Neale, A., Derome, D, Blocken, B and Carmeliet, J. 2006. CFD calculation of convective heat transfer coefficients and validation. IEA Annex 41 report A41-T3-C-06-5.

Perschk, A. 2000. Gebäude-Anlagen-Simulation unter Berücksichtigung der hygrischen Prozesse in den Gebäudewänden. Dissertation TU Dresden (Germany).

Plathner, P. and M. Woloszyn. 2002. Interzonal air and moisture transport in a test house. Experiment and modelling. Buildings and Environnement, vol. 37/2, 189-199.

Rode, C. and K. Grau. 2003. Whole Building Hygrothermal Simulation Model. In: ASHRAE Transactions - American Society of Heating Refrigerating Air-Conditioning Engineers. 2004, 109 (1). pp. 572-582.

Sahlin P., L. Eriksson, P. Grozman, H. Johnsson, A. Shapovalov and M. Vuolle (2004) Whole-building simulation with symbolic DAE equations and general purpose solvers. Building and Environment Volume 39, Issue 8, Pages 949-958.

Sasic Kalagasidis A. 2004. HAM-Tools. An Integrated Simulation Tool for Heat, Air and Moisture Transfer Analyses in Building Physics. Doctoral thesis. Chalmers University of Technology, Gothenburg, Sweden

Sasic Kalagasidis A., Mattsson, B. 2005. Modelling of Moisture Conditions in a Cold Attic Space. In: Proceedings of the 26th AIVC-Conference 'Ventilation in Relation to the Energy Performance of Buildings', Brussels, ISBN 2-9600355-8-5, INIVE EEIG.

Sasic Kalagasidis, A. 2007. Hygrothermal response of a house with dynamical insulation in the roof. IEA Annex 41 report A41-T1-S-07-1.

Schijndel, A.W.M. van. 2007a. Integrated Heat Air & Moisture Modeling and Simulation, PhD thesis, Eindhoven University of Technology, ISBN 978-90-6814-604-2

Sofic M, Bednar T. 2007. Analyses of the accuracy of monthly energy balances for assessment of cooling energy demand (Analyse Der Genauigkeit Des Monatsbilanzverfahrens Zur Ermittlung Des Kühlbedarfs Von Nichtwohngebäuden). Bauphysik, 29(3): 202 − 207. (in German).

Steeman H.J., Janssens A, De Paepe M. 2005b. CFD modelling of HAM transport in buildings: The importance of local indoor climate. IEA Annex 41 report A41-T1-B-05-8.

Steeman H.J., Janssens A., Carmeliet J., De Paepe M. 2008. Modelling indoor air and hygrothermal wall interaction in building simulation: Comparison between CFD and a well mixed zonal model, accepted for publication in Building and Environment.

Stovall T, Karagiozis A. 2004. CFD Analysis of a Ventilated Brick Cavity. Annex 41 report A41-T1-US-04-2.

Tariku, F. 2008. PhD Thesis in Progress. University of Concordia, Canada

Woloszyn M, Rode C. 2008. Annex 41, Subtask 1: Modelling principles and common exercises. Draft Final Report for the ECBCS executive committee of the International Energy Agency.

Woloszyn, M., J. Shen, A. Mordelet and J. Brau. 2005. Numerical simulations of energy performance of a ventilation system controlled by relative humidity. In: Proceedings of the 26th AIVC-Conference 'Ventilation in Relation to the Energy Performance of Buildings', Brussels, ISBN 2-9600355-8-5, INIVE

Wurtz E., F. Haghighat, L. Mora, K.C. Mendonca, C. Maalouf, H.Zhao, P. Bourdoukan. 2006. An integrated zonal model to predict transient indoor humidity distribution, ASHRAE Transactions (112)2: 175-186.

Zhai, Z. 2006. Applications of Computational Fluid Dynamics in Building Design: Aspects and Trends. Indoor and Built Environment 15(4): 305-313.

HAM-Tools – a whole building simulation tool in Annex 41

Angela Sasic Kalgasidis, Assistant professor
Chalmers University of Technology, Dep. of Civil and Environmental Engineering, Sweden;
Angela.Sasic@chalmers.se; www.chalmers.se

Carsten Rode, Associate professor
Department of Civil Engineering, Technical University of Denmark
car@byg.dtu.dk; www.byg.dtu.dk

Monika Woloszyn, Associate professor
Université de Lyon, Lyon, France ; CETHIL
monika.woloszyn@insa-lyon.fr; www.insa-lyon.fr

KEYWORDS: HAM-Tools, Whole building simulations, HAM simulations, Annex 41

SUMMARY. HAM-Tools is a building simulation software. The main task of this tool is to simulate transfer processes related to building physics, i.e. heat, air and moisture transport in buildings and building components in operating conditions. The scope of the ECBCS Annex 41 "Whole Building Heat, Air and Moisture Response" was of a high relevance for the testing, development, validation and promotion of the HAM-Tools. The majority of the numerical studies made by this programme were provided for Subtask 1 "Modelling principles and common exercises". This paper gives an overview of the modelling capabilities of HAM-Tools and some results provided for Subtask 1.

1. Introduction

HAM-Tools is a building simulation software. 'HAM' stands for *H*eat, *A*ir and *M*oisture transport processes in buildings and building envelopes that can be simulated by this program, and 'Tools' describes its modular structure. The main objective of this tool is to obtain simulations of transfer processes related to building physics, i.e. heat, air and moisture transport in buildings and building components in operating conditions.

Using the graphical programming language Matlab/Simulink®, the code was developed as a library of predefined calculation procedures (tools) where each supports the calculation of the HAM transfer processes in a building part or an interacting system. Thus, the tool can be used for the investigations of the above mentioned transfer mechanisms and for the analyses of the overall hygro-thermal response of buildings.

HAM-Tools was developed by Sasic (2004), within a PhD work that was conducted at the Building Physics research group at Chalmers University of Technology. The structure of the programme, it's interface and documentations provided are standardized according to the guidelines given in the International Building Physics Toolbox in Simulink (www.ibpt.org). IBPT is an open source of calculation tools for building physics application. It is a result of the cooperative work between Chalmers University of Technology and the Building Physics Department from Technical University of Denmark (see Weitzmann et. al 2003). As a part of IBPT, HAM-Tools is also an open tool and publicly available for free downloading.

Due to the complexity of the physics that is in-built in the programme, the need for an active development of the tools and to the costly modelling platform in Matlab/Simulink®, HAM-Tools is more suitable for research and education than for a commercial use. Some examples of the research applications can be found in Sasic and Mattsson (2005), Ramos (2006), Hagentoft and Sasic (2007), Essah et. al (2008), Nik and Nielsen (2008). A significant effort has been put on the validation of the existing modules. Results of the validation are presented in Hagentoft et. al (2002), Sasic (2004 b, 2007 b) and, as it is shown below, in the final reports from Annex 41.

1.1 HAM-Tools in IEA Annex 41

The scope of the ECBCS[1] Annex 41 "Whole Building Heat, Air and Moisture Response" (ECBCS, 2008) was of a high relevance for the testing, development, validation and promotion of the HAM-Tools.

The majority of the numerical studies made by this programme were provided for Subtask 1 "Modelling principles and common exercises" (Woloszyn and Rode, 2008), the working group who dealt with the modelling of heat, air and moisture transfer processes that take place in "whole buildings". HAM-Tools solutions were provided for five out of six calculation exercises that were presented in Subtask 1, as it is summarized in Table 1. All these cases present one of the three possible validation methods: analytical validation, e.g. the problem where an exact mathematical solution is known, comparison with other codes and empirical validation. In addition, in the frame of this Subtask, two numerical studies on the influence of air infiltration on the hygro-thermal states in buildings were performed by HAM-Tools and presented in Sasic and Mattsson (2005) and Sasic (2007 a).

TABLE. 1: HAM-Tools solutions provided to the calculation exercises in Subtask 1. The marker "•" denotes solutions from Chalmers University of Technology, "∗" are solutions from CSTB[2] using HAM-Tools and "X" marker denotes the skipped cases. Validation methods are indicated as: /A/-analytical, /C/-comparison with other codes, /E/-empirical.

CE 0 /C/	600	•	CE 2 /E/	Case 1-1	•,∗	CE 3 /E/	Step 1	•				
	900	•		Case 1-2	•,∗		Step 2	•				
	600 FF	•		Case 1-3	•,∗		Step 3	•				
	900 FF	•		Case 2-1	•,∗		Step 4	X				
CE 1 and 1B /A, C/	600-0A	•		Case 2-2	•,∗	CE 4 /C/		A	B	C	D	E
	600-0B	•		Case 2-3	•,∗		Step 1	•	•	X	X	X
	600-Open	•		Case 2-4	•,∗		Step 2	•	•	X	•	X
CE 1A /A/	0A	•		Case 2-5	•,∗		Step 3	•	•	X	•	X
	0B	•		Case 2-6	•,∗	CE 5 /A, E/	X					

Some results were also provided for Subtask 2 "Experimental analyses of moisture buffering" (Roels, 2008). These were the numerical solutions to the benchmark cases on moisture buffering in a layer of gypsum boards under transient conditions. As measured data are available for all benchmark cases in Subtask 2, they represent a set of problems for the empirical validation of one-dimensional hygro-thermal calculations in a wall. Table 2 gives the overview of the cases and the HAM-Tools solutions provided. Besides, Ramos (2006) presented a separate study on moisture buffering of coated gypsum boards under transient conditions. The study encloses the measured data from a small chamber test, supported by numerical investigations done by HAM-Tools.

TABLE. 2: HAM-Tools solutions provided within Subtask 2. The "X" marker denotes the skipped cases.

Benchmark 1	Step - naked	•	Benchmark 2	Test 1	•
	Step - acryl	•		Test 2	•
	Step - latex	•		Test 3	•
	Cyclic-naked	•		Test 4	•
	Cyclic- acryl	•		Test 5	•
	Cyclic- latex	•		Hysteresis and 100 cycles	X

There were no particular contributions from HAM-Tools to Subtask 3 "Boundary conditions and whole building HAM analyses" (Kumaran and Sanders, 2008). However, the modelling of wind and wind pressure coefficients has been included in the above mentioned studies from Subtask 1, which deal with air

[1] Energy Conservation in Buildings and Community Systems

[2] CSTB Centre de Thermique de Lyon, France

infiltration in buildings, (see for example Sasic 2007 a). Also, the modelling of the surface transfer coefficients has been addressed in the studies from Subtask 2.

One study based on numerical investigations by HAM-Tools was presented in the frame of Subtask 4 "Moisture-engineering application" (Holms, 2008). The study shows the moisture safety assessment in cold attics under different ventilation regimes. (Hagentoft and Sasic, 2007).

The HAM-Tools description and a selection of modelling issued from Annex 41 Subtask 1are presented hereafter.

2. Object oriented modelling approach in HAM-Tools

The general problem of HAM-Tools simulations is depicted in Figure 1, where main systems and transfer processes involved are indicated. These are: building enclosure (e.g. walls, windows, floor, ceiling, etc), building services (HVAC systems and components), occupants and appliances. The scope of the simulation is to find thermal and moisture states in a building enclosure and in enclosed air volumes, as the result of the building usage in specified operating conditions (in given climate conditions and internal activities). This knowledge enables a number of further analyses such as: calculation of energy consumption for heating and cooling in buildings, assessment of indoor comfort, analyses of risks for higher moisture content levels in a building construction and indoor air, functionality of HVAC systems, air flow distribution through openings on building enclosure, etc.

The main idea in HAM-Tools is to model a building as a system of cooperating objects. This approach is known as object-oriented programming (see for example Coyne et. al, 1989), as opposed to a traditional view in which a programme may be seen as a group of tasks to compute.

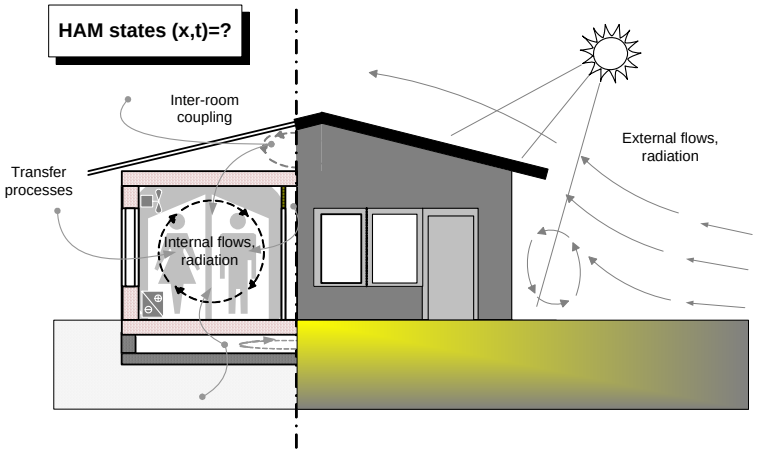

FIG.1 The general simulation problem in HAM-Tools.

2.1 Library

Using the graphical programming language Simulink® (Matlab), the code is developed as a library of predefined calculation procedures (tools) where each supports the calculation of the HAM transfer processes in a part of a building or in an interacting system. Tools are grouped according to their functionality into five sub-systems:

- Constructions (building envelope parts),
- Zones (air volumes and cavities),
- Systems (HVAC systems),
- Helpers (weather data and basic modelling tools) and
- Gains (casual gains).

When all sub-systems are coupled together and solved simultaneously, the resulting simulation represents the highest level of integration in the HAM-Tools.

In the Simulink graphical approach, the HAM-Tools library appears as it is shown in Figure 2, where the above mentioned five subsystems appear as separate folders. Representatives of tools or blocks[3] from each of the subsystem are shown in the same figure below. Blocks can be modelled separately from each other, with different modelling techniques and with different levels of accuracy.

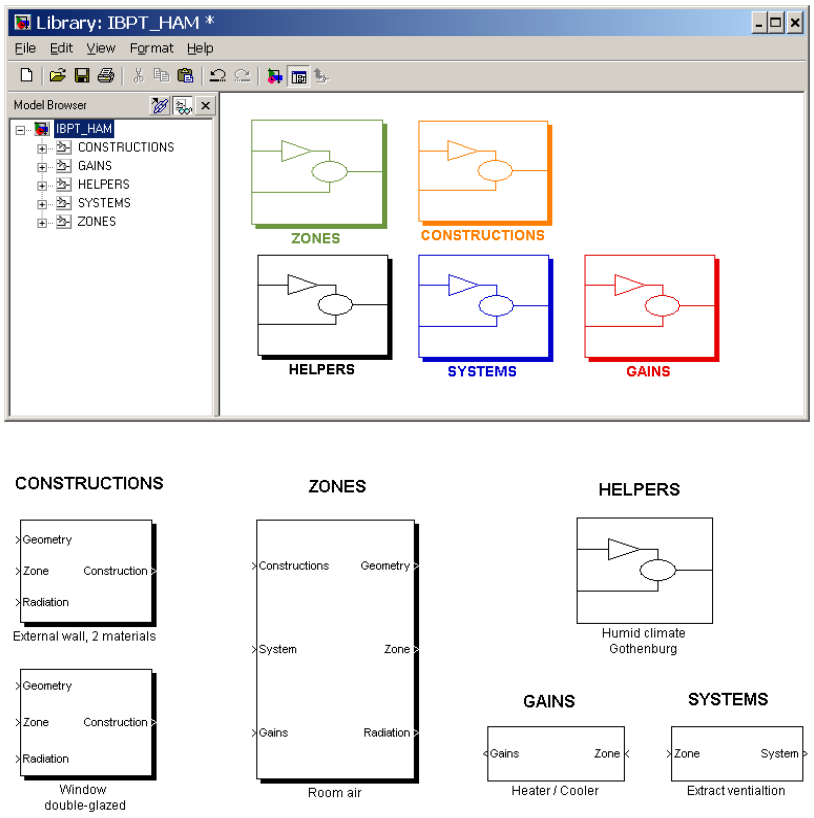

FIG.2 HAM-Tools library in Simulink, and some tools.

2.2 Interface

The blocks “communicate” with each other by exchanging data through communication ports. Input ports are usually grouped on a left-hand side of a block, while the output ports are placed on the right-hand side. The ports tolerate or provide the data that are organized in arrays or signals, which have predefined and rigid structures. In this way, the block communication is always ensured even then when they are developed by different users. The set of rules for the data exchange between the blocks is called interface.

For the highest level of integration in HAM-Tools, e.g. at the level where a model of a building is assembled, the set of seven signals is used. These are:

- Surface weather data

[3] A ”block” is a common term in Simulink for any kind of modelling elements – operations, routines, subsystems, etc.

- Construction array
- System array
- Geometry array
- Zone array
- Radiation array
- Gain array

The same interface is valid for all tools enclosed in IBPT (see Rode et. al 2002).

2.3 Building a model of a building

By combining different tools such as a single-layer wall in a multi-layer wall, a couple of different walls in a zone, several zones in a building, and finally together with climate load and HVAC equipment, it is possible to build a house as a system. Basically, all HAM-Tools models used in the common exercises of Subtask 1 were one-zonal models. A system with several air zones, a dwelling and two air cavities in a roof can be found in Sasic (2007a).

2.4 Granularity

Woloszyn and Rode (2008) use the term "granularity" to describe the size and the dimension of the numerical girds used in whole building simulation tools, e.g. the spatial discretization of air spaces and building envelopes in the numerical models. There are four levels of granularity: coarse, intermediate, fine and very fine. Coarse models assume well-mixed air in a zone and do not provide the hygro-thermal states in a building envelope. "Very fine" refers to the models that are, for example, based on computational fluid dynamics (CFD) calculations. Table 3 shows the classification of the models used in Annex 41 Subtask 1.

TABLE. 3: Typical associations of model granularities, from Woloszyn et.al (2008)

	Envelope			
Air	Coarse	Intermediate	Fine	Very fine
Coarse	X	X		X
Intermediate	X	X	X	X
Fine		X		
Very fine		X		X

These are the programming capabilities of HAM-Tools:

- 1D calculations of transient heat, air and moisture transfer through a building envelope
- Transient heat and moisture balances in air zones, assuming well mixed air. At the same time, the mass balance of air can be performed on a multi-zonal grid.
- Coupling between air zones, e.g multi-zonal calculations
- Modelling of wind and temperature induced air pressure differences around a building
- Moisture uptake by surface materials during rain
- Condensation of surfaces
- Modelling of the radiation heat exchange with surroundings based on a building orientation.
- Modelling of the radiation heat exchange within air zones based on exact view factors
- Detailed modelling of internal HAM gains and HVAC equipment
- Coupling to oher codes / procedures developed in Matlab, C++ and Femlab

According to Woloszyn and Rode (2008), HAM-Tools can be classified as an intermediate to fine-grained model. For example, HAM-Tools provides 1D calculations in a building envelope and thus it can be classified as intermediately-grained. But in terms of the represented physical processes, such as coupled HAM transfer in a building envelope, including liquid transport and temperature and moisture dependent material properties, the programme can be classified as "fine".

2.5 Limitations

The programme has following the limitations:

- Temperature should be in the range of –30 °C to +80 °C
- Effects associated with phase change liquid from/to ice, are neglected.
- Hysteresis is not considered.
- Gravity effects are not considered.
- Chemical reactions are not considered.
- Drainage between material layers is not considered.
- Ageing effects or changes in geometrical dimensions are neglected.

3. HAM-Tools calculation model for HAM transport in whole buildings

This chapter encloses the detail description of the governing equations for the calculation of heat, air and moisture transfer in a whole building, in HAM-Tools.

3.1 HAM states in a building enclosure – the model for the construction blocks

HAM states in a wall, e.g. temperature T (°C) and moisture content w (kg/m^3) can be found from the following energy and mass balance equations:

$$c\rho\frac{\partial T}{\partial t} = -\frac{\partial q}{\partial x} \quad (1.)$$

$$\frac{\partial w}{\partial t} = -\frac{\partial g}{\partial x} \quad (2.)$$

Both the temperature and the moisture content are the functions of time t and the space coordinate x.

The heat and moisture flows in a wall, q (W/m^2) and g (kg/m^2), are governed by the differences in temperature T (°C), vapour pressure p_v (Pa) and suction pressure s (Pa):

$$q = \underbrace{-\lambda\frac{\partial T}{\partial x}}_{\text{heat conduction}} + \underbrace{g_a \cdot c_a}_{\text{heat convection}} + \underbrace{g_v \cdot h_e}_{\text{source due to evaporation}} \quad (3.)$$

$$g = g_v + g_a \cdot x_a + g_l = \underbrace{-\delta_p\frac{\partial p_v}{\partial x}}_{\text{vapour diffusion}} + \underbrace{g_a \cdot x_a}_{\text{vapour convection}} + \underbrace{\lambda_{m,l}\frac{\partial s}{\partial x}}_{\text{suction}} \quad (4.)$$

The air flow rate through a wall g_a (only one-dimensional, along x coordinate) is governed by the difference in air pressure across the wall. This flow is either prescribed in advance or calculated by another module.

The humidity ratio x_a (kg/kg) is approximated as:

$$x_a = 6.21\cdot 10^{-6}\cdot p_v \quad (5.)$$

3.2 HAM states in a zone – Zone blocks

HAM states in a zone, e.g. air temperature $T_{a,in}$ (°C), moisture content in the air v_{in} (kg/m^3) and air pressure $P_{a,in}$ (Pa) can be found from the energy and mass balance equations:

$$c\rho V\frac{dT_{a,in}}{dt} = \sum_i Q_i \quad (6.)$$

$$V\frac{dv_{in}}{dt} = \sum_j M_{v,j} \quad (7.)$$

$$0 = \sum_k M_{a,k} \qquad 8.$$

The first two equations describe the storage of energy and water vapour in air. The last equation describes the mass conservation of dry air in a zone.

The HAM-Tools zone model is based on the assumption of a well-mixed air. This means that special variations of the air temperature and moisture content in air are neglected. i.e. the corresponding gradients are zero:

$$\nabla T_{a,in} = 0 \quad \text{and} \quad \nabla v_{in} = 0 \qquad 9.$$

The right-hand sides enclose HAM flows to and from the zone, such as:

$Q_1 = \sum_p h_p A_p \left(T_{surface,p} - T_{in}\right) +$ Heat flows due to a convective heat exchange between the air and the adjacent surfaces 10.

$Q_2 = \sum_q \dot{m}_{a,q} c \left(T_{inlet,q} - T_{in}\right) +$ Heat flows due to ventilation and infiltration

$Q_3 = \sum_r Q_{sources,r}$ Heat sources due to eating/cooling/humidifying equipment, solar gains through windows, lighting, appliances, etc. Only the convective parts are of interest.

$M_{v,1} = \sum_l \beta_l A_l \left(p_{surface,l} - p_{in}\right) +$ Vapour flows due to convective moisture exchange with adjacent surfaces 11.

$M_{v,2} = \sum_m \dot{V}_m \left(v_{inlet,m} - v_{in}\right) +$ Vapour flows due to ventilation and infiltration

$M_{v,3} = \sum_s M_{sources,s}$ Vapour generated within a zone by cooking, evaporation from a water surface, etc.

Q_1 and $M_{v,1}$ are organized in the Construction array, Q_2 and $M_{v,2}$ are in the System array while Q_3 and $M_{v,3}$ are in the Gain array.

$$\sum_k M_{a,k} = \sum_k \rho_{a,inlet,k} C_k \left(P_{a,inlet,k} - P_{a,in}\right)^n \qquad 12.$$

Air flows governed by mechanical ventilation systems, through openings and leakages in a building envelope

Depending on the source of air, the flows $M_{a,k}$ can be either in the Construction or in the System array. The air pressure in a zone, $P_{a,in}$, can be found from equation 8 and 12 by iterations.

3.3 HAM balance at outdoor surfaces (external boundary conditions)

Heat balance at an outdoor wall surface is given as:

$$-\lambda \frac{\partial T_{surface}}{\partial x} = h_c \cdot (T_{a,ext} - T_{surface}) + q_{rad} + \left(g_a \cdot c_a + g_{rain} \cdot c_l\right) \cdot T_{a,ext} + g_v \cdot h_v \qquad 13.$$

The first two terms on the right-hand side represent the convective and radiative heat exchange with the surrounding air. The third and the fourth parts refer to the specific enthalpy flows for air and water, when either an air ex-filtration or rain is taking place. The specific enthalpy flow for the water vapour is presented only by the latent part, the last term, while the sensitive part is neglected. The reference temperature for the sensible specific enthalpy is zero. In case of the air infiltration, the enthalpy of air is based on $T_{surface}$.

Net radiant energy absorbed by a wall surface originates from incoming solar radiation (direct and diffuse parts, I_{dir} and I_{diff}) and long-wave radiation exchange with surroundings:

$$q_{rad,ext} = \alpha_{sol} I_{sol} \cdot + \sum_k F_k \varepsilon_k \cdot \sigma \cdot \left(T_k^4 - T_{surface}^4 \right) \quad 14.$$

Temperature of surrounding surfaces, T_k,, view factors F_k and emissivities ε_k should be prescribed. Solar radiation intensity on a sloped (exterior) surface, I_{sol}, is calculated by the model presented in Perez (1986). Intensity of solar radiation through windows is a function of angle of incidence, number of panes and coatings.

Vapour balance at an outdoor surface is given as:

$$-\delta_p \frac{\partial p_{v,surface}}{\partial x} = \beta_p \cdot \left(p_{v,a,ext} - p_{v,surface} \right) + \begin{cases} g_a \cdot x_{a,ext}, & \text{for air ex - filtration } (g_{air} > 0) \\ g_a \cdot x_{a,surface}, & \text{for air infiltration } (g_{air} < 0) \end{cases} \quad 15.$$

In case of rain, the suction of water takes place for capillary active surface materials. The liquid inflow becomes the minimum of

$$\lambda_{m,l} \frac{\partial s_{surface}}{\partial x} \text{ and the prescribed flow } g_{rain}. \quad 16.$$

The rain load from a wind driven rain should be supplied from other calculations – there is no a specific calculation procedure for it.

3.4 HAM balance at indoor surfaces (internal boundary conditions)

Heat balance at an interior wall surface is given as:

$$-\lambda \frac{\partial T_{surface}}{\partial x} = h_c \cdot (T_{a,in} - T_{surface}) + q_{rad,in} + g_a \cdot c_a \cdot T_{a,in} + g_v \cdot h_e \quad 17.$$

when indoor air is flowing into the construction (infiltration). For the case of air flowing out from the wall, the enthalpy of air is based on $T_{surface}$.

Long-wave radiation exchange between internal surfaces can be modelled either in a simplified way, by using the so called “star model” or in an exact way, using additional modules for the calculation of exact view factors between the surfaces in an enclosure. In the first model, the net radiation that is coming to a surface is calculated as

$$q_{rad,i} = \frac{\Phi_r}{\sum_i A_i} + h_r \cdot \left(T_{star} - T_i \right) \quad 18.$$

where the first part on the right-hand side, Φ_r, represents a sum of all radiative heat sources in the zone, e.g both short wave and emitted long wave. The second part presents the radiative heat flow from the surrounding surfaces. The temperature of the “star”, T_{star} represents the mean surface temperature of all surfaces in an enclosure. In this way, all opaque surfaces absorb the same amount of energy per unit of surface area. The part that reaches a transparent surface (a window) is counted as a loss (see de Wit, 2000).

3.5 Gains and Systems

HAM sources in a zone, such as those originating from HVAC equipment or gains from transmitted solar radiation, people, appliances, wind and temperature induced air flows through intentional and unintentional openings, can be modelled in details by using the standard Simulink library tools.

3.6 Numerical model and solvers

The system of energy and mass balance equations presented above is solved numerically using the control volume technique and explicit time discretization scheme. The space discretization is done on a non-uniform stationary discretization mesh. As a part of the Matlab package, Simulink has built-in state-of-the-

art ordinary differential equation (ODE) solvers, which are automatically configured at run-time of the model. Thus, time discretization is done by the solver, and not by user. More details about the numerical model can be found in Sasic (2004 a)

4. Modelling issues in Subtask 1 that were exclusively addressed by HAM-Tools

As shown in Table 1, HAM-Tools was used in five of the six modelling exercises that were presented in the frame of Subtask 1. This section includes a selection of additional numerical studies that were made by HAM-Tools.

4.1 Thermal problem in Common Exercise 0

Common exercise 0 considered rather standard thermal problems - energy consumption for heating and cooling in lightweight and heavyweight test buildings (cases 600 and 900 in Table 1), and free-running indoor temperatures (cases FF in Table 1). All cases are based on the testing procedure that is known as BESTEST (Judkoff and Neymark, 1995).

As in BESTEST, the results obtained within Annex 41 for this exercise fairly diverged from one programme to another (see Woloszyn and Rode, 2008). In order to investigate some possible causes for the differences found, Sasic (2004 c) made a sensitivity analysis on one modelling aspect in energy calculations – modelling of a long-wave radiation heat exchange inside the test building. The analysis was done by HAM-Tools.

Two options can be found in HAM-Tools for the calculation of a long-wave radiation heat exchange in an enclosure: by using the approximate model that is given in equation 18 or by using a procedure for the calculation of exact view factors between surfaces. For the latter, the view factor between surfaces *i* and *j* is found from the following expression:

$$F_{ij} = \frac{1}{A_i} \int_{A_i} \int_{A_j} \frac{\cos(\theta_i)\cos(\theta_j)}{\pi r^2} dA_i dA_j \qquad 19.$$

where A_i and A_j are the areas of the surfaces *i* and *j*; θ_i and θ_j are the view angles between the surfaces; *r* is the distance between the surfaces.

The view factor F_{ij} gives the fraction of radiation that leaves A_i and is intercepted by A_j (see for example Hagentoft, 2001). The integration in equation 19 can be performed numerically; in HAM-Tools this is done by a separate module that is presented in Karlsson and Hagentoft (2005). In this way, instead of using a common radiative heat transfer coefficient for all surfaces, h_r, an exact amount of radiative heat flow is calculated for each surface.

Results of energy calculations for CE 0 in respect to the model used for long-wave radiation exchange are summarized in Table 3. As it can be seen, the exact model for the long-wave radiation gives substantially lower annual average free-running temperatures (up to 3 ^{o}C) and lower energy demands for cooling (around 5 %).

4.2 Moisture-buffering capacity of finishing materials in Common Exercise 3

The simulation problem in Common exercise 3 is based on a real one storey test building with two rooms, which are located at the outdoor testing site of the Fraunhofer Institute of Building Physics in Holzkirchen, Germany. The internal surfaces in the reference room were covered by standard gypsum boards with a latex paint. The walls in the test room were firstly fully coated with aluminium foil and then, in further tests, covered with gypsum boards. The indoor air temperature in both rooms was kept at 20 ^{o}C. The moisture production in both rooms was also the same: a high production of 0.4 kg/h in the morning, from 6-8 a.m., and moderate but longer production in the afternoon - 0.2 kg/h from 4-10 p.m. The rooms were exposed to the outdoor climate conditions in Fraunhofer.

TABLE. 3 HAM-Tools results for Common Exercise 0 in respect to the model used for the long-wave radiation heat exchange in enclosure

	Equation 18	Equation 19	Equation 18	Equation 19
	Case 600 FF		Case 900 FF	
Annual mean indoor temperature	27.8	24.2	27.8	24.3
Maximum indoor temperature	69	62.2	46.4	44.7
Minimum indoor temperature	-15.3	-15.7	-1.4	-4.6
	Case 600		Case 900	
Annual energy for heating, kWh	4700	4700	1700	1800
Annual energy for cooling, kWh	5800	5600	2400	2300
Peak effect in heating, W	3800	3800	3400	3400
Peak effect in cooling, W	5700	5500	3000	2800

The scope of this exercise was to investigate the influence of moisture-buffering capacity of different finishing materials on the indoor relative humidity. The set of measured data collected in the test and the reference room during January-April 2005 was used for the validation of the simulation tools. The exercise was organized in four steps (see Table 1). The results for the first step, obtained by HAM-Tools, are presented hereafter.

During the first step, the walls in the test room were covered by aluminium foil and the indoor relative humidity was completely controlled by ventilation. As it was found from the tracer gas measurements, the ventilation flow rate was 0.66 1/h. As it is shown in Figure 3, the HAM-Tools results for the test room and for the first step are in excellent agreement with the measured data.

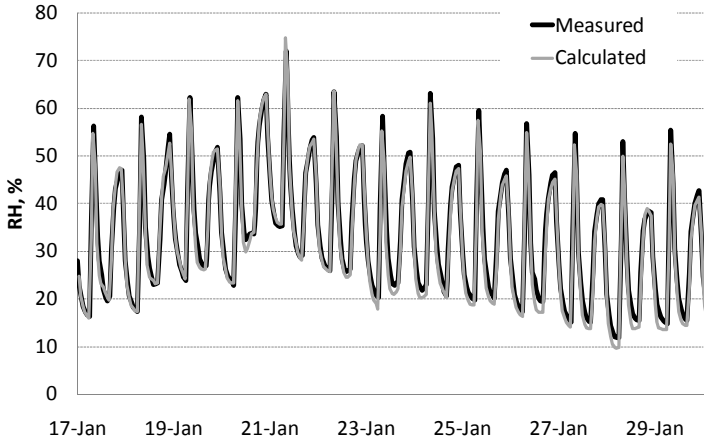

FIG. 3. Common exercise 3, Step 1: relative humidity in the test room. Black line shows the measured values, the grey line shows the calculated values with the ventilation flow rate of 0.66 1/h.

For the reference room, the ventilation flow rate was 0.63 1/h and the vapour resistance of the latex paint on the gypsum boards was specified to 0.15 m (s_d value). HAM-Tools simulations, however, point to a higher vapour resistance of the gypsum boards in the reference room than specified. As it can be seen in Figure 4, the calculated peaks in relative humidity are always lower than the measured ones. When a higher vapour resistance for the paint was used, s_d = 0.4 m instead of 0.15 m, a very good agreement with the measurements was achieved.

In HAM-Tools, the vapour resistance of the latex paint was incorporated in equivalent surface flow coefficient as:

$$\beta_{equivalent} = \beta_p + \delta_{p,air} / s_d \qquad 20.$$

where β_p is the surface vapour transfer coefficient in air and $\delta_{p,air}$ is the vapour diffusivity in air. The equivalent surface transfer coefficient is than used in the model (see equation 11).

None of the participants in this exercise reported the similar observations. And it is not even certain that the calculations can be corrected in this way. However, there are indications that the moisture buffering capacity in the reference room could be lower than it is expected. Lengsfeld et. al (2005) reported similar observations during the measurements for the step 4, where the relative humidity in the test room was lower than in the reference room. For this step, the walls in the test room (area 45 m^2) were covered by painted gypsum boards, with the resistance of the paint s_d=0.34 m. At the same time, the walls and the ceiling in the reference room were covered by the latex-painted gypsum boards (area 67 m^2), the same as in the step 1. Another reason for the discrepancies between the HAM-Tools simulations and measurements can be the non-uniformity of air inside the reference room. Similar indications can be found in the results for Common exercise 2 of Subtask 1.

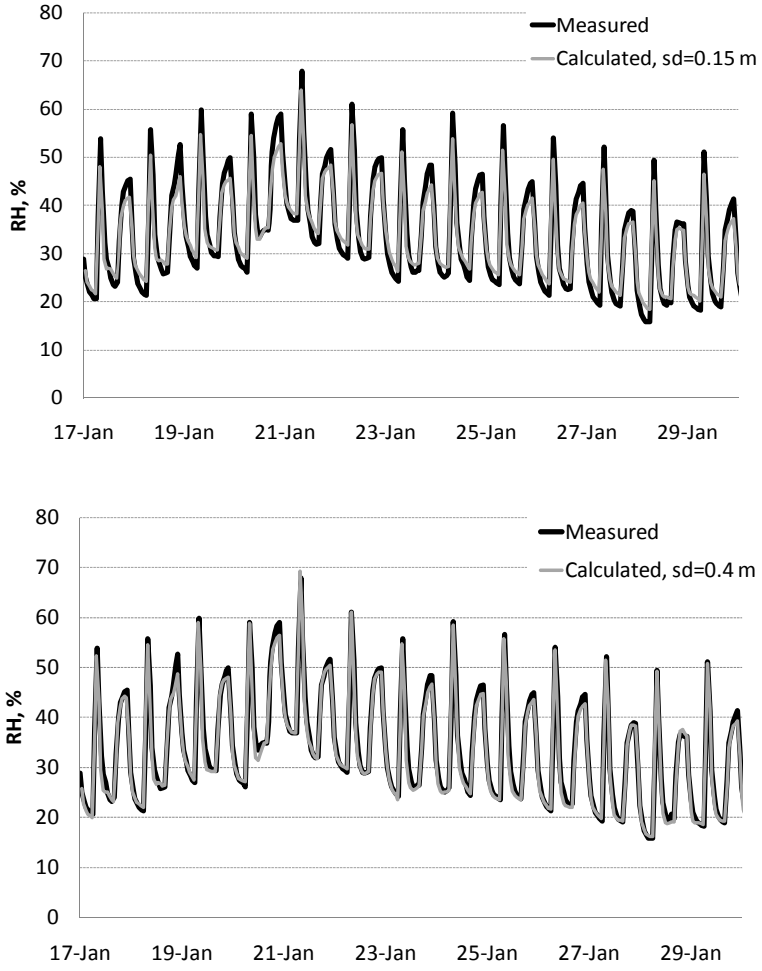

FIG. 4. Relative humidity in the reference room. Black line shows the measured values, the grey line shows the calculated values with sd=0.15 in the upper figure and 0.4 m in the lower figure. The ventilation flow rate is 0.63 1/h in all cases.

4.3 Convective heat and moisture flow through walls

As discussed in Woloszyn and Rode (2008), temperature and pressure gradients across a wall may lead to the onset of air convection inside air permeable materials and cavities, or to air filtration through the wall. Depending on the magnitude and direction of the air flow, the convective transport of heat and moisture, induced in this manner, may become a dominant transfer mechanism in comparison to heat conduction and vapour diffusion.

Air filtration through a wall has sometimes positive effects as, for example, when it is used for the heat recovery of the energy losses due to ventilation of a building. When passing through the insulation layer, the air is partly pre-heated by the heat that would be otherwise lost from a wall by heat conduction. The effective or the dynamical U-value of the wall is thus reduced and the overall efficiency of the insulation is improved.

Sasic (2007 a) investigated the energy efficiency of such concept and the hygro-thermal response of a house in relation to the overall air tightness of the house. The numerical investigation was made by HAM-Tools, on the model house from Common exercise CE 1- 600-Open (see Table 1). The original conventional roof in the test house was replaced by the roof with dynamical insulation. The airtightness of the building envelope was varied from 2 to 0.1 1/h airflow rates at 50 Pa pressure difference; in this way, the house can be classified as considerably airtight, according present standards, to extremely airtight. All other data were the same as in CE 1.

The coupled convective-diffusive heat and moisture transfer in the dynamical insulation was studied by using one-dimensional approach (see for example equations 3 and 4). The air flow through the house was studied by taking into account temperature and wind-induced pressure differences across the building envelope, as well as the action of an exhaust fan. For the calculation of the pressure distribution inside the house, the original one-zone model was upgraded with a quasi multi-zone model. Thus, the modelling equation 12 was extended for 12 more nodes (two pressure nodes in front of each internal surface).

Results of this study are summarized in figures below. As it can be seen in Figure 5, the energy efficiency of the dynamical insulation in the roof is directly correlated to the airtightness of the house. The maximum savings for heating, 17 % in comparison to the reference case from CE 1- 600-Open, are achieved for the extremely airtight house. For this case, the cooling energy demand is increased for 3 % in comparison to the reference case. In other two cases, the energy savings for heating and cooling are in the range of 2-4 %.

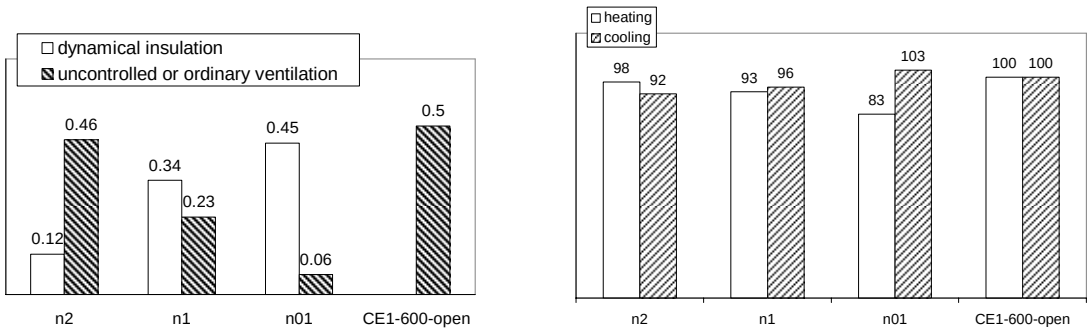

FIG 5. Left: Airflow rates (annual averages) through the dynamical insulation in the roof and thorough the air leakages in the building envelope, in relation to the overall airtightness of the building envelope. n2 stands 2 1/h at 50 Pa pressure difference, etc. The case CE1-600-open refers to the calculation exercise CE 1, with a lightweight and vapour-open construction. Right: Annual energy consumption for heating and cooling in kWh, for the cases from the figure to the left.

The maximum indoor relative humidity in CE 1-600-Open was 66 %, as calculated by HAM-Tools. When the dynamical insulation is used, the maximum relative humidity is around 70 % as it is shown in Figure 6. The highest value is reached for the extremely airtight house, while it is just the same as in the reference case for other airtightness classes. Note, however, that the internal wooden cladding provides very efficient

moisture buffering here. If a more vapour tight cladding is used, indoor relative humidity may be much higher in the house with the dynamical insulation (more details can be found in Sasic, 2007 a).

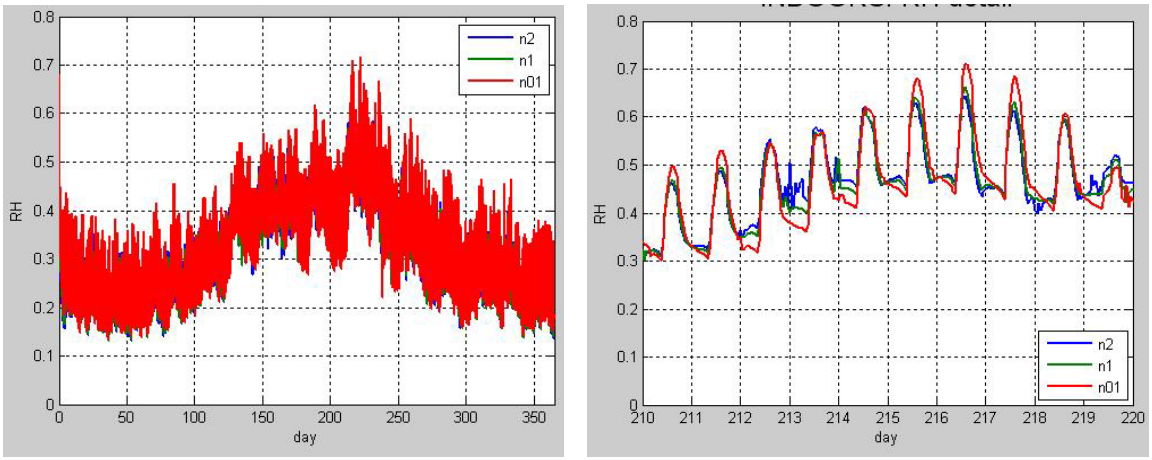

FIG. 6. Left: relative humidity in the indoor air, over a year. Right: the indoor air relative humidity reaches maximum in the middle of August (detail from the figure to the left).

5. Outlook

Annex 41 gathered around 15 building simulation tools that were capable for the calculation of combined heat, air and moisture transfer in whole buildings. The paper presents one of them, the building simulation program HAM-Tools, which participated in the most of the benchmark cases that were presented within Subtask 1 and 2.

The main quality of HAM-Tools is that it has been developed from a beginning as a whole building heat, air and moisture simulation tool. The programming environment of the Matlab/Simulink and the modelling approach used – the object oriented development of the calculation modules, enable a variety of the modelling possibilities in HAM-Tools. Some of them are presented in this work.

Though successfully validated and used in the exercises and topics that were enclosed within Subtask 1 and 2, HAM-Tools provides rather limited information on the hygro-thermal states in buildings – one dimensional distribution of temperature and moisture in the building envelope parts and "one-node" hygro-thermal states for the air zones. Therefore, the future development of this programme will be directed towards the refinement of the special granularity in air zones and building envelopes.

Nomenclature

A	Area, m^2	h_c	Convective surface heat transfer coefficient, W/m^2K
C	Flow characteristic, $m^3/s/Pa^n$	h_e	Heat of evaporation, J/kg
F	View factor	h_r	Radiative surface heat transfer coefficient, $W/m^2/K$
I_{sol}	Intensity of solar radiation, W/m^2	m_a	Density of mass flow of air, $kg/m^2/s$
M	Mass flow to a zone, kg/s	n	Flow exponent in equation 12
P_a	Air pressure, Pa	p	Partial pressure of vapour in air, Pa
Q	Heat flow to a zone, W	q	Density of heat flow, W/m^2
T	Temperature, ^{o} C	s	Suction pressure, Pa
V	Volume, m^3	s_d	Vapour resistance of a coating, m
$\dot{V}$	Volumetric flow rate, m^3/s	t	Time, s

c	Specific heat capacity, J/kg/K	v	Humidity by volume, kg/m^3
g	Density of mass flow, kg/m^2/s	w	Moisture content in material, kg/m^3
g_{rain}	Intensity of rain, kg/ m^2/s	x	Space coordinate, m

Greek letters

α_{sol}	Absorptivity for solar radiation
β_p	Vapour surface transfer coefficient, m/s
δ_p	Vapour permeability, kg/smPa
ε	Emissivity
λ	Thermal conductivity, W/mK
$\lambda_{m,l}$	Liquid moisture conductivity, s
σ	Stefan-Boltzmann constant W/m^{2}K^4
θ	Angle, deg
Φ_r	Radiative source of heat in a zone, W

Subscripts

a	Air
inlet	At inlet
l	Liquid
rad	Radiative
surface	At surface
v	Vapour
i,j,k,p,q,r	indices
ext	Exterior, outdoor
in	Interior, indoor

References

Coyne, R.D., Rosenman, M.A., Radford A.D., Balachandran, M., Gero, J.S. 1989. Knowledge-based design systems. University of Sidney. Addison-Wesley Publishing Company.

de Wit, M. 2000. A simulation model for the thermal and hygric performance of a building. Technical University Eindhoven, the Netherlands.

ECBCS. 2008. Annex 41 Whole Building Heat, Air and Moisture Response (MOIST-ENG) www.ecbcs.org/annexes/annex41.htm

Essah, A.E., Sanders, C., Baker, P., Galbraith G., Sasic Kalagasidis. A. 2008. Simulating the Energy Benefits and Reduction in Condensation Formation that is obtained from Houses with Cold Pitched Roofs. In Proceedings of the 8th Nordic Building Physics Symposium, Copenhagen, Denmark.

Hagentoft, C-E, 2001. Introduction to Building Physics. Studentlitteratur. Lund, Sweden.

Hagentoft, C-E. 2002. HAMSTAD WP2 Modelling, Version 4. Report R-02:9. Department of Building Physics, Chalmers University of Technology, Gothenburg, Sweden. Also available on www.buildphys.chalmers.se

Hagentoft, C-E., Sasic Kalagasidis, A. 2007. Controlled ventilation of cold attics. Moisture safety aspects. IEA Annex 41 meeting in Florianopolis, Brazil, April 2007.

Holms, A. Annex 41, Subtask 4. Moisture-engineering applications. Final report. To be published.

IBPT. International Building Physics Toolbox in Simulink. www.ibpt.org

Judkoff, R, Neymark, J. 1995. Building Energy Simulation Test and Diagnostic Method – BESTEST. National Renewable Energy Laboratory. Golden, Colorado.

Karlsson, H., Hagentoft, C-E. 2005. Modelling of long-wave radiation exchange in enclosure with building integrated heating. Proceedings of the 7th symposium on Building Physics in the Nordic Countries, Reykjavik, Island.

Kumaran, K., Sanders, C. 2008. Annex 41, Subtask 3. Boundary conditions and whole building HAM analyses. Final report. To be published.

Lengsfeld, K., Krus, M., Holm, A. 2005. Investigations of gypsum boards with regard to the moisture-buffering-effects. Annex 41 publication FhG May 2005 Paper A41-T2-D-05-4

Matlab / Simulink. www.mathwork.com.

Perez, R. et al., 1986. An anisotropic hourly diffuse radiation model for sloping surfaces: description, performance, validation, site dependency evaluation. Solar Energy 36, 481–575.

Ramos, N., de Freitas, V. 2006. Testing and modelling coated gypsum products' hygric behaviour under transient conditions. IEA Annex 41 meeting in Lyon, France, October 2006.

Rode, C., Gudum, C., Weitzmann, P., Peuhkuri, R., Nielsen, TR, Sasic Kalagasidis, A, Hagentoft CE. 2002. International Building Physics Toolbox, General report. R-024. Division of Building Technology, Chalmers University of Technology, Sweden. Available on www.ibpt.org.

Roels, S. 2008. Annex 41, Subtask 2. Experimental analyses of moisture buffering. Final report To be published.

Sasic Kalagasidis A., Mattsson, B. 2005. Modelling of Moisture Conditions in a Cold Attic Space. 26th AIVC conference, Brussels, Belgium.

Sasic Kalagasidis, A. 2004 a. HAM-Tools, An Integrated Simulation Tool for Heat, Air and Moisture Transfer Analyses in Building Physics. Doctoral thesis. Department of Building Technology, Building Physics division, Chalmers University of Technology, Gothenburg, Sweden.

Sasic Kalagasidis, A. 2004 b. The whole model validation for HAM-Tools. Case study: hygro-thermal conditions in the cold attic under different ventilation regimes and different insulating materials. Report R:03-6. Department of Building Technology, Chalmers University of Technology, Gothenburg, Sweden. Also available for free downloading on www.ibpt.org.

Sasic Kalagasidis, A. 2004 c. Common exercise 1. Modelling details and results. Annex 41 publication CTH Oct 2004 Paper A41-T1-S-04-3.

Sasic Kalagasidis, A. 2007 a. Hygrothermal response of a house with dynamical insulation in the roof. Case study: Test house from CE 1, Subtask 1, IEA Annex 41. IEA Annex 41 meeting in Florianopolis, Brazil, April 2007.

Sasic Kalagasidis, A. 2007 b. Calculation of cooling energy demand for a space. Modelling and validation. Internal report. Division of Building Technology, Chalmers University of Technology, Sweden.

Weitzmann, P., Sasic Kalagasidis, A., Nielsen, T.R., Peuhkuri, R., Hagentoft, C-E. 2003. Presentation of the International Building Physics Toolbox for Simulink. Proceedings of the 8th International Building Performance Simulation (IBPSA) Conference. Eindhoven, the Netherlands. Available on www.ibpsa.org.

Woloszyn, M., Rode, C. 2008. Annex 41, Subtask 1: Modelling Principles and Common Exercises. Final report. To be published.

Woloszyn, M., Rode, C., Sasic Kalagasidis, A., Janssens, A., De Paepe, M. 2008. From EMPD to CFD – overview of different approaches for Heat Air and Moisture modelling in IEA Annex 41. Submitted to ASHRAE Transactions (American Society of Heating, Refrigerating and Air-conditioning Engineers).

Common Exercises in Whole Building HAM Modelling

Carsten Rode, Assoc. Prof.
Technical University of Denmark;
car@byg.dtu.dk; www.byg.dtu.dk

Monika Woloszyn, Assoc. Prof.
Université de Lyon, Lyon, France ; CETHIL;
monika.woloszyn@insa-lyon.fr; www.insa-lyon.fr

KEYWORDS: Heat, Air and Moisture; Modelling; Common Exercise; Benchmarking; Model development.

SUMMARY:
Subtask 1 of the IEA Annex 41 project had the purpose to advance the development in modelling the integral heat, air and moisture transfer processes that take place in "whole buildings". Such modelling comprises all relevant elements of buildings: The indoor air, the building envelope, the inside constructions, furnishing, systems and users. The building elements interact with each other and with the outside climate. The Annex 41 project and its Subtask 1 has not aimed to produce one state-of–the-art hygrothermal simulation model for whole buildings but rather to stimulate the participants' own development of such models, or advanced use of related existing models.

Subtask 1 dealt with modelling principles and the arrangement and execution of so-called common exercises with the purpose to gauge how well we can succeed in the modelling. The paper gives an overview of the Common Exercises which have been carried out in the Subtask. Based on this activity, some general experiences are reported about how well we are able today to carry out such advanced modelling, and some recommendations for future developments are indicated.

1. Introduction

Indoor air humidity is an important factor influencing air quality, energy consumption of buildings and the durability of building materials. Indoor air moisture depends on several factors, such as moisture sources (human presence and activity, equipment), airflow, sorption from/to solid materials and possible condensation. As all these phenomena are strongly interdependent, numerical predictions of indoor air humidity need to be integrated into combined heat-airflow simulation tools. Subtask 1 of IEA Annex 41 has set out to advance the development in modelling the integral heat, air and moisture transfer processes that take place in "whole buildings".

The past few decades have seen the development and professional use of tools which, for some of the processes or some of the building elements, describe their building physical conditions.

For instance, fairly comprehensive tools for transient building energy simulation have been well established for more than a decade – see for instance http://www.eere.doe.gov/buildings/tools_directory. Such tools comprise the whole building with a granularity going from the suite of rooms that make up the building down to the individual building materials and individual parts and controls of the heating, ventilation and air-conditioning system. However, the building energy simulation tools are relatively poor tools to describe the moisture transfer processes in buildings.

Air flow simulation tools at building level, e.g. COMIS, CONTAM, or at room level, e.g. CFD codes like Fluent, STAR-CD, make good descriptions of air exchange between the zones of a building and the outer environment. Some of them deal with airborne moisture transport, and even take into account moisture impact on the airflow. They also represent the heat transfer in the air and in the envelope. However most of them do not take into account the moisture flow between the air and porous surfaces.

Detailed, transient tools for combined heat, air and moisture transfer (HAM) within individual building components were developed in conjunction with the IEA Annex 24 project, which ran from 1991 to 1995 [Hens 2002]. The results of calculations with the building envelope HAM-tools may however be very dependent on the assumptions made about for instance the climatic boundary conditions. Many HAM-tools for building envelopes have fairly good procedures to represent the outdoor environmental exposures, e.g. from weather data files, but

the indoor environment would often have to be assumed and specified by the user. However, it should also be realized that the collection of building elements themselves form one of the most important factors to determine the indoor climate, and thus there is a mutual link between the envelope and room conditions.

For building envelopes, detailed tools exist for the multidimensional flow of heat, as for instance around thermal bridges. In some cases, models also exist for predicting multidimensional air or moisture flows in envelope constructions.

Thus, there has been a motivation to combine the capabilities of earlier tools in order to make it possible to describe all relevant hygrothermal processes in a composite building, i.e. to bring a holistic perspective to building physics modelling. This has been the outset ambition for Subtask 1 of IEA Annex 41.

2. Common Exercises

The purpose of the common exercises being part of Subtask 1 of the Annex has been to test the current possibilities to use modeling as a means to predict the integrated hygrothermal behavior of buildings and to stimulate new development in this area. This could be done either by clever use of already existing models, or by new modeling, where models were developed either from scratch or as extensions to already existing models which have some of the desired performances.

The following Common Exercises (CE) have been carried out as part of Subtask 1 of Annex 41:

- Common Exercise 0. Validation of thermal aspects of the employed models.
- Common Exercise 1. Expanding on CE0 ase by considering moisture interactions..
- Common Exercise 2. Experimental climate chamber tests in the laboratory.
- Common Exercise 3. Double outdoor climatic chamber test.
- Common Exercise 4. Extension of CE3 with moisture management to reducing energy consumption.
- Common Exercise 5. Real life row house case.
- Common Exercise 6. Two-story test-hut data determeined in Environmental Chamber

2.1 BESTEST Case as Common Exercises 0 and 1

Both Common Exercise 0 and Common Exercise 1 have studied the IEA BESTEST building of IEA SHC Task 12 & ECBCS Annex 21 (Judkoff and Neymark, 1995). The building is shown in FIG 1. The building is superficial, so no measurement data exist.

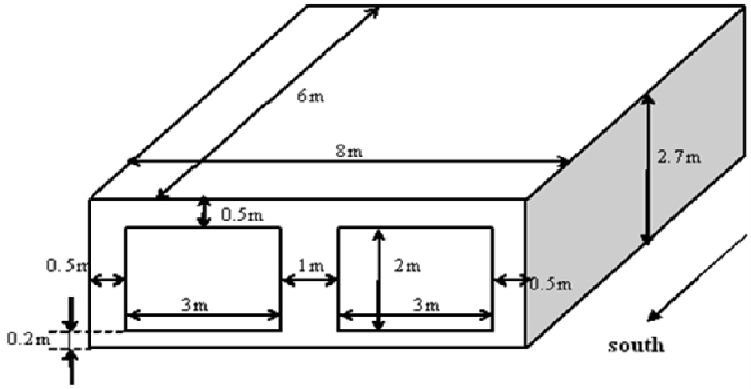

FIG. 1 BESTEST base case building.

The BESTEST case serves to provide comparison between different modeling results. For the thermal analyses of CE0 it would of course be possible to compare against the previous endeavors of IEA BESTEST, but otherwise, and due to the good participation in the exercises, it has been the intention to make comparisons between the different participants in this exercise.

2.1.1 CE 0 Thermal building simulation.

For the purpose of Annex 41, four cases were chosen from the original BESTEST procedure, appropriate for whole building approach (see Table 1). The four cases are indicated by their BESTEST code “600” for a

building made of lightweight construction, “900” for a heavyweight building, and the code “FF” indicates if the building was simulated under free floating thermal conditions without heating or cooling systems. These four cases were chosen because they represent well the whole building approach, according to the scope of Annex 41 without focusing too much on some very specific issues such as solar shading or transfers to the ground.

Table 1 Four cases tested as Common Exercise 0.

Case	Building structure	Heating and cooling
600 FF	plasterboard, insulation, wood	None
600	plasterboard, insulation, wood	
900 FF	concrete, insulation, wood	None
900	concrete, insulation, wood	20°C < Tint < 27°C

13 sets of results were collected coming from 10 institutions from 9 countries using 11 different programs (see Table 2). The programs participating in CE0 were both public domain and commercial software, and their common feature is continuous development of physical models. For numerical resolution, different solution methods were used, such as explicit and implicit finite difference algorithms, or response factor methods. Both fixed and auto-adaptive time steps were equally represented.

Table 2 Overview of the participating institutions and the used simulation tools in CE0 and CE1

Institution	**Country**	**CE0 May 2004**	**CE 1 Oct 2004**	**CE 1A Jan 2005**	**CE 1B May 2005**
CETHIL	France	Clim2000 TRNSYS	Clim2000	-	-
CTH	Sweden	HAM-Tools	HAM-Tools	HAM-Tools	HAM-Tools
DTU	Denmark	BSim	BSim	BSim	BSim
FhG	Germany	Wufi+	Wufi+	Wufi+	Wufi+
KIU	Japan	-	Xam	Xam	Xam
KUL	Belgium	TRNSYS ESP-r	-	-	-
KYU	Japan	-	Original Code	Original Code	Original Code
ORNL	USA	EnergyPlus	EnergyPlus	-	-
PUCPR	Brazil	-	-	PowerDomus 1.0	PowerDomus 1.0
SAS	Slovakia	-	Esp-r+Wufi+NPI	NPI	Esp-r + NPI
TTU	Estonia	IDA ICE	IDA ICE	IDA ICE	IDA ICE
TUD	Germany	-	TRNSYS ITT	TRNSYS ITT DELPHIN	TRNSYS ITT DELPHIN
TUE	Netherlands	HAMLab	HAMLab	HAMBase	HAMLab
TUW	Austria	ESP-r	HAM-VIE	HAM-VIE	HAM-VIE
UCL	UK	EnergyPlus	EnergyPlus	EnergyPlus Canute_beta	EnergyPlus
UG	Belgium	-	(analytical solution)	TRNSYS	1DHAV+ TRNSYS 16
ULR	France	-	-	TRNSYS SPARK	-

Some differences in the results could be expected because of the differences in the reconstruction of outdoor climate from meteorological data. Some programs use linear interpolation while others assume that the climate remains constant over the sampling interval.

All models used include moisture in the balance of the air zone, but at the time of executing CE0 only a few programs represent moisture transfer through the envelope.

The results gathered comprised indoor air temperatures, heating and cooling loads (for cases 900 and 600) as well as solar radiation description (incident radiation at all the walls and gains through the windows). Both detailed hourly values were collected as well as global results (annual loads, mean temperature, etc.)

Indoor temperature variation during one day is shown in FIG 2. The difference between heavy- and lightweight structures can be clearly seen. Similarly, a spread of several degrees between different sets of results can be seen on the graph. The differences are mainly due to different modeling capabilities of the codes, and especially to differences in calculating solar gains through windows. However it should be noted that the results concerning heating and cooling loads mostly corresponded well with the original range of results from BESTEST.

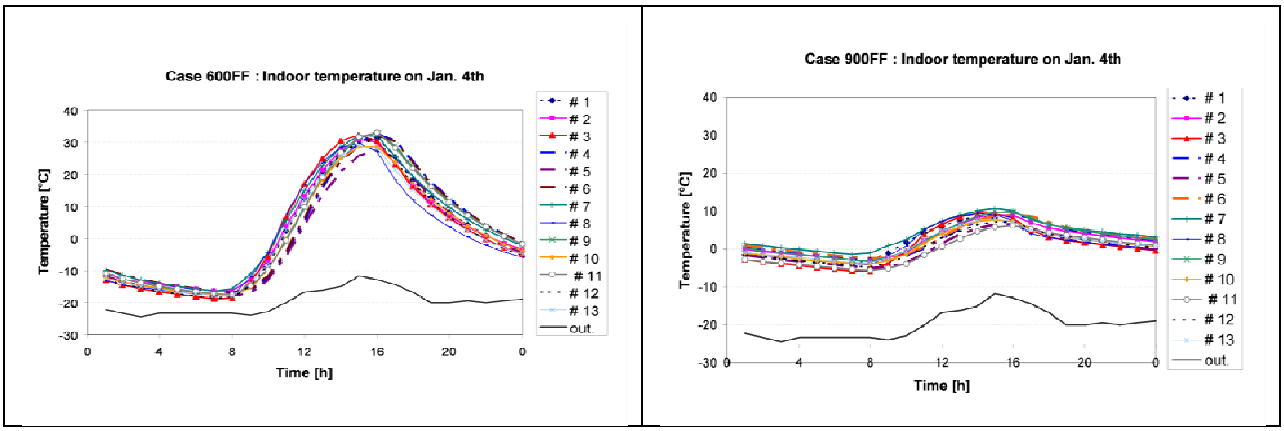

FIG. 2 Common Exercise 0: Indoor and outdoor temperature (°C) on Jan.4th, for both lightweight structure (left – 600FF) and heavyweight structure (right – 900FF for all 13 sets of results.

2.1.2 CE 1 Hygrothermal building simulation.

Common Exercise 1 extended on Common Exercise 0 by adding some analysis of the indoor and building envelope moisture conditions for the BESTEST building used in CE0. The original plan for CE1 was to add the moisture problem parts directly to the problem from CE0.

Table 3 Overview of variations of Common Exercise 1.

CE1 Numerical cases in principle like in CE0. Natural climate.	**CE1A** Monolithic walls w. simple material properties. Isothermal conditions. No internal or solar gains.	**CE1B** Monolithic walls with realistic properties. Natural climate.
- 600 0A Analytical, Vapor tight - 600 0B Analytical, Vapor open - 600 Open Numerical, vapor open - 600 Paint & VR Numerical, painted - 900 Open Numerical, vapor open	- 0A Tight Analytical, vapor tight - 0B Open Analytical, vapor open	- T_{indoor} 20°C no external radiation - T_{indoor} 20 - 27°C no external radiation - T_{indoor} 20 - 27°C with solar and long-wave radiation

The first results of the Common Exercise 1 showed, however, that the original case had too many uncertainties even within the thermal calculation, e.g. the presentation of the material data, window models etc. Therefore, a step back was taken with Common Exercise 1A (an analytical case) and Common Exercise 1B (a more "realistic", numerical case). The constructions were monolithic, the material data were given as constant values (CE1A) or as functions (CE1B), and the solar gain through windows was modeled simplified. An overview of these variants is given in Table 3.

For all cases there was an internal moisture gain of 500 g/h from 9:00 - 17:00 every day. The air change rate was always 0.5 ach. The heating and cooling controls for all the non-isothermal cases kept the indoor temperature between 20 and 27ºC. The system was a 100 convective air system and the thermostat was on air temperature.

Table 2 shows the used simulation codes. Some of the institutions have used the same code for all the exercises – with or without modifications from case to case – while others have used 2 different codes or have not taken part in particular exercises.

Results from the original CE1. "CE1" was the original case of an exercise for simulations which include moisture exchange. It was posed with a relatively high degree of freedom for modelling a realistic building, based on the descriptions for thermal BESTEST cases. The results from different participants showed a very large spread. Big differences in results were coming from different assumptions that have been made on some of the input conditions both for energy and moisture modelling. Facing the difficulty to interpret such data, it was decided to review the exercise giving much more details on the input data and on the way of modelling the problem.

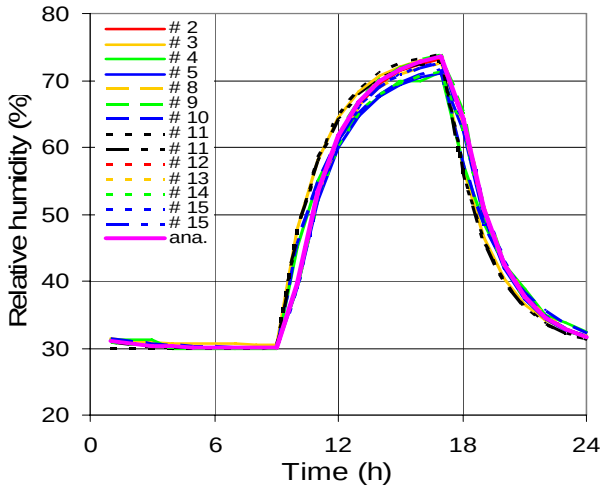

FIG. 3 CE 1A, Case 0A. Analytical test. Isothermal exposure. Construction surfaces are tight. The results are given as the numerical results compared with the analytical consensus solution of the indoor RH. The main deviation is due to the way the hourly values are given: either actual or mean hourly values.

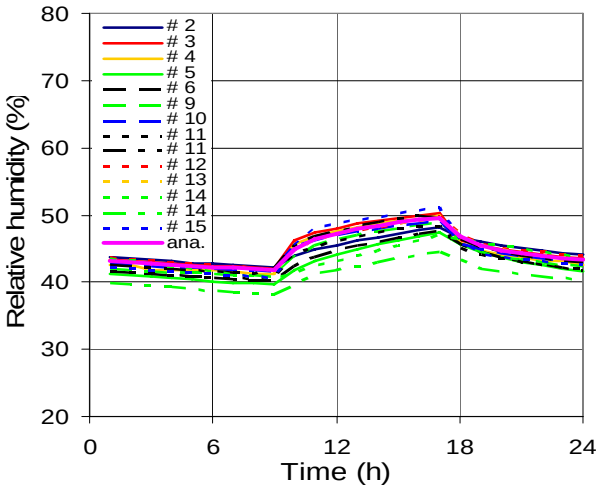

FIG. 4 CE 1A, Case 0B. Analytical test. Isothermal exposure. Construction surfaces are open. The results are here given as the numerical results compared with the analytical consensus solution of the indoor RH.

Results from CE 1A Analytical cases. This exercise applied the simplest conditions in terms of material properties and boundary conditions and used properties which facilitate the possibility to solve the case analytically. Compared to the original CE1, the following changes were made: Constructions were supposed to be made of monolithic aerated concrete with constant/linear properties. Tight membranes on the outside, and in case 0A also on the inside, prevented loss of vapour from the building by transport all the way through the walls. The exposure was completely isothermal, i.e. the same temperature outside as inside the building. The building had no windows. The initial conditions were given, an dthe calculagtoins were run until quasi-steady conditions..

It was possible also to solve the cases by using numerical tools. The numerical results are shown in FIG 3 and FIG 4 for tight and open surfaces respectively, together with an analytical consensus solution (Bednar and Hagentoft, 2005). For this simple case all models used showed a very good agreement with the consensus solution.

Results from CE1B "Realistic" cases. This exercise was the second part of the revised CE 1: The constructions were still more simple than in the original CE1 and a more humid location, which is also close to sea level, was chosen: Copenhagen. All the envelope constructions were made of monolithic aerated concrete and faced outdoor air. There were no coatings or membranes on any sides, not even for the roof. Variations were run either for isothermal or non-isothermal conditions, and the non-isothermal conditions were run either with or without solar gains in the building. The results were again given as the indoor relative humidity. Given the important spread between different numerical solutions, judging the results in terms of "correct" or "not correct" was very difficult. It was then preferred to go to Common Exercises 2 and 3 where measured data give target solutions and help to validate the modelling approach.

2.2 Common Exercise 2 - Small climate chamber test

In order to design residential spaces for indoor humidity control, it is important to investigate the influence of ventilation rate and hygrothermal materials. The objective of this common exercise was to simulate the small chamber (called "THU test room") which is located in a climate chamber. Two kinds of experiments were carried out. The first examined the influence of ventilation rate, while the second examined the influence of both the quantity and location of the hygrothermal materials within the chamber. The moisture buffering material investigated was gypsum board (the same gypsum board used in the round robin test of Anbex 4's Subtask 2).

Experimental settings. Each experiment consisted of a preconditioning period followed by 6 hours of humidification and 12 hours without humidification, during which variations of indoor temperature and humidity within the small chamber were evaluated.

A schematic view of the test chamber is shown in FIG. 5. The test chamber was located in the climate room at the Akita Prefectural University. In the climate room, it is possible to control indoor temperature in a range from 10 °C to 40 °C. and humidity from 30 %RH to 90%RH. This test chamber is approximately half the size of a typical residential room. The internal volume of the test chamber is 4.60 m^3 and the area of interior surfaces is 16.62 m^2. The walls, ceiling and floor of the chamber consist of an internal surface of 12.5 mm of gypsum board behind which is 100 mm of polystyrene. In order to keep vapour- and airtight conditions in the chamber, an aluminium sheet is installed between the polystyrene and the gypsum board. The inlet and outlet for mechanical ventilation are located at the bottom and top of two opposite walls respectively. A small ventilation duct is connected to the outlet of the chamber to measure the ventilation rate accurately.

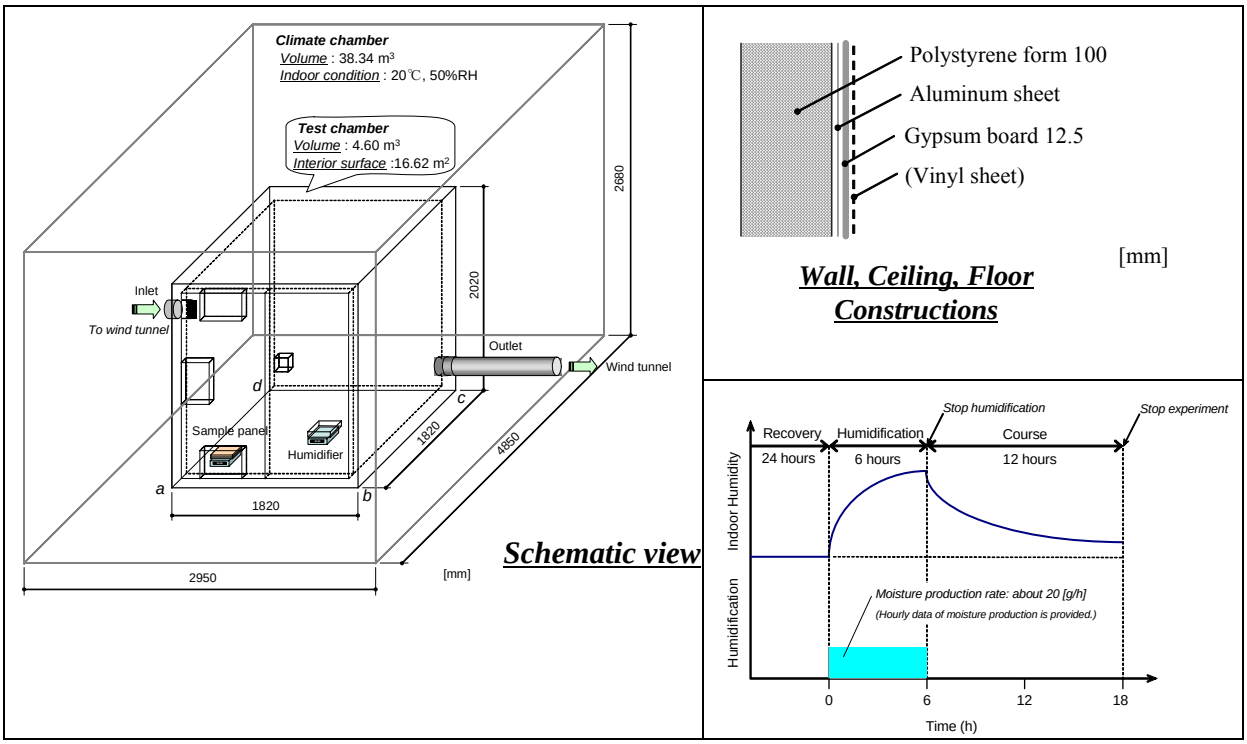

FIG. 5 Schematic view of the test chamber, the construction, and the schedule

Constructions Wall, ceiling and floor constructions are shown in FIG. 5. The gypsum board on the walls, ceiling and floor is covered with the vinyl sheet according to the experimental cases in order to prevent moisture absorbing and desorbing from the surface. Gypsum board is not installed on the door of the chamber in any of the experimental cases.

Internal Gains and schedules Humidification took place by evaporating moisture from two water reservoirs that were heated by an electric heating element. The water reservoir tray was weighed by an electric balance to measure the quantity of humidification water. The target moisture production rate was about 20 g/h. The experimental schedule is shown in FIG. 5.

Comparison between simulation and experimental results. In all the cases there was a rise of approximately 1.5-2°C in the air temperature, due to vapour production. It was correctly represented by all the models except one, which assumed almost isothermal conditions. As the power used to heat the water in the reservoirs was not known, the participant did not want to "guess" the size of heat source.

Experimental data were higher than simulated values in all the cases. Moreover:

- Experimental values agreed well with simulated values in cases which focused on: *High ventilation*, *One hygroscopic surface on the wall*, and *No hygroscopic surfaces*.
- The simulation tools underestimated the peak absolute humidity by approximately 1g/kg in cases with: *five hygroscopic surfaces*, *three hygroscopic surfaces on the wall*, and 2-5 *one hygroscopic surface on the ceiling*.
- The simulation tools underestimated the peak absolute humidity by approximately 2g/kg in cases with *five hygroscopic surfaces and no ventilation*, and *one hygroscopic surface on the floor*.

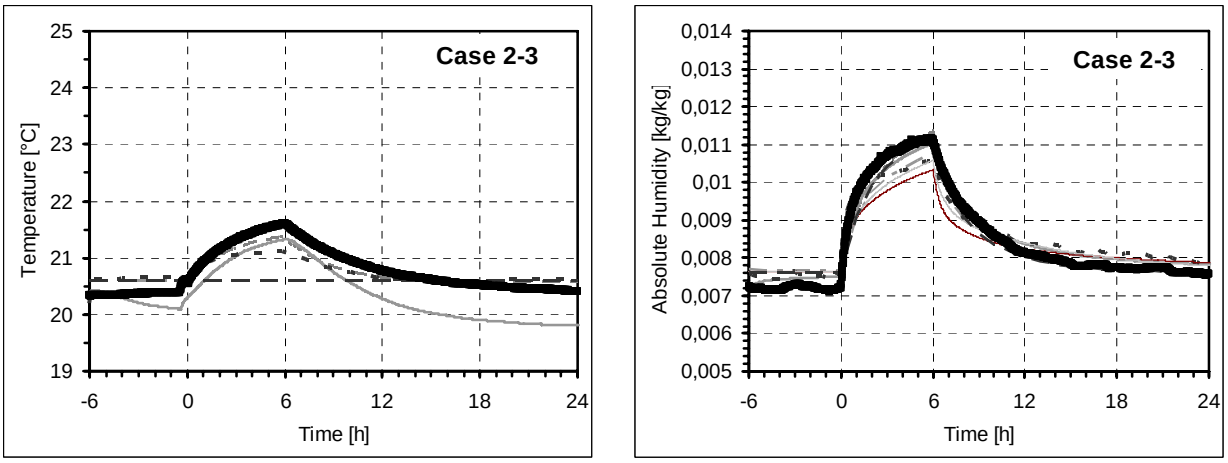

FIG. 6 Comparison between measured values and simulation results (Case 2-3)

The agreement was better when the impact of moisture buffering is lower (high ventilation and no hygroscopic surfaces). The biggest differences occurred in cases with no ventilation and with hygroscopic surface on the floor. It may indicate that besides moisture adsorption on hygroscopic surfaces there was some stratification of the indoor air. Indeed with no ventilation the air was very still in the test chamber, so there was no mixing. Moreover water vapour is lighter than dry air, so it has a tendency to rise, which is a factor to be considered when the hygroscopic material is on the floor.

Conclusion from Common Exercise 2. Simulation results of humidity in Case 1-3, Case 2-3 and Case 2-6 indicated comparatively good agreement with the experimental values. When comparing the results of the simulation programs, a spread in the range of predicted humidity was noted. The reasons for the differences between the experimental and simulation results were not clear but could be due to measurement error and the influence of the distribution of indoor temperature

2.3 Common Exercise 3. Double outdoor climatic chamber test

The intention of this common exercise was to simulate two real test rooms which are located at the outdoor testing site of the Fraunhofer Institute of building physics in Holzkirchen. Tests were carried out during winter and spring period with the aim to compare the measurements with the models developed within this Annex 41. As moisture buffering material served gypsum boards (the same gypsum board was used as was tested in a round robin test from Subtask 2).

The results of the measurements showed the influence of different materials in comparison to the relative humidity in the rooms. In the reference room was used a standard type of gypsum board with a latex paint (s_d = 0.15 m). The walls and the ceiling of the test room were fully coated with aluminium foil. For the experiments the test materials can be attached to the walls and ceiling of the room.

The tests in the rooms were made for the following four steps:

1. Reference room - Test room only with aluminium foil. During the first test stage no material was attached to the walls in the test room and measurements were run for a period of 17 days. This test showed the difference between the reference room and the test room with aluminium foil where no sorption effects were possible.

2. Reference room – Test room with gypsum boards on the walls. In the second step gypsum boards were attached on the surface of the walls with aluminium foil in the test room so that it covered the area of the walls, this experiment was run for a period of 35 days. For the test were used gypsum boards with or without paint.

3. Reference room - Test room with gypsum boards on the walls and the ceiling. For this experiment additional gypsum boards were installed in the room with aluminium foil, so also the ceiling was covered (in total now approximately 65 m²). The test was carried out for a period of 26 days. For this test were again used gypsum boards with or without paint.

4. Same as the previous tests but now also with solar gains in the rooms. In Step 4 the influence of solar radiation through the windows are considered and additionally the indoor climate conditions are measured with and without a heating system. The test room was empty and only covered with aluminium foil.

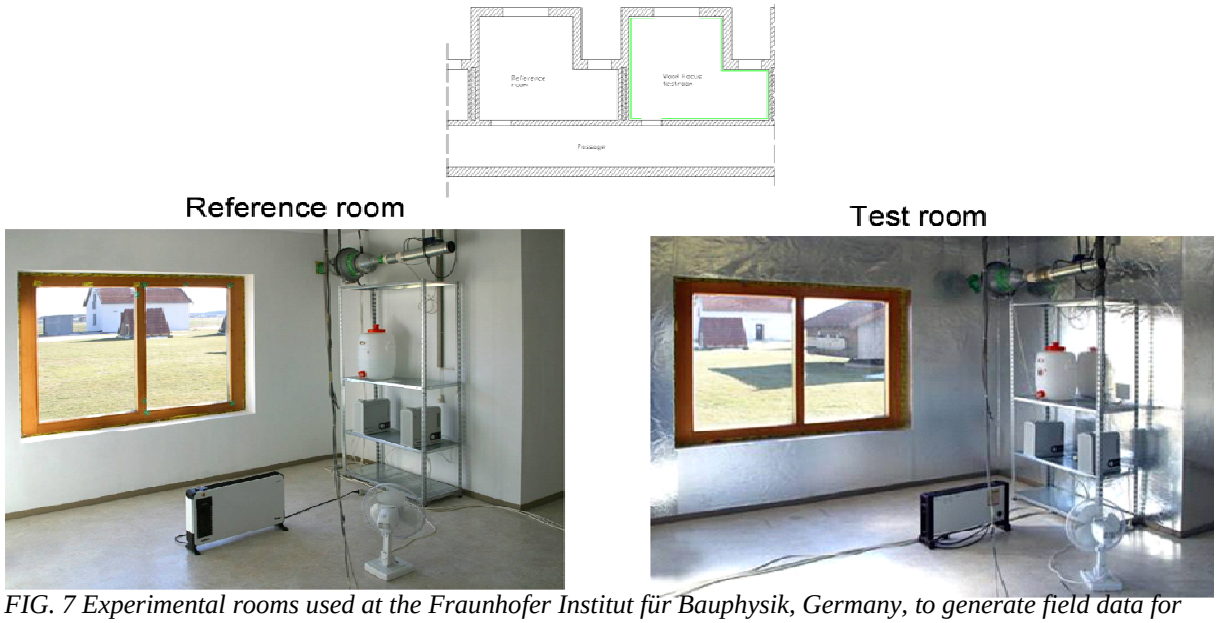

FIG. 7 Experimental rooms used at the Fraunhofer Institut für Bauphysik, Germany, to generate field data for Common Exercise 3. "Reference room" (left): The surfaces of the walls and the ceiling are coated with common gypsum plaster and paint (s_d=0.15m). "Test room" (right): Surfaces of the walls and the ceiling are completely coated with aluminum foil.

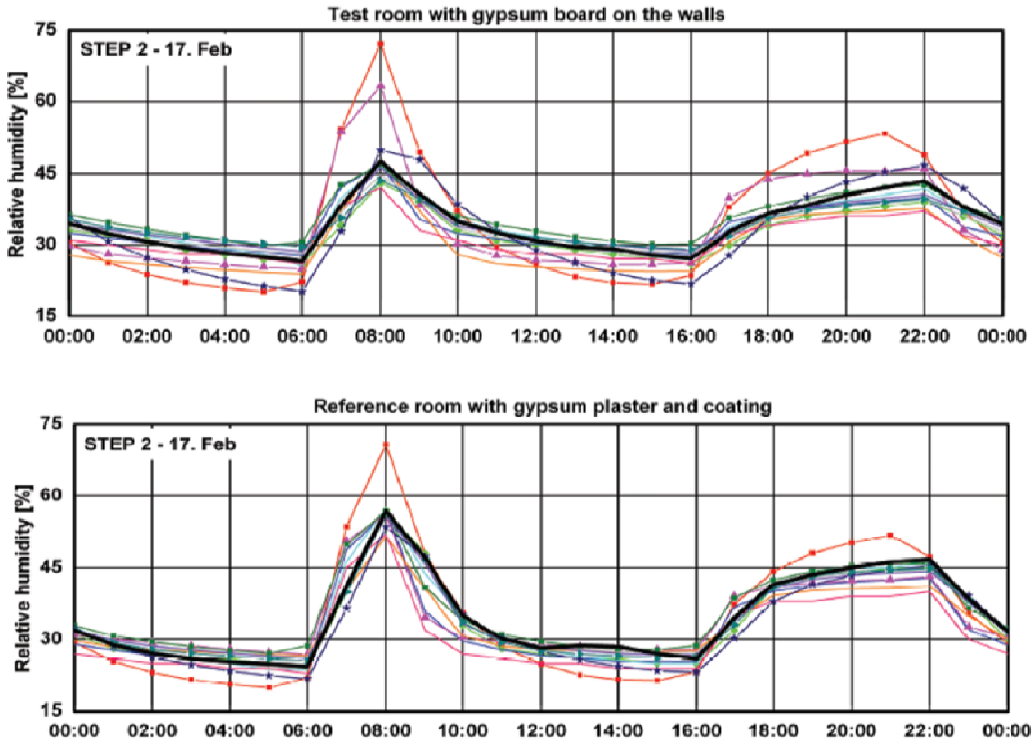

FIG. 8. Results of simulations for Common Exercise 3. Rooms with gypsum boards on the walls which were either untreated (top graph) or painted (bottom). Bold line represents the measured values and the thin lines represent 12 computed solutions.

Output from the investigations . For each calculation hourly averaged air temperatures and relative humidity was reported for the air in each of the rooms. In addition, the required energy to maintain the desired temperature

in the rooms was reported. The results of relative humidity predictions and measured results for a day of Step 2 are shown in *FIG. 8*.

In comparison with CE1 a rather good agreement between different solutions was obtained. It should be noticed that the authors of the "extreme" numerical solutions reported some misunderstanding of the input data. Improving of overall results between CE1 (2004/2005) and CE3 (2006) are an encouraging proof that some progresses in whole building HAM modelling were accomplished within the Annex 41.

2.4 Common Exercise 4. Moisture management for reducing energy consumption

The intention of this common exercise was to show that an appropriate management of the indoor moisture conditions could reduce the building's energy consumption. The objective of the exercise was to use a relative humidity controlled (RHC) ventilation system combined with the effects of moisture buffering materials in order to reduce the energy consumption and improve the indoor climate.

The exercise was based on the two real test rooms which were used in CE3. The RHC ventilation adapts the flow rate to the indoor relative humidity. The target relative humidity values of the indoor air were between 40 and 50%, as proposed by EN 15251:2007 for class A buildings.

The participants were asked to perform 5 simulations changing ventilation system data and moisture buffering capacity of the envelope:

- Run A: the original results from CE3, with constant ventilation
- Run B: using original finishing materials and the Relative Humidity Controlled ventilation system,
- Run C: using original finishing materials and a Relative Humidity Controlled ventilation system with maximum and minimum airflow values modified by the participants
- Run D: using the original RHC ventilation system from run B, but changing the moisture buffering capacity of materials by using different material properties and different surfaces.
- Run E: combining both: the ventilation and the materials in order to reduce the energy consumption and improve indoor RH.

The simulations were run for a period from January to April covering cold and mild periods. 6 solutions were provided by 6 diffreent participants. Even if some differences in results were noticed, an overall good agreement was found for the different simulations. FIG. 9 shows the indoor relative humidity in the cold period for two ventilation systems. It can be noticed that RHC ventilation reduces the spread between the minimum and the maximum values of relative humidity. It was also found that the use of and RHC system could reduce the mean ventilation rate of about 30 to 40 % in the cold period and generate 12 to 17 % of energy savings. It should be stressed that the energy savings are done with keeping the peak RH values at the same level, therefore without raising the risk of condensation. However, during the mild period the savings were much lower (~2%), mainly because of the higher moisture content outside. It was also confirmed by the participants that the use of moisture buffering materials enables a significant reduction of the amplitude of daily moisture variations.

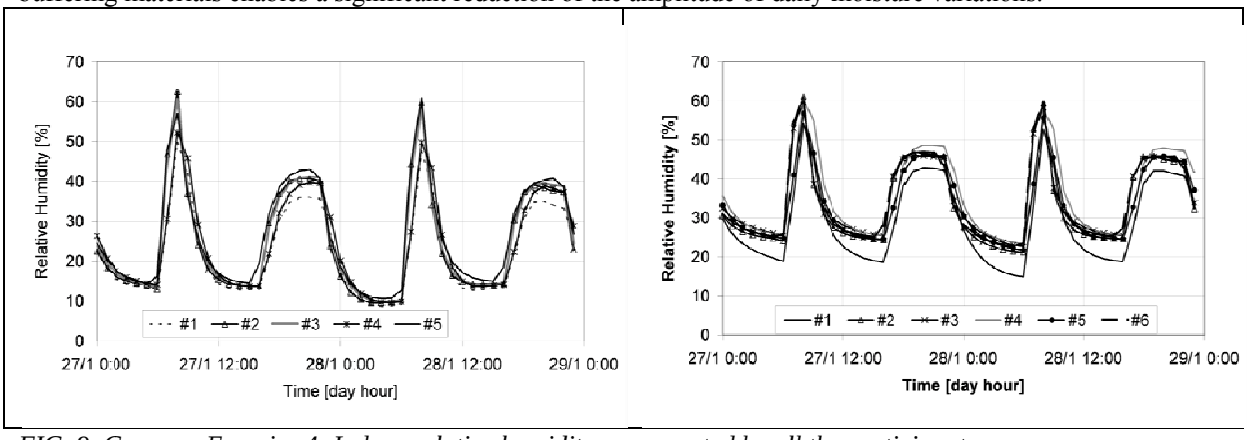

FIG. 9. Common Exercise 4: Indoor relative humidity as computed by all the participants.
(a) constant ventilation rate *(b) relative humidity controlled ventilation*

2.5 Common Exercise 5

With exercise 5, a practice-related case was introduced within the Annex 41 common exercises. First, the case study dwelling is described, then its translation into a common exercise is explained, ending with the reference solution and a comparison with the results introduced by the participants.

FIG. 10 The dwelling considered

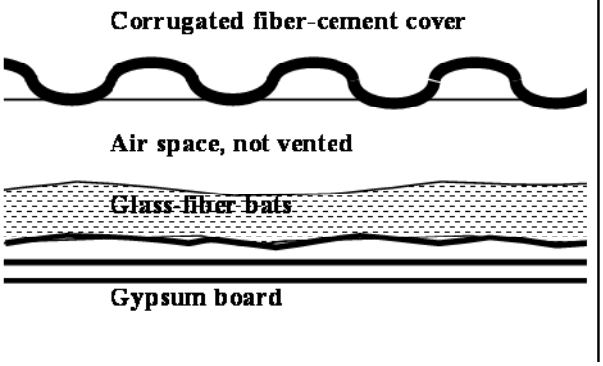

FIG. 11 Roof section

The case concerns a low income estate of 48 two storey houses built in the 1970s (FIG 10). The only difference between the 48 dwellings is the orientation of the main façade: 9 NW, 4 NNW, 16 NE, 5 E, 5 SE and 8 SW. All had a non-insulated floor on grade, non insulated cavity walls, double glazed aluminium windows on the ground floor, single glazed aluminium windows on the first floor and a cathedral ceiling composed of (from inside to outside) (1) gypsum boards mounted with open joints, (2) 6 cm thick glass-fibre bats with a vapour retarder on the underside, (3) an un-vented air space and (4) corrugated fibre cement plates as roof cover (FIG 11). The two floors were linked by an open staircase in the living room. The dwellings were adventitiously ventilated, while purge ventilation was provided by opening windows.

85% of the dwellings showed traces of moisture on the cathedral ceiling, while a large number of inhabitants complained about dripping moisture in the bedrooms after cold nights. A detailed inspection of some roofs revealed poor installation of the glass-fibre bats, abundant traces of condensation at the underside of the corrugated fibre-cement plates, mould on the rafters and traces of condensate at the back of the internal lining.

The suggested solution was: (1) retrofit the roof in accordance to the better solution; (2) upgrade the overall poor insulation quality of the dwellings; (3) equip the dwellings with a purpose designed ventilation system.

The exercise. The objective of the exercise was not comparing software-based solutions, but evaluating if the Annex 41 participants could solve an engineering problem using simplified approaches. For that reason, the exercise was kept as a eady state problem, based on a cold week.

The exercise was split in three successive steps:

- Step 1: ground floor and first floor heated, daily vapour release constant over the week, air leakage through the façade distributed proportional to the surface
- Step 2: ground floor heated, first floor not, vapour release on both floors given on an hourly basis, air buffering only, air leakage through the façade distributed proportional to the window perimeter lengths
- Step 3: as step 2 plus moisture buffering by the fabric included

Conclusions from Common Exercise 5. The exercise proved that solving real life problems, using simplified methods, is not as simple as expected. One has to know a lot about what could happen before the calculations. The simple models used should be physically correct. Nodes for air balance calculations must be chosen carefully. Hand calculations of these balances are hard to perform as iteration is needed. Modelling in a spreadsheet programme anyhow is easily done. The material or system property values used should be realistic. Mass balances for air and vapour must fit. Heat balances should be correctly constructed and solved. And, finally, the results have to be interpreted correctly.

2.6 Common Exercise 6. Two-story test-hut data from Environmental Chamber

The objective of the experimental study was to generate reliable datasets that will serve first to advance the understanding of the whole building response to heat, air, and moisture (HAM), and secondly to validate ongoing and future numerical models. For this objective, tests were carried out in a two-story test-hut that was assembled inside the Environmental Chamber at Concordia University.

In the first stage, the test rooms were isolated and the HAM transfer and moisture buffering parameters were monitored. Each room was tested independently to study the moisture buffering capacity of two finishing materials and furniture, and to study airborne moisture distribution within a room. These tests are referred herein as the "single room" tests. In the second stage, the upper and lower rooms were coupled by a horizontal opening to study the inter-zonal HAM transport through this opening and the resulting airborne moisture distribution in both rooms. These tests are referred herein as the "two-room" tests.

Environmental Chamber and test-hut construction The Environmental Chamber was used to provide the desired outdoor temperature. The temperature condition in this large chamber was controlled by two cooling systems and two electric heaters. A blower (5.7 m3/s) and small portable fans provided the air circulation in the large chamber.

A two-story test-hut was built inside the Environmental Chamber (FIG 11A). The test-hut consisted of two rooms with internal dimensions of 3.62m x 2.44m x 2.43m each (FIG 11b). The test-hut represents typical wood-framed construction of Canadian houses. In each floor, a small foyer was built adjacent to the north wall to reduce disturbance to the test rooms when doors were opened to set new conditions inside the rooms and to house part of the data acquisition system.

The east and west walls (see FIG 11b) were used to study the moisture buffering capacity of two different finishing materials, uncoated gypsum board and pine paneling. The rest of the indoor surfaces were covered with aluminum sheets (0.8 mm thickness) to avoid any additional moisture buffering effect. For the non-hygroscopic cases, the east and west walls were covered with polyethylene sheets (0.15 mm thickness).

Materials used in this study were generic. Hygrothermal properties of similar materials were tested at IRC (NRCC). Also, surface mass transfer coefficients for uncoated gypsum board and pine paneling were measured at the University of Saskatchewan.

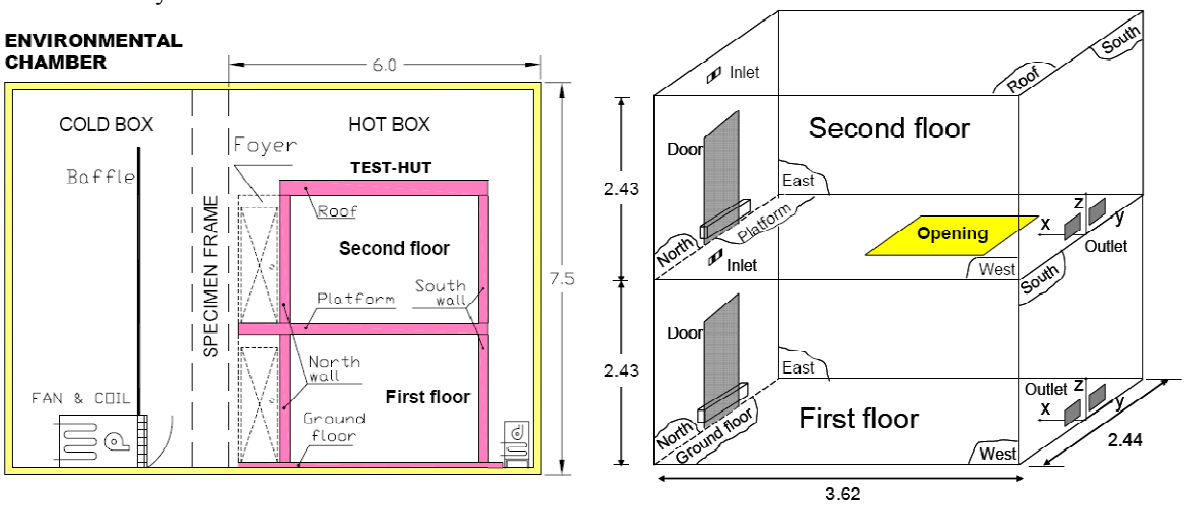

FIG. 12 a) Schematic drawing of the two-story test-hut inside the Environmental Chamber. b) Interior dimensions of the two-story test-hut and name of the test-hut components (dimensions are in meters)

Air leakage of the test-hut was measured at operating conditions. Air leakage varied from 0.014 to 0.044 h^{-1} for single room tests, and from 0.018 to 0.027 h^{-1} for two-room tests.

Conclusions from Common Exercise 6. Full-scale tests in single rooms and two rooms coupled vertically by a horizontal opening were carried out in an environmental chamber. The aim of these tests was to generate complete datasets that allow the study of the moisture buffering capacity of two finishing materials and furniture, airborne moisture distribution within the rooms and inter-zonal HAM transport through horizontal openings. In

total, 20 datasets are provided in electronic format, which may be used to validate ongoing and future Whole Building HAM and CFD models.

A complete report with further details and explanations of the experimental setup, test conditions, details of the constructions, specifications of sensors and instruments, and the contributions from the University of Saskatchewan (Experimental determination of the convective mass surface transfer coefficients for gypsum board and pine paneling) and from IRC (Moisture buffering capacities of five North American building materials) are provided in the electronic appendix.

3. Some conclusions to draw from all common exercises

The Common Exercises have illustrated the complexity of whole building hygrothermal modelling. It was possible to find some consensus among solutions only for an extremely simple isothermal case: a monolithic building without windows and no contact with the ground.

But the Common Exercises have stimulated some developments of different software as well as some original use of already existing programs. Mainly in CE0 some energy models were improved in more moisture oriented programs, and in CE1 moisture modelling was enhanced in more energy oriented tools. The improvement of the models was noticed in CE3, when the obtained agreement was much better that in CE1.

All common exercises showed that there is a need for some consensus data concerning heat and moisture properties of the materials, and more generally about all the input data. Same remark concerns the outputs: as energy and moisture are closely influenced by each other, some spread in relative humidity values can be easily explained by the spread in temperature values. Therefore moisture content should be preferred over relative humidity for comparison purposes.

Also in such an integrated modelling all elements are very important: For example some differences in the indoor relative humidity may be induced by modelling of solar gains or long wave radiations, and not at all by the differences in the moisture model. Moreover some participants stressed the importance of wall discretization. Differences are important for energy vs. moisture modelling; they can lead to numerical divergence.

A crucial question was raised during the discussion: how can we evaluate if the solution is GOOD or BAD? This is especially important when there are no measured data. In such cases, could one say that the consensus solutions are good? The question remains open.

Globally the most encouraging results of all the Common Exercises are:

- Existing models have been “tested” for their suitability for the whole building hygrothermal simulation
- New models have been created, including upgrading and developing existing models to be able to handle also new aspects in “H”, “A” or “M”.
- Several existing computational tools were found to be able to deal with coupled heat, moisture and ventilation problems at the whole building level - they all give similar results.

4. Acknowledgements

The authors would like to thank all the participants in Annex 41 project for their contributions and for financial support from the French Energy Agency ADEME, and from the Danish Technical Research Council, Danish Energy Research Programme, and Martha and Paul Kerrn-Jespersen foundation.

5. References

Hens, H. 2002. Technical Synthesis Report on Heat, Air and Moisture Transfer in Highly Insulated Building Envelopes. UK, Faber Maunsell Ltd.

Bednar, T. & C.-E. Hagentoft. 2005. Analytical solution for moisture buffering effect - Validation exercises for simulation tools. Nordic Building Physics Symposium. Reykjavik. June 13-15, 2005.

Judkoff, R., & J. Neymark. 1995. Building energy simulation test (BESTEST) and diagnostic method. NREL/TP-472-6231. Golden, CO.: National Renewable Energy Laboratory.

Woloszyn, M. & C.Rode, 2007. Annex 41, Subtask 1: Modelling Principles and Common Exercises. Final report. International Energy Agency, Buildings and Community Systems Programme

An overview of LFC-FEUP recent research on hygric buffering

Nuno Ramos, Assist. Professor,
Department of Civil Engineering, Faculty of Engineering – University of Porto;
nuno.ramos@fe.up.pt

Vasco Peixoto de Freitas, Full Professor,
Department of Civil Engineering, Faculty of Engineering – University of Porto;
vpfreita@fe.up.pt

KEYWORDS: Moisture Buffering, Hygroscopic Inertia, Experiments, Simulation.

SUMMARY:
This article describes the recent research conducted at LFC-FEUP on the subject of moisture buffering and its contribution to the hygroscopic inertia of a room. An extensive experimental campaign complemented with numerical simulation provided the main results of that research. The characterization of painted renderings properties provided a deeper insight on the buffering potential of common finishing solutions. The experimental assessment of hygroscopic inertia at room level was implemented using a flux chamber designed specifically for this experiment. A daily hygroscopic inertia index, $I_{h,d}$, was defined using MBV as a basis for the assessment of materials contribution to the buffering capacity of a room. The correlation between that index and peak dampening was proved both numerically and experimentally. The benefits of daily hygroscopic inertia were analysed with the help of full hygrothermal simulation of a bedroom.

1. Introduction

The variation of inside Relative Humidity (RH) is influenced by the moisture exchange between air and building elements. The relevance of that exchange is linked to the active moisture buffer capacity present in a room, which can be identified with its hygroscopic inertia. The evaluation of that capacity can be approached in three different levels.

At material level, international standards already support the determination of the basic properties that condition moisture storage performance, such as sorption isotherms and vapour permeability. Recently, a new property defined as MBV, Moisture Buffer Value, was proposed by (Rode et al, 2005), allowing for a direct experimental measure of the moisture accumulation capacity of a material under transient conditions.

At element level, where several materials can be combined by their application in different thicknesses, MBV can also be applied as an experimental measure of each specific element configuration moisture accumulation capacity.

At room level, the authors believe that the daily hygroscopic inertia index, $I_{h,d}$, can be a measure of the active moisture buffer capacity promoted by the room's interior configuration.

This text presents an overview of the research work conducted at these three levels by LFC-FEUP.

2. Material properties

2.1 Materials

The elements selected for the experimental part of the study are presented in Table 1. Both base materials and coatings are representative of the typical finishing solutions used in Portuguese bedrooms.

TABLE. 1: Tested elements.

Sample	Base material	Primer	Finishing coating
GC	Gypsum board	—	—
GC2	Gypsum board	—	Vinyl - 50 μm (2 layers)
GC2A	Gypsum board	25 μm (1 layer)	Vinyl - 50 μm (2 layers)
GC3A	Gypsum board	25 μm (1 layer)	Acryl - 50 μm (2 layers)
GP	Gypsum plaster	—	—
GP2	Gypsum plaster	—	Vinyl - 50 μm (2 layers)
GP2A	Gypsum plaster	25 μm (1 layer)	Vinyl - 50 μm (2 layers)
GP3A	Gypsum plaster	25 μm (1 layer)	Acryl - 50 μm (2 layers)

2.2 Sorption Isotherms

Sorption isotherms were determined for the base materials, on a first stage according to the method described in the instruction document used in Annex41 Subtask 2 inter-laboratory tests (Roels 2004). The first adsorption was obtained by finding the equilibrium moisture content at four different RH points. Then desorption was obtained by obtaining equilibrium moisture content at the lower RH points. A second adsorption curve was produced by taking again a set of specimens, which had made the main desorption curve, stepwise from low to high RH. The results are presented in Figures 1 and 2. Also the actual curves used in numerical simulations are presented.

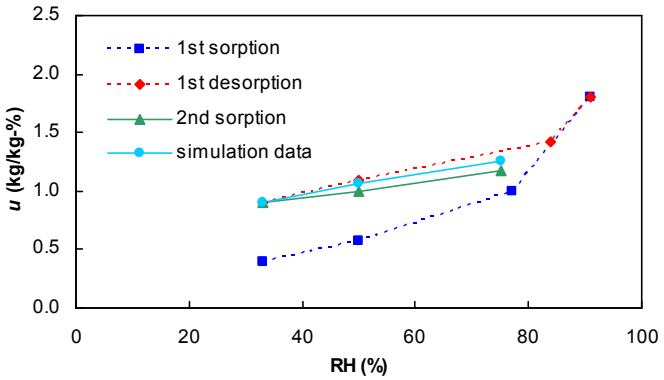

FIG. 1: Gypsum board sorption isotherms.

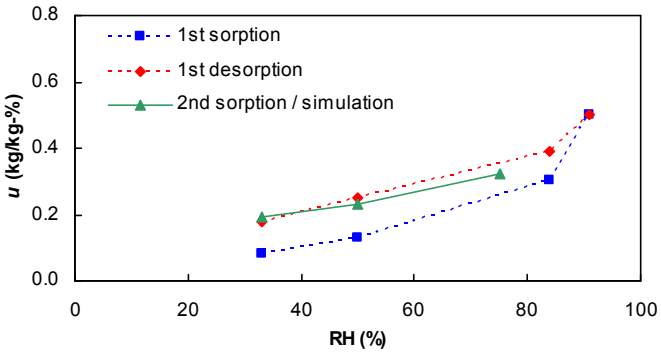

FIG. 2: Gypsum plaster sorption isotherms.

2.3 Vapour permeability

Vapour permeability tests were conducted using the cup method under three different conditions: dry cup (0%-50%), wet cup (50%-93%) and (85%-93%). The tests were done in agreement with the (EN ISO 12572, 2001). The analysis of the cup tests results is usually very direct, and a material's vapour permeability can be determined from Fick's law. But testing coated samples introduces a higher complexity in that analysis. And as the final objective of these tests was the determination of vapour permeability as a function of relative humidity, that complexity increased.

The fitting of a mathematical function to a set of cup test results performed in different RH ranges took as reference the method proposed by (Galbraith, 1998, Galbraith, 1999).

The result of each cup test, for a given element configuration, can be expressed as an equivalent air layer thickness value for that element. But if it consists of different material layers it can be decomposed in a sum of the equivalent air layer thicknesses of each material, as suggested by the scheme in Figure 3.

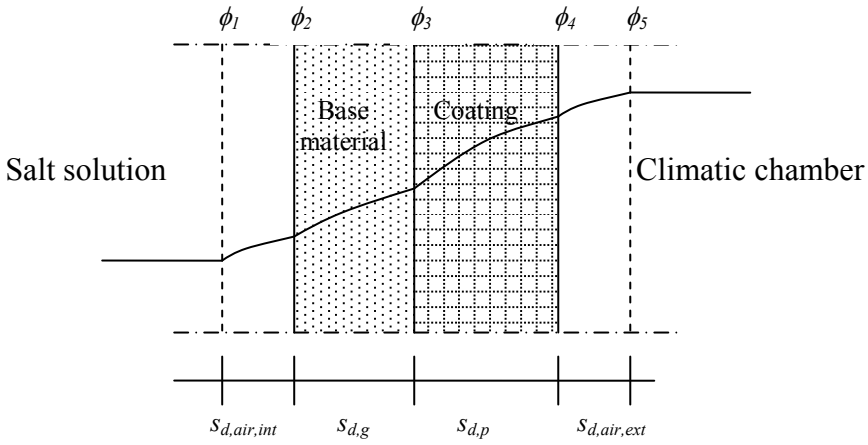

FIG. 3: Relative humidity variation inside a sample during cup tests.

Based on the scheme in Figure 3, the functions for the vapour permeability of the base materials and the applied coatings can be obtained. The results are summarized in Figures 4 and 5.

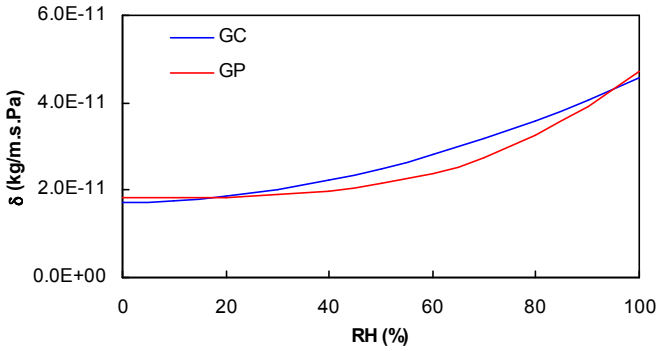

FIG. 4: Base materials vapour permeability.

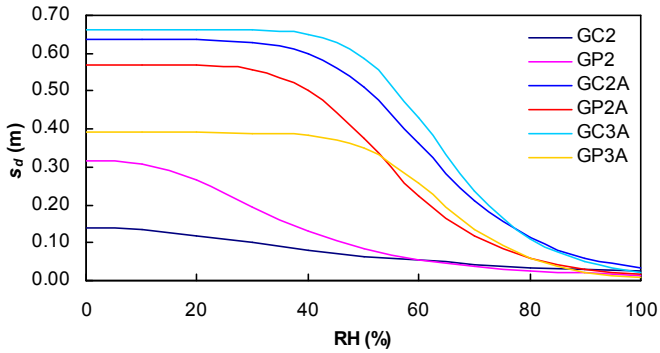

FIG. 5: Equivalent air layer thickness for applied coatings.

The graphics presented above highlight three points. The vapour resistance of the tested coatings is highly dependent on RH. The base material affects the actual vapour resistance of a coating. The vapour resistance of the primer is of major importance to the resistance of the finishing layer.

2.4 MBV

A set of MBV experiments were conducted on the selected elements, in agreement with the procedures defined by (Rode, 2005), using a climatic chamber and a balance for continuous weighing. The gypsum board samples were 12.5 mm thick and the gypsum plaster samples were 21 mm thick. The coating characteristics correspond to Table 1 data. The resulting mass variation of the tested samples is presented on Figure 6. As it can be seen in the graphics, the transient behaviour of the samples can be strongly influenced by the coatings. But the same type of coating had a different effect on the samples, as it would be expected from the vapour permeability test results.

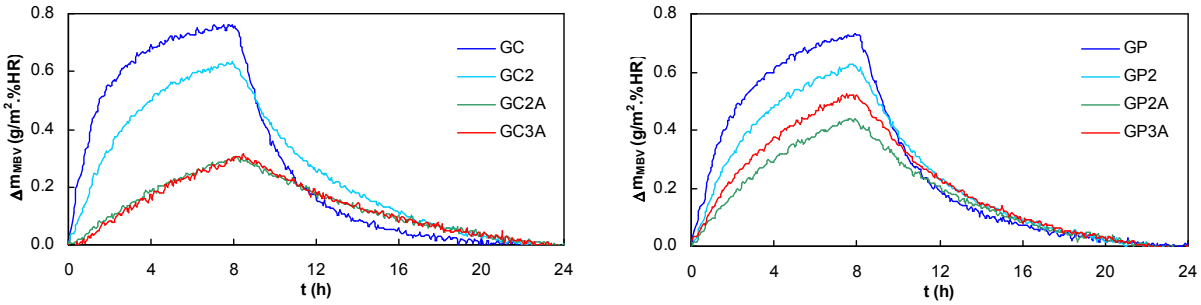

FIG. 6: MBV stable cycles.

3. Hygroscopic Inertia experiments

3.1 Flux chamber

A way of evaluating the impact of renderings and furnishings on the moderation of inside relative humidity variation is to actually determine the peak reduction of that variation caused by those materials. Ideally, that evaluation would be conducted in full size rooms where each combination of hygroscopic materials could be tested, facing real climate situations. As it would be impossible for LFC-FEUP to build such rooms, due to the costs involved, a decision was made to try to replicate those conditions in a small scale flux chamber. The facility, inspired by Padfield's flux chamber (Padfield, 1998), is presented in Figure 7. Other experimental setups have been recently used for hygroscopic inertia effect assessment (Rode et al, 2002, Yoshino et al, 2005).

The flux chamber was built inside an existing climatic chamber, allowing for the control of temperature (15ºC – 35ºC) and relative humidity (30% - 90%) of the whole system. The flux chamber consists of a Plexiglas box, placed over two steel tables, with three openings that can be used to gain access to the interior of the box. Its inside dimensions correspond to 1500x524x584 mm^3.

The ventilation system uses a pump that extracts air in two points inside the box. An inlet on top allows for the air to get in and, at the same time, prevents pressure differences. The air that enters the box comes directly from the climatic chamber, and therefore its characteristics are known. The air flux value is controlled by two flow meters allowing for a range of 2-130 l/min, corresponding to a range of air renovations of 0.26-17 h^{-1}.

The data acquisition system uses a set of Rotronic® sensors for measuring temperature and relative humidity. These sensors connect to a data logger, which transmits to a personal computer. The results can be stored in EXCEL format files.

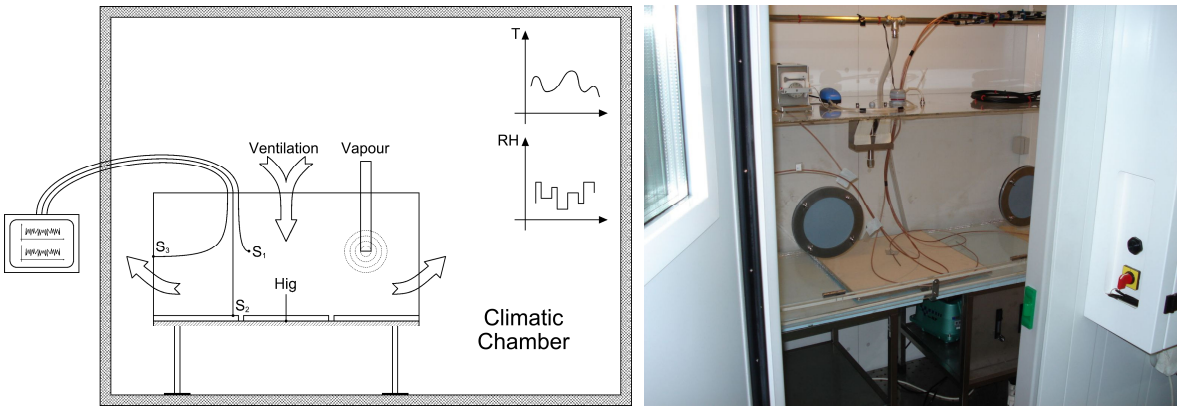

FIG. 7: Test facility principle and picture of the actual flux chamber inside a climatic chamber.

Although the flux chamber has an independent vapour production device, for the specific tests presented in this text, the combined effect of ventilation and climatic chamber RH variations was used to emulate vapour production effect on the mass balance.

The authors believe that this facility, although providing a small scale experiment, can be an interesting contribution to the experimental measurement of hygroscopic inertia effect. The simplicity in changing the test configuration or swap samples inside the flux chamber allows for the development of test scenarios in a relatively short time. At the same time, there's a high level of control of hygrothermal parameters, allowing for a rigorous analysis of the results.

3.2 Results

One of the tests performed in the flux chamber consisted of the definition of the stable daily RH cycle for a hygrothermal scenario. The selected scenario was defined assuming a ventilation rate, Rph, of 0.5 h^{-1} and a vapour production of 2 g/h, during 8 hours in the daily cycle. As the temperature of the system was fixed at 23º C, the vapour production was obtained with the RH variation of the climatic chamber between 40% and 80% RH. Using that scenario, different combinations of samples were placed inside the flux chamber, resulting in

different RH cycles. The samples used in these tests had the same configuration as the ones in MBV tests. For each configuration, the daily hygrothermal cycle is repeated until the flux chamber RH falls in a stable cycle.

The results of a few of the tests are referred in Table 2 and Figure 8 displays the RH variation inside the flux chamber for the tested combinations. For quantification of the test results, the difference between the average RH and the RH 90th percentile, RH_{90} - RH_m, is used. The average RH value obtained for each stable cycle showed a small variation, demonstrating the high control level of the experiments.

These results clearly illustrate the application of the flux chamber in measuring the actual RH dampening caused by the presence of different levels of moisture buffering in contact with inside air.

TABLE. 2: Configurations and results in Flux Chamber tests.

Test	Samples	RH_m (%)	RH_{90} (%)	RH_{90} - RH_m (%)
HI1	-	54.6	73.2	18.6
HI2	0.75 m^2 GC2A	54.6	68.3	13.7
HI3	0.75 m^2 GC	54.5	64.6	10.1
HI4	0.75 m^2 GC + 0.75 m^2 GC3	55.1	61.2	6.1

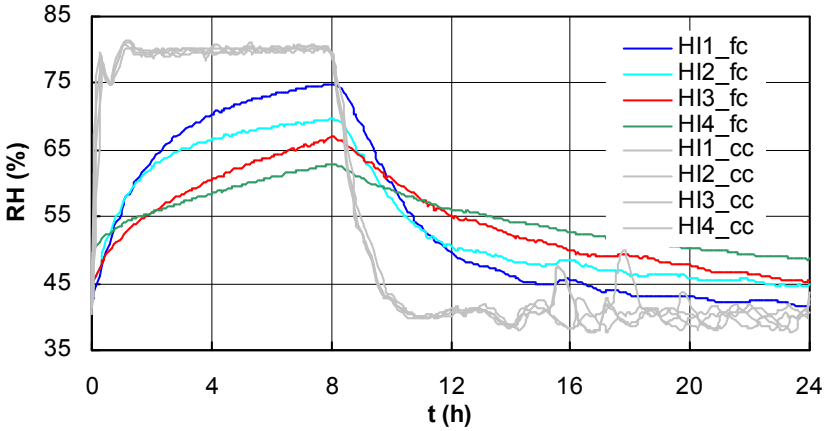

FIG. 8: Flux chamber tests HI1-HI4 stable cycles (fc – flux chamber, cc – climatic chamber).

4. Numerical Simulations

4.1 MBV

A modelling exercise based on the MBV experiments is presented in this section. The HAM-Tools model (Kalagasidis, 2004) was used in this exercise and the material data was obtained from the sorption isotherm and vapour permeability tests presented above. The main goal of this modelling exercise was to provide a base for discussing the different alternatives for simulating the coating effect on the transient hygric behaviour of a building system.

The base material layer was modelled with an eight node discretization.

Three options were used for modelling the coating effect:

- Application of a constant additional vapour resistance included in the surface transfer coefficient, corresponding to the average RH value of the test interval, which in the case of the MBV tests is 54%. (ref. zsurfavg)
- Application of a variable additional vapour resistance included in the surface transfer coefficient, calculated in each simulation step with the average RH value between the material surface and the air. (ref. zsurfvar)

— Modelling the coating as a layer, using a two node discretization. As there were no measurements of the coatings' sorption curve, that specific data for simulation was taken from literature (Goossens, 2004). (ref. zlayer)

The hygrothermal solicitation of the simulated specimen was defined with the actual RH variation measured inside the climatic chamber that supported the MBV laboratory tests.

A comparison between simulations and MBV tests on uncoated specimens is presented in Figure 9. The MBV simulations are highly dependant on the sorption curve used in the simulations. The second adsorption curve seems to produce a good agreement to the experiments, but in the case of the gypsum board the best agreement is only reached by a curve slightly different from that one.

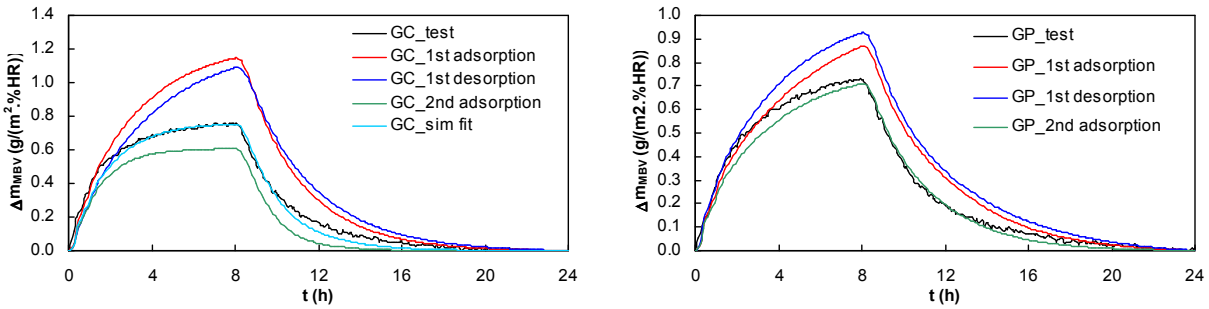

FIG. 9: MBV simulations for uncoated base materials.

The simulation of coated specimens also provided interesting results. In Figure 10, the results for the simulations of the vinyl coated specimens are presented. In this case, where the additional surface resistance was small, the agreement between tests and simulations is acceptable and a small difference was found when looking at the three modelling options of the coating effect.

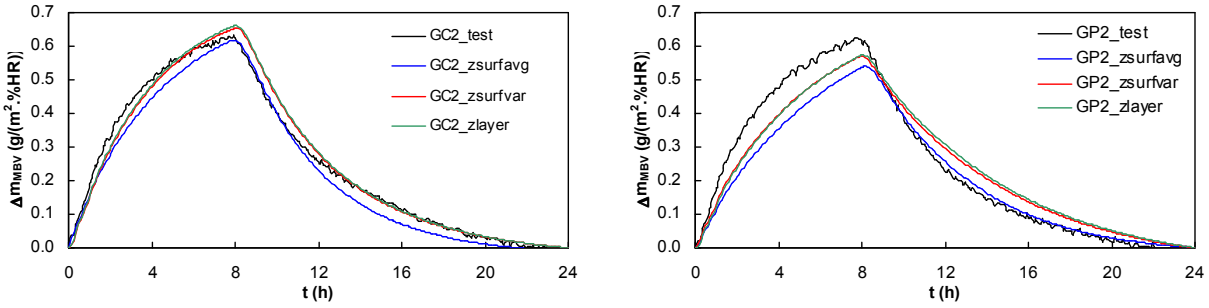

FIG. 10: MBV simulations for vinyl coated specimens.

In Figure 11, the results for primer plus acryl coating are presented. In this case, the different modelling options produced different results, but all underestimated the results. So another attempt was made, reducing the coating resistance to two thirds of its value, in the three options. The results of this set are presented in Figure 12, where an agreement improvement can be observed. The results for the simulation of primer plus vinyl coating effect were similar to the ones regarding primer plus acryl coating. The reduction to two thirds of the coating resistance showed, in general, an improvement of the agreement between tests and simulations, but a physical justification for this is lacking. If one considers that the coating resistance is a function of water content and not RH, the eventual influence of hysteresis may explain some of the fitting required for adapting simulations to experiments.

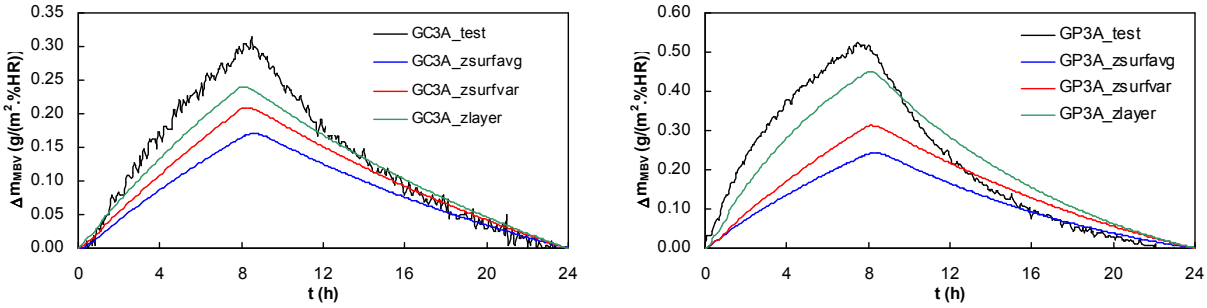

FIG. 11: MBV simulations for primer plus acryl coated specimens.

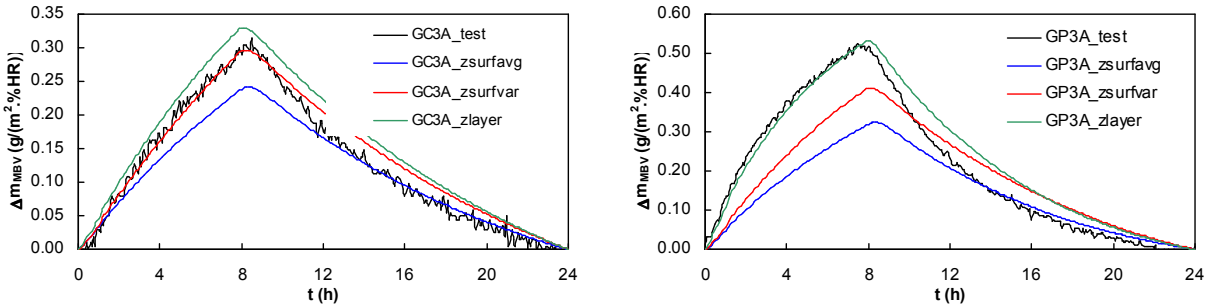

FIG. 12: MBV simulations for primer plus acryl coated specimens using reduced values of the coating's vapour resistance.

Some points of discussion can come from these observations:

- The coating's vapour permeability, determined by the cup method, had the expected effect on the MBV tests, since higher vapour resistances produced a higher MBV reduction;
- The simulation of the base materials MBV already revealed some difficulties due to the influence of the sorption isotherm data;
- Coated elements were simulated using three different strategies;
- The simulation of the coated elements showed that using the vapour permeability data from the cup tests would underestimate the MBV, with the worst results for a constant surface resistance and the best ones for the simulation of the coating as a layer;
- Simulating the coating as a material layer can be the best way of producing a good agreement between tests and numerical results, but the determination of the coating sorption isotherm, applied on a base material, is not easy to produce;
- The difficulties in simulating the coatings may not be linked to the material data at all, but to the model itself, and eventually different physical principles must be applied;
- Or, if we need to include the coating effect in a model, calibrating the data obtained in static tests by simulating simple dynamic tests may be an acceptable solution.

4.2 Virtual Bedroom

A different HAM-Tools modules association allowed for the simulation of a room's hygrothermal behaviour in yearly cycles. The virtual room is 3.5x3.5x2.5 m^3, with one exterior wall, containing a 1 m^2 window, facing south. The surrounding rooms are assumed to have similar conditions of temperature and relative humidity as the simulated room. The climate conditions were defined for Lisbon, using Meteonorm software. The inside temperature was allowed to float between Tmin and 28 ºC, and RH was allowed to float below 90%. The ventilation rate is constant and the vapour production takes place between 0h and 8h, with a constant value. On walls and ceiling the admitted material was gypsum board and on the floor spruce.

Table 3 describes the conditions that were changed for simulations SG1 and SG2 that are presented as an example where SG1 stands for the room with no hygroscopic inertia, the reference room.

TABLE. 3: Room configurations.

Simulations	Walls		Ceiling		Floor	
	Area (m^2)	β (s/m)	Area (m^2)	β (s/m)	Area (m^2)	β (s/m)
SG 1	34	2e-12	12.25	2e-12	12.25	2e-12
SG 2	34	2e-8	12.25	2e-8	12.25	2e-12

Partial results from simulations SG1 and SG2 are presented in Fig. 13, illustrating the tested scenarios. The hygroscopic inertia effect is clear when looking at RH peak dampening from SG1 to SG2.

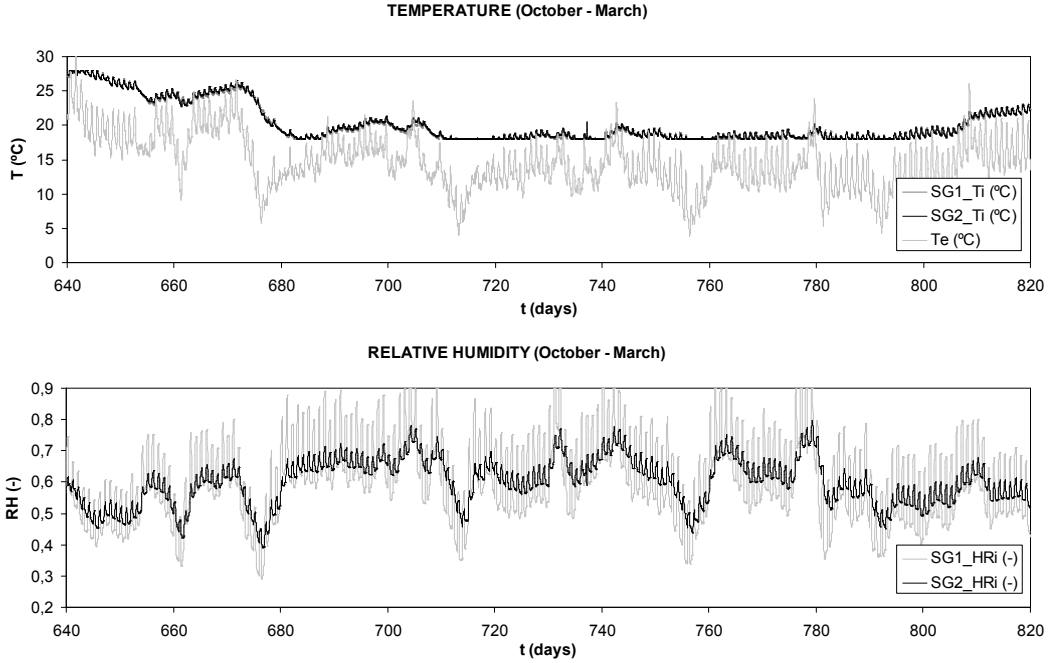

FIG. 13: Results from simulations SG1 and SG2.

5. Daily Hygroscopic Inertia Index, $I_{h,d}$

5.1 Concept

There is a need for a single parameter that can characterize the daily hygroscopic inertia of a room and correlate to the expected dampening of the RH variation of that room.

The proposed daily hygroscopic inertia index, $I_{h,d}$, is defined by Ramos (2007) as a function of MBV, according to expression (1), where MBV_i = Moisture buffer value of element i ($g/(m^2.\%RH)$); S_i = surface of element i; MBV_{obj} = Moisture buffer value of complex element j (g/%RH); C_r = Imperfect mixing reduction coefficient (-); Rph = air exchange rate (h^{-1}); V = room volume (m^3); TG = Vapour production period (h). The $I_{h,d}$ can be understood as the room MBV, homogenized to air renovation conditions and vapour production period variations.

$$I_{h,d} = \frac{\sum_{i}^{n} C_{r,i} \cdot MBV_i \cdot S_i + \sum_{j}^{m} C_{r,j} \cdot MBV_{obj,j}}{Rph \cdot V \cdot TG} \quad \left[\frac{g}{m^3 \cdot \%RH}\right] \tag{1}$$

The AMDR parameter was defined according to expression (2), where HR_m is the average relative humidity variation and $\overline{HR_{90}}$ stands for the daily average of the 90th percentile of the relative humidity variation. The index *ref* refers to the base scenario of a room without hygroscopicity and *sim* identifies a scenario under study for that same room. The AMDR parameter can therefore be interpreted as relative daily average amplitude of a RH variation of a room hygroscopic configuration. This parameter is interesting since the average RH variation in long term analysis will not be affected by daily hygroscopic inertia.

$$AMDR = \frac{\left(\overline{HR_{90}} - HR_m\right)_{sim}}{\left(\overline{HR_{90}} - HR_m\right)_{ref}} \tag{2}$$

Analysis of both numerical and experimental results confirmed the correlation between AMDR and $I_{h,d}$. The graphic relation between the two parameters is presented in Fig. 14

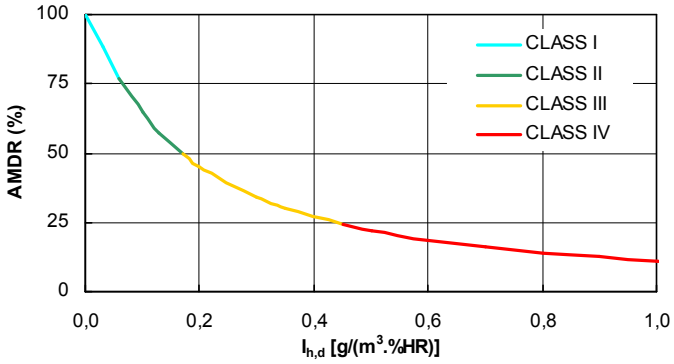

FIG. 14: Graphic relation between AMDR and $I_{h,d}$.

6. Conclusions

This study allows for the following conclusions:

- Moisture buffering tests were conducted at element level. Renderings finished with different coatings were tested for MBV determination, allowing for buffer effect comparison. The finishing coating has a relevant influence on that effect.
- Hygroscopic inertia tests were conducted in a flux chamber that represents a small scale room. The influence of different elements on RH variation was obtained. The experimental evidence of daily hygroscopic inertia was demonstrated.
- Numerical simulations provided elements for discussion on the difficulties in simulating the dynamic hygroscopic behaviour of painted renderings.
- The benefits of hygroscopic inertia associated to RH peak dampening can be observed in full hygrothermal modelling of bedrooms.
- A daily hygroscopic inertia index was proposed and verified with both experimental and numerical data.

7. Acknowledgement

This study was financially supported by Fundação para a Ciência e Tecnologia (FCT) and project POCI/ECM/57722/2004 co-financed by FEDER.

8. References

Galbraith, G. H., Mclean, R. C., Guo, J., Kelly, D., Lee, C. (1999) The use of differential permeability in moisture transport modelling. Proceedings of Building Simulation '99.

Galbraith, G. H., Mclean, R. C., Guo, J.S. (1998) Moisture permeability data presented as a mathematical relationship. Building Research & Information, 26, 157-168.

Goossens, E., Van Der Zanden, A., Van Der Spoel, W. (2004) The measurement of the moisture transfer properties of paint films using the cup method. Progress in Organic Coatings, 49, 270-274.

Kalagasidis, A. S. (2004) HAM-Tools: An Integrated Simulation Tool for Heat, Air and Moisture Transfer Analyses in Building Physics. Department of Building Technology, Building Physics Division. Gothemburg, Chalmers University of Technology.

Padfield, T. (1998). The role of absorbent building materials in moderating changes of relative humidity. Department of structural engineering and materials. Lyngby, The technical university of Denmark.

Ramos, N. (2007). The importance of hygroscopic inertia in the hygrothermal behaviour of buildings (in Portuguese). PhD Thesis. Department of Civil Engineering, Faculty of Engineering – University of Porto.

Ramos, N., Freitas, V. (2006). Evaluation Strategy of finishing materials contribution to the hygroscopic inertia of a room. Research in Building Physics and Building engineering – Proceedings of the Third International Building Physics Conference, pp. 543-548. Concordia University, Montreal, Canada, 27-31 August.

Rode, C., Peuhkuri, R., Mortensen, L., Hansen, K., Time, B., Gustavsen, A., Svennberg, K., Arfvidsson, J., Harderup, L., Ojanen, T. and Ahonnen, J. (2005) Moisture Buffering of Building Materials. Report BYG-DTU R-126. Department of Civil Engineering. Technical University of Denmark.

Rode, C., Mitamura, T., Schultz, J., Padfield, T. (2002) Test cell measurements of moisture buffer effects. 6th symposium on building physics in the Nordic countries. Trondheim, Norway.

Roels, S. (2004). Inter-laboratory comparison on measurement of moisture buffering properties of gypsum board - Instruction document. Annex 41 MOIST-ENG.

Yoshino, H., Mitamura, T., Hasegawa, K., Matsumoto, S., Adachi, M. (2005) Experiment for synthetic evaluation of moisture buffering effect in a room. IEA Annex 41 meeting. Trondheim, Norway.

IEA Annex 41 Subtask 2: interlaboratory comparison of vapour transmission properties and sorption isotherm of gypsum board

Staf Roels, Professor,
Department of Civil Engineering, K.U.Leuven;
staf.roels@bwk.kuleuven.be

KEYWORDS: *round robin testing, cup test, vapour diffusion, sorption isotherm, gypsum board*

SUMMARY:
The precision and reliability of common methods used for the determination of the hygric properties of porous building materials was investigated. The study was performed in the framework of Annex 41 of the International Energy Agency, dealing with hygric buffering of finishing materials. Fourteen laboratories measured the vapour permeability and sorption isotherm of coated and uncoated gypsum board. Apart from an off set based on the conditions during the oven-drying, the measured sorption isotherms showed acceptable agreement. But for the vapour transmission tests, though performed according to a standard, a wide spread in the measured data was found.

1. Introduction

Subtask 2 of IEA/ECBCS Annex 41 has been devoted to the experimental analyses of moisture buffering. Within the subtask it was decided to perform first an interlaboratory comparison of the measurement of the hygric properties of porous building materials by means of a round robin test. The main goal of the round robin testing was twofold: on the one hand to assess the reliability of material property measurements relevant for Annex 41, on the other hand to collect reliable data that could be used in the benchmark cases of Subtask 1 and 2. The first goal was partly inspired by the European HAMSTAD-project which showed that even commonly used measurement methods could not always determine the material properties with an acceptable level of precision and repeatability (Roels et al., 2004). BCR (1992) reported a similar observation when describing the results of a round robin test in which 13 laboratories performed water vapour permeability tests on two different materials. Better results were obtained in (Time and Uvslokk, 2003), a project in which six Nordic countries performed cup tests on three different materials.

In the framework of Annex 41, to gain time, no real round robin was performed, but samples of the same batch were randomly distributed among the participating laboratories. It was decided to restrict to one kind of finishing material: gypsum board, but measured both uncoated and finished with a priming coat and two kind of finishing coat. Not all material properties have been measured, but the round robin focussed on those properties relevant for indoor moisture buffering: the water vapour transmission properties and the sorption isotherm. In total fourteen laboratories participated in the round robin test. The results are presented in this paper. In "*IEA/ECBCS Annex 41 Subtask 2 Common Exercise on Transient Heat and Moisture Transfer in a Bed of Gypsum Boards*" the dynamic behaviour of gypsum board as measured in a laboratory experiment was compared with numerical simulations with the measured material properties of the round robin test as input (James et al, 2008). The large number of participants also allowed a sensitivity study of the numerical simulations, in which the influence of the uncertainty in material properties and boundary conditions was investigated.

2. Test materials and test series

In the Annex 41-project of the International Energy Agency a lot of research has been on indoor hygric buffering. Therefore, a finishing material was selected as test material, gypsum board. Though, the material had to be measured both uncoated and finished with a priming coat and two kind of finishing coat. The gypsum board and primer have been supplied by *GYPROC BPB, Belgium*. The gypsum board is from the type '*GYPROC A ABA-board'* with overall dimensions of 1200x2400 mm² and a thickness of 12.5 mm. For the finishing coats two types, labelled A and L, have been used. Both were supplied by *BOSS Paints, nv Bossuyt, Belgium*. Finishing coat A is an acrylic paint (type Decomat, BOSS paints) and was coloured light blue. Finishing coat L is a latex paint (Bolatex, BOSS paints) and was coloured light yellow.

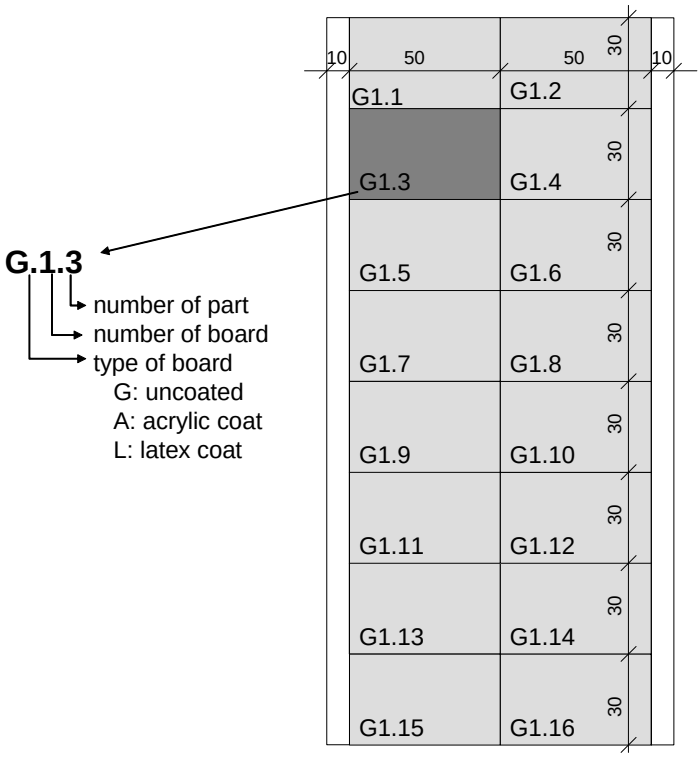

FIG. 1: Subdivision of the gypsum boards in 16 parts of 50x30 cm² As an example the numbering for the first uncoated gypsum board (G.1) is indicated.

Three test series have been measured: 1) the uncoated gypsum board; 2) the gypsum board covered with the priming coat and acrylic finishing coat A; 3) the gypsum board covered with the priming coat and latex coat L. This three series allow to asses the reliability to measure the vapour permeability of a layer of paint. In total 20 plates of gypsum board (2400x1200x12.5 mm³) have been cut in different parts of 500x300 mm² (see Figure 1). All parts were labelled with a letter (G for uncoated board, A for board covered with the acrylic finishing coat, L for board covered with the latex finishing coat), followed by the number of the board and the number of the part. To randomise the test samples as much as possible parts form different boards were sent to each partner. Each partner had to cut specimens out of these parts in a way that for each measurement set-up specimens of different boards are measured. For series 2 and 3 the priming coat and finishing coat were applied with a paint roller by the University of Leuven and the painted gypsum board samples were distributed among all participants.

3. Water vapour transmission test

3.1 Test method and test conditions

The water vapour transmission properties have been determined in accordance to EN ISO12572:2001 *Hygrothermal performance of building materials and products – determination of water vapour transmission properties*. A complete description of the test method and procedure can be found in (EN ISO 12572:2001). Specific attention had to be paid to the following remarks in the standard:

1) if the specimen area is less than 0.02 m², five specimens shall be tested; otherwise three specimens shall be tested.
2) Preparation of the cups: the desiccant or aqueous solution shall be placed with a minimum depth of 15 mm in the bottom of each cup. The air space between the desiccant or aqueous solution and the specimen shall be 15±5 mm.
3) Annex A: methods suitable for self supporting materials shall be followed. If molten sealants are used, the edge of the specimens shall be sealed with tape or an epoxy resin to avoid penetration of the molten sealant into the gypsum board.

All three main test series (the uncoated gypsum board, the gypsum board covered with primer and paint A and the gypsum board covered with primer and paint L) had to be measured at three test conditions as given in Table 1. Test condition C1 and C2 correspond respectively to set A and set C in chapter 7.1. of (EN ISO 12572:2001). Test condition C3 was included to apply an analytic fit to the measured data, which could be used in numerical simulations. If CaCl2-flocks were used as desiccant in test condition C1, it was asked to make sure to start from fully dried (at 200-250 °C) flocks. Specific prescriptions for the preparation and more details on the applied test assemblies can be found in (Roels et al., 2008).

TABLE. 1: Test conditions for the determination of the water vapour transmission properties

Set	*conditions*	*temperature*	*Relative Humidity*	
	°C – RH		*Climatic chamber*	*Cup*
C1	*23 – 0/50*	*23 ± 0.5 °C*	*Aqueous solution 53 % $Mg(NO_3)_2$*	*Desiccant $CaCl_2$-flocks or $Mg(ClO_4)_2$*
C2	*23 – 50/93*	*23 ± 0.5 °C*	*Aqueous solution 53 % $Mg(NO_3)_2$*	*Aqueous solution 94 % KNO_3*
C3	*23 – 86/93*	*23 ± 0.5 °C*	*Aqueous solution 85 % KCl*	*Aqueous solution 94 % KNO_3*

3.2 Main results

The results of the water vapour transmission tests are presented as equivalent air layer thickness (s_d-values in m). Figure 2 shows the probability density functions of the mean values as measured by the different participating laboratories, when no corrections for the air layers or for the masked edge are performed. The uncoated gypsum board is found to be very vapour open. In fact, only the dry cup value (test condition C1) exceeds an equivalent air layer thickness of 0.1 meter, the criterion used in the standard as minimum value to make cup tests applicable due to the increasing uncertainty on the measurement results for more vapour open materials. Applying a primer and finishing coat on the gypsum board changes the vapour permeability considerably, but the type of coat seems to be very important. Applying an acryl finishing coat triples the equivalent air layer thickness (mean value of all laboratories for test condition C1), while the latex coat multiplies the equivalent air layer thickness with almost a factor 30! But, the dependency of the vapour permeability on relative humidity is far more pronounced for the coated gypsum board than for the uncoated gypsum board. Put otherwise, the vapour resistance of the finishing coat strongly decreases with increasing relative humidity. This feature is far more pronounced for the latex coat than for the acrylic coat. Compared to the uncoated gypsum board where the wet cup value of the equivalent air layer thickness (test condition C3) is ± 70% of the dry cup value, a reduction with almost a factor three is found for the acryl coat and a reduction with a factor seven for the latex coat.

Comparing the results of the different laboratories, the data show remarkable high differences. Knowing that the measurements are carried out according to the prescriptions of an existing standard, unacceptable deviations are found. Furthermore, the more vapour tight the specimen is (dry cup values of gypsum board covered with latex coat), the more pronounced the differences become. However, when comparing the individual results of each of the laboratories the deviations are much smaller than the deviations between the laboratories. Note that these data are not included here, but can be found in (Roels et al., 2008). This suggests that there could be systematic differences between the participating laboratories. However, when plotting the data of the three test series versus one another, no indication for systematic differences between the participating laboratories could be found.

3.3 Discussion

The results presented in Figure 2 correspond to uncorrected data. Depending on the test set-up assembly two types of corrections have to be applied. According to Annex G of (EN ISO 12572:2001) a correction for the vapour resistance of the layer of air in and above the cup has to be applied for very permeable materials. Very permeable materials are defined as materials with an equivalent air layer thickness less than 0.2 m.

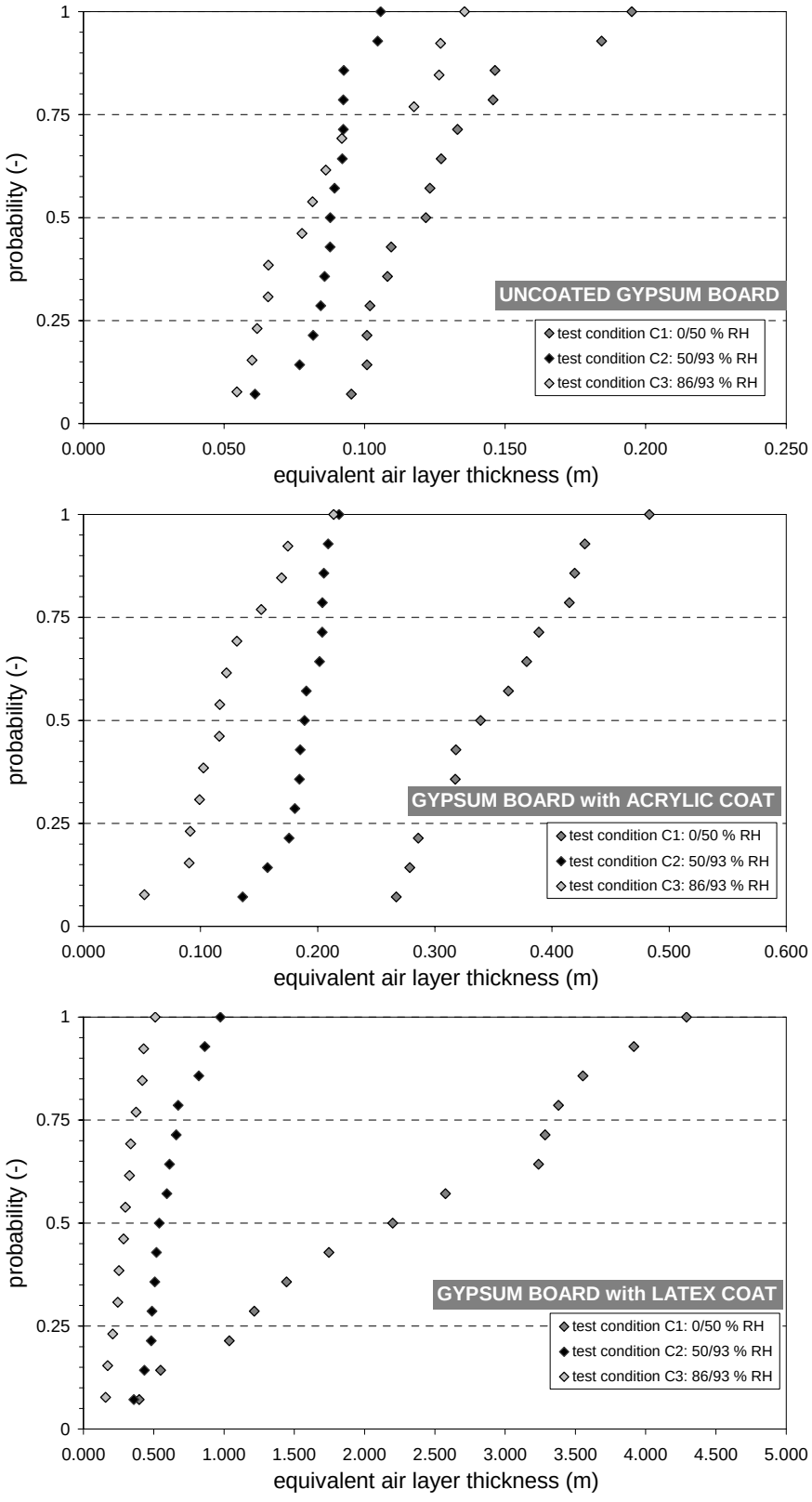

FIG. 2: Cumulative distribution function of the mean values of the equivalent air layer thickness as determined by the participating laboratories.

This is the case for the uncoated gypsum board and for the gypsum board with acrylic finishing coat under test condition C2 and C3. (note that for uncoated gypsum board only test condition C1 is within the scope of the standard). For the air layer in the test cup the measured permeance has to be corrected with the permeance of the stagnant air layer in the cup. Since most of the laboratories followed the prescriptions very well, which stated that the air space between the desiccant or aqueous solution and the specimen had to be within the range of 15±5 mm, all correction are in the same order of magnitude. In this way applying a correction for the air layer in the cup just reduces the calculated equivalent air layer thickness (mean value after correction 0.107 meter instead of 0.128 meter), but has hardly any difference on the spread in results. To ensure that the resistance of the air layer above the cup is negligible, EN ISO12572:2001 request to stir the air in the test chamber and to ensure an air velocity above each specimen of at least 2 m/s. Furthermore it is advised to use cups without a high rim. For most laboratories the air velocity in the test chamber is much lower than 2 m/s (Roels et al., 2008). Furthermore, different types of cups have been used, some with, others without rim. However, no correlation could be found between the measured values and the air velocity above the cups or the presence (and height) of the rim.

Some participants use cup types with 'masked edges', which means that the edge of the specimen overlaps the edge of the cup. This overlap zone is a possible route for two dimensional vapour transfer, leading to an overestimate of the vapour permeance, since the total flow through the specimen in the test assembly is greater than that through the exposed area of the specimen. Annex F of (EN ISO12572:2001) proposes a correction if a masked edge is present. This is done by dividing the measured vapour flow with a correction factor. For the cup assemblies with the most extreme masked edge (a square cup with a masked edge of 21% of the exposed area and a circular cup with a masked edge of 24% of the exposed area) the correction factor is 1.089 and 1.106 respectively. This influences the obtained equivalent air layer thickness by approximately 10%, but it hardly influences the variation on the results and can not explain the deviations found between the different laboratories.

Most striking when comparing the data and looking at the cumulative distribution function of the measured mean values, is the wide spread found in the dry cup data (test condition C1) of the gypsum board finished with the latex coat. The measured mean equivalent air layer thickness varies between 0.4 and 4.3 meter ! Since this is the most vapour tight material, a possible explanation could be leakage through the seal. To investigate this, Figure 3 replots the probability function of the measured mean values, with the type of seal indicated. Except for two outliers, cups with a wax seal seem to perform much better than all other kinds of seals. The lowest value of the two outliers corresponds to a special way of sealing where the wax is poured into a collar. The second outlier, with a value of 2.2 meter corresponds to a mean value of two measurements around 3.4 meter and three measurements around 1.4 meter. So, there it seems that the seal is imperfect for three of the five cases.

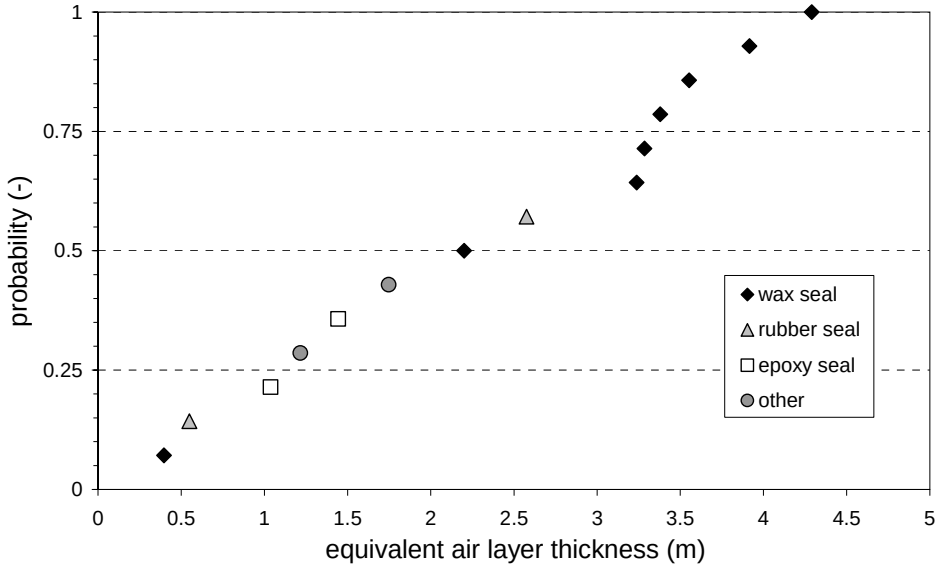

FIG. 3: Influence of the type of seal on the measured equivalent air layer thickness of gypsum board with a latex finishing coat for test condition C1 (dry cup) .

4. Sorption isotherm

4.1 Test method and test conditions

Since the hygroscopic behaviour of the finishing paint is in the precision range of most weighing devices, it was decided to determine the sorption isotherm only on the uncoated gypsum board. For the determination of the isothermal adsorption curve initially oven dried samples had to be conditioned at different relative humidity and at constant temperature until a static sorption equilibrium was attained between the relative humidity of the environment and the moisture content of the specimen. Equilibrium between moisture content and relative humidity is said to have been achieved when repeated weighing, at intervals of at least one week, show a difference in mass of 0.1 percent or less. The equilibrium moisture content mass by mass of the specimens is calculated as

$$u = (m_w - m_o)/m_o \quad (2)$$

with m_w the mass of the moist specimen and m_o the mass of the specimen in dry state. To control the relative humidity of the environment the samples had to be placed in desiccators that contain different aqueous solutions. To control the temperature, the desiccators had to be stored in temperature controlled climatic chambers at 23 ± 1°C. The measurements are performed at four relative humidities: 33, 53, 79.5 and 94%.

For the adsorption curve different specimen could be used for the different relative humidity. So specimen were not taken stepwise from low to high relative humidity, but to gain time the adsorption isotherm was determined in all data points at the same time. When equilibrium was achieved all specimen had to be taken stepwise from high to low relative humidity to study the desorption curve starting from different starting points. So both the specimen at 53%, 79.5% and 94% were stepwise taken from high to low relative humidity. In this way some of the intermediate scanning curves between the ad- and desorption isotherm were measured.

To allow a statistic analysis, each participant had to prepare from the delivered boards 5 test specimen for each relative humidity, each of them with a surface area of 60x60 mm². All specimens had to be dried beforehand at a temperature of 50°C and this as long as the weight loss between two successive measurements, with a time interval of at least 24 hours, remained more than 0.1%. Drying at a higher temperature was found not recommendable since also chemically bounded water may be removed. Some preparatory measurements indicated that drying at 50°C performed in a vented oven was not dehydrating the gypsum but was also not removing all the hygroscopically bounded water. This means that the starting point of the sorption isotherm (the intended dry weight) is not corresponding to the origin of the sorption isotherm graph. The shape of the curve, though, will not be influenced and since the main focus of Annex 41 is the dynamic hygric behaviour of the material, the measured slope of the sorption isotherm is of main interest. More details on the prescriptions of preparation and measurements of the specimen can be found in (Roels et al., 2008).

4.2 Results

Figure 4 shows the adsorption curves (mean of five specimen) as measured by the participating laboratories. Figure 5 shows a typical example of the measured desorption and intermediate scanning curves starting from the different positions on the adsorption isotherm. As could be expected a significant difference in absolute values can be observed for the adsorption isotherm (Figure 4). This can be attributed to the different oven drying conditions and corresponding correction for the dry weight. When comparing the slopes of the curves (see Figure 6) a much better agreement is found. Between 30 and 80% RH the slope of the adsorption curve is –ignoring one outlier – for all institutes in the same order of magnitude. For the higher RH's (above 80%) a larger spread is obtained.

For the desorption curves – data not included, but presented in (Roels et al., 2008) – it was observed that, apart from the first desorption step, the slope of the adsorption, desorption and scanning curves is almost the same. So it seems that hysteresis on the hygric capacity plays mainly a role in the first part, in the current case when the switch is made from loading to unloading.

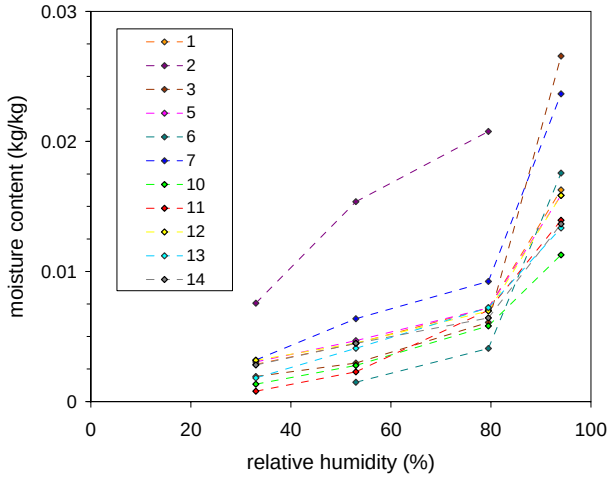

FIG. 4: Adsorption curves as determined by the participating laboratories on uncoated gypsum board. Each data point corresponds to the mean of five or six specimen.

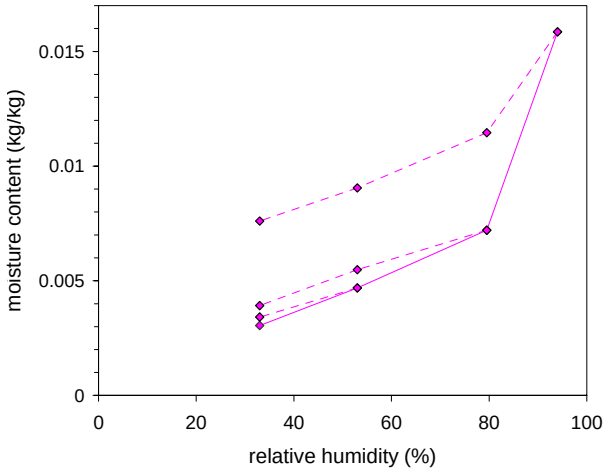

FIG. 5: Typical example of adsorption curve (continuous line) and desorption and intermediate scanning curves (dotted lines) as measured by one of the partners.

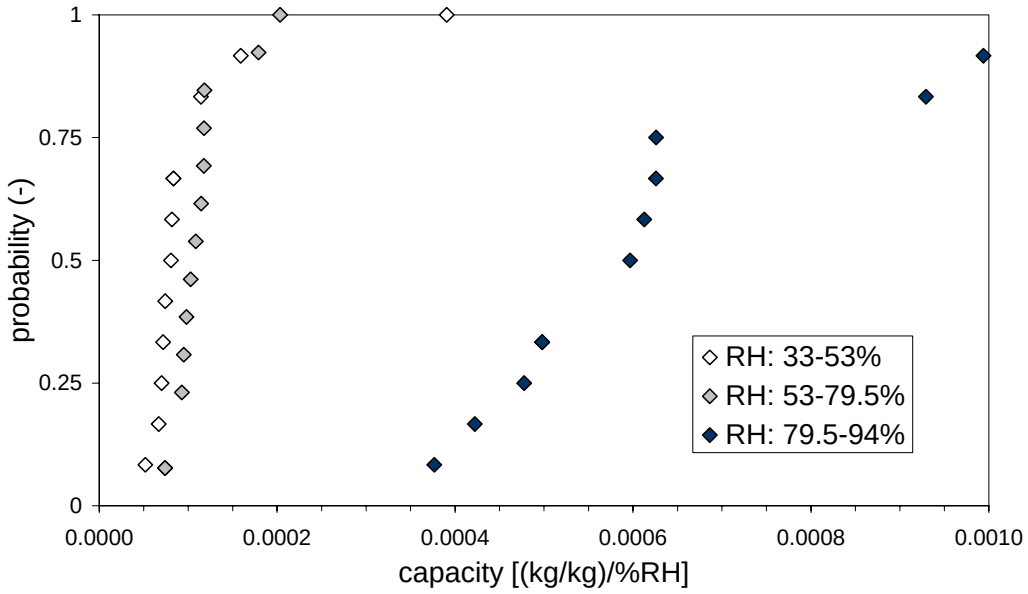

FIG. 6: Cumulative distribution function of the mean values of the piecewise capacity determined for the absorption curve by the participating laboratories .

5. Conclusions

In the framework of IEA-Annex 41 a round robin testing was set up. Aim was to investigate whether it is possible to determine the necessary moisture properties with respect to moisture buffering with an acceptable level of precision and repeatability. In total fourteen laboratories measured the vapour permeability and sorption isotherm of gypsum board.

The vapour transmission properties have been measured on three test series: uncoated gypsum board, gypsum board covered with a priming coat and acrylic finishing coat and gypsum board covered with a priming coat and latex finishing coat. The tests were carried out in accordance to EN ISO12572:2001. Three test conditions (0/50, 50/93 and 86/93 %RH) were considered. Comparing the results, it was found that the obtained vapour

resistance data show surprisingly high differences. The differences are most pronounced for vapour tight specimen. The highest measured mean dry cup value of gypsum board finished with latex paint is more than ten times larger than the lowest measured mean value. And, though the deviations within the results of each laboratory are much smaller than the deviations between the laboratories, no systematic differences could be found between the participating laboratories. Neither could the type of desiccant in the dry cup, the masked edge or the vapour resistance of the air layers in and above the cups explain the observed differences. Yet, when analysing the type of seal, it was found that the highest equivalent air layer thicknesses were measured on cups sealed with wax. It can be concluded that for experiments carried out according to an existing ISO standard, the obtained results show unacceptable differences. This is in agreement with previous round robin testing and stresses the need for further research on the reliability of cup tests to come to an adequate revision of the existing standards.

Both the sorption isotherm, desorption isotherm and some intermediate scanning curves have been determined on uncoated gypsum board. Though, due to differences in the determined dry weight the absolute curves deviate significantly, the measured slopes of the sorption isotherm correspond much better. Therefore, comparison of the results was based on the piecewise capacity of the sorption isotherm. Based on the mean values as measured by each of the participating laboratories it can be concluded that a rather good agreement is found in the adsorption curve as long as the relative humidity remains below 80%. At higher values the differences between the laboratories increases. Both for the main desorption curve as well as for the intermediate scanning curves hysteresis was mainly found to play a role in the first desorption step. For the following desorption steps the piecewise capacity was nearly the same as determined on the adsoption curve.

6. References

BCR (1992). The BCR programme on applied metrology and chemical analysis, projects and results *1988-1992, Office for publications of the European Communities, Luxemburg.*

EN ISO 12572:2001 (2001). Hygrothermal performance of building materials and products – determination of water vapour transmission properties. *European Committee for Standardization, Brussels, Belgium.*

James C, Talukdar P, Simonson C (2008). IEA/ECBCS Annex 41 Subtask 2 Common Exercise on Transient Heat and Moisture Transfer in a Bed of Gypsum Boards. *Workshop on IEA/ECBCS Annex 41 at the 8th Symposium of Building Physics in the Nordic Countries*, Technical University of Denmark.

Roels S, Carmeliet J, Hens H, Adan O, Brocken H, Cerny R, Pavlik Z, Hall C, Kumaran K, Pel L and Plagge R, (2004). Interlaboratory comparison of the measurement of basic hygric properties of porous building materials. *Journal of Thermal Envelope and Building Science*, 27(4): 307-325.

Roels S, James C, Janssen H, Talukdar P, Simonson CJ (2008), Experimental analysis of moisture buffering, Annex 41, Subtask 2 Final report, (2008), in press.

Time B., Uvslokk S. (2003). Intercomparison on measurement of water vapour permeance. *Nordtest-project agreement 1529-01*.

IEA/ECBCS Annex 41 Subtask 2 Common Exercise on Transient Heat and Moisture Transfer in a Bed of Gypsum Boards

Chris James[1], Prabal Talukdar[2] and Carey J. Simonson[1]

[1]Department of Mechanical Engineering, University of Saskatchewan, 57 Campus Drive, Saskatoon, SK, S7N 5A9, Canada
[2]Department of Mechanical Engineering, Indian Institute of Technology Delhi, Hauz Khas, New Delhi 110016, India

Abstract: Numerical models of heat, air and moisture (HAM) transfer in whole building continue to advance, but there remains a need for accurate and well-documented experimental data for model validation. Therefore, Subtask 2 of IEA/ECBCS Annex 41 conducted a common exercise on 1-D and transient heat and moisture transfer in a gypsum bed to generate an experimental and numerical data set for benchmarking numerical models [1]. This common exercise is summarized in this paper, which presents experimental data measured using the transient moisture transfer (TMT) facility at the University of Saskatchewan and numerical data from 10 different numerical models. In nearly all cases, the agreement between the data is within the experimental and numerical uncertainty bounds.

1. Introduction

As computing power increases and numerical models for whole building heat, air and moisture (HAM) transfer advance, there remains a general need for more experimental data that quantify HAM transport in porous building materials. For example, recent benchmarks for validating 1-D HAM simulation models produced in a large international project [2] rely solely on numerical and analytical data because well-documented and accurate 1-D data are scarce. An important part of the research in IEA/ECBCS Annex 41 has been on heat and moisture transfer between indoor air and hygroscopic materials during transient changes in indoor humidity because there is evidence that moisture buffering may improve comfort, air quality and energy consumption in buildings [3-8]. To validate models that simulate moisture buffering of hygroscopic materials, new experimental data are needed that accurately quantify heat and moisture transfer between humid air and hygroscopic materials during transient changes in the air humidity.

Experimental data are available in the literature, but most data are not well suited to benchmark detailed numerical models because carefully planned laboratory experiments are often needed for model validation [7-17]. In addition many of the experiments in the literature are conducted on non-hygroscopic materials, where a majority of the moisture accumulation is due to condensation and frosting near a cold boundary. Furthermore, in many cases the thermal transients dominate the problem. To benchmark models that intend to consider moisture buffering of hygroscopic materials in contact with indoor air, experimental data are needed where the air humidity is changed in a transient manner as presented in this paper.

The objective of this paper is to compare experimental and numerical data for 1-D heat and moisture transport in a bed of gypsum boards, which was conducted as part of Subtask 2 of IEA/ECBCS Annex 41 [1]. Comparing the numerical and experimental data serves a dual purpose of validating the numerical models as well as confirming the experimental data.

Together, the experimental and numerical data form a valuable data set for benchmarking numerical models where the expected range of agreement between the measured and simulated data is identified.

2. Experimental Facility

The test section of the transient moisture transfer (TMT) facility (Figure 1) is designed to provide and measure 1-D heat and moisture transfer between a humid air stream and porous media [4, 16]. The air flow in the test section is hydrodynamically fully developed with known convective transfer coefficients [18, 19] and is drawn from two environmental chambers resulting in stable and well controlled temperature and humidity boundary conditions above the porous media [4, 16]. All the sensors used in the TMT facility (i.e. temperature, relative humidity, mass and pressure sensors) are carefully calibrated with known standards before and after the tests [4, 16]. All the sensors used in the experiments show good agreement between the pre-test and post-test calibrations and the total 95% uncertainties bounds, including bias and precision uncertainties, are summarized in Table 1.

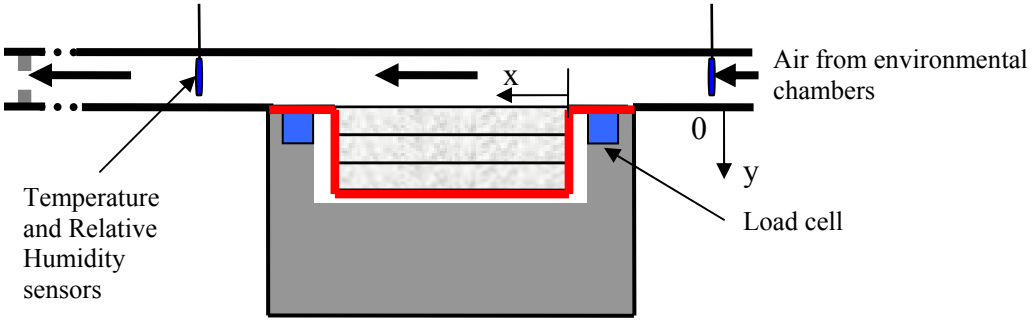

Figure 1. Schematic of the test section of the TMT facility at the University of Saskatchewan.

Table 1. Description of the measurement sensors and uncertainties in the experiment.

Measurement and sensor description	95% Uncertainty bounds
Temperature of the air stream (RTD)	±0.1°C
Temperature in the gypsum bed (thermocouple)	±0.1°C
Relative humidity of the air stream (capacitance based sensor)	±1%
Relative humidity in the gypsum bed (capacitance based sensor)	±2%
Moisture accumulation in the gypsum bed (gravimetric load sensors)	±2g
Mass flow rate of air (orifice plate)	±6%
Reynolds number	±8%

In this paper, the TMT facility is used to measure the temperature, relative humidity and moisture content in a bed of gypsum that consists of three gypsum boards (each 500 mm long, 280 mm wide and 12.5 mm thick) as shown in Figure 2. Although several sensors are used at each depth in the bed, only averages are presented in this paper because the temperature and relative humidity fields are very nearly 1-D in the experiment as evidenced by the small variation (±0.1°C and ±2% RH) between each sensor reading and the average value at each depth in the bed [1]. To minimize the effects of the sensor and leads, they are placed in small grooves machined in the upper surface of the middle and bottom gypsum boards (Figure 3). The grooves make up 1.8% and 0.7% of the surface area of the middle and bottom gypsum boards. In addition,

6 nylon screws (3 mm in diameter) were used to hold the gypsum bed together and minimize air gaps between the boards. The holes for the nylon screws on the top gypsum board and the edges of all gypsum board were covered with aluminum tape to minimize moisture transfer in these areas.

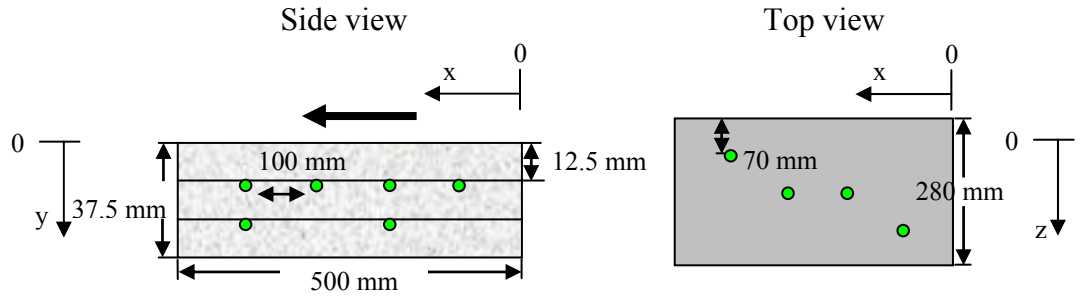

Figure 2. Location of the humidity and temperature sensors within the gypsum bed.

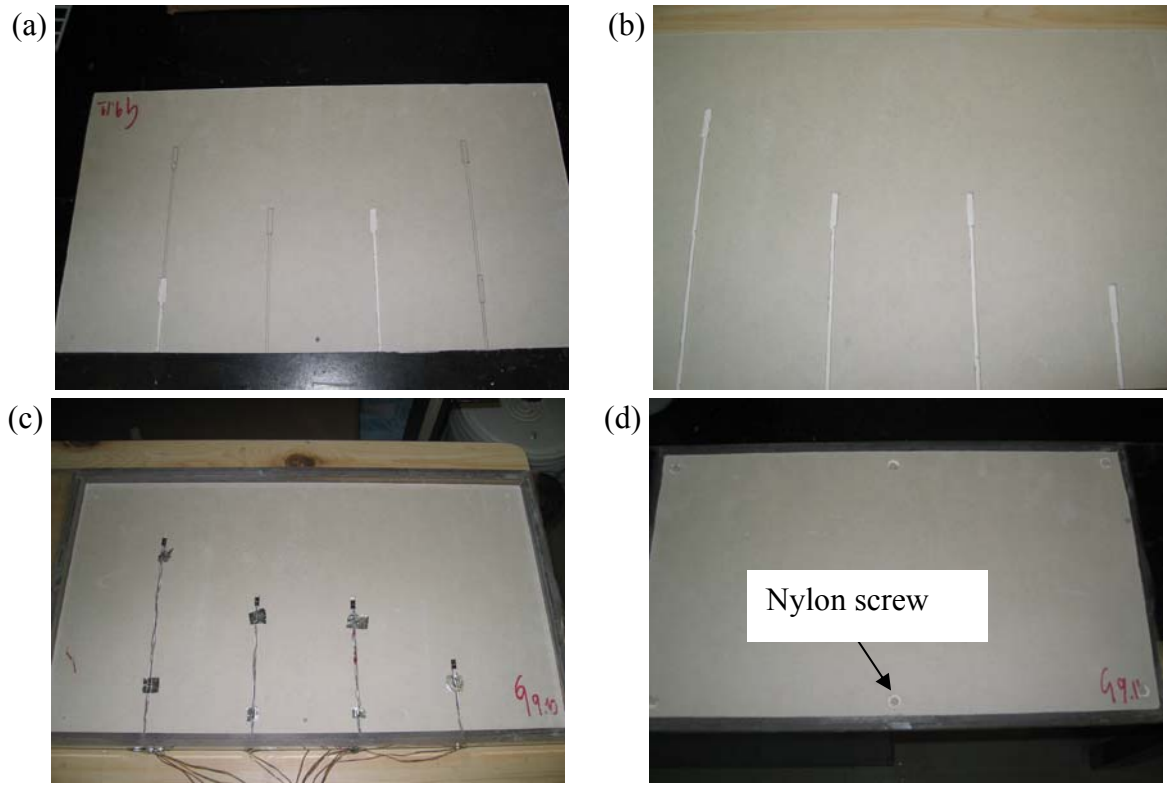

Figure 3. Gypsum boards showing the machined grooves to hold sensors in the (a) bottom board, (b) middle board and (c) middle board with sensors in place, and the (d) entire bed held together with six nylon screws.

3. Tests Cases

In the tests, initially dry gypsum boards (30% RH) are subject to a high humidity air flow (70% RH) for a period of 8 or 24 h, followed by an equal period of dry air flow (30% RH). A total of five tests are conducted to investigate: the effect of cycle length (8 or 24 hours), Reynolds number (2000 or 5000) and coatings on the top layer of the gypsum bed (uncoated, acrylic paint coated and latex paint coated). Table 2 provides the test conditions for the five tests. The

convective moisture and heat transfer coefficients for each test and a complete listing of material properties (density, specific heat, thermal conductivity, vapor permeability and sorption) can be found in the final report of Subtask 2 of IEA/ECBCS Annex 41 [1].

Table 2. Test conditions and material used in the tests.

Test	Description of gypsum boards	Re	Initial conditions		Air flow conditions		
			T_i (ºC)	RH_i(%)	T_∞ (ºC)	RH_∞ (%)	Time (h)
1	All 3 gypsum boards uncoated	2000	23.3	30	23.8	71.9	24
					22.5	29.6	24
2	All 3 gypsum boards uncoated	2000	23.7	32.1	23.6	71.2	8
					23.6	31.9	8
3	All 3 gypsum boards uncoated	5000	22.7	31.6	23.2	71.4	24
					23.2	30.9	24
4	Acrylic coated board on top of 2 uncoated boards	2000	24	34.6	23.2	72.2	24
					23.2	30.8	24
5	Latex coated board on top of 2 uncoated boards	2000	24.1	31.4	23.4	70.9	24
					23.4	31.2	24

4. Numerical Models

The numerical models used in the common exercise are 1-D or 2-D models for diffusive heat and moisture transfer within a porous bed. In most of the models, the convective heat and moisture transfer between the air and the porous bed are calculated using convective boundary conditions with specified transfer coefficients; however, two models use computational fluid dynamics (CFD) to calculate the heat and moisture transfer between the moist air and the gypsum bed. Numerical results from the following countries, institutes and models are used in this paper:

- Katholieke Universiteit Leuven, Belgium [20]
- Slovak Academy of Science, Slovakia [21]
- Concordia University, Canada [9]
- Concordia University, Canada
- IRC-NRC, Canada [9]
- Technical University of Dresden, Germany
- Chalmers University of Technology, Sweden [22]
- Thermal Science Centre of Lyon, France [23]
- Ghent University, Gent , Belgium
- University of Saskatchewan, Canada [17, 24]

The effect of the paint layer on the gypsum bed is investigated with two different methods. In one method, the moisture transfer resistance of the paint is included in the moisture transfer coefficient between the gypsum and the air. In the other method, the paint layer is modeled as a separate porous layer.

5. Experimental and Numerical Results

5.1 Transient Data A comparison of relative humidity and temperature measured and simulated at depths of 12.5 mm and 25 mm in the gypsum bed are provided in Figure 4 for uncoated gypsum. Each simulation is identified as a number from 1 to 10 for anonymity. The thicker dashed lines represent the two CFD models. The data from the different numerical simulations are in good agreement and follow the same trend as the experimental data with the exception of

one of the CFD models. The simulation results are closer to the experimentally measured results at a depth of 12.5 mm than at a depth of 25 mm in the bed. The simulations also agree better during the adsorption phase than during the desorption phase of the test.

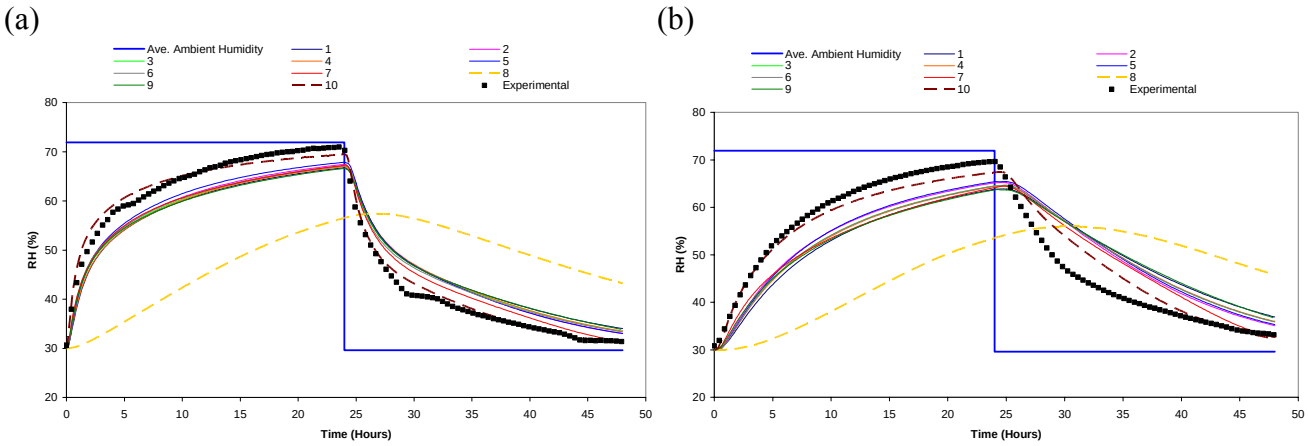

Figure 4. Measured and simulated relative humidities at depths of (a) 12.5 mm and (b) 25 mm in a bed of uncoated gypsum boards (test 1).

The experimental and numerical temperatures in the gypsum boards at depths of y = 12.5 and 25 mm are presented in Figure 5. At the beginning of the adsorption phase, the temperature in the gypsum rises above the air temperature due to the phase change energy released as water vapor adsorbs in the dry gypsum bed. Similarly, there is a noticeable cooling effect at the beginning of the desorption phase. Near the end of the adsorption and desorption phases, the temperature of the boards approach the temperature of the air flow. The temperatures at depths of 12.5 and 25 mm in the gypsum bed are nearly equal because the test is nearly isothermal. In fact, some numerical simulations used a constant temperature throughout the bed for the duration of the test, with little apparent influence on the calculated moisture transfer.

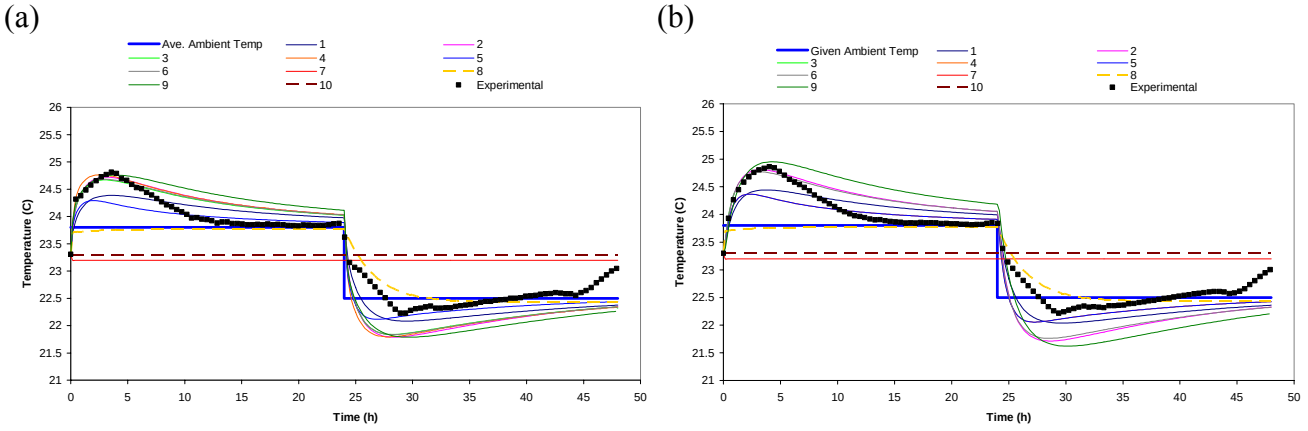

Figure 5. Measured and simulated temperatures at depths of (a) 12.5 mm and (b) 25 mm in a bed of uncoated gypsum boards (test 1).

The measured and simulated vapor pressures are presented in Figure 6 and show very good agreement for most of models.

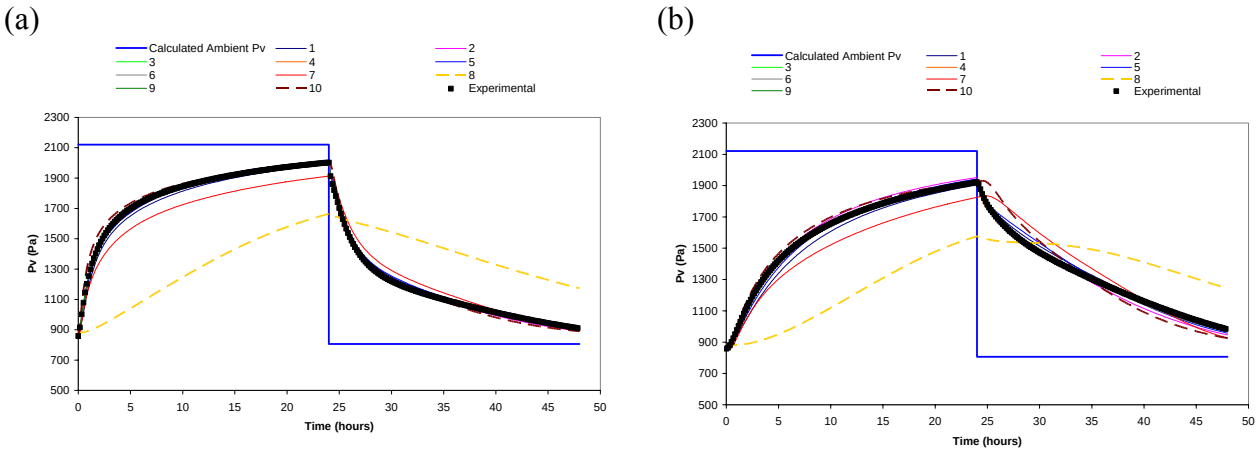

Figure 6. Measured and simulated vapor pressure at a depth of (a) 12.5 mm and (b) 25 mm in the uncoated gypsum bed for test 1.

The measured and simulated changes in moisture content for the uncoated gypsum bed (test 1) are presented in Figure 7. Considering the uncertainty in the measured data, the agreement between the experimental and numerical data is quite good. All of the experimental and numerical data agree within the experimental uncertainty bounds, except for CFD simulation 8.

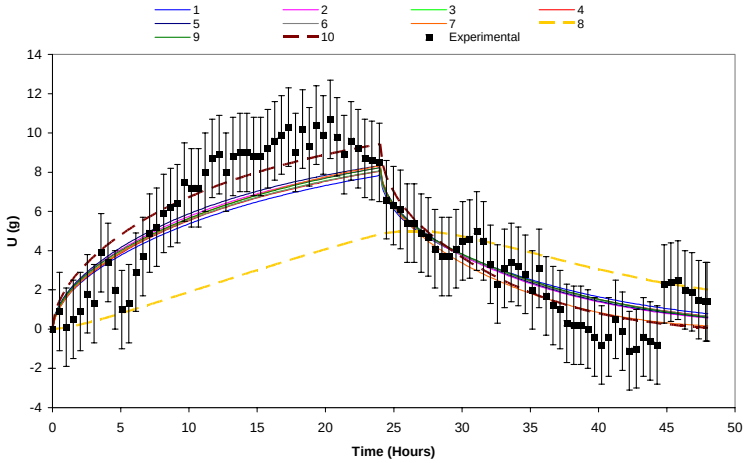

Figure 7. Measured and simulated change in mass during test 1 in the uncoated gypsum bed.

5.2 Quasi-steady Data The transient data for the other four tests also show good agreement between the experimental and numerical data [1]. A convenient way to compare the different tests and quantify the agreement between the numerical and experimental results is to compare the maximum change during the adsorption and desorption cycles. The maximum change is calculated as the difference between the conditions at the end of a cycle and the conditions at the beginning of the cycle:

$$\Delta X = X_{\text{end of cycle}} - X_{\text{beginning of cycle}} \quad (1)$$

where ΔX is the calculated change in relative humidity or mass accumulation between the end of the adsorption/desorption cycle ($X_{\text{end of cycle}}$) and the beginning of the same cycle ($X_{\text{beginning of cycle}}$). Figures 8-10 contain the results for the maximum change in humidity and mass during each cycle for all five tests. The CFD simulations and distinguished with small square symbols.

Figures 8 and 9 show that the simulation results are closer to the experimental results during the adsorption cycle than during the desorption cycle, indicating that hysteresis may be important. The numerical results from the painted bed (tests 4 and 5) show better agreement among each other when the paint is treated as an extra resistance in the surface transfer coefficient than when it is treated as a separate porous media. An increased transfer coefficient (test 3 with Re=5000) above the gypsum bed has a negligible effect on the relative humidity in the bed when compared to the base case (test 1 with Re=2000). The numerical results at a depth of y = 25 mm in the gypsum bed have a larger spread than the results at y = 12.5 mm.

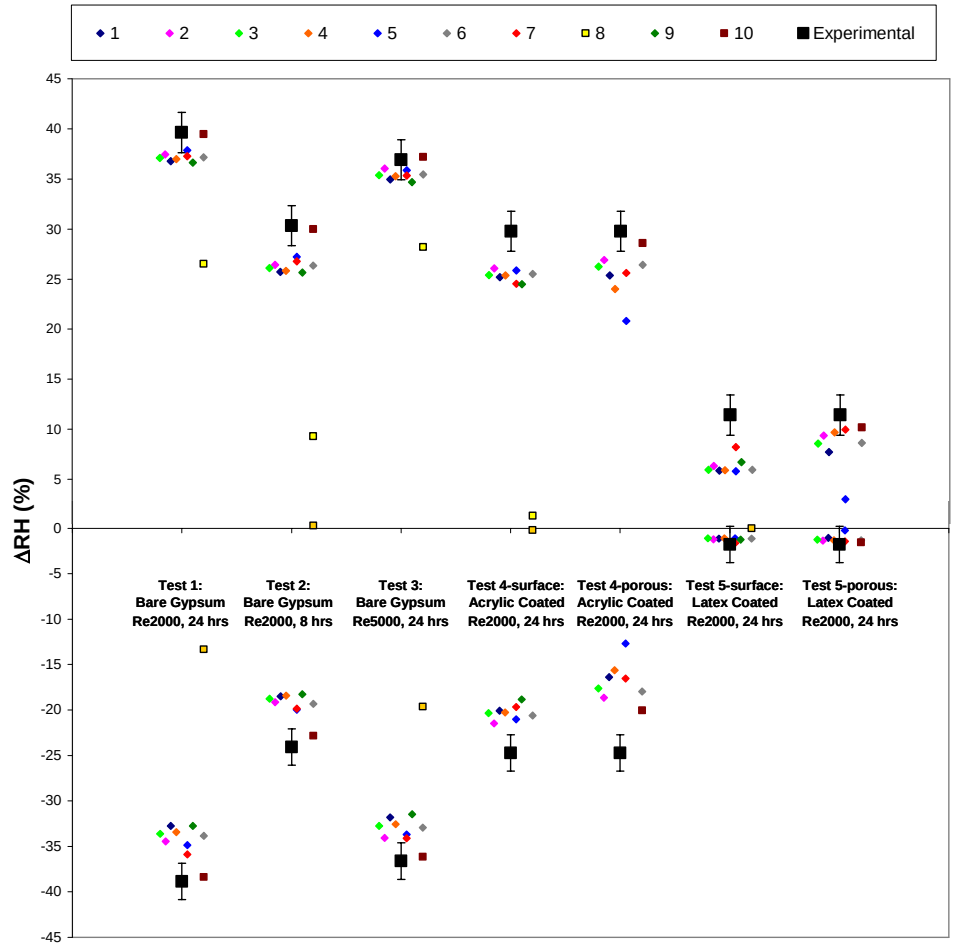

Figure 8. Change in relative humidity during each cycle at a depth of 12.5 mm in the gypsum bed.

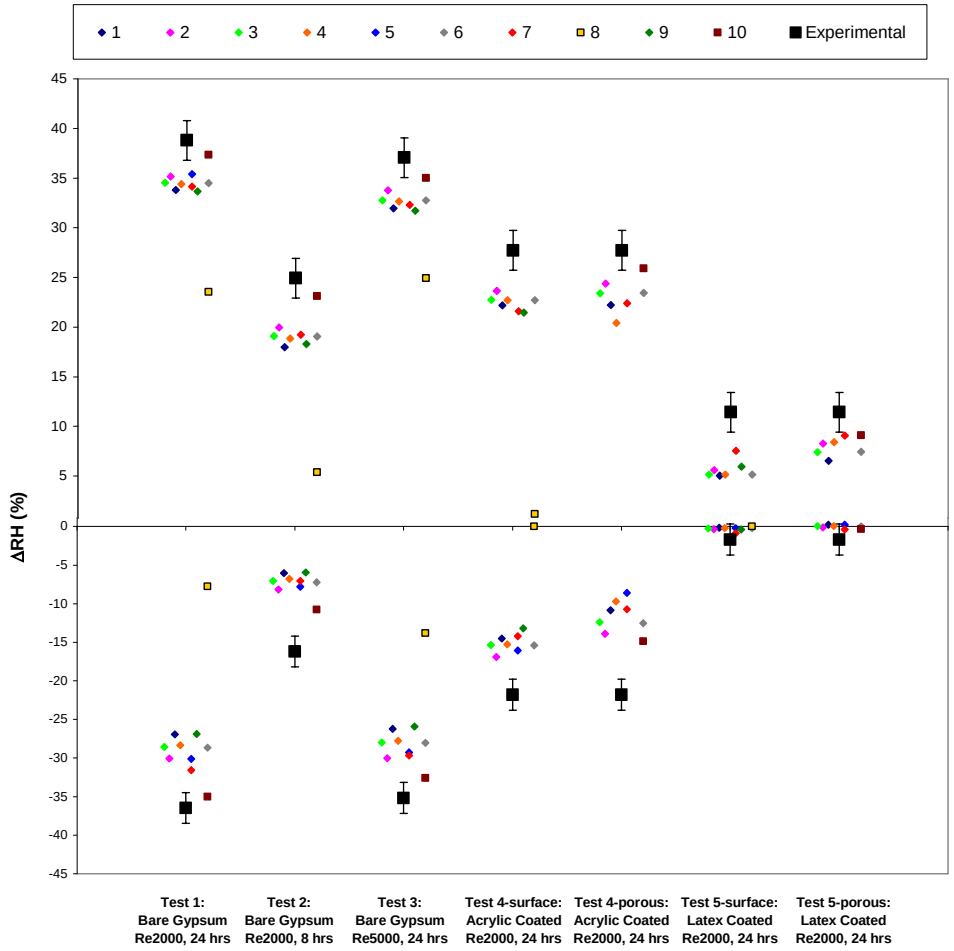

Figure 9. Change in relative humidity during each cycle at a depth of 25 mm in the gypsum bed.

Figure 10 contains the measured and simulated change in mass during the adsorption and desorption phases for all five tests. In general, the moisture gain and loss is simulated quite accurately. There is also good agreement between the different simulations for each test.

(a) (b)

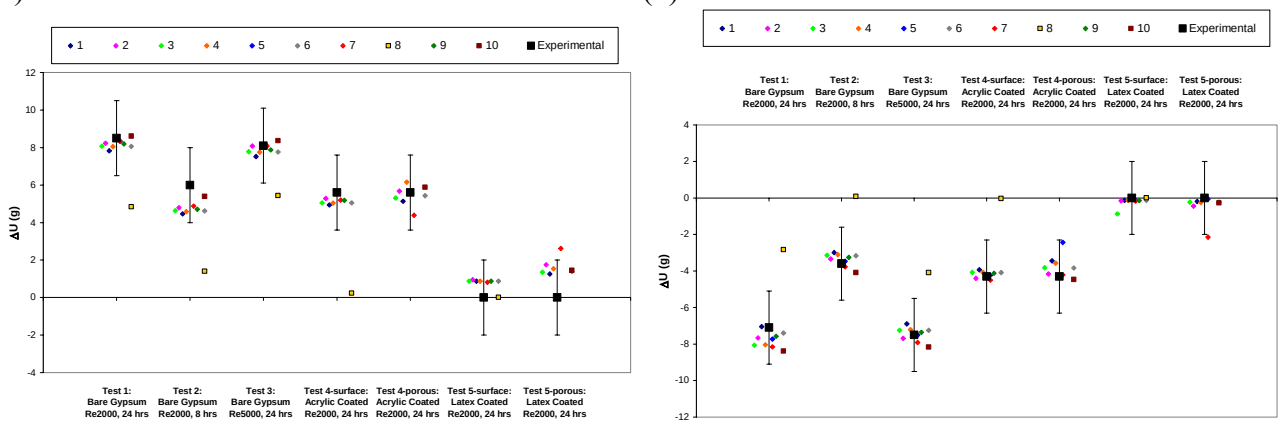

Figure 10. Moisture (a) gain during the adsorption phase and (b) loss during the desorption phase.

5.3 Sensitivity Study In the common exercise, a sensitivity study is performed to show which material properties (sorption, vapor diffusion, or transfer coefficients) have the greatest effect on heat and moisture transfer in the gypsum bed and to demonstrate the sensitivity of the results to uncertainties in the input property data. In the sensitivity study, the variations in the material property data are based on measurement uncertainties [1]. On average, the equilibrium moisture content (sorption curve) is decreased by 10% or increased by 20%; the vapor permeability is varied by ±20%, ±30% and ±20% for the uncoated gypsum board, the acrylic coating and the latex coating respectively, while the heat and moisture transfer coefficients are varied by ±10%. Each sensitivity study is carried out individually. The effect of sorption hysteresis is also investigated as discussed in the final report of Subtask 2 [1]. Figure 11 shows the effect of changing the properties on moisture accumulation. Humidity data are presented in reference [1].

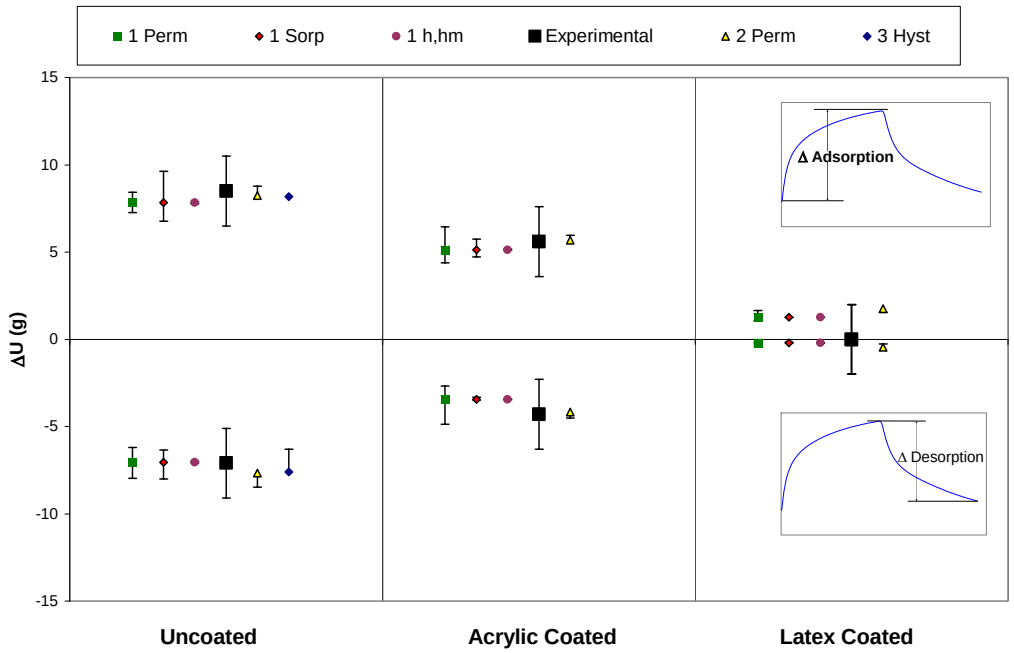

Figure 11. Results of the sensitivity study for moisture accumulation in the uncoated (test 1), acrylic coated (test 4) and latex coated (test 5) gypsum beds.

Figure 11 shows that a change of ±10% in the transfer coefficients has a small effect on the moisture accumulation. The -10%/+20% change in the sorption isotherm has the largest effect on the moisture accumulation in the uncoated gypsum bed while the ±20% or ±30% change in vapor permeability has the largest effect on the moisture accumulation in the coated beds. Hysteresis can be seen to have an effect that is similar to varying the sorption isotherm or the water vapor permeability.

6. Conclusions

The IEA/ECBCS Annex 41 Subtask 2 common exercise summarized in this paper validated numerous numerical simulations with carefully measured experimental data. The experimental and numerical data set can be used to benchmark models of 1-D heat and moisture transfer within a gypsum bed subject to step changes in the relative humidity (from 30% RH to 70% RH and back to 30% RH) of the air flowing above the bed. The relative humidity and temperature at

two depths in the gypsum bed were measured and simulated for five different cases. Three cases were for unpainted gypsum boards: one with a 24 hour period between step changes, one with an 8 hour period between step changes and one with a higher, non-laminar, airflow above the bed. Two cases were for a coated bed where the top gypsum board was painted with acrylic or latex paint.

The results in this paper show very good agreement between most of the experimental and numerical data and between most of the models. Of the ten models used in the exercise, only one model gave results that differed significantly from the experimental data and the numerical data of the other models. In general, the agreement between the experimental and numerical data was better during the adsorption cycle and nearer the convective surface of the gypsum bed, than during the desorption cycle and deeper within the bed.

A sensitivity study was performed to determine the effect of measurement uncertainties in the material properties (sorption isotherm, vapor permeability and convective transfer coefficients) and sorption hysteresis on the simulated moisture accumulation. The results show that the uncertainty in the sorption isotherm had the largest effect in the uncoated gypsum bed, while the vapor permeability had the largest effect in the coated gypsum beds. The uncertainty in the convective transfer coefficients showed little influence on the moisture transfer. The simulation data showed that including hysteresis will improve the agreement between the numerical and experimental data during the desorption phase, and the influence is similar to the influence of the sorption and vapor permeability uncertainties.

The paint layer had a substantial effect on the moisture transfer to/from the gypsum bed and was simulated by two different methods. One method included the paint in the surface transfer coefficient while the other treated the paint as a separate porous layer with its own material properties. Incorporating the paint into the surface transfer coefficient proved to be very accurate and provided results that were comparable to treating the paint as a separate porous layer.

The most important factor when simulating 1-D heat and moisture transfer in a gypsum wall is the type of surface coating applied to the gypsum. Of the parameters studied in this exercise, the surface coating had the largest effect on the moisture transfer in the gypsum. The next most important factor is accurate property data for the sorption isotherm and vapor permeability.

Acknowledgements
This work was carried out as part of IEA/ECBCS Annex 41. The data, inspiration and insight provided by the participants in the Annex are greatly appreciated. Financial support from the Natural Science and Engineering Research Council of Canada (NSERC) Special Research Opportunity Program and the Canada Foundation for Innovation (CFI) are also noted.

References

[1] S. Roels, C. James, H. Janssen, P. Talukdar, C.J. Simonson, Experimental analysis of moisture buffering, Annex 41, Subtask 2 Final report, (2008), *in press*.

[2] C-E. Hagentoft, A.S. Kalagasidis, B. A-Zarrabi, S. Roels, J. Carmeliet, H. Hens, J. Gruenwald, M. Funk, R. Becker, D. Shamir, O. Adan, H. Brocken, K. Kumaran, R. Djebbar, Assessment Method of Numerical Prediction Models for combined heat, air and

moisture transfer in building components: Benchmarks for one-dimensional cases, Journal of Thermal Envelope and Building Science, 27 (4) (2004) 327-352.

[3] C.J. Simonson, M. Salonvaara, and T. Ojanen, The effect of structures on indoor humidity – possibility to improve comfort and perceived air quality, Indoor Air, 12 (2002) 243-251.

[4] O.F. Osanyintola, C.J. Simonson, Moisture buffering capacity of hygroscopic building materials: Experimental facilities and energy impact, Energy and Buildings, 38 (2006) 1270-1282.

[5] C. Rode, N. Mendes, K. Grau, Evaluation of moisture buffer effects by performing whole-building simulations, ASHRAE Transactions, 110 (2) (2004) 783-794.

[6] C.J. Simonson, M. Salonvaara, and T. Ojanen, Moderating indoor conditions with hygroscopic building materials and outdoor ventilation, ASHRAE Transactions, 110 (2) (2004) 804-819.

[7] A.H. Holm, H.M. Kuenzel, K. Sedlbauer, Predicting indoor temperature and humidity conditions including hygrothermal interactions with the building envelope, ASHRAE Transactions, 110 (2) (2004) 820-826.

[8] C.J. Simonson, M. Salonvaara, T. Ojanen, Heat and mass transfer between indoor air and a permeable and hygroscopic building envelope, Part I – Field measurements, Journal of Thermal Envelope and Building Science, 28(1), 63-101

[9] F. Tariku, K. Kumaran, Hygrothermal modeling of aerated concrete wall and comparison with field experiment, 3rd International Building Physics Conference, Montreal, Canada, 321-328, August 27-31 (2006).

[10] C.J. Simonson, T. Ojanen, M. Solonvaara, Moisture performance of an airtight, vapour permeable building envelope in a cold climate, Journal of Thermal Envelope and Building Science, 28 (3) (2005) 205-226.

[11] K. Svennberg, K. Lengsfeld, L-E Harderup, A. Holm, Previous experimental studies and field measurements on moisture buffering by indoor surface materials, Journal of Building Physics, 30 (2007) 261-274.

[12] T. Kalamees, J. Vinha, Indoor humidity loads and moisture production in lightweight timber-frame detached houses. Journal of Building Physics, 29 (3) (2006) 219-245.

[13] J.A. Jenssen, S. Geving, R. Johnsen, Assessments on indoor air humidity in four different types of dwelling randomly selected in Trondheim, Norway, Proceedings of the 6th Symposium on Building Physics in the Nordic Countries, Trondheim, Norway (2002).

[14] H. Hens, Indoor climate in student rooms: Measured values. IEA-Annex 41 MOIST-ENG, Working Meeting, Glasgow, 2004.

[15] M. Qin, R. Belarbi, A. Ait-Mokhtar, Alain Seigneurin, An analytical method to calculate the coupled heat and moisture transfer in building materials, International Communications in Heat and Mass Transfer, 33 (1) (2005) 39-48.

[16] P. Talukdar, S.O. Olutimayin, O.F. Osanyintola, C.J. Simonson, An experimental data set for benchmarking 1-D, transient heat and moisture transfer models of hygroscopic building materials, Part I: Experimental facility and material property data, International Journal of Heat and Mass Transfer, 50 (2007) 4527-4539.

[17] P. Talukdar, O.F. Osanyintola, S.O. Olutimayin, C.J. Simonson, An experimental data set for benchmarking 1-D, transient heat and moisture transfer models of hygroscopic building

materials, Part II: Experimental, numerical and analytical data, International Journal of Heat and Mass Transfer, 50 (2007) 4915-4926.

[18] C.R. Iskra, C.J. Simonson, Convective mass transfer coefficient for a hydrodynamically developed airflow in a short rectangular duct, International Journal of Heat and Mass Transfer, 50 (2007) 2376-2393.

[19] P. Talukdar, C.R. Iskra, C.J. Simonson, Combined heat and mass transfer for laminar flow of moist air in a 3D rectangular duct: CFD simulation and validation with experimental data, International Journal of Heat and Mass Transfer, (2007) *in press*, http://dx.doi.org/10.1016/j.ijheatmasstransfer.2007.08.034.

[20] H. Janssen, B. Blocken, J. Carmeliet, Conservative modelling of the moisture and heat transfer in building components under atmospheric excitation, International Journal of Heat and Mass Transfer, 50 (2007) 1128-1140.

[21] H.M. Kunzel, Verfahren zur ein- und zweidimesionalen Berechnung des dekoppelten Warme und Feuchtetransports in Bauteilen mit einfachen Kennwerten. Dissertation. Universitat Stutgart (1994).

[22] A.S. Kalgasidis, HAM-Tools. An integrated simulation tool for heat, air and moisture transfer analyses in building physics, Doctoral thesis (2004) ISBN 91-7291-439-4

[23] J. Kwiatkowski, K. Feret, M. Woloszyn, J.J. Roux, Predicting indoor relative humidity using buildings simulation tools, 6th International Conference on Indoor Air Quality, Ventilation & Energy Conservation in Buildings, Sendai, Japan, October 28-31 (2007).

[24] S. Olutimayin and C. Simonson, Measuring and modelling vapor boundary layer growth during transient diffusion heat and moisture transfer in cellulose insulation, International Journal of Heat and Mass Transfer,48 (2005) 3319-3330.

INDOOR CLIMATE CONDITIONS AND HYGROTHERMAL LOADS IN FINNISH AND ESTONIAN DWELLINGS

Targo Kalamees, Ph.D.,
Chair of Building Physics and Architecture, Tallinn University of Technology;
Department of Civil Engineering, Tampere University of Technology;
Laboratory of Heating, Ventilating and Air-Conditioning, Helsinki University of Technology;
targo.kalamees@ttu.ee

Juha Vinha, Dr.Tech., Minna Korpi, M.Sc,
Department of Civil Engineering, Tampere University of Technology;
juha.vinha@tut.fi, minna.korpi@tut.fi

Jarek Kurnitski, Dr.Tech.,
Laboratory of Heating, Ventilating and Air-Conditioning, Helsinki University of Technology;
jarek.kurnitski@tkk.fi

KEYWORDS: *indoor climate, hygrotthermal loads, moisture excess, moisture production, moisture buffering*

SUMMARY:
The actual indoor temperature is the most important data to assess indoor climate and thermal comfort as well as for energy consumption. To understand how ventilation and structures influence the indoor climate, the use of field measurements is a valuable tool that makes it possible to show the importance of structures under real use in houses. This paper summarises, the results of field measurements of indoor climate conditions in Finnish and Estonian dwellings, made during IEA Annex 41. The temperature and RH were continuously measured in 128 houses and in 13 apartments at one–hour intervals over a one-year period.
An extended period of high indoor temperatures during summer suggests that thermal comfort was not considered in the original design. During winter, despite of almost ideal average temperatures, the variations in temperature was larger than expected to be produced by modern heating systems and well insulated envelopes. Small differences in the daily amplitude of the relative and absolute humidity were shown in the comparison of the hygroscopic and non-hygroscopic cases. A very similar dampening effect was seen when balanced ventilation was compared to other ventilation systems. The building orientation and a large number of uncontrolled factors had an important effect on the indoor climate because the variation of indoor climate parameters was much higher between single houses than between subdivisions compared.
For the hygrothermal analysis of the building envelope, the critical values of the moisture excess were determined by using the measurement results from single–family detached houses. The determined design curve of moisture excess curve on the 10 % critical level is +4 g/m^3 during the cold period ($T_{out} \leq +5$ °C) and +1.5 g/m^3 during the warm period ($T_{out} \geq +15$ °C) for detached houses (commonly low occupancy and normal ventilation). The determined moisture excess for apartments with high occupancy and low ventilation was +6 g/m^3 during the cold period. During the winter season, the average moisture production in the studied houses was 6 kg/day/house and 2 kg/day/person, which can be considered a reasonable value for many indoor climate simulations. During the winter season, the average value of daily maximum moisture production values from different houses was 13 kg/day/house and 4 kg/day/person.

1. Introduction

As people spend more time indoors, the quality of the indoor environment is becoming very important. The actual indoor temperature is the most important data to assess indoor climate and thermal comfort as well as for energy consumption. Absolute humidity and relative humidity (RH) are important parameters for hygrothermal design and indoor climate, respectively. Temperature and humidity have also a significant impact on perceived air quality. A major result caused by moisture damages is health effects on the occupants. The evidence of a causal association between dampness and health effects is strong. However, the mechanisms are unknown, as shown in comprehensive reviews by Bornehag et al. (2001 and 2004).

Due to the cold climate, buildings in Finland and in Estonia are normally designed according to the outdoor climate conditions in winter. Since now, outdoor climate conditions in summer have not usually been taken into account. However, recently after heat waves in 2003 and 2006, a discussion of summer thermal comfort has begun. In addition, the understanding about the quality of indoor environment has changed over the last decades. Due to rising living standards, requirements for thermal comfort and healthy indoor air have been raised. As air conditioning and special shadings for solar protection have become normal solutions in modern office buildings, these may become common in dwellings as well. In cold climate in winter, low outdoor humidity combined with overheating may result in indoor humidifying that would strongly increase humidity loads. Portative humidifiers used in bedrooms of sensitive people provide a lower effect, but it is still to be taken into account.

It is also to be taken into account in the hygrothermal performance as specifications in the indoor climate and ventilation codes and standards influence directly indoor hygrothermal loads. Indoor climate and ventilation specification together with occupant behaviour produce real indoor loads. In many cases the methods, how boundary conditions are defined, may strongly influence the results of hygrothermal simulations. Holm and Künzel (2001) point out that the influence of the exterior and interior climate conditions on the results of hygrothermal simulations is comparable (sometimes even higher) to the influence of the material property variation. Although boundary conditions are very important parameters, there have usually been given small attention for him. Often constant values are given for variable values and durability calculations are made with average climatic data. As many factors affect indoor loads, probably the most reliable way to determine the relevant design values is to perform long-term field measurements in a representative sample of dwellings.

This paper summarises, the results of field measurements of indoor climate conditions in Finnish and Estonian dwellings, made during IEA Annex 41 (Vinha et al. 2005, Kalamees et al. 2006, Kalamees 2006a, Kalamees 2006b, Kalamees et al. 2007). The temperature and RH were continuously measured in 128 detached houses (125 bedrooms, 96 living rooms) and in 13 apartments at one–hour intervals over a one-year period. The level and the stability of indoor temperature and relative humidity as well moisture excess and moisture production were analyzed in the subdivisions of houses categorized according to outdoor temperature, ventilation system and type of envelope assembly.

2. Methods

2.1 Dwellings studied

To study the indoor climate and hygrothermal loads in dwellings, the field measurements were carried out in 128 lightweight timber-frame detached houses occupied by single–families in Finland (mainly close to Tampere and Helsinki region) and in Estonia (mainly close to Tallinn region). The houses were randomly selected from the databases of the manufacturing and construction companies. The houses were relatively new, built, on average, four-five years prior to the measurements. The studied houses had three different types of ventilation systems: passive stack ventilation (referred to as natural ventilation in this study), mechanical exhaust ventilation and the mechanical supply and exhaust ventilation (referred to as balanced ventilation in this study). In all of the studied rooms, windows were available for airing purposes.

To study the hygrothermal loads in dwellings with higher occupancy, measurements were carried out in a small control group: in 13 apartments. All the apartments were supplied with the natural ventilation (passive stack ventilation and window airing) in all apartments.

Table 1 shows the main characteristic of the studied dwellings.

Table 1 Main characteristic data of the measured dwellings

	Finnish detached houses, n=101	Estonian detached houses, n=27	Estonian apartments, n=13
Measurement period	July 2002 … June 2004	April 2003….July 2005	Dec. 2005…April 2006
Floor area	153 m^2	135 m^2	55 m^2
Volume	386 m^3	344 m^3	136 m^3
Occupancy	43 m^2/person	46 m^2/person	17 m^2/person
Envelope air leakage rate	4.0 $m^3/(h \cdot m^2)$	4.2 $m^3/(h \cdot m^2)$	5.0 $m^3/(h \cdot m^2)$
at 50 Pa	3.9 1/h	4.9 1/h	6.7 1/h
Ventilation rate	0.38 ach 13 l/(s·pers.), 0.26 l/(s·m^2)	0.41 ach 13 l/(s·pers.), 0.28 l/(s·m^2)	

2.2 Measurements

The values of temperature and RH were measured with data loggers at one–hour intervals from inside and outside the building over a one-year period (in apartments over a four-month period). The indoor loggers were located on separating walls in bedrooms and living rooms. The outdoor loggers were located on the north facade, protected from direct solar radiation and driving rain. The accuracy of the loggers was checked before and after both measurement years. As in the Finnish study after the second measurement year, the measuring accuracy of almost all outdoor data loggers was below the acceptable level, for the second measurement year, the outdoor climate was retrieved from the nearest weather station.

The exhaust air flow rates were measured with anemometers and manometers. In the Finnish study, in addition to instantaneous measurements in 74 houses, the air change rates were measured using a homogenous constant emission (passive) method (Nordtest, 1997). Small perfluorocarbon tracer gas (PFT) samplers were distributed in the house (7-13 samplers per house depending on house volume and number of rooms). The tracer gas was continuously released at a constant rate to the room air. Passive diffusion samplers were placed in each room to sample tracer gas at steady state room air concentration. Measurement period in each house lasted three weeks. After the sampling period, the samplers were capped and analysed in laboratory. The actual air change rates in apartments were not known, because these depend a lot on climatic conditions and the use of window airing.

The air leakage of each house and apartment was measured with the standardized (EN 13829:2000) fan pressurization method. To compare different buildings, the air flow rate at the pressure difference 50 Pa was divided by the internal volume of the building (result n_{50} value) or by the external envelope area (resulting air leakage rate at 50 Pa).

A questionnaire was completed for each house and apartment, where the building characteristics, used building materials, type of HVAC systems and its use, occupants' habits, typical complaints and symptoms related to indoor air quality, etc. were interviewed from occupants acting as contact persons of the study. For purposes of comparison, similar questionnaires were used in Estonian and in Finnish studies.

2.3 Assessment of indoor climate and indoor humidity loads

Assessment of indoor climate was done according to the Finnish classification of the indoor climate (FiSIAQ 2001) and to the Estonian standard of the indoor climate (EVS 839:2003). Both references set the target values for three categories, Table 2. The lowest and average categories were chosen to compare the results.

Table 2 Target values for the indoor temperature (T) and RH

	Finland, (FiSIAQ 2001)				Estonia, (EVS 839:2003)			
	Summer		Winter		Summer		Winter	
	T, °C	RH, %	T, °C	RH, %	T, °C	RH, %	T, °C	RH, %
A and S1	23-24	-*	21-22	25-45	24-25	30-70	21-23	25-45
B and S2	23-26	-*	20-22	-*	23-26	30-70	20-24	25-45
C and S3	22-27	-*	20-23	-*	22-27	30-70	19-25	25-45

*As categories S2 and S3 do not specify RH values, the range 20…60 % was used as a criterion for the acceptable RH in Finnish houses.

The values of the moisture excess Δv (the difference between the indoor and outdoor air's absolute humidity, Eq. 1) were calculated on the basis of the measured results of the indoor and outdoor temperatures and RH. Absolute humidity values were averaged for weekly average values.

$$\Delta v = v_i - v_e , \qquad (1)$$

where Δv indicates the moisture excess [g/m^3], v_i humidity by volume of the indoor air [g/m^3] and v_e humidity by volume of the outdoor air [g/m^3].

On the basis of the dependence of moisture excess on the outdoor temperature, frequency distributions of moisture excess during the cold period ($T_{out} \leq 5$ °C) were analyzed separately from other data ($T_{out} > 5$ °C). To analyze the dependence of the moisture excess on the outdoor temperature and to determine the critical moisture excess values, the data from each room were sorted according to the outdoor air temperature, using a 1 °C step of the outdoor temperature. From these sorted values, 10 % critical levels were calculated. On the basis of moisture excess and indoor temperature dependence on the outdoor temperature, the critical moisture excess levels are given for the cold period ($T_{out} \leq 5$ °C) and on the basis of the dependence of the indoor temperature on the outdoor temperature, the critical moisture excess levels are presented for the warm period ($T_{out} \geq 15$ °C).

On the basis of the air change rate during winter and the moisture excess during the cold period, the daily average moisture production G, [kg/day] was estimated in detached houses, Eq. 2:

$$G = q_v \cdot \Delta v, \qquad (2)$$

where Δv indicates the moisture excess [kg/m^3], and q_v stands for the air change rate [m^3/day].

Moisture production was calculated from the measured air change rate during winter. The actual air change rates during summer were not known, because these depend on the use of window airing and infiltration. As the ventilation air change rate was measured for the whole building, the moisture excess values were the average values of the results of bedroom and living room measurements.

3. Results

Temperature and RH measurements were carried out during 2002-2005 in Finland and in Estonia. Measurements lasted for one year in each house. Indoor temperature and humidity conditions were analyzed separately during the summer and the winter season in two measurement years. In Finland, the analyzed summer season was during the first measurement year, between 1.7…10.9.2002 (average T_{out} +19 °C) and during the second measurement year, between 4.7…25.08.2003 (average T_{out} +19 °C). The winter season analyzed in the measured houses lasted for three winter months: from the beginning of December to the end of February. The average outdoor temperature during the first measurement winter was -8 °C (minimum -29 °C) and during the second measurements winter it was T_{out} -4 °C (minimum -22 °C). In Estonia, the analyzed summer season lasted for three summer months: from the beginning of June to the end of August. The average outdoor temperature during the first measurement summer was +17 °C and during the second measurements summer it was +18 °C. The average outdoor temperature during the first measurement winter was -2 °C (minimum -16 °C) and during the second measurements winter it was T_{out} -1 °C (minimum -15 °C).

3.1 Indoor temperature and humidity conditions during summer seasons

The average indoor temperature during the summer seasons in Finnish detached houses was +24.8 °C (min. average being +22.2 °C and max. average +28.5 °C) and the average indoor RH was 51 % (min. average being 34 % and max. average 60 %). During the first summer 19 % of the rooms and during the second summer only 2 % of the rooms remained below the higher limit of the indoor climate category S2. Thermal requirements of the indoor climate category S3 fulfilled 53 % of rooms during the first summer and 63 % of rooms during the second summer. In Estonian detached houses the average indoor temperature during the summer seasons was +23.5 °C (min. average being +21.0 °C and max. average +25.7 °C) and the average indoor RH was 55 % (min. average being 43 % and max. average 72 %). During summer, only 13 % of the rooms (with 5 % excess) met the requirements of the temperature in indoor climate category C. Figure 1 shows all the temperature (left) and RH (right) measurement results in measured detached houses during summer seasons. Average values of the temperature, RH and humidity by volume during summer seasons divided into subdivisions according to the ventilation systems are shown in Table 3.

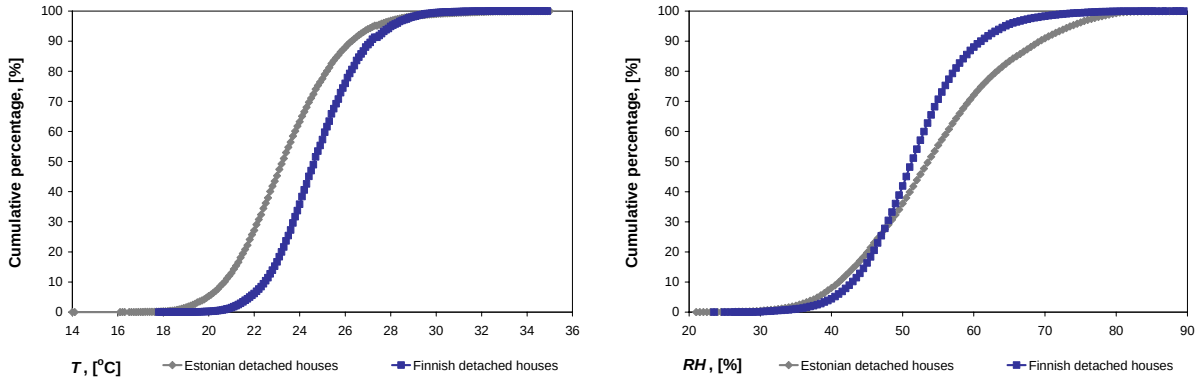

Figure 1 Distribution of the hourly indoor temperature (left) and RH (right) during two summer seasons in Finnish and Estonian detached houses

Table 3 Average values of the temperature (T), RH and the humidity by volume (v) during summer

	Finnish houses						Estonian houses					
	Summer I: 46 houses, 78 rooms			Summer II: 50 houses, 97 rooms			Summer I: 12 houses, 22 rooms			Summer II: 15 houses, 17 rooms		
	T, °C	RH, %	ν, g/m^3	T, °C	RH, %	ν, g/m^3	T, °C	RH, %	ν, g/m^3	T, °C	RH, %	ν, g/m^3
Natural vent.	+24.2	52	11.4	+24.4	53	11.8	+22.9	62*	12.7*	+23.4	54	12.2
Exhaust vent.	+24.7	50	11.3	+24.8	51	11.7	+23.3	56*	11.6*	+23.5	55	10.8
Balanced vent.	+24.6	51	11.4	+25.0	51	11.9	+24.2	49*,*	10.8*,*	+23.8	51	10.9
All data	+24.6	51	11.3	+24.9	51	11.8	+23.4	56	11.6	+23.6	53	11.0

* The difference is significant, P < 0.05

3.2 Indoor temperature and humidity conditions during the winter seasons

The average indoor temperature during the winter seasons in Finnish detached houses was +21.6 °C (min. average being +16.9 °C and max. average +26.5 °C) and the average indoor RH was 26 % (min. average being 14 % and max. average 47 %). The thermal requirements of the indoor climate category S3 fulfilled 2 % of rooms during the first winter and 4 % of rooms during the second winter. The average indoor temperature during studied winter seasons from all Estonian detached houses was +21.3 °C (min. average being +17.1 °C and max. average +26.1 °C) and the average indoor RH was 32 % (min. average being 23 % and max. average 48 %). Only 18 % of rooms met the requirements of the temperature in indoor climate category B and the requirements of indoor climate category C were met by 45 % of the rooms (with 5 % excess). All the temperature and RH measurement results in the measured dwellings during winter seasons are shown in Figure 2. Average values of the temperature, RH and humidity by volume during winter seasons in subdivisions according to the ventilation systems are shown in Table 4.

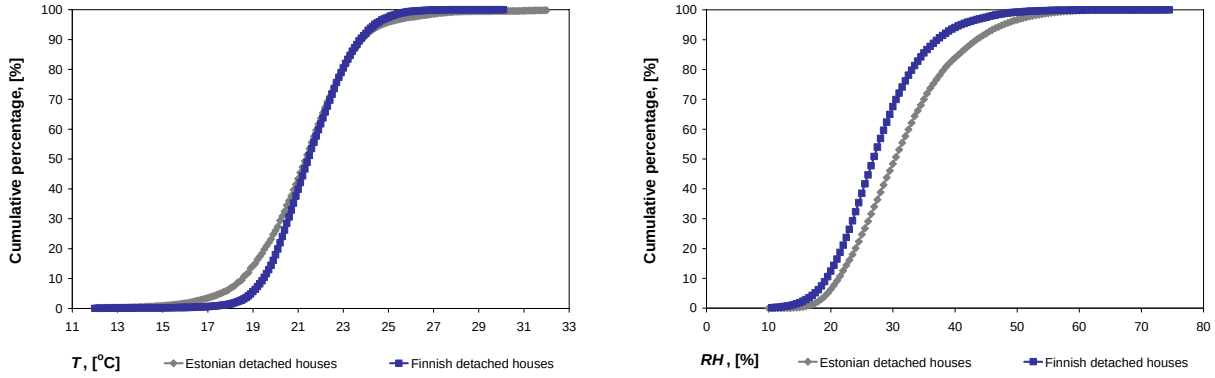

Figure 2 Distribution of the hourly indoor temperature (left) and RH (right) during two winter seasons in Finnish and Estonian detached houses

Table 4 Average values of the temperature (T), RH and the humidity by volume (v) during winter

	Finnish houses						Estonian houses					
	Winter I: 44 house, 78 rooms			Winter II: 50 house, 98 rooms			Winter I: 12 house, 22 rooms			Winter II: 15 house, 17 rooms		
	T, °C	RH, %	ν, g/m^3	T, °C	RH, %	ν, g/m^3	T, °C	RH, %	ν, g/m^3	T, °C	RH, %	ν, g/m^3
Natural vent.	+20.8	26	4.7	+21.4	28	5.1	+20.7	32	5.7	+20.7	34*	6.1*
Exhaust vent.	+22.0	23	4.5	+21.3	31*	5.8	+21.5	32	5.9	+21.5	28*	5.3*
Balanced vent.	+21.7	23	4.3	+21.8	28*	5.4	+21.6	29	5.5	+21.2	34	6.3
All data	+21.7	23	4.4	+21.6	29	5.5	+21.4	31	5.7	+21.1	32	5.9

* The difference is significant, P < 0.05

3.3 Average daily amplitude of the temperature, RH, and the absolute humidity

To study the fluctuations of the temperature and humidity on daily level, the amplitudes of 24 hours, i.e. the difference between the daily maximum and minimum values were calculated. An average value of these daily amplitudes over all the summer and winter season were considered as a measure of the fluctuation of the parameter studied. The ventilation systems significantly influenced the stability of the indoor climate values on

daily level in most of cases. The values of the average daily amplitude in subdivisions of ventilation systems and interior surface hygroscopicity of the room envelopes (rooms with the hygroscopic interior surface materials and the rooms with the fully non-hygroscopic interior surface materials) during summer and winter seasons are shown in Table 5.

Table 5 Values of the average daily amplitude of indoor temperature (ΔT), RH (ΔRH) and the absolute humidity (Δv) during the first (I) and second (II) summer (S) and winter (W)

	Finnish houses												Estonian houses											
	Summers						Winters						Summers						Winters					
	ΔT, °C		ΔRH, %		Δv, g/m³		ΔT, °C		ΔRH, %		Δv, g/m³		ΔT, °C		ΔRH, %		Δv, g/m³		ΔT, °C		ΔRH, %		Δv, g/m³	
	S I	S II	S I	S II	S I	S II	W I	W I	W I	W I	W I	W I	S I	S II	S I	S II	S I	S II	W I	W I	W I	W I	W I	W I
Natural vent.	2.5*	1.8	9	9	2.0	2.0	2.2*	1.5	5	6	1.2	1.3*	2.2	2.4	11*	9	2.3*	2.2	2.2*	3.5*	9	8	1.8	1.8
Exhaust vent.	2.1*	2.0*	10*	10*	2.2*	2.3*	1.5*	1.4	6	7	1.5	1.6*	3.6	2.6	10	10	2.1	2.2	2.7*	2.8*	8	8	1.9	1.5
Balanced vent.	1.6*	1.6*	8*	8*	2.0*	2.0*	1.5*	1.4	6	6	1.3	1.3	3.4	2.3	7*	10	1.7*	2.0	1.6*	1.2*	8	7	1.7	1.4
Hygroscopic	1.8	1.6	8*	9	1.9*	2.1	1.5	1.3*	6	6	1.3	1.4												
Non-hygroscopic	1.8	1.9	9*	9	2.1*	2.1	1.6	1.5*	6	7	1.4	1.4												
All data	1.8	1.7	9	9	2.0	6	1.6	1.4	6	6	1.3	1.4	3.3	2.6	9	10	2.0	2.2	2.3	2.5	8	8	1.8	1.6

* The difference is significant, P < 0.05

In Finnish study during the first summer, the average daily amplitude of the temperature was significantly lower (and showed the lowest variation) in rooms with balanced ventilation compared to rooms with natural ventilation (P<0.0001) and exhaust ventilation (P<0.001). Balanced ventilation showed a significantly lower variation of humidity by volume (P<0.01) and RH (P<0.0005)) than mechanical exhaust ventilation. The vapour tightness of the building envelope did not show any significant difference in average daily amplitudes of temperature, RH and absolute humidity. In rooms with hygroscopic indoor surfaces, the average daily amplitude of the humidity by volume (P<0.05)) and RH (P<0.05) was significantly lower than in rooms with non-hygroscopic indoor surfaces. During the second summer, the average daily amplitudes of the temperature (P<0.005)), RH (P<0.005), and humidity by volume (P<0.001) were significantly lower in rooms with balanced ventilation compared to rooms with exhaust ventilation. During the first winter, the average daily amplitudes of the temperature were significantly higher in rooms with natural ventilation than in rooms with balanced ventilation (P<0.005) and mechanical exhaust ventilation (P<0.01). During winter there was not any significant difference in average daily amplitude of the humidity by volume between rooms with hygroscopic and non-hygroscopic indoor surface materials. In Estonian study during the first summer balanced ventilation showed a significantly lower variation of humidity by volume (P<0.01) and RH (P<0.05)) than natural ventilation. During both winters balanced ventilation showed a significantly lower variation of temperature compared to rooms with natural ventilation and exhaust ventilation (P<0.05).

3.4 Internal moisture excess and moisture production

From each measured room moisture excess values were averaged over the cold period ($T_{out} \leq +5$ °C) and over the remaining time ($T_{out} > +5$ °C). Figure 3 shows the distribution of moisture excess in Estonian and in Finnish dwellings over the cold period and over the remaining time. The average value of weekly average moisture excess values from different rooms over the cold period in Estonian detached houses was +1.5 g/m^3 and over the remaining time +0.2 g/m^3 and in Finnish detached houses +1.8 g/m^3 and during the remaining time +0.5 g/m^3. In Estonian apartments during the cold period, the average value of the weekly average moisture excess was +3.2 g/m^3.

The average values of moisture excess were compared between different subdivisions, see Table 6. In Estonian detached houses during the period when $T_{out} > +5$ °C, the moisture excess was significantly lower in houses with balanced ventilation compared to houses with exhaust (P<0.02) and natural ventilation (P<0.04). In Finnish detached houses, the moisture excess during the cold period was significantly lower in rooms with balanced ventilation compared to rooms with natural (P<0.05) and mechanical exhaust ventilation (P<0.05). During the

rest of the time (T_{out} > +5 °C), balanced ventilation showed a markedly lower moisture excess (P<0.003) than natural ventilation.

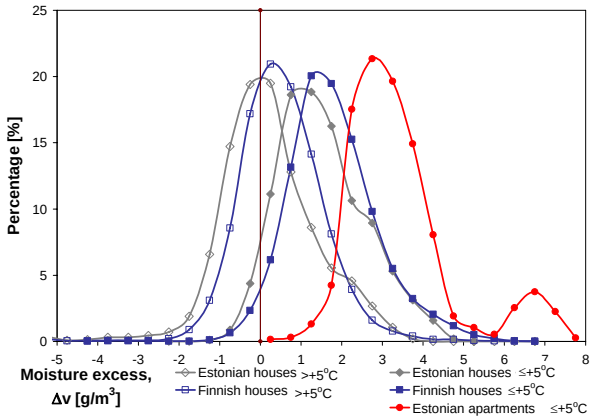

Figure 3 *Distribution of the moisture excess values during the cold period (T_{out} ≤ +5 °C) and during the rest of time (T_{out} > +5 °C)*

Table 6 *Average values of weekly average moisture excess during the cold period (T_{out} ≤ +5 °C) and during the remaining time (T_{out} > +5 °C)*

	Finnish detached houses		Estonian detached houses	
	T_{out} ≤ +5 °C AVG	T_{out} > +5 °C AVG	T_{out} ≤ +5 C AVG	T_{out} > +5 °C AVG
Bedrooms	+1.9	+0.5	+1.6	+0.3
Living rooms	+1.7	+0.4	+1.4	+0.2
Natural ventilation	+2.1*	+0.9*	+1.6	+0.8*
Exhaust ventilation	+2.0*	+0.5	+1.4	+0.2*
Balanced ventilation	+1.7*,*	+0.4*	+1.6	-0.1*,*
≤3 occupants	+1.7	+0.4	+1.4	+0.2
>3 occupants	+1.8	+0.5	+1.6	+0.3

* The difference is significant, P < 0.05

To analyze the influence of different moisture excess components on the humidity load in Estonian detached houses, the houses with lower (<+1 g/m^3) and higher (>+2 g/m^3) average moisture excess during the cold period were compared. Detached houses with higher average moisture excess are characterized with higher occupancy (39 m^2 vs. 52 m^2 floor area per occupant), lower ventilation rate (8 l/(s·pers.) vs. 12 l/(s·pers.)) and significantly higher (P<0.02) air tightness of the building envelope (3.5 m^3/hm^2 vs. 7.4 m^3/hm^2). Similarly, in the Finnish study, houses with average moisture excess during the cold period >+3 g/m^3 and <+1.5 g/m^3 were compared. Houses with higher moisture excess had significantly lower (P<0.00003) air change rate (0.25 vs. 0.4 ach in average) and had significantly higher (P<0.01) air tightness of the building envelope (n_{50}=2.4 vs. n_{50}=4.0 ach at 50 Pa). The questionnaire conducted in the houses with higher moisture excess showed the following: markedly less window airing (P<0.02), more houseplants (P=0.05) and higher occupancy (41 m^2 vs. 51 m^2 per occupant).

Figure 4 (left) shows the dependence of the maximum moisture excess from the studied dwellings on the higher 10 % critical level on the outdoor temperature. The proposed moisture excess design curve is on the basis of the trend line of these curves.The determined design curve of moisture excess A is +4 g/m^3 during the cold period (T_{out} ≤ +5 °C) and +1.5 g/m^3 during the warm period (≥ +15 °C) for dwellings with low humidity load (detached houses: commonly low occupancy (~45 m^2/occupant) and normal ventilation), design curve of moisture excess B is +5 g/m^3 during the cold period and +2 g/m^3 during the warm period for dwellings with average humidity load (occupancy ~30 m^2/occupant or humidification during cold period (RH_{in}>25%)) and normal ventilation) and design curve of moisture excess C is +6 g/m^3 during the cold period and +2.5 g/m^3 during the warm period for dwellings with high humidity load (apartments: commonly high occupancy (~20 m^2/occupant) and low ventilation).

The air change rate has a direct influence on the indoor humidity loads. The effect of the air change rate on the maximum and average moisture excess in Finnish detached houses during the cold period is shown in Figure 4 (right). This dependence is on the basis of the actual air change rate measurements in each house with the PFT technique during the winter season.

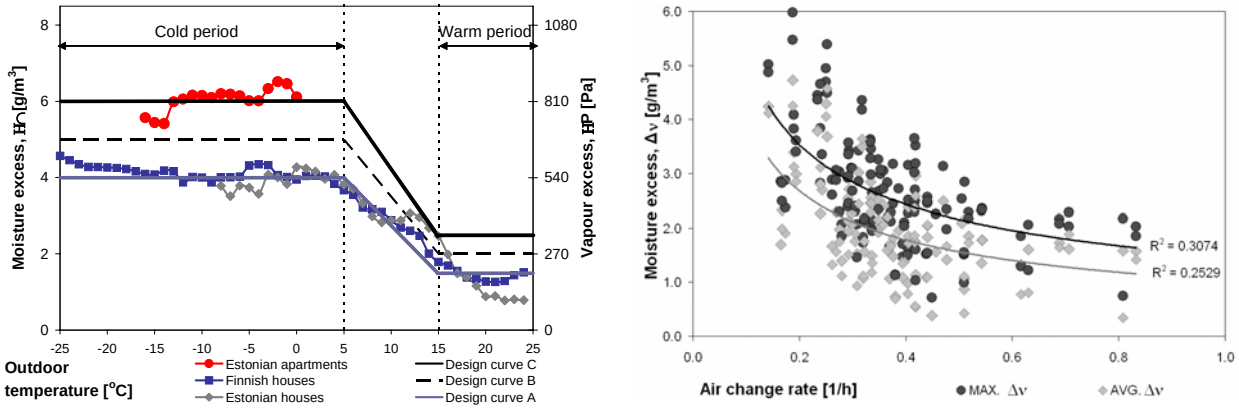

Figure 4 *Moisture excess on the higher 10 % critical level and the design curve of moisture excess (left) and the effect of the air change rate on the maximum and average moisture excess during cold period*

To do hygrothermal calculations and sensitivity analyzes under different hygrothermal loads, it is necessary to know the distribution of different moisture excess levels in the whole outdoor temperature range. To analyze the moisture excess performance through the full range of moisture production, different curves were calculated from the maximum moisture excess curves of each room, sorting the curves such that during the cold period, the average values of moisture excess would be as follows: +1 g/m^3, +2 g/m^3, +3 g/m^3, +4 g/m^3, +5 g/m^3, and +6 g/m^3. Different moisture excess levels and approximation curves from these levels that show the moisture performance of houses through the full range of moisture production are shown in Figure 5. These curves show that if the moisture excess changes by 1 g/m^3 during the cold period, it does by about 0.5 g/m^3 during the warm period.

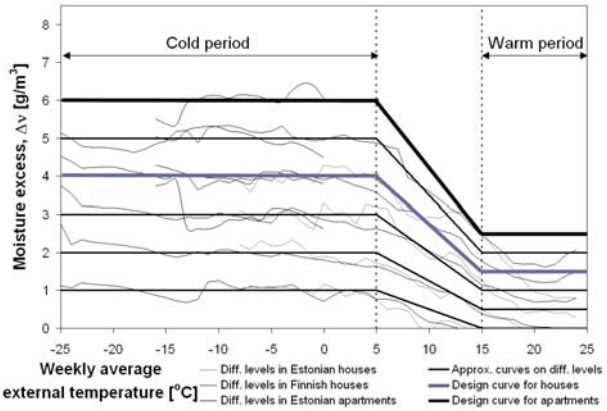

Figure 5 *Simplified moisture excess curves on different humidity load levels*

On the basis of the air change rate and the moisture excess, the daily average moisture production rates from each house were estimated (Eq. 2).

Table 3.7 *Moisture production in the studied detached houses*

	Finnish detached houses	Estonian detached houses
Daily average moisture production	5.9 kg/day/house 1.9 kg/day/person	5.4 kg/day/house 1.6 kg/day/person
Average value from the daily maximum moisture production values	12.7 kg/day/house 4.0 kg/day/person	13.0 kg/day/house 4.1 kg/day/person

3.5 Performance of the indoor hygrothermal load model

In the following, it will be tested how to achieve realistic indoor humidity conditions by using the design curve of moisture excess all the year round. As the moisture excess approach is a robust simplified approach, thus, it should be checked that the model would not calculate too low or too high RH values. Correct RH values, in addition to absolute humidity values, are especially important for mould growth calculations in the internal part of the envelope. To calculate indoor RH correct room temperature value or curve is needed.

Measurements showed dependence between the indoor temperature and the outdoor temperature (Figure 6, left). There is a turning point at +15 °C daily average outdoor temperature. Over +15 °C of average daily outdoor temperature, the slope of the indoor temperature is larger. Over +15 °C of average daily outdoor temperature, the indoor temperature reaching over +21…22 °C and heating is not necessary any more. These are two main factors, which may be interpreted that a heating season would change to the summer season at this +15 °C of average daily outdoor temperature in cold climates. The average indoor temperature curve in Estonian detached houses rises from +20 °C (at T_{out} -25 °C) to +22 °C (at T_{out} +15 °C) in the heating season, reaching +27 °C (at T_{out} +25 °C) during summer. The indoor temperature model in Finnish detached houses is 1° C higher during the heating season. These indoor temperature models can be used in the indoor temperature calculations, where the indoor temperature is not generated by the room model of the simulation program.

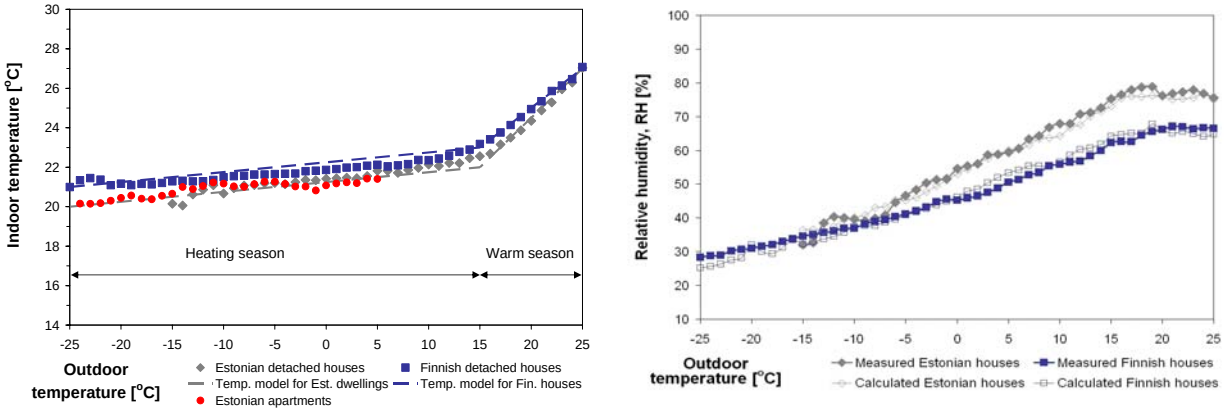

Figure 6 Dependence of average daily indoor temperature on the average daily outdoor temperature (left) and the comparison of measured and calculated daily average indoor RH on higher 10 % level (right)

In Figure 6 right, the measured indoor RH in detached houses on the higher 10 % level is shown by the curve with filled squares and rhombs. The corresponding calculated values are shown by the no filled squared and rhombed curve. This was calculated with the use of the design curve of moisture excess in detached houses (Figure 4, left), the average temperature curve (Figure 6, left) and the outdoor climate during two measurement years in Estonia and in Finland. Calculated RH values were sorted according to the outdoor air temperature from where the 10 % critical level was calculated (curve with no filled squares and rhombs). As indoor temperature models and outdoor climate were different in two (Finnish and Estonian) studies, also the performance of indoor RH dependency on outdoor temperature is different. Nevertheless, in both studies, the measured and the calculated indoor RH showed a good agreement, which allows the dependence of the indoor temperature and the moisture excess on the outdoor temperature to be used in calculations of indoor RH values as boundary conditions for hygrothermal simulation.

The present results are compared with solutions of different standards (EN ISO 13788, prEN 15026 and ASHRAE SPC 160P) in Figure 7. In standards (prEN 15026 and ASHRAE SPC 160P) the indoor humidity is not provided by vapour or moisture excess, but the indoor temperature and RH depend directly on the daily mean outdoor temperature. Moisture excess was calculated according indoor climate parameters, described in the standards and was averaged for weekly average values. Moisture excess levels according to standards are close to the results of the current study during the cold period. During the warm period, the difference is larger. If the indoor boundary conditions are given directly by temperature and RH (not moisture excess), the humidity loads will have significant variation following the fluctuation of the outdoor humidity.

Therefore, it would correspond to more realistic moisture production to provide humidity loads by moisture or vapour excess. Figure 7 shows that giving the indoor hygrothermal loads by temperature and RH will generate abnormal peaks to the moisture load curve that are not valid when calculated according to moisture production and ventilation rate profiles.

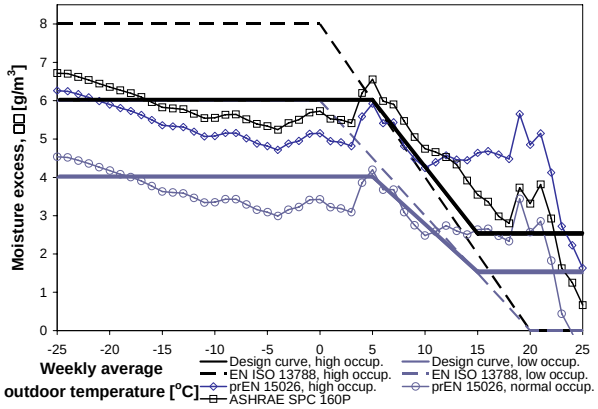

Figure 7 Comparison of the moisture excess design curves with solutions of different standards.

4. Discussion

In this study, the level and the stability of indoor temperature and relative humidity as well moisture excess and moisture production in Finnish and Estonian dwellings were analyzed. The results were compared based on the outdoor temperature, ventilation system and type of envelope assembly.

When the indoor climate parameters were compared, some limitations and uncertainties were to be taken into account. The architecture, orientation, and the surroundings of the dwellings were different in every case. Especially during the summer time, solar radiation had the main influence on the indoor temperatures. As the temperature and the RH sensors were located in one room, the orientations of these rooms played an important role. As all the houses were different and situated in different areas, urban or natural surroundings, the neighboring houses or trees may have had the direct influence on the indoor conditions. Additionally, the occupants' behaviour may have played an important role, for example, on the temperature level. On the other hand the influences of these factors decrease, when the number of houses is large, as in this study.

The effectiveness of ventilation and heating systems play an important role in establishing the indoor climate. Among the houses with balanced ventilation were most of the houses that met these recommendations for the indoor temperature of the indoor climate standard. Balanced ventilation was found to have the strongest influence on temperature stability on a daily level. A questionnaire about the houses found that the noise level of ventilation was the main problem for occupants in the houses with mechanical ventilation and often limited its use. Stuffy air was related to natural ventilation alone.

In field conditions it was also difficult to identify real values of material properties. It was impossible to divide houses with no distinction between houses that are highly, moderate, weakly or non hygroscopic. Only rough classification was possible: the rooms with the hygroscopic interior surface materials and the rooms with the fully non-hygroscopic interior surface materials. It was possible the houses that were classified as non-hygroscopic, were not completely non-hygroscopic, because each house could have significant amount of furniture, textiles, books etc.

Usually the dynamic simulations show, that in room with hygroscopic interior surface materials the fluctuation of humidity is significantly decreased compared to room with non-hygroscopic interior surface materials. In the field measurements, the difference in average daily amplitude of the indoor humidity was much less. Usually in the dynamic simulation the compared rooms are ideally hygroscopic and ideally non-hygroscopic. In the field measurements it was not possible to find houses built with as fully hygroscopic and non-hygroscopic surfaces as have been used in laboratory measurements or simulations. In the field measurements, the main hygroscopic surface material of walls was wooden boarding, wallpaper on wood chipboard or on plasterboard. Still, there were only a few rooms that were completely covered with unfinished wooden boarding. To protect wood surfaces from becoming discolored by UV-radiation or to make the surface cleanable, the surfaces were usually

coated. In many cases the dynamic simulations are carried out without furniture or any other hygroscopic mass, such as indoor textiles etc. This is not common in real houses. Textiles, furniture or other furnishing may play an important role in dampening the humidity fluctuation of indoor air. This is probably the reason why ideally non-hygroscopic houses do not exist in real life. Houses with non-hygroscopic indoor surface materials can still show similar behaviour to hygroscopic houses, if there is some other hygroscopic mass present. Therefore in future classifications of hygroscopicity of houses must be more detailed and distinguish between degrees of hygroscopicity.

According to statistics, the average living area per occupant in new detached houses is in Estonia 45 m^2/pers. (Statistics Estonia 2005) and in Finland 38 m^2/pers. (Statistics Finland 2003). In Estonian apartments this value is 21 m^2/pers. and in overall Estonian housing stock 28 m^2/pers. The average living density in measured Estonian detached houses was about 46 m^2/pers. and 17 m^2/pers. in apartments and 43 m^2/pers. in Finnish detached houses. Thus, the studied detached houses correspond to houses with low occupancy and the studied apartments represent to slightly higher occupancy than the average.

The design loads presented in this study cannot be directly used for other types of buildings, such as commercial or educational or sports halls etc. As moisture excess is obviously dependent on moisture production and ventilation profiles.

Humidity load levels in Finnish detached houses with massive walls were similar to this study. Finnish apartments, with lower occupation and better ventilatsion, had lower humidity loads, Salminen et al (2008).

For hygrothermal calculation the critical moisture excess values were calculated as weekly average values over the whole year. A week was selected as the reference time period because week is certain living cycle and it represents more accurately indoor climate than for example a month. If we use month for the reference time period, the averaging period is to long: we don't get values for the whole outdoor temperature range (especially for the cold period) and the result is not as comprehensive. If we use a shorter reference time period, the hygrothermal dynamic and different moisture production profiles can influence the results too much.

The EN ISO 13788:2001 standard suggests using a safety margin 1.1 for moisture excess values, when the steady-state calculation method described in that standard is used. The introduction of this safety factor is intended only to allow the inaccuracies of the steady–state calculation method described in that standard. This safety factor does not include the behaviour of the occupants that can have a significant effect on ventilation or moisture production and thus on moisture excess. It should be taken into account by raising the safety factor. Commonly, safety factors are not used in hygrothermal design. The reason may be that the damage caused by hygrothermal problems is less catastrophic and dangerous compared to that of structural design. Parallels may also be drawn to the analyzes of the limiting state of service on the structural design where safety factors are not used. On the other hand, in order to determine the normative loads, the critical level is lower in hygrothermal loads. The overall consensus (Sanders, 1996) is that the return period once every 10 years seems to be appropriate in the hygrothermal analyzes, while, in the design of the bearing capacity of structures, the return period once in 50 or 100 years is used. The humidity loads are usually the most important agent, leading to the deterioration of the building envelope and limiting the service life of a building. Therefore, neglecting the safety factors in hygrothermal design deserves some criticism. In particularly, because hygrothermal loads are building use dependent. The owner, occupants, i.e. the user behaviour may change during the service life of the building, but the building envelope and servicing systems usually remain the same. In many cases, the use of safety factors in the hygrothermal design would not raise the building costs.

5. References

ASHRAE Standard 160P (2004). Design Criteria for Moisture Control in Buildings, Working Draft, Nov. 2004.

Bornehag, C. G., Sundell, J., Bonini, S., Custovic, A., Malmberg, P., Skerfving, S., Sigsgaard, T., Verhoeff, A. (2004). Dampness in buildings as a risk factor for health effects, EUROEXPO: a multidisciplinary review of the literature (1998-2000) on dampness and mite exposure in buildings and health effects. Indoor Air 2004; 14 (4): 243–257.

Bornehag, C.G., Blomquist, G., Gyntelberg, F., Järvholm, B., Malmberg, P., Nordvall, L., Nielsen, A., Pershagen, G., Sundell, J. (2001). Dampness in Buildings and Health. Nordic Interdisciplinary Review of the Scientific Evidence on Associations between Exposure to "Dampness" in Buildings and Health Effects (NORDDAMP). Indoor Air 2001; 11 (2): 72-86.

EN 13829:2000. Thermal performance of buildings - Determination of air permeability of buildings - Fan pressurization method (ISO 9972:1996, modified). European Committee for Standardization, 2000.

EN ISO 13788:2001. Hygrothermal performance of building components and building elements – Internal surface temperature to avoid critical surface humidity and interstitial condensation – Calculation methods. International Organization for Standardization, 2001.

EVS 839:2003. Sisekliima (Indoor climate). Estonian Centre for Standardisation. Estonian Centre for Standardisation, 2003 (in Estonian).

FiSIAQ (2001). Classification of Indoor Climate 2000. Finnish Society of Indoor Air Quality and Climate, Espoo, Finland.

Kalamees, T., Vinha, J., Kurnitski, J. (2006). Indoor Humidity Loads and Moisture Production in Lightweight Timberframe Detached Houses. Journal of Building Physics, 29(3), 219 - 246.

Kalamees, T. (2006a). Hygrothermal Criteria for Design and Simulation of Buildins. Doctoral Thesis, Tallinn University of Technology, Tallinn: TTU Press

Kalamees, T. (2006b). Indoor Hygrothermal Loads in Estonian Dwellings. In: The 4th European Conference on Energy Performance & Indoor Climate in Buildings. The 27th Conference of the Air Infiltration & Ventilation Centre: Lyon, France, 20-22 November. 2006, (2), 541 - 546.

Kalamees, T., Kurnitski, J., Vinha, J., Korpi, M. (2007). Indoor Climate Conditions in Lightweight Detached Houses in Cold Climate. In: The International Conference on Indoor Air Quality, Ventilation and Energy Conservation in Buildings, IAQVEC 2007: Oct 28-31, 2007, Sendai, Japan. , 2007, (CD-ROM), 8 pp.

Nordtest (1997). Ventilation: Local Mean Age Of Air – Homogenous Emission Techniques. Nordtest Method NT VVS 118. Finland, Nordtest.

prEN 15026 (2006). Hygrothermal performance of building components and building elements - Assessment of moisture transfer in building components by numerical simulation. Draft European Standard.

Sanders, C. (1996). Environmental conditions. Final Report, Volume 2, Task 2. International Energy Agency, Energy Conservation in Buildings and Community Systems Program, Annex 24 Heat, Air and Moisture Transfer in Insulated Envelope Parts (HAMTIE), Belgium, K.U.-Leuven, 1996, 96pp.

Statistics Estonia (2005). Statistical office of Estonia. Statistical database. (in Estonian).

Statistics Finland (2003). Rakennukset, asunnot ja asuinolot 2002. 2003:9 (Buildings, Dwellings and Housing Conditions 2002) (in Finnish).

Vinha J., Korpi M., Kalamees T., Eskola L., Palonen J., Kurnitski J., Valovirta I., Mikkilä A. & Jokisalo J. 2005. Puurunkoisten pientalojen kosteus- ja lämpötilaolosuhteet, ilmanvaihto ja ilmatiiviys. (Research report 131: Indoor temperature and moisture conditions, ventilation and airtightness of Finnish timber framed one-family and row houses), Tampere University of Technology. (in Finnish)

Salminen, M. et al (2008). Excess moisture in residential buildings in Finland. Submitted to the 8th Symposium on Building Physics in the Nordic Countries, Copenhagen, Denmark,

6. Acknowledgements

This study was part of the cooperative project Annex 41 “Whole Building Heat, Air and Moisture Response” of the International Energy Agency’s (IEA) Energy Conservation in Buildings and Community Systems (ECBCS) program. All participants of the IEA Annex 41 are acknowledged for the cooperation and useful discussions. The study utilizes the measuring data and previous analysis of national research projects “Moisture-proof healthy detached house” in Finland and “Construction, renovation and indoor climate of wooden buildings” in Estonia. These studies were financed by National Technology Agency of Finland, the Estonian Science Foundation (grant 5654) and Tallinn University of Technology (V352, B605) and Finnish and Estonian companies and associations. The authors are grateful to researchers Ilkka Valovirta, Antti Mikkilä, Heli Toukoniemi, Hanna Aho from Tampere University of Technology, Lari Eskola, Miimu Airaksinen, Juha Jokisalo, Kai Jokiranta and Jari Palonen from Helsinki University of Technology, and Andreas-Henn Otsmaa, Helen Parkman, Jaak Volberg, Roland Vaikmäe, Toomas Kliimask from Tallinn University of Technology, who have carried out the measurements.

Surface phenomena of wind-driven raindrops on porous building walls

Masaru Abuku, PhD student,
Laboratory of Building Physics, Department of Civil Engineering, Katholike Universiteit Leuven;
masaru.abuku@bwk.kuleuven.be

Hans Janssen, Assistant Professor,
Department of Civil Engineering, Technical University of Denmark;
haj@byg.dtu.dk

Jean Poesen, Professor,
Physical and Regional Geography Research Group, Katholieke Universiteit Leuven;
jean.poesen@geo.kuleuven.be

Staf Roels, Professor,
Laboratory of Building Physics, Department of Civil Engineering, Katholike Universiteit Leuven;
staf.roels@bwk.kuleuven.be

KEYWORDS: *wind-driven rain, raindrop impact, absorption, evaporation, moisture transfer, building facade.*

SUMMARY:
In this paper, the reliability of the traditional approach to implement wind-driven rain loads in hygrothermal building envelope models is investigated by experimental and/or numerical means. Laboratory experiments were carried out to study the impact of water drops with different diameters, impact speeds and impact angles on a porous building material surface (ceramic brick). The measurements showed that large drops with high impact speeds splash, whereas drops with high impact speeds and small impact angles bounce. The measurements, furthermore, recorded the maximum spreading length and width of the drops as a function of drop diameter, impact speed and impact angle. A numerical analysis to study the distribution of impact speed and angle for raindrops hitting the facade of a 4 × 4 × 10 m^3 tower building is then documented. The results demonstrated typical and important tendencies of impact angle and speed across the facade. Finally, the experimental and numerical data were used in a more detailed three-dimensional simulation of impact, absorption and evaporation of random and discrete wind-driven raindrops. This was compared with the traditional one-dimensional simulation of absorption and evaporation at the facade considering a continuous uniform rain load as boundary condition. Significant differences between the two approaches were observed.

1. Introduction

Wind-driven rain (WDR) is one of the most important moisture sources for building facades and is thus of great concern in building science (Sanders, 1996; Blocken and Carmeliet, 2004; Abuku et al., 2008). The behaviour of WDR is governed by the combined effects of the airflow around the building, the geometry of the building and its surroundings, and the horizontal rainfall intensity. In reality the WDR load on building facades is the impingement of individual raindrops whose spatial and temporal distribution is discrete and random. As a matter of fact, WDR is such a complicated boundary condition that in numerical simulations of heat and moisture transfer in building components, it is commonly implemented as a moisture flux averaged over space and time: over the surface area and over the time step of (hourly) climate data (e.g. Künzel, 1994; Hagentoft et al., 2004). This is a simplified approach which allows a speedy numerical simulation, but does not correspond to reality. Such simplification of raindrop loads may lead to a significant difference between the model and reality: e.g. the wet spots caused by individual raindrops hitting the wall surface have a much higher vapour pressure than the averaged surface vapour pressure in the simplified approach. Also when a raindrop splashes or bounces off the wall surface, a fraction of the raindrop is neither absorbed into the wall nor does it evaporate at the wall surface.

The phenomenon of drop impact has been studied by scientists and engineers in several research fields, so reviews of this topic have been made from different points of view. For example, Bennett and Poulikakos (1993)

and Healy et al. (1996) focus on a semi-empirical model to estimate the maximal spreading of a droplet impacting on a solid surface; Rein (1993) made a comprehensive review of the liquid drop impact on solid and liquid surfaces and Yarin (2006) reviewed recent advances. Also much research, via numerical modelling and simulation of drop impact, has targeted a better understanding of the detailed behaviour of a droplet on impact. Recent simulation results demonstrate remarkable validity (Fujimoto et al., 2007). So far however, while the impact of a water drop on a solid surface (e.g. glass surface, steel etc.) has been intensively investigated experimentally and numerically, limited research has studied drop impact on porous materials (Alleborn et al., 2003; Reis et al., 2004; Zadražil et al., 2006). The latter publications show that the behaviour of a drop, at impact on a porous material, depends on droplet diameter, impact speed, impact angle, viscosity, surface tension, temperature, material properties and so forth. Because a raindrop is generally considered as pure liquid water, viscosity and surface tension can be assumed constant under the temperature and pressure of the liquid phase of water, and are not of interest for this study. The current study focuses on the absorption and evaporation of multiple drops after impact as in driving rain loads on building facades.

The first part of this study focuses on the raindrop impact on a porous building wall surface (ceramic brick). In laboratory experiments, the behaviour of water drops when hitting the building material surface is investigated for droplets with different diameters, impact speeds and impact angles. In the second part, these data are combined with numerical investigations of specific catch ratio (Blocken and Carmeliet, 2004), impact speed and impact angle that can be expected for raindrops hitting the facade of a tower building. Finally the standard approach, a one-dimensional simulation considering a spatially and temporally averaged rain impact as boundary condition, is compared with a detailed three dimensional simulation of the discrete and random raindrop load.

2. Measurement of water drop impact on a porous building material surface

The behaviour of a liquid drop at and after impact on a porous building material consists of spreading, splashing, bouncing, absorption, evaporation, and so forth. The definitions of spreading, splashing and bouncing in this paper are illustrated in Fig. 1 based on the figure in Rein (1993). Compared to spreading, splashing or bouncing, which occurs in a few milliseconds, absorption of the droplet by the porous material and the simultaneous evaporation are considered to last at least 100 times longer. The measurements shown here investigate experimentally how a water drop behaves in the first milliseconds after its impact and to what shape it is transformed after spreading. Specifically the maximal spreading length and width are discussed. This data will be used in §4 as input for the detailed three-dimensional simulations of the absorption and evaporation of WDR on building envelopes.

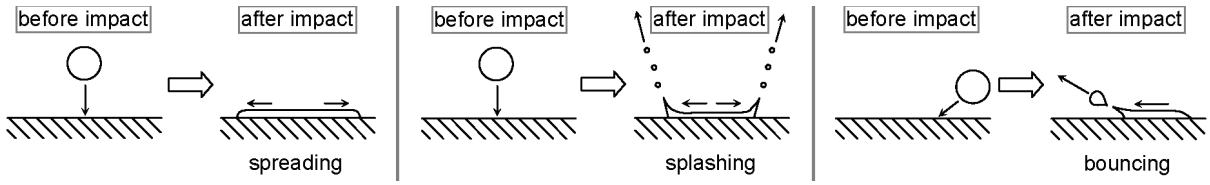

FIG. 1: Definitions of spreading, splashing and bouncing (based on the figure in Rein (1993)).

2.1 Measurement set-up

The impact of water drops on a ceramic brick surface was measured in the laboratory. For the material properties of the ceramic brick used in this study, the reader is referred to Hagentoft et al. (2004). For the experiment a specimen was cut out of a fired clay brick, resulting in a smooth surface as shown in Fig. 3. Note however that no physical data concerning surface roughness are available. The drops, with diameters of 2.0 mm (±0.1 mm) and 3.9 mm (±0.1 mm), were released from a hypodermic needle or a pipette placed at different heights, hence with different impact speeds, and at several impact angles. The diameter, impact speed and impact angle were determined by high speed camera (MotionXtra HG-100K, Redlake) images (1000 pictures per second). At the same time, the shape of the wet spot on the surface (the adherence shape of the water drop) was captured with a digital camera. Fig. 2 shows a schematic overview of the measurement set-up.

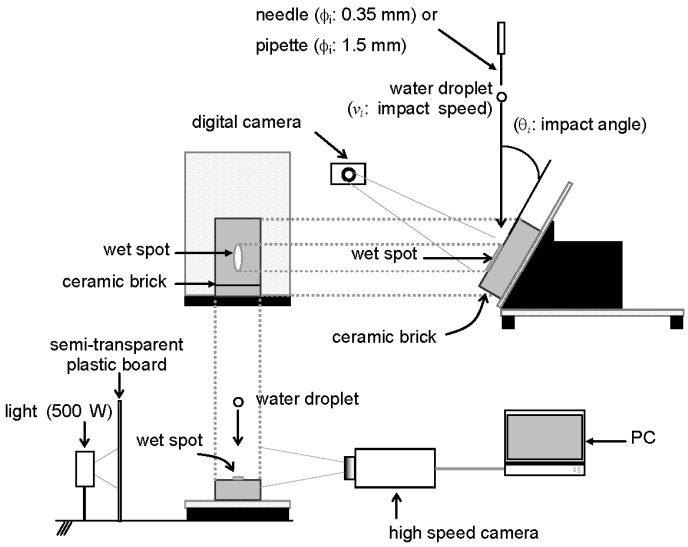

FIG. 2: Schematic overview of the measurement set-up of water drop impact at building material surfaces. ϕ_i: inner diameter (mm) of the needle or the pipette to generate a water drop.

2.2 Results and discussion

As an example, Fig. 3 shows some pictures of the spots wetted when the water drop spread, spread and splashed, or spread and bounced on the brick surface. Fig. 3 (a) and (b) compare the wet spots by 2.0 mm drops falling at 6.8 m/s with 2 different impact angles; Fig. 3 (c) and (d) compare those by 3.9 mm drops falling at 7.5 m/s with 2 different impact angles. Apart from spreading, splashing and bouncing were observed. Splashing was observed for the larger drops (3.9 mm). Bouncing was observed for drops with a lower impact angle of 24.5º for the 2 mm drops and 15.0º for the 3.9 mm drops. It is difficult to determine from the pictures what volume of water bounced and splashed, nevertheless, the observed splashing and bouncing indicate that the volume of rain during a certain period typically measured by a wall mounted rain gauge (Blocken and Carmeliet, 2004), can differ from the volume of rain acting as a moisture source for the building wall. The wall mounted gauge collects most raindrops which may sometimes splash or bounce on porous building wall surfaces, although part of the collected rain can be adhered to the surface and evaporate.

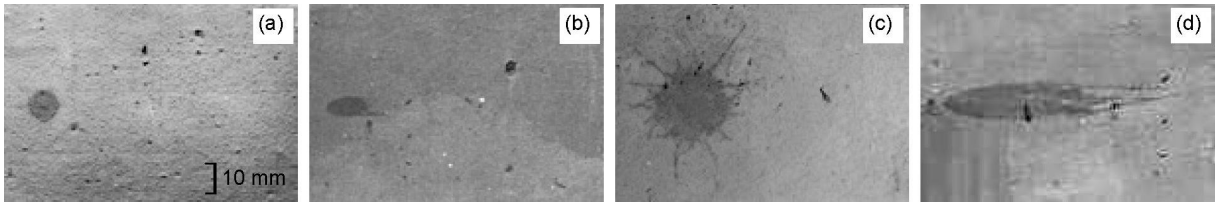

FIG. 3: Pictures of wet spots on ceramic brick surface. Drop diameter: (a, b) 2.0 mm (±0.1 mm) and (c, d) 3.9 mm (±0.1 mm); impact speed: (a, b) 6.8 m/s and (c, d) 7.5 m/s; impact angle: (a) 90.0º, (b) 24.5º, (c) 90.0º and (d) 15.0º. The drops in (b) and(d) bounced. The drop in (c) splashed.

Fig. 4 plots the measured maximum spreading length and width of the different drops as a function of impact angle. Each symbol in Fig. 4 represents data of a single drop. Note that, when looking at Fig. 3, the wet spots are sometimes irregularly shaped, making an exact definition of spreading length and width unclear. Here, the maximum spreading length and width of wet parts were determined by taking the middle of the fingering parts, which are irregularly shaped edges of wet spots as seen in Fig. 3 (c).

In general the spreading length l_s (Fig. 4 (a)) remains almost constant when the impact angle is above a threshold value and it increases with a decrease of impact angle once below this threshold. But the spreading length of 2.0 mm drops at 6.8 m/s impact speed decreases between 33.3º and 24.5º impact angle due to bouncing. On the other hand, the spreading length of the 3.9 mm drop with an impact angle of 15º is still longer than the one with 38.0º, although the former drop bounced and the latter drop splashed. The spreading length of a 2.0 mm drop at an

impact speed of 2.0 m/s remains almost the same when the impact angle is larger than 21.0º and steeply increased with a decrease of impact angle from 21.0º to 10.5º.

The spreading width w_s of the corresponding drops is shown in Fig. 4 (b). w_s for a given drop diameter and impact speed slightly increases with an increase of impact angle as a general trend. This relation between the spreading width and the impact angle is almost linear. Yet the spreading width of the three drops which bounced is distinctly smaller than that of the drops with a larger impact angle.

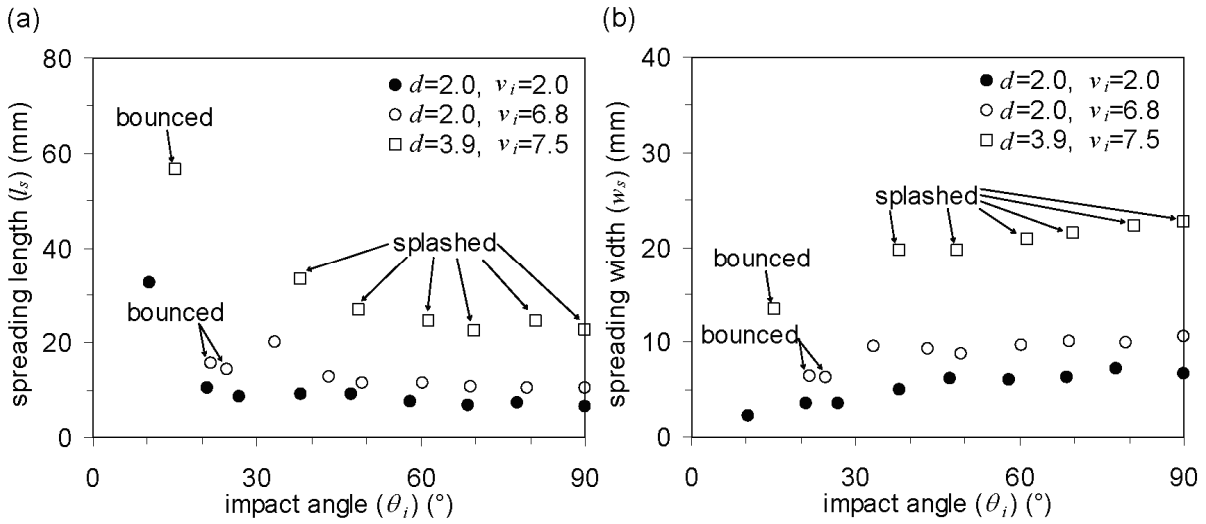

FIG. 4: (a) Spreading length (l_s) and (b) spreading width (w_s) of water drops at a ceramic brick surface. d: drop diameter (mm); v_i: impact speed (m/s); θ_i: impact angle (the minimum angle between the wall and the direction of impact) (º). Each symbol represents data of a single drop. Note that 3 drops bounced and 6 drops splashed.

3. Numerical determination of the impact speed, impact angle and size distribution of raindrops at a building facade

The measurements described in the previous section showed that the behaviour of a raindrop at its impact on the ceramic brick surface under study is mainly determined by the size, impact speed and impact angle of the drop. During a natural rain event, impact speeds and angles of raindrops are determined by the trajectory from sky to building facade and will strongly depend on the size of the raindrops, the airflow around the building and the geometry of the building. This section numerically investigates the distribution of these parameters on the facade of a tower shaped building with overall dimensions of $4 \times 4 \times 10$ m^3.

The size of raindrops falling in stagnant air is distributed and its distribution depends on the horizontal rainfall intensity. Although the size distribution of raindrops can not be generalised as a function of horizontal rainfall intensity, the measurements of Best (1950a) are often used as the most general relation between size distribution and horizontal rainfall intensity. The speed of these falling raindrops depends on the size of the raindrop and reaches a certain terminal value while falling. This terminal speed for a given raindrop diameter was given by Best (1950b) and empirically modelled by Gunn and Kinzer (1949).

Raindrops falling near to an obstacle such as buildings or hills show that the size distribution and terminal speed are strongly influenced by the airflow patterns around the obstacle. Choi (1993) proposed a numerical simulation of the distribution of raindrops on the surface of such obstacles to determine wind-driven rain loads on building facades; a lot of efforts to validate this method were made in several researches (e.g. Blocken and Carmeliet, 2002, 2007). Choi's method can also be used to determine the impact speed and impact angle of raindrops for a given diameter and location on the facade. The procedure comprises three steps:

(1) the steady-state airflow pattern around the building is calculated with computational fluid dynamics;

(2) raindrop trajectories are obtained by injecting raindrops of different sizes in the calculated airflow pattern and solving their equations of motion;

(3) the impact speed, impact angle and catch ratio of raindrops with a specific diameter are determined via the calculated raindrop trajectories.

In the calculation of the raindrop trajectory, the turbulent dispersion of raindrops remains an issue of disagreement amongst researchers. Other limitations of wind-driven rain simulation are discussed in Blocken and Carmeliet (2002). Although the validation of Blocken and Carmeliet clearly proved that an accurate determination of the wind-driven rain distribution on building facades can be performed, the specific determination of raindrop trajectories still remains to be validated. The trajectories of small raindrops are particularly influenced by the wind, but their effect is less important in the validation of wind-driven rain simulations, especially for moderate to high rainfall intensity.

Numerical simulation of raindrop trajectories hitting the facade of a tower of $4(x) \times 4(y) \times 10(z)$ m^3 with wind perpendicular to the facade was conducted with the method of Choi. For different wind speeds the spatial distribution of the impact speed, impact angle and size distribution of raindrops on the facades is investigated. Although the accuracy of the above-mentioned method is not validated for the calculation of impact angle and speed of raindrops, the simulation demonstrated here is considered to be accurate enough to privide an overall picture of the distribution of impact angle and speed across the facade.

First, simulation of the airflow field was performed with Fluent 6.2.16. A computational domain with overall dimensions $404(x) \times 204(y) \times 110(z)$ m^3, in which the centre of the tower is placed at x = 202 m and y = 102 m on the ground level, was subdivided into 2.1 million tetrahedral cells based on grid sensitivity analysis. The aerodynamic roughness length z_0 to generate the profile of the wind speed, turbulence energy, and energy dissipation rate at the inlet (x = 0 m) was set at 0.1 (m). The profile of wind speed, turbulence energy, and energy dissipation rate at the upstream (x = 0~150 m) and downstream (x = 254~404 m) parts of the computational domain was treated by use of the wall function with the equivalent sandgrain roughness height k_S = 0.098 (m) and the roughness constant C_s = 10 (-) (Blocken et al., 2007). At the outlet of the domain, an "outflow boundary condition" was used, in which no streamwise gradient is assumed. At the top and the sides of the domain, symmetric boundary conditions were used. With these conditions, the 3D Reynolds-Averaged Navier-Stokes (RANS) equations and the continuity equation were solved using the control volume method. Closure was obtained through the realizable k-ε model. The SIMPLE algorithm was used for the pressure-velocity coupling. Pressure interpolation was second order. A second order discretisation scheme was used for all convection and viscous terms.

In the next step, the trajectory of raindrops with a diameter of 0.3, 0.4, 0.5, 0.6, 0.7, 0.8, 0.9, 1.0, 1.2, 1.4, 1.6, 1.8, 2.0, 3.0, 4.0, 5.0 and 6.0 mm was simulated with the method of Choi. But now, not only the specific catch ratio, typically needed to determine the wind-driven rain load on building facades, but also the impact speed and angle distribution were calculated. Fig. 5 shows examples of the numerically determined impact angle, impact speed and specific catch ratio of raindrops at the centre (x = 200 m, y = 102 m, z = 0.2~9.8 m) on the facade of the tower. Fig. 5 (a), (c) and (e) show the results simulated with a reference wind speed U_{10} of 4m/s (U_{10} taken at 10 m height above the ground level); Fig. 5 (b), (d) and (f) with U_{10} = 8 m/s.

Fig. 5 (a) and (b) show that the impact angle increases along the height of the tower. The smaller the raindrop size, the more widely distributed the impact angle. The impact angle at a low position simply increases with an increase of drop diameter, but that at a high position first increases and then decreases with increasing drop diameter. Also, the higher the wind speed, the higher the impact angle. Fig. 5 (c) and (d) show the impact speed. The figures illustrate that the spatial distribution of impact speed for a given diameter is not that large. Combining both figures, it can be seen that the impact speed of a small raindrop decreases with an increase of the impact angle. Fig. 5 (e) and (f) show the specific catch ratio for a given drop diameter and position. The smaller the raindrop size, the more widely distributed the specific catch ratio.

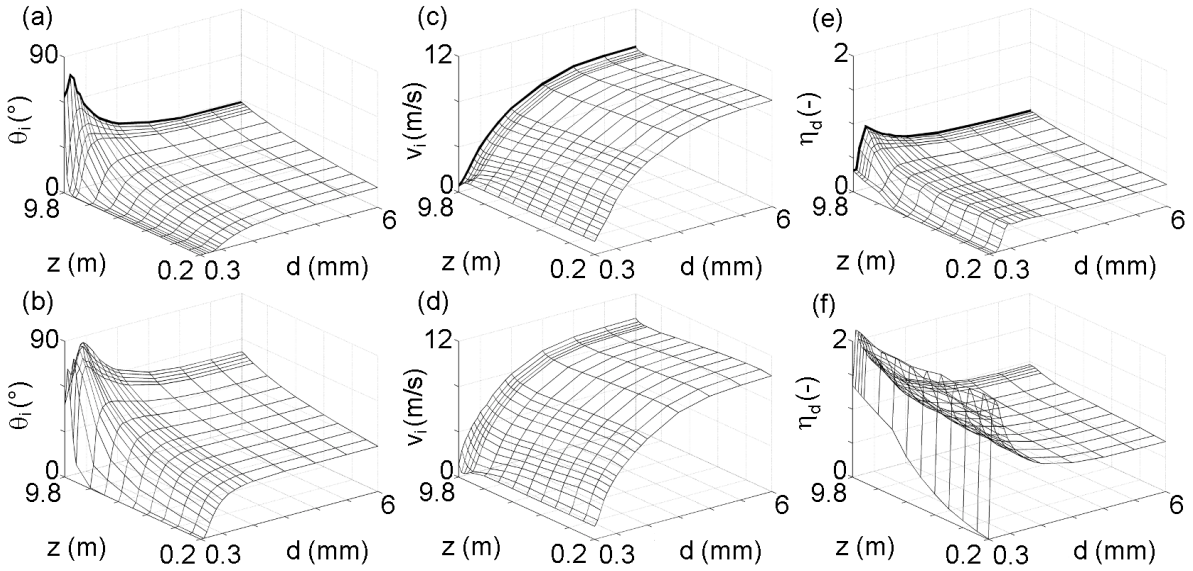

FIG. 5: Numerically determined (a,b) impact angle θ_i, (c,d) impact speed v_i and (e,f) specific catch ratio η_d of raindrops at centre on the facade of the tower. The reference wind direction is perpendicular to the facade. U_{10} = 4 m/s for (a), (c) and (e); U_{10} = 8 m/s for (b), (d) and (f). The bold lines are used in the simulations of Section 4. z: z-coordinate (m); d: raindrop diameter (mm).

4. Comparison of traditional and detailed approaches

In this section the commonly used simplified approach in hygrothermal building envelope models to implement WDR as a continuous and uniform boundary flux is compared to a much more detailed three-dimensional simulation taking into account the discrete and random impact of individual raindrops. The input for the latter model is based on results obtained in the previous two sections. First the two numerical models are described in more detail. Then both models are applied to two rain events and the differences between the obtained simulation results are discussed.

4.1 Traditional approach to implement WDR loads as boundary condition

In most hygrothermal building envelope models, the moisture stress due to WDR on a vertical wall is typically simulated with the assumption of the WDR load spatially averaged over the material surface and temporally averaged over a certain period. Without runoff, the moisture flux at the wall surface g_m can be expressed as (e.g. Hall and Hoff, 2002; Janssen et al., 2007):

$$g_m = -\beta(p_e - p_s) - I_{WDR} \qquad (1)$$

Here, β is the surface film coefficient, p_e is the vapour pressure of the air adjacent to the external wall surface, p_s is the vapour pressure at the external wall surface, and I_{WDR} is the source term of the moisture due to WDR.

I_{WDR} can be obtained through climatic data files and standard procedures (Sanders, 1996; Blocken and Carmeliet, 2004) or numerically with the aid of computational fluid dynamics (CFD) and the method of Choi (1993) and its extension to deal with climatic data sets by Blocken and Carmeliet (2002).

4.2 Detailed approach to implement WDR loads as boundary condition

In a much more detailed approach to implement WDR as boundary condition, the random spatial and temporal distribution of impinging raindrops, satisfying the statistical character of the WDR load, can be taken into account. To do so the WDR amount is distributed into a number of raindrops and each raindrop impinges on a certain position on the wall at a certain time. This approach is more realistic than the classical one, but intrinsically requires a three-dimensional simulation of the moisture or the heat and moisture transfer in the

material. Of course, for practical cases this results in unacceptably time-consuming simulations, but here such simulation is employed to check the validity of the classical simplified approach.

A number of spatially and temporally discrete raindrops are generated by use of a random generator. The procedure is as follows:

(1) the (global) horizontal rainfall intensity is transformed into specific horizontal rainfall intensities (rainfall intensity for a certain range of raindrop diameter) by use of the relation of Best (1950a);

(2) the specific horizontal rainfall intensity is transformed into the specific wind-driven rain intensity by use of the specific catch ratio;

(3) the specific wind-driven rain which is still spatially and temporally averaged is transformed into specific raindrops randomly falling at a certain time onto a certain location by use of a random generator.

For the current study the specific catch ratio data for a reference wind speed of 4 m/s at 9.8 m above the ground at the centre on the facade of the tower building is used (see the bold line in Fig. 5 (e)). With these catch ratio data, two fictitious 90-minute rain events, with horizontal rainfall intensities 0.1 and 0.5 mm/h, were transformed into raindrop sequences (I_{WDR} = 0.062 and 0.345 mm/h) as mentioned above. To investigate the effect of both absorption and evaporation, a rain schedule of 90 minutes start with a rain period of 20 minutes, followed by a dry period of 10 minutes, again 20 minutes of rain and finally a dry period for the remaining 40 minutes. For the two rain schedules, 92 and 292 raindrops with several different diameters (< 1.7 mm) were generated. Fig. 6 shows the time course of the diameters of the raindrops. These raindrops are randomly falling at a certain moment onto a certain location on a material surface with an area of 180mm^2. Note that the load of these raindrops is quantitatively equal to the temporally and spatially averaged WDR load with an intensity of 0.062 and 0.345 mm/h respectively.

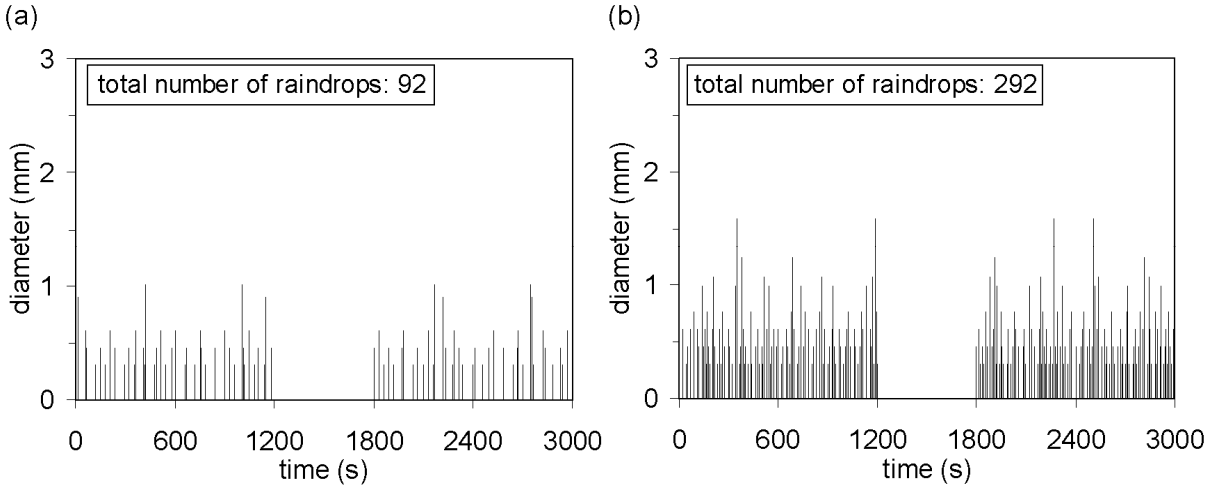

FIG. 6: Time course of the diameter of numerically generated raindrops over the brick wall surface (180 mm^2) on the facade of the tower. (a) I_h = 0.1 mm/h (I_{WDR} = 0.062 mm/h); (b) I_h = 0.5 mm/h (I_{WDR} = 0.345 mm/h). Note that there is no rain load from 3000 s to 5400 s.

Due to the corresponding impact angle and speed (see the bold lines in Fig. 5 (a) and (c)) of the raindrops generated (< 1.7 mm) no splashing or bouncing of impinging raindrops will occur. So only spreading occurs and in the current model a raindrop impinging at the building facade is transformed into an infinitely thin water film with both the volume and mass of the raindrop and with a rectangular effective surface area for absorption and evaporation, described by the maximum spreading length l_s (mm) and spreading width w_s (mm). Although this transformation facilitates the easier generation of a better mesh, the difference between a real shape and the transformed shape may have some minor influence on the results in this section. However it is considered that the insights from the simulation results presented below remain valid. Under isothermal conditions, the viscosity and surface tension can be considered constant and spreading length and width can be modeled as a function of the droplet diameter d, impact speed v_i and impact angle θ_i. Based on Fig. 5 (a), only impact angles larger than 30° are expected in the current study. Therefore the equations of l_s and w_s were made based on the measured data for water drops hitting the ceramic brick surface with impact angles larger than 30°:

$$l_s = 6.1 \times \left(\frac{d^3}{0.127d + 0.209} \right)^{0.5} \times \left\{ 1 - \frac{1.49}{(v_i + 4.9)^{0.36}} \right\} \times \left\{ 1 + 0.24 \left(\frac{\theta_i}{90} + 0.51 \right)^{-10} \right\} \quad (2)$$

$$w_s = 4.6 \times \left(\frac{d^3}{0.127d + 0.209} \right)^{0.5} \times \left\{ 1 - \frac{1.49}{(v_i + 4.9)^{0.36}} \right\} \times \left\{ 1 + 0.31 \left(\frac{\theta_i}{90} \right) \right\} \quad (3)$$

Each equation is based on the 13 measurement data. Note, because no theoretical study of empirical equations of maximum spreading length and spreading width is seen for oblique drop impact on porous materials, arbitrary forms of function were chosen for both equations. However d^3 in both equations signifies that l_s and w_s are dependent on the volume of a drop. A comparison of l_s (mm) and w_s (mm) as a function of the impact angle given by Eqs. (2) and (3) with the measurement data is shown in Fig. 7. Note that these equations are only valid for $\theta_i > 30$ º, because l_s and w_s for $\theta_i < 30$ º are often very different from the Eqs. (2) and (3) due to splashing and bouncing. Though the equations were not validated for $d < 2.0$ mm, a possible deviation of the equations from the real value is considered to be less significant for smaller raindrops, because the value of l_s and w_s of small raindrops is not so large. Therefore the Eqs. (2) and (3) are adopted for $d < 2.0$ mm and for a low impact speed of small raindrops in the simulations reported in this paper. Furthermore the temperature dependency of l_s and w_s is not considered here. Note that Eqs. (2) and (3) were only derived for the type of ceramic brick used in this study. If materials with different surface roughness or porosity are used, these equations may no longer hold.

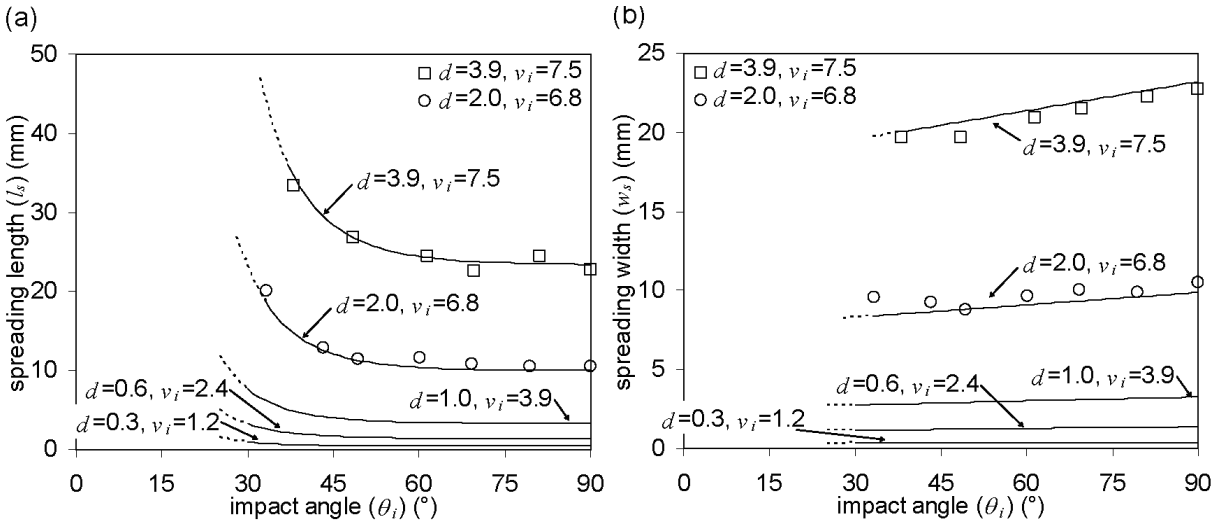

FIG. 7: (a) Spreading length (l_s) and (b) spreading width (w_s) of water drops at a ceramic brick surface for θ_i >30º. The symbols (□ and ○) show the measurement data. The lines show Eqs. (3) and (4). The lines of raindrops with a diameter of 2.0 and 3.9 mm are compared to the measurement data. The impact speed for the three lines of raindrops with a diameter of 0.3, 0.6 and 1.0 mm is the terminal speed given by Best (1950b). d: drop diameter (mm); v_i: impact speed (m/s); θ_i: impact angle (the minimum angle between the wall and the direction of impact) (º).

4.3 Numerical simulation of absorption and evaporation of WDR

The absorption and evaporation for the two fictitious rain events are numerically simulated under isothermal condition (10.8 ºC) by the traditional one-dimensional averaging model (1-d model) and the detailed three-dimensional model (3-d model). As in the laboratory experiments, ceramic brick is used in the simulations as facade material. The material properties are taken from a previous international modelling benchmark case (Hagentoft et al., 2004). The initial relative humidity of the ceramic brick is set at 75 %. The relative humidity of the moist air on the external front side was kept constant at 75 % and the surface film coefficient for the moisture transfer at the external front side was also kept constant at 1.54×10^{-7} kg/m^{2}sPa. All other boundaries were assumed impermeable. The total number of nodes in mesh (Fig. 8) for the simulation of the moisture transfer by

the finite element method (Janssen et al., 2007) for the 3-d model is 4194; the number of nodes at the exterior surface of the wall is 1701; and the number of nodes at the interior surface is 150.

Note that when the raindrops impacted the wall surface in the discrete simulations, it was assumed that the raindrops immediately spread at the wall surface and the time step was reduced to 10^{-6} s. The following assumptions were also adopted in the discrete simulations:

(1) when a raindrop overlaps a wet spot, the mass of the water at the crossover of two wetted parts becomes the sum of the mass of their crossovers;

(2) a cyclic boundary condition was imposed on determining the position of wet spots: e.g. when a wet spot intersects with an edge of the external material surface, one of the split spots by the edge that is not on the external material surface comes at the edge on the other side of the surface.

Fig. 9 compares the simulation results of the 1-d model with the results of the 3-d model. Fig. 9 (a) and (b) show the time change of the average moisture contents; Fig. 9 (c) and (d) show the time course of the evaporation rate at the entire wall surface; and Fig. 9 (e) and (f) show the time change of the amount of the cumulative WDR for both models, cumulative evaporation for both models, the water in the brick for both models and the total adhered water for the 3-d model. Note that no excess water appeared in the simulations with the 1-d model.

As a general trend the average moisture content of the top layer (1 cm) of the brick increased due to the WDR load during rain events and then decreased due to evaporation. The raindrops which spread on the brick surface were immediately evaporated or absorbed into the brick interior (Fig. 9 (e) and (f)). A comparison of the two models for each case shows an important difference between the two models.

For the horizontal rainfall intensity of 0.1 mm/h, the average moisture content simulated with the 3-d model was higher than with the 1-d model. This difference can be attributed to the evaporation rate at the material surface. As seen in Fig. 9 (c), the evaporation rate at the entire wall surface for the 1-d model was usually higher than for the 3-d model, even though the evaporation rate at and around the small wet spots for the 3-d model was locally very high. Only when a steep increase of the vapour pressure at and around a wet spot was noticed in the 3-d model, the evaporation rate for the 3-d model became higher than the one for the 1-d model. This difference can be explained more clearly by comparing the amount of evaporated water for the two models in Fig. 9 (e).

For the rain event of 0.5 mm/h, on the contrary, the average moisture content simulated with the 1-d model became approximately 2 times higher at the maximum than when predicted with the 3-d model. The reason being that in the simulation with the 1-d model, the moisture content at the material surface remained below the saturated moisture content and the vapour pressure at the material surface was kept uniformly at a certain relatively low value. On the other hand, in the simulation with the 3-d model, the water of the raindrops quickly spread into the wall inside and evaporated because of the high vapour pressure at and around the wet spots. So for a higher WDR intensity, while the 1-d model allows easy absorption, maintaining low surface vapour pressure and slow evaporation, the 3-d model yields a locally high absorption and evaporation, sustaining several scattered islands of high vapour pressure at the material surface.

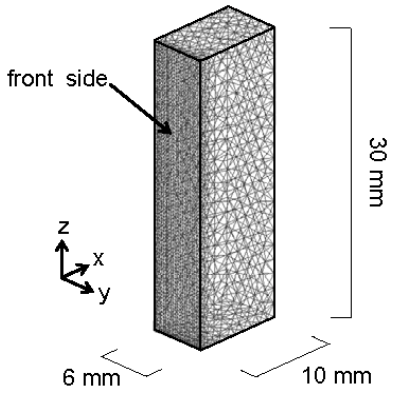

FIG. 8: Mesh over the material surface for FEM simulation (3D).

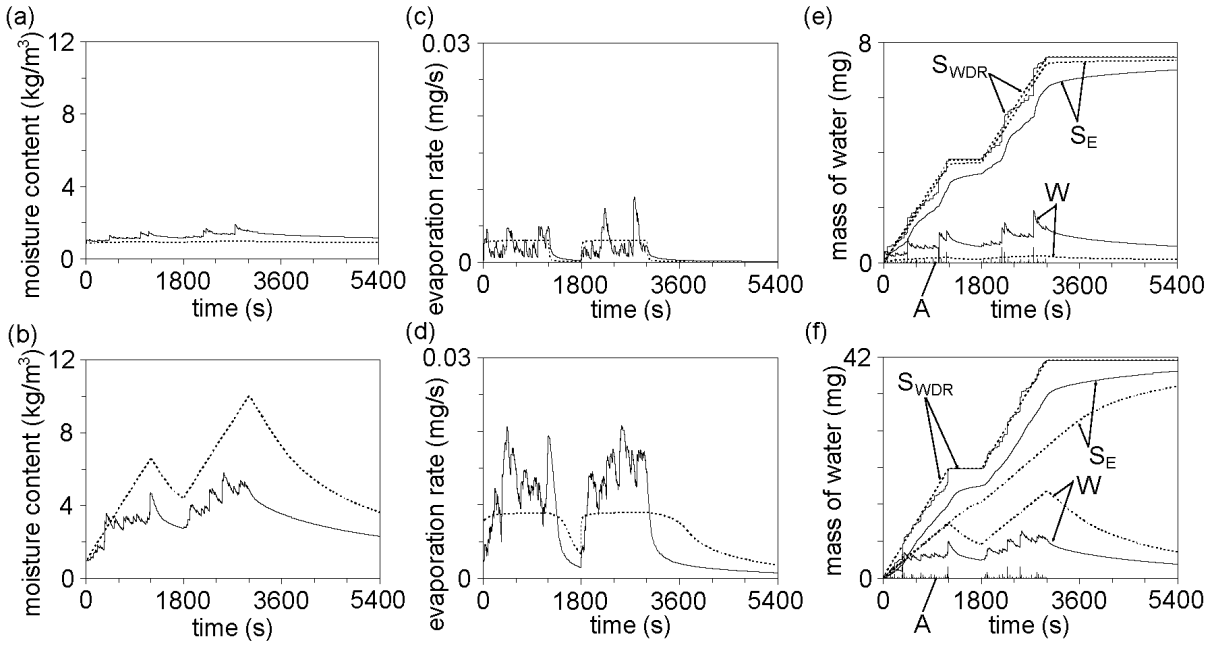

FIG. 9: Simulation results. (a) and (b) Average moisture content in brick; (c) and (d) evaporation rate at the entire surface; (e) and (f) cumulative mass of water. In (a), (c) and (e), I_h = 0.1 mm/h and I_{WDR} = 0.062 mm/h; in (b), (d) and (f), I_h = 0.5 mm/h and I_{WDR} = 0.345 mm/h. The dash lines show the results of the 1-d simulations with the traditional model for WDR loads; the solid lines show those of the 3-d simulations with the detailed model for WDR loads. A: adhered water at the wall surface (mg); S_E: cumulative evaporation (mg); S_{WDR}: cumulative WDR (mg); and W: water in brick due to WDR (mg).

5. Conclusions

The reliability of the traditional approach to implement wind-driven rain (WDR) as boundary condition in hygrothermal building envelope models was experimentally and numerically investigated and elaborated in detail.

The first part of this paper experimentally investigated the behaviour of raindrops in a few milliseconds after impact on building material surfaces: the water drop impact on a porous material's surface (ceramic brick) was measured. The results showed that a drop with a diameter of 3.9 mm splashes at its impact and a drop with a small impact angle and speed bounces. These observations indicate that the volume of raindrops corrected by a driving rain gauge can differ from the moisture load due to rain on the building facade, because side walls of the gauge may collect a part of the water that has splashed or bounced on the gauge, while part of the raindrops which impact the building facade may not be loaded onto the building facade due to splashing and bouncing. Furthermore splashing and bouncing can differ for facade and gauge surfaces due to different surface phenomena. Also the maximum spreading length and width of raindrops, which are key parameters for investigating the absorption and evaporation of rain at the building facade, were determined. The spreading length increases with a decrease of impact angle and an increase of drop diameter and impact speed; the spreading width increases with an increase of impact angle, drop diameter and impact speed. Furthermore, the occurrence of bouncing reduces the maximum spreading length and width.

Secondly the impact angle, impact speed and specific catch ratio of the raindrops at the facade of the tower building were numerically determined, which revealed some trends:

(1) the impact angle and specific catch ratio of small raindrops are spatially widely distributed; those of large raindrops are spatially rather uniform;

(2) the impact angle is often large where the specific catch ratio is large;

(3) the impact speed of all raindrops is spatially rather uniform regardless of the airflow speed around the building;

(4) the impact speed of raindrops at the building facade is considerably close to their terminal speed (e.g. Gunn and Kinzer, 1949); and

(5) the impact angle, impact speed and specific catch ratio on the building facade increases with an increase of the reference wind speed when the cardinal wind is perpendicular to the building facade.

When these findings are confronted with the measurement results of drop impact, for the building studied, the wind-driven rain is more important at a high location on the facade than at a low location, not only because the high location is exposed to more wind-driven rain, but also because a raindrop at the low location often has a small impact angle and thus bounces and is not entirely loaded onto the facade as a moisture source.

Finally the classical spatial and temporal averaging of the WDR load on building enclosures was compared to a detailed three-dimensional simulation, in which the discrete impact of individual raindrops was modelled. The average moisture contents simulated in both ways were quite different. In one case for a horizontal rainfall intensity of 0.1 mm/h, the simulation with the commonly used 1-d model led to an underestimation of the average moisture content due to an overestimation of the evaporation rate. In the other case for 0.5 mm/h, the simulation with the 1-d model led to an overestimation of the average moisture content due to an underestimation of the evaporation rate. Note that, in the current simulations, a part of the kinetic energy of raindrops which forces the water into the wall interior was ignored, though influences of this energy on the absorption might be of some importance.

6. References

Abuku M, Janssen H, Roels S. (2008). Impact of wind-driven rain on mould growth, indoor climate and energy consumption in cold and humid climate, *Energy and Buildings*, in review.

Alleborn N, Raszillier H, Anthonissen K, Lievens O. (2003). Spreading and sorption of a droplet on a porous substrate, In: Schweizer PM, Cohu O. editor. *Proceedings of the 5th European Coating Symposium, Advances in Liquid Film Coating Technology*, Fribourg, Switzerland, p. 246-251.

Best AC. (1950a). The size distribution of raindrops, *Quarterly Journal of the Royal Meteorological Society*, Vol. 76, p. 16-36.

Best AC. (1950b). Empirical formulae for the terminal velocity of water drops falling through the atmosphere, Quarterly Journal of the Royal Meteorological Society, Vol. 76, p. 302-311.

Bennett T, Poulikakos D. (1993). Splat-quench solidification: estimating the maximum spreading of a droplet impacting a solid surface, *Journal of Materials Science*, Vol. 28, p. 963-970.

Blocken B, Carmeliet J. (2004). A review of wind-driven rain research in building science, *Journal of Wind Engineering and Industrial Aerodynamics*, Vol. 92(13), p. 1079-1130.

Blocken B, Carmeliet J. (2002). Spatial and temporal distribution of wind-driven rain on low-rise building, *Wind and Structures*, Vol. 5(5), p. 441-462.

Blocken B, Stathopoulos T, Carmeliet J. (2007). CFD simulation of the atmospheric boundary layer: wall function problems, *Atmospheric Environment*, Vol. 41, p. 238-252.

Choi ECC. (1993). Simulation of wind-driven-rain around a building, *Journal of Wind Engineering and Industrial Aerodynamics*, Vol. 46&47, p. 721-729.

Fujimoto H, Shiotani Y, Tong AY, Hama T, Takuda H. (2007). Three-dimensional numerical analysis of the deformation behaviour of droplets impinging onto a solid substrate, *International Journal of Multiphase Flow*, Vol. 33, p. 317-332.

Gunn R, Kinzer GD. (1949). The terminal velocity of fall for water droplets in stagnant air, *Journal of Meteorology*, Vol. 6, p. 243-248.

Hall C, Hoff WD. (2002). Water transport in brick, stone and concrete, London: Spon Press.

Hagentoft CE, Kalagasidis AS, Adl-Zarrabi B, Roels S, Carmeliet J, Hens H, Grunewald J, Funk M, Becker R, Shamir D, Adan O, Brocken H, Kumaran K, Djebbar R. (2004). Assessment method of numerical prediction models for combined heat, air and moisture transfer in building components: benchmarks for one-dimensional cases, *Journal of thermal envelope and building science*, Vol. 27(4), p. 327-352.

Healy WM, Hartley JG, Abdel-Khalik SI. (1996). Comparison between theoretical models and experimental data for the spreading of liquid droplets impacting a solid surface, *International Journal of Heat and Mass Transfer*, Vol. 39(14), p. 3079-3082.

Janssen H, Blocken B, Carmeliet J. (2007). Conservative modelling of the moisture and heat transfer in building components under atmospheric excitation, *International Journal of Heat and Mass Transfer*, Vol. 50, p. 1128-1140.

Künzel HM. (1994). Verfahren zur ein- und zweidimensionalen Berechnung des gekoppelten Wärme- und Feuchtetransports in Bauteilen mit einfachen Kennwerten, PhD thesis, Universty of Stuttgart.

Rein M. (1993). Phenomena of liquid drop impact on solid and liquid surfaces, *Fluid Dynamics Research*, Vol. 12, p. 61-93.

Reis NC, Griffiths RF, Santos JM. (2004). Numerical simulation of the impact of liquid droplets on porous surfaces, *Journal of Computational Physics*, Vol. 198, p. 747-770.

Sanders C. (1996). Heat, air and moisture transfer in insulated envelope parts, *IEA Annex 24, Final report – Vol. 2, Task 2: Environmental conditions*, Leuven: Acco Leuven.

Zadražil A, Stepanek F, Matar OK. (2006). Droplet spreading, imbibition and solidification on porous media, *Journal of Fluid Mechanics*, Vol. 562, p. 1-33.

Yarin AL. (2006). Drop impact dynamics: splashing, spreading receding, bouncing…, *Annual Review of Fluid Mechanics*, Vol. 38, p. 159-192.

Acknowledgements

The results in this paper have been obtained within KUL OT/04/28, ‘Towards a reliable prediction of the moisture stress on building enclosures’, funded by the K.U.Leuven and IWT 050154, ‘Heat, air and moisture performance engineering: a whole building approach’, funded by the Flemish Government. This financial support is gratefully acknowledged.

Measurements of drop impact were performed with the high speed camera of the Department of Biosystems, K.U.Leuven. We would like to thank Prof. Ramon and his co-workers for fruitful collaboration.

Climate Change and its Implications for Hygrothermal Modelling

Chris Sanders
Centre for Research on Indoor Climate and Health, Glasgow Caledonian University
c.h.sanders@gcal.ac.uk http://www.caledonian.ac.uk/rich/

KEYWORDS: *Climate change, external, boundary conditions, risk .*

SUMMARY:

The external boundary conditions that we use for hygrothermal modelling of building performance are changing and will continue to change over the present century as greenhouse gases accumulate in the atmosphere. This paper discusses the processes of generating future climate scenarios that are relevant to buildings and construction and describes data sets of hourly values of future climate parameters. Data from two locations were analysed: Heathrow in southern England and Eskdalemuir in upland Scotland. The results suggest that seasonal mean temperatures will increase by between 3°C and 6°C and extreme temperatures and periods of successive days with high temperatures become more common. Conversely, low temperatures will become less common.

Seasonal rainfall totals will rise in winter and fall in summer, extreme high rainfall events may become more common, although the data set used may not predict these reliably. Similarly, seasonal mean windspeeds will tend to increase. Sunshine totals will fall slightly in the winter, but increase significantly in summer. Vapour pressure will rise slightly, but because of the rises in temperature, relative humidities will fall significantly. Because of the rising temperatures, frost damage to masonry will fall sharply. Driving rain will increase in winter, but fall in summer.

1. Introduction

One of the main determinants of the external boundary conditions is the large scale external climate imposed on the building. In the past we have been able to assume that the statistics from the climate of the recent past could be used to assess the performance of buildings in the future, however this is no longer the case.

There is now general agreement that the climate of the earth is changing more rapidly than has ever been recorded before and that this change is driven by the increasing concentration of 'greenhouse' gases in the atmosphere (IPCC 2007). The most important of these is carbon dioxide (CO_2) produced from burning fossil fuels, with deforestation also adding to atmospheric concentrations. Methane (CH_4), nitrous oxide (N_2O) and halocarbons also provide significant contributions. While there is a general consensus that the global temperature will rise steadily over the present century with more or less complex local effects, the possibility of more dramatic effects, which are physically plausible, but difficult to quantify, has also been raised. The most important of these are a) the thermohaline circulation, which drives the Gulf Stream in the North Atlantic, may be reduced because of fresh water from increased precipitation and melting ice caps; this would lead to a very marked cooling of northern Europe, with major consequences for economy, agriculture and energy demand; b) there might be major releases of methane as the soil warms, especially in the tundra in northern Canada and Russia; this would increase warming very significantly over present estimates with major impacts on local and global climate.

Because future climate predictions rely on assumptions about future global greenhouse gas emissions and global economic development, there is uncertainty in any estimate. To deal with this, different emissions scenarios have been developed by the Intergovernmental Panel on Climate Change (IPCC) to reflect possible patterns of global development (IPCC, 2000).

In recent years the potential impacts of climate change on buildings and construction have been studied in a number of countries, particularly the UK, Norway and Sweden. This is of particular interest in the UK, where much of the housing stock is old, with over 40% dating back before the middle of the 20th century (DCLG 2007). There are currently about 22.7 million dwellings in the UK, with current construction and demolition rates of 167,000/year and 20,000/year respectively. If these rates were continued unchanged, about 75% of the dwellings

in the UK in 2050 would those existing at present, with a significant number of these built before the 20th century. Even if construction and demolition rates were both doubled, still about 60% of dwellings in 2050 would be those with us now. Therefore measures to conserve energy in the house stock and protect individual buildings from the stresses of climate change must cover the adaptation of existing buildings as well as the improved design of new ones.

2. Future Climate Data

2.1 The UK Climate Impacts Programme

The United Kingdom Climate Impact Programme (UKCIP) is a major government funded programme to investigate the potential impacts of climate change on all aspects of life in the UK, including construction, energy use, infrastructure, industry, agriculture, society and the natural environment. A large number of sector specific and regional studies have been carried out under the co-ordination of the UKCIP. At an early stage of the programme in the 1990s it was realised that there was a danger of confusion between different projects using different assumptions about future climate change. To reduce this risk it was decided to develop a series of future climate 'scenarios' each of which was underpinned by clearly defined assumptions and reflected the best available understanding at the time. An initial set was produced in 1998; much more detailed scenarios were produced in 2002 and a very ambitious set of complex scenarios are due in October 2008 (delayed from 2006 owing to the complexity of the task). The analysis in this paper is based on the UKCIP02 Scenarios.

2.2 The UKCIP02 Scenarios

2.2.1 Emissions scenarios

How climate changes in the future depends on future emissions of greenhouse gases and other pollutants, which in turn depend upon how population, economies, energy technologies and societies develop. The IPCC Special Report on Emissions Scenarios (IPCC 2000) developed a range of projections of possible future emissions based on a series of 'storylines' about future global development. Four of these were chosen by the UKCIP (designated B1, B2, A2 and A1FI) which span nearly the full range (Table 1).

TABLE 1: Storyline assumptions behind the IPCC SRES Emissions Scenarios

Storyline	Description
A1Fl	Very rapid economic growth; population peaks mid-century; social, cultural and economic convergence among regions; market mechanisms dominate, with reliance on fossil fuels;
A2	Self-reliance; preservation of local identities; continuously increasing population; Economic growth on regional scales
B1	Clean and efficient technologies; reduction in material use; global solutions to economic, social and environmental sustainability; improved equity; population peaks mid-century
B2	Local solutions to sustainability; continuously increasing population at a lower rate than in A2; less rapid technological change than in B1 and A1

The amount of carbon emitted over the twenty-first century under each of these emissions scenarios is shown in Figure 1. Summed over the century, A1FI has the highest total emissions (2189 giga, or billion, tonnes of carbon; GtC), more than twice the mass of the lowest scenario, B1 (983 GtC). The atmospheric concentrations of carbon dioxide resulting from these emissions are shown in Figure 2.

The UK Met Office Hadley Centre global climate model was used to simulate changes in climate due to each of these emissions scenarios. The changes in global-average surface air temperature and CO_2 concentrations from the various scenarios are shown in Table 2. It is noticeable that, despite quite large differences in emissions between the four scenarios, there is relatively little difference between the global temperature changes they produce until after the middle of the century. This is partly because much of the change in climate over the next 30 to 40 years has already been determined by historic emissions and partly because the effects on climate of scenario differences in changes in greenhouse gas and sulphate aerosol concentrations initially offset each other. After 2050, however, the temperatures diverge more substantially.

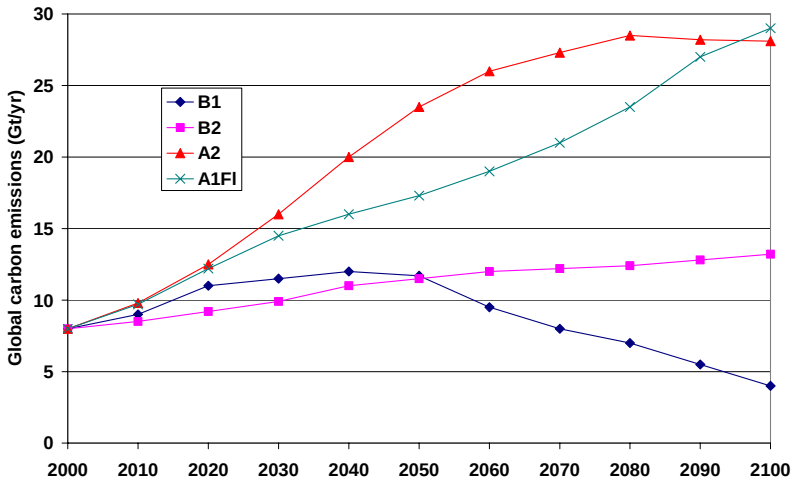

Figure 1: Global carbon emissions from all sources (energy, industry and land-use changes) from 2000 to 2100 for the four scenarios

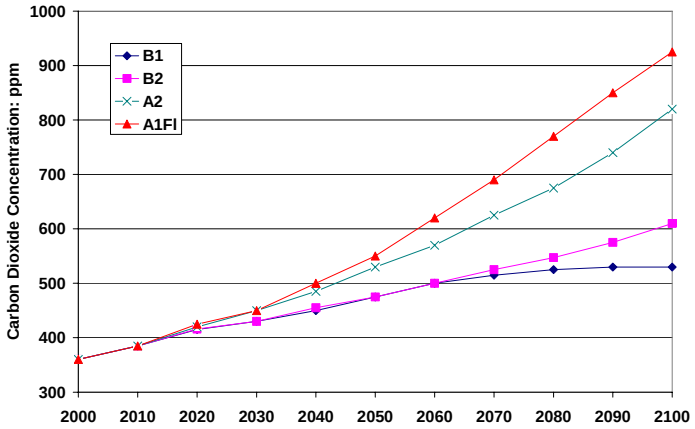

Figure 2 : Global carbon dioxide concentration (parts per million) from 2000 to 2100 for each of the four emissions scenarios.

Table 2: Global average temperatures and CO_2 concentrations under the four scenarios

	2020s		2050s		2080s	
	ΔT (°C)	CO_2 (ppm)	ΔT (°C)	CO_2 (ppm)	ΔT (°C)	CO_2 (ppm)
Low	0.79	422	1.41	489	2.00	525
Medium Low	0.88	422	1.64	489	2.34	562
Medium High	0.88	435	1.87	551	3.29	715
High	0.94	437	2.24	593	3.88	810

The results from the scenarios are available on a 50km grid for three time slices covering the 2020s, the 2050s and the 2080s. As an example Figure 3 show the predicted percentage change in winter rainfall, compared with the 1960 – 1990 averages, under the High Scenario (Hulme et al., 2002).

Figure 3 : Percentage change in winter rainfall compared to the 1960 – 1990 average under the High Scenario

2.3 The UKCIP08 Scenarios

It is not possible to assign any relative probabilities to the four UKCIP02 Scenarios. This will change significantly in the UKCIP08 scenarios to be launched in October 2008. The implications of the multiple assumptions and choices that needed for climate modelling are being explored. This is being achieved by varying certain model parameters within the Hadley Centre climate model (HadCM3) within plausible limits, with each combination of parameter values providing a different model version. In total 31 parameters were varied to provide around 300 model versions, creating a large ensemble of projections of future global climate, all using the Hadley Centre climate model. These ensembles will be weighted by how well the relevant model explains currently observed trends in the atmosphere. This is based on the assumption that models which are better at representing current climate and recent trends will also be better at representing future climate.

The data will be available for each 25 x 25 km UK grid squares; for three future scenarios of greenhouse gas emissions (labelled as Low, Medium and High); for the period 2010-2099, using seven overlapping 30-year time-slices that move forwards in decade steps (i.e. 2010–2039, 2020–2049, etc. until 2070–2099); for changes in monthly, seasonal and annual averages, perhaps with additional information expected about changes to extreme events (e.g. hottest day of summer, wettest day of winter).

The data can be used to drive a weather generator (see below), a tool that will provide a statistical expression of baseline and projected climate at daily time-scales that are consistent with the UKCIP08 probabilistic climate projections.

2.4 Building Knowledge for a Changing Climate

One part of the overall UKCIP programmes on climate change was a programme of linked projects looking in detail at impacts on the built environment and infrastructure, Building Knowledge for a Changing Climate, (BKCC). This covered urban heat islands, drainage and flooding, economic and social impacts, and impacts on the energy supply industry. As part of this, Glasgow Caledonian University and University College London collaborated in Engineering Historic Futures, which examined the impacts of driving rain and flooding on historic buildings, which are particularly vulnerable to climate change impacts (Cassar & Hawkings, 2007).

One of the major inputs to the BKCC projects was a set of hourly future climate scenarios specifically designed for research in the construction industry, produced under a project called Built EnvironmenT: Weather scenarios for investigation of Impacts and eXTremes (BETWIXT) The need for high-resolution climate change scenarios tailored to the needs of the construction research was identified from these discussions with potential academic partners and stakeholders. The starting point for the work is the UKCIP02 climate change scenarios which have been developed for shorter time periods and point locations, to meet the particular requirements of the built environment, including information about changes in weather extremes.

BETWIXT developed two types of model to construct these scenarios.

1. The RainClim software package was developed by the University of Newcastle building on previous work on the Neyman-Scott Rectangular Pulses (NSRP) point-process rainfall model applied in hydrological modelling.

The software can be used to generate rainfall time series for the present day and future time periods up to 2100 for 18 sites in the UK, with time resolutions of 5 minutes and 1 hour.

2. This was linked to the weather generator developed by the Climatic Research Unit (CRU) at UEA to construct self-consistent daily time series scenarios for the present day and future time periods for eight variables (maximum and minimum temperature, precipitation, sunshine, vapour pressure, relative humidity, wind speed and potential evapotranspiration) and 10 BKCC case-study locations (including Manchester, Glasgow, Bradford, Birmingham and Heathrow). An hourly version of the weather generator, linked to RainClim, has also been produced.

The BETWIXT data from two locations in the UK was used to assess the affects of climate change on the boundary conditions for hygrothermal modelling.

3. Effect of Climate change on Boundary Conditions

3.1 Data used

Two of the BETWIXT data sets were used:

Heathrow on the western edge of London, 51° 28' N, 0° 27' W, 24m above sea level, is typical of the conditions that affect most building in the south of England.

Eskdalemuir in the Southern Uplands of Scotland, 55° 19' N, 3° 12' W, 242m above sea level, is representative of the most severe conditions likely to be experienced by almost all the buildings in the UK.

Figures 4 and 5 show the current monthly mean temperatures and rainfall totals from the two stations.

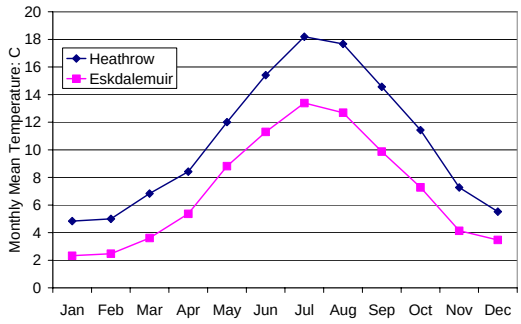

Figure 4: Current monthly mean temperatures at Heathrow and Eskdalemuir

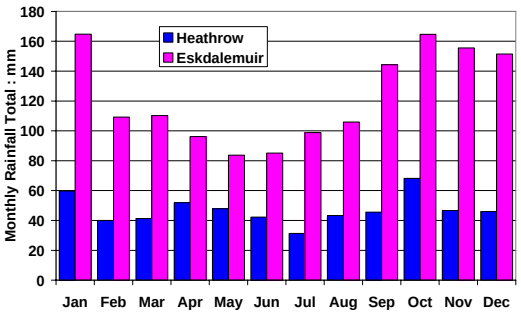

Figure 5: Current monthly rainfall totals at Heathrow and Eskdalemuir

The BETWIXT files are representative of the 1970 climate and the four UKCIP02 scenarios for the 2020s, the 2050s and the 2080s. Each file contains 30 years of hourly values of:

- Temperature in °C
- Vapour pressure in kPa
- Rainfall in mm
- Wind speed in m/s
- Fraction of hour with bright sunshine

These were used to calculate daily and monthly mean temperatures, rainfall and sunshine totals, and the daily maximum and minimum temperatures. A number of other derived parameters were also calculated. The sections below discuss the effect of climate change on various parameters relevant to the hygrothermal performance

3.2 Temperature

3.2.1 Mean temperatures

The simplest effect of climate change or 'global warming' as it used to be known, is rising temperature. To give an impression of the range of effects predicted, Figure 6 shows the seasonal mean temperatures at Heathrow from 1970 and from the Low and High scenarios from 2020, 2050 and 2080. Figure 7 shows the same information from Eskdalemuir.

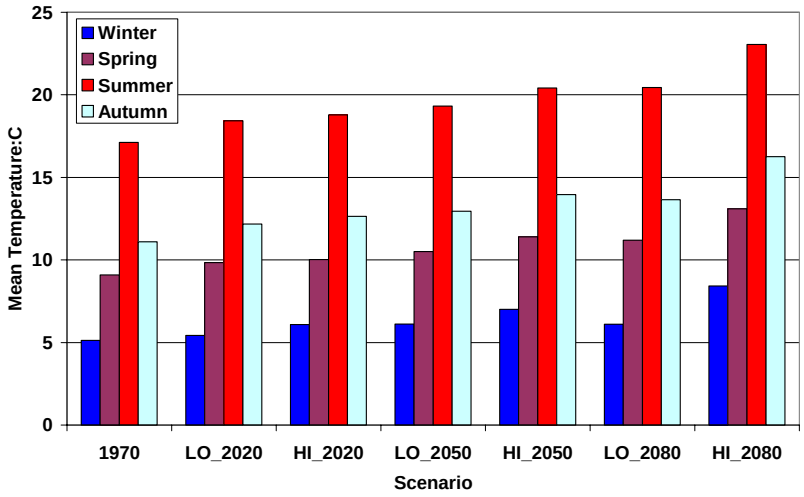

Figure 6 : Seasonal mean temperatures from Heathrow for 1970, and the Low and High Scenarios for 2020, 2050 and 2080.

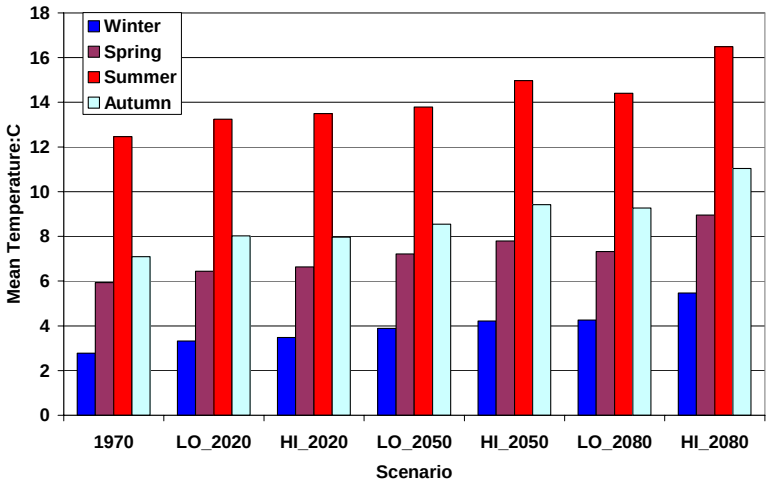

Figure 7: Seasonal mean temperatures from Eskdalemuir for 1970, and the Low and High Scenarios for 2020, 2050 and 2080.

By 2080 the mean summer temperature at Heathrow is predicted to rise by between 3°C and 6°C, with rises of between 2°C and 4°C at Eskdalemuir. The winter temperature rises are rather smaller.

3.2.2 Extreme Temperatures

In many practical applications extreme temperatures are of more importance than the means. Unusually high summer temperatures can cause discomfort, and in extreme cases, affect human health. In this respect high overnight minimum temperatures can be more of a problem than high daytime maxima. Also if high summer

temperatures become more common, there is a possibility that air conditioning in housing, which is currently extremely rare in the UK, might be more commonly installed, with significant consequences for energy use. Tables 3 and 4 show that high maximum and minimum temperatures will become very much more common at Heathrow. There will be similar rises at Eskdalemuir, although at lower temperature levels.

Table 3: Number of days/year with maximum temperature >30°Cand 34°C at Heathrow

	1970	HI_2020	HI_2050	HI_2080
Tmax>30°C	1.5	5.5	15.1	22.7
Tmax>34°C	0.0	0.1	1.8	3.7

Table 4: Number of days/year with minimum temperature >24°Cand 28°C at Heathrow

	1970	HI_2020	HI_2050	HI_2080
Tmin>24°C	0.0	0.1	1.9	10.4
Tmin>28°C	0.0	0.0	0.0	0.9

As high temperatures become more common, low temperatures will become less common. Table 5 shows the fall in low overnight minima at Eskdalemuir.

Table 5: Number of days/year with minimum temperature <0°C and -6°C at Eskdalemuir

	1970	HI_2020	HI_2050	HI_2080
Tmin<0°C	55.0	37.9	24.3	11.0
Tmin<-6°C	2.7	1.6	0.6	0.4

3.2.3 Successive days with extreme temperatures

Particular problems in cooling buildings can arise when there are sequences of successive very hot days. Table 6 shows the number of occasions/year when there are sequences of 2, 3, 4 and 5 successive days at Heathrow with a maximum temperature greater than 30°C. The very marked increase in occurrence by 2080 is clear.

Table 6: Number of occasions at Heathrow with 2, 3, 4 and 5 successive days with maximum temperature >30°C

No. of successive days	1970	HI_2020	HI_2050	HI_2080
2	0.1	0.2	3.5	15.7
3	0	0.1	2.1	11.2
4	0	0	1.3	8.2
5	0	0	0.7	6

The possibilities of passive cooling of buildings overnight are limited and the discomfort to occupants increases when minimum overnight temperatures are high. Table 7 shows the number of occasions/year at Heathrow when there are 2, 3 and 4 successive days with maximum temperature over 30°C and minimum over 25°C. While there are fewer occurrences than in Table 6, the increase by 2080 is again clear.

Table 7: Number of occasions at Heathrow with 2, 3 and 4 successive days with maximum temperature >30°C and minimum temperature >25°C

No. of successive days	1970	HI_2020	HI_2050	HI_2080
2	0	0	0.23	3.43
3	0	0	0.07	1.73
4	0	0	0	1

The cooler climate of Eskdalemuir means that that these high temperature sequences do not occur, even by 2080.

Problems with heating systems being able to maintain the desired internal temperatures can occur when there are several successive unusually cold days. With the general rise in temperature, these will become less common as shown in Table 8

Table 8: Number of days/year with maximum temperature <0°C at Eskdalemuir

No. of successive days	1970	HI_2020	HI_2050	HI_2080
2	2.2	1.1	0.8	0.2
3	1.2	0.5	0.4	0.1
4	0.7	0.2	0.2	0

3.3 Rainfall

Table 9 shows the seasonal mean daily rainfall totals for Heathrow and Eskdalemuir. Both show significant rises in the winter (40% by 2080 at Heathrow, 22% at Eskdalemuir) and falls in the summer (55% at Heathrow and 31% at Eskdalemuir. Over the whole year there is an 8% fall at Heathrow and a 4% rise at Eskdalemuir.

Table 9 : Seasonal mean daily rainfall total at Heathrow and Eskdalemuir: mm/day

	Heathrow				**Eskdalemuir**			
	1970	HI_2020	HI_2050	HI_2080	1970	HI_2020	HI_2050	HI_2080
Winter	1.62	1.84	2.03	2.30	4.73	5.26	5.50	5.80
Spring	1.53	1.48	1.40	1.26	3.15	3.37	3.72	3.49
Summer	1.27	1.14	0.91	0.58	3.15	3.12	2.62	2.18
Autumn	1.76	1.98	1.69	1.55	5.10	5.01	5.28	5.39

Very high daily rainfall totals are significant in causing flooding, that is perceived to be one of the major impacts of climate change on buildings. However the process of development of the scenarios does not take good account of the severe storms that produce extremes. There is some indication, shown in Table 10, that high totals will increase, especially at Eskdalemuir.

Table 10 : Number of days/year with rainfall >25mm and >50mm at Heathrow and Eskdalemuir

	1970	HI_2020	HI_2050	HI_2080
Heathrow >25mm	0.7	0.9	1.0	1.1
Heathrow >50mm	0	0.1	0	0.1
Eskdalemuir >25mm	7.3	8.0	9.4	9.9
Eskdalemuir >50mm	0.2	0.3	0.6	0.8

3.4 Windspeed

Windspeed is both the most important climate parameter that can effect the structure of buildings and the most difficult to predict in the future. In the development of the BETWIXT scenarios considerable effort went into refining wind speed predictions however much less confidence can be placed in them that in predictions of the other parameters. Wind direction is even more complex with no predictions available

Table 11 shows the seasonal mean windspeeds for Heathrow and Eskdalemuir. Both show small rises in the winter (9% by 2080 at Heathrow, 13% at Eskdalemuir) and summer (11% at Heathrow and 8% at Eskdalemuir). Over the whole year there are rises of 10% at Heathrow and 11% at Eskdalemuir.

Table 11 : Seasonal mean wind speed at Heathrow: m/s

	Heathrow				Eskdalemuir			
	1970	HI_2020	HI_2050	HI_2080	1970	HI_2020	HI_2050	HI_2080
Winter	3.7	3.8	3.9	4.1	4.02	4.27	4.37	4.56
Spring	3.8	3.9	3.9	4.0	3.94	4.02	4.22	4.38
Summer	3.2	3.3	3.4	3.6	3.32	3.42	3.54	3.60
Autumn	3.1	3.3	3.4	3.5	3.62	3.63	3.91	4.03

For structural considerations, extreme windspeeds are much more important than the means. However the process of development of the scenarios does not take good account of the severe storms that produce extremes. There is some indication, shown in Table 12, that high speeds will increase, especially at Eskdalemuir.

Table 12: Number of hours/year with wind speed >10m/s at Heathrow and Eskdalemuir

	1970	HI_2020	HI_2050	HI_2080
Heathrow	12	13	13	16
Eskdalemuir	151	169	295	202

3.5 Solar Radiation

Obviously, the changing concentration of greenhouse gases will not affect the solar geometry in relation to the surface of the earth and the consequent intensity of the incoming solar radiation. The changing composition of the atmosphere will also have a negligible effect on the transmission of incoming radiation through clear skies. However possible changes in cloudiness will have significant effects on the hours of sunshine at the earth's surface and therefore the energy absorbed at building surfaces.

The BETWIXT data sets contain the proportion of each hour that the sun is shining at each location. These have been summed up to give the daily totals of bright sunshine. Average values for the two locations for each season and the four time periods are summarised in Table 13. This shows small falls in the winter in both areas and more substantial rises in the summer (14% at Heathrow and 12% at Eskdalemuir by 2080)

Table 13: seasonal averages of sunshine hours/day at Heathrow and Eskdalemuir

	Heathrow				Eskdalemuir			
	1970	HI_2020	HI_2050	HI_2080	1970	HI_2020	HI_2050	HI_2080
Winter	2.09	2.08	2.03	1.94	1.42	1.39	1.39	1.37
Spring	4.99	5.09	5.42	5.51	4.28	4.22	4.22	4.30
Summer	6.53	6.80	7.10	7.51	5.19	5.24	5.58	5.80
Autumn	3.69	3.63	3.62	3.62	2.65	2.68	2.69	2.69

The number of very sunny summer days, with more than 10 hours or more than 12 hours of sunshine rises sharply at Heathrow as shown in Figure 8, with increases of 40% and 47% respectively.

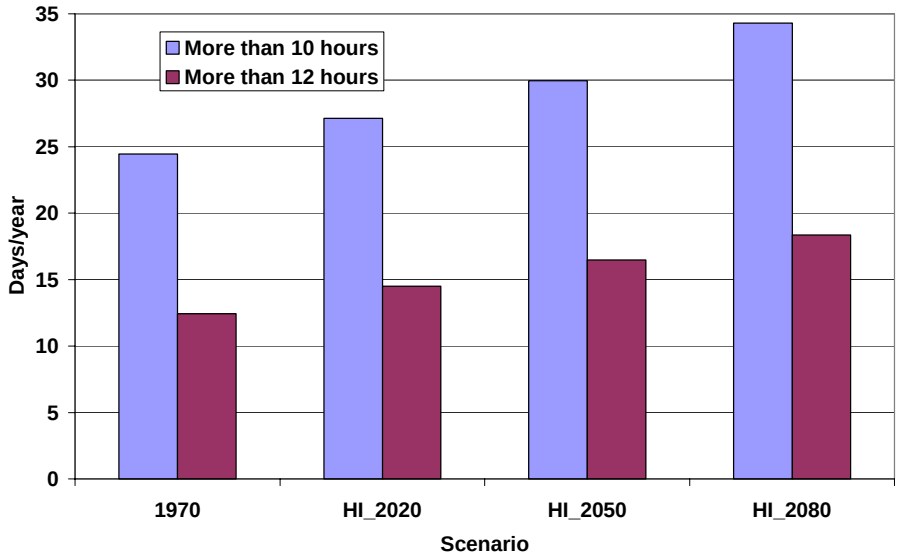

Figure 8 : Number of days/year at Heathrow with more than 10 hours and more than 12 hours of sunshine.

Conversely, the number of winter days with less than one hour of sun rises at Eskdalemuir from 43.9 in 1970 to 46.8 in 2080.

3.6 Atmospheric humidity

As shown in Table 14, small rises in seasonal mean vapour pressure are predicted by 2080, when combined with the rising temperatures, discussed in section 3.2, these lead to the significant falls in relative humidity shown in Table 15.

Table 14 : Seasonal mean vapour pressure in kPa at Heathrow and Eskdalemuir

	Heathrow				**Eskdalemuir**			
	1970	HI_2020	HI_2050	HI_2080	1970	HI_2020	HI_2050	HI_2080
Winter	0.77	0.77	0.78	0.80	0.68	0.70	0.70	0.71
Spring	0.90	0.91	0.93	0.95	0.78	0.78	0.81	0.82
Summer	1.38	1.42	1.45	1.48	1.21	1.23	1.26	1.27
Autumn	1.12	1.14	1.15	1.17	0.93	0.94	0.96	0.97

Table 15 : Seasonal mean relative humidity,%, at Heathrow and Eskdalemuir

	Heathrow				**Eskdalemuir**			
	1970	HI_2020	HI_2050	HI_2080	1970	HI_2020	HI_2050	HI_2080
Winter	70	64	59	52	82	77	71	63
Spring	54	49	44	38	65	61	56	50
Summer	36	32	27	22	51	46	41	35
Autumn	54	47	42	33	69	63	55	47

3.7 Frost damage

Repeated freezing and thawing of wet masonry disrupts the material, causing surface layers to spall off, damaging the appearance of the building and increasing the risk of rain penetration. This is a greater problem in temperate climates where the temperature moves through 0°C many times a winter, than in colder climates. A long series of trials of exposed brickwork samples carried out by BRE Scotland in the 1990s (Stupart & Phillipson, 1998) established a frost index, which would increase by one on each day when a) the minimum temperature was below -2°C and the maximum was above 0°C and b) there had been at least 10mm of rain in the previous 7 days. The total index for the winter gave the risk of damage to brickwork at any location.

Table 16 shows the change in the individual components of the frost index independently and the frost index itself. The rising temperatures mean that there is a distinct fall in the frost index in both locations.

Table 16: Temperature and rainfall components of the frost index (occasions/year) from Heathrow and Eskdalemuir.

	Heathrow				**Eskdalemuir**			
	1970	HI_2020	HI_2050	HI_2080	1970	HI_2020	HI_2050	HI_2080
Temperature component	5.7	2.6	0.6	0.1	18.6	11.3	7.2	2.7
Rain component	151.7	153.3	139.8	134.9	274.6	287.0	265.2	264.9
Frost Index	1.3	1.4	0.2	0	13.5	9.4	5.1	2.1

3.8 Driving rain

The combination of rain and wind to form driving rain is a very important input to the moisture load on any building. The classic equation for the total load on a vertical surface over any period is (Lacy, 1997):

$$I'_S = \frac{2}{9}\sum v \cdot r^{8/9} \cdot \cos(D - \Theta)$$

Where v is the wind speed in m/s
r is the rainfall rate in mm/hour
D is the wind direction
Θ is the angle of the normal to the wall relative to north
The sum is taken over all occasions when cos(D-Θ) is positive, i.e. the wind is blowing against the wall

As we do have any wind direction data in the scenarios, it is not possible to calculate the complete index, however if we assume that the directions are not going to change, it is possible calculate relative indices from different periods. Table 17 shows that there are significant increases in winter at both locations, with corresponding falls in the summer

Table 17: Seasonal percentage change in total driving rain compared to 1970

	Heathrow			**Eskdalemuir**		
	HI_2020	HI_2050	HI_2080	HI_2020	HI_2050	HI_2080
Winter	7.2	25.8	47.7	14.1	25.2	42.1
Spring	2.7	-10.0	-11.4	3.9	26.4	19.8
Summer	-7.0	-18.6	-42.9	-0.7	-11.6	-26.7
Autumn	20.8	6.2	0.3	-2.4	12.6	17.6

4. Conclusions

This paper has used a data set of hourly values of future climate parameters developed specifically for construction research, to assess the changes in those parameters relevant to boundary conditions for hygrothermal modelling, that are likely to occur by 2080. Data from two locations were analysed: Heathrow in southern England and Eskdalemuir in upland Scotland. The main results that have come from this are:

- Seasonal mean temperatures will increase by between 3°C and 6°C and extreme temperatures and periods of successive days with high temperatures become more common. Conversely, low temperatures will become less common.
- Seasonal rainfall totals will rise in winter and fall in summer, extreme high rainfall events may become more common, although the data set used may not predict these reliably.
- Similarly seasonal mean windspeeds will tend to increase.
- Sunshine totals will fall slightly in the winter, but increase significantly in summer.
- Vapour pressure will rise slightly, but because of the rises in temperature, relative humidities will fall significantly.
- Because of the rising temperatures, frost damage to masonry will fall sharply
- Driving rain will increase in winter, but fall in summer.

5. References

BETWIXT http://www.cru.uea.ac.uk/cru/projects/betwixt/

Cassar, M.C, Hawkings, M. (2007) Engineering Historic Futures, Stakeholders Dissemination and Scientific Research Report, UCL. www.ucl.ac.uk/sustainableheritage/publications.htm

DCLG (2007), English House Condition Survey 2005: Annual Report, ISBN 139781851128822, UK Department of Communities and Local Government

Hulme,M., et al. (2002) Climate Change Scenarios for the United Kingdom: The UKCIP02 Scientific Report, Tyndall Centre for Climate Change Research, School of Environmental Sciences, University of East Anglia, Norwich, UK.

IPCC (2000) Special report on emissions scenarios (SRES): A special report of Working Group III of the Intergovernmental Panel on Climate Change, Cambridge University Press, Cambridge, UK, 599pp.

IPCC (2007), Climate Change 2007 - The Physical Science Basis, Working Group I Contribution to the Fourth Assessment Report of the IPCC, Cambridge University Press , http://www.ipcc.ch/

Lacy, R.E. (1977) Climate and Building in Britain, BRE, Department of the Environment, 1977.

Stupart, A W, Phillipson, M C (1998), Frost indexing for clay brickwork Masonry International. Vol. 12, no. 1, pp. 13-16.

Walsh, C.L. et al (2007). Building Knowledge for a Changing Climate: collaborative research to understand and adapt to the impacts of climate change on infrastructure, the built environment and utilities. Newcastle University, March 2007. http://www.k4cc.org/news/bkcc-publication

UKCIP http://www.ukcip.org.uk/

Modelling of mould growth in building envelopes

Ruut Peuhkuri, Ph.D.
ruut.peuhkuri@vtt.fi

Hannu Viitanen, Ph.D.
hannu.viitanen@vtt.fi

Tuomo Ojanen, M.Sc.
tuomo.ojanen@vtt.fi

VTT Technical Research Centre of Finland

KEYWORDS: *mould, modelling, experiments, sensitivity analysis.*

ABSTRACT:

The requirements for durability of the buildings and indoor air quality are growing. Therefore the focus in hygrothermal modelling of whole buildings is moving towards a kind of risk analysis. One of the main risks in this sense is the mould growth and following indoor air quality problems, and also decay of the constructions. This paper gives a state-of-art of models predicting mould growth. But what is more important, this paper also discusses the whole problem of modelling such a phenomenon. A sensitivity analysis of modelled mould growth and comparison with measured mould growth are also presented in order to enhance the strength and weakness of approaches to model mould growth in building envelopes.

1. The nature of mould growth

The important starting point for the whole mould issue is to understand that mould spores are all over in our surroundings. Therefore we will never get totally rid of mould: The mould growth outdoors will always happen in our temperate climate, unless the building exterior surface is treated with fungicides and/or cleaned regularly. However, to provide durable and healthy buildings, we need to manage the conditions – especially the microclimate and the envelope constructions – in order to reduce the risk for mould growth. In this section, necessary conditions for mould growth are discussed shortly.

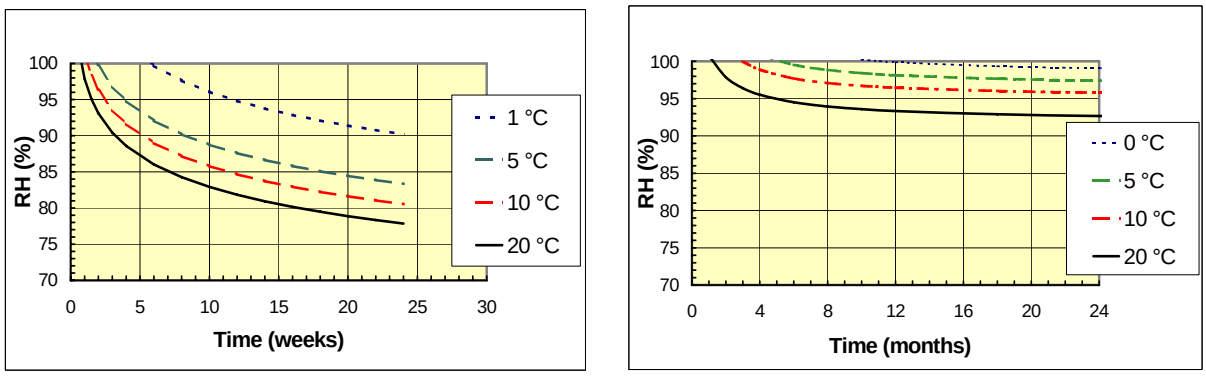

FIG. 1. Critical humidity (RH %), time (weeks / months) and temperature needed for the start of ***mould*** *growth on pine sapwood (A) and early stage of* ***brown rot*** *development (B) in pine sapwood (Viitanen et.al 2000).*

A certain **duration** of suitable exposure conditions is required before microbial growth will start or the damage will reach a certain grade. Particular emphasis is focused on this time period, the so-called response time or response duration in different humidity and temperature conditions for mould growth or decay development (Viitanen 1996). The lowest humidity level for mould growth is around RH 75 – 80 % and for decay development above RH 95 - 98 %. The response times proved to be short (from a few days to a few weeks) in

pine sapwood in conditions favourable to the growth of micro-organisms and long (from a few months to a year) in conditions close to the minimum and maximum moisture or temperature levels. Time periods needed for decay development are also significant longer than that for mould growth. Critical humidity levels at different temperatures for mould and rot, respectively, are shown in FIG. 1. Notice the different time scales for mould and brown rot!

Another classical way to express the suitable exposure conditions is to use so-called isopleth diagrams (see FIG. 2A). (Ayerst 1969) studied the effect of moisture and temperature on growth and spore germination for some mould fungi on agar medium. For each mould species and temperature level there is a minimal amount of moisture needed for these processes. These growth conditions – for germination times or growth rates – can be described in an isopleth diagram. Outside the lowest line (isopleth) the mould is not active. The isopleths are determined under steady state conditions, i.e. constant temperature and relative humidity.

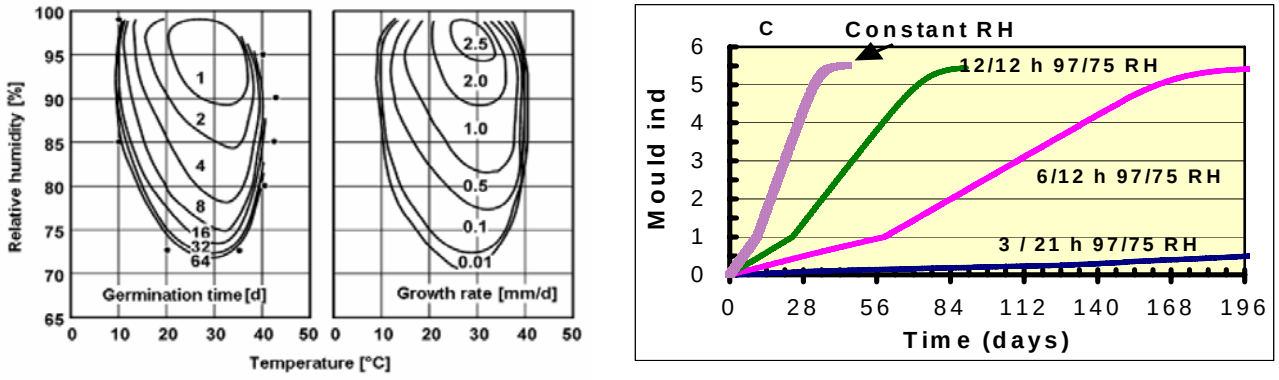

FIG. 2: A) An example on isopleth systems. Measured germination time and growth rate of Aspergillus restrictus (Ayerst 1969). B) Modelled impact of cyclically varying moist and dry periods on mould growth according to VTT model (Hukka. & Viitanen 1999),(Viitanen et.al 2000)

Other important studies on mould growth are e.g.(Block 1953), who studied the humidity requirements for mould growth on different materials. (Smith & Hill 1982) studied the effect of temperature and water activity on germination and growth of selected mould fungi. They showed the isoplets of the growth conditions of the mould fungi on agar medium. (Grant et.al 1989) analysed and modelled the moisture requirements of some mould fungi isolated from dwellings. A certain succession depending on the moisture requirements of different fungal species: primary, secondary and tertiary colonizers, was found.

Within fluctuating humidity conditions (see FIG. 2B), the total exposure time for response of growth of mould fungi is affected by the time periods of high and low humidity conditions as well as the humidity and temperature level. Short periods at high humidity conditions will not cause a fungal growth if the time periods at low humidity preventing mould growth are long enough (Viitanen & Bjurman 1995). When the period at high RH is longer than 24 hours, the effect of cumulative time at high humidity is more linear, but if the dry periods are very long, very low or neglected growth response will be expected. An exposure period at low RH prevents the growth and has a direct effect on the total response time required for mould growth.

In practical cases it means, that the short high humidity causes no risk for mould, if the moisture of structures are not increased for longer time. For example RH 95 % for 2 hours in each day causes no harm, if continuous microclimate conditions of materials are below RH 75 %. Temperature fluctuation can cause condensation of water or high RH near the surface, if RH of indoor air is high (e.g. above 50 % during winter time). In fluctuating temperature conditions at a high RH, a fall in temperature will add or even condense moisture on the surface of materials and drastically enhance the available moisture for microbial growth.

2. Existing models for predicting mould growth

In this section, the aim is to give a rather comprehensive overview of the existing work conducted in order to understand the methods behind the calculation models for predicting mould growth under given conditions. The authors are themselves deeply involved in mould modelling activity and therefore the model they know best is introduced first and most detailed. However, it is widely accepted in scientific community that the VTT model is

one of the most advanced models in predicting dynamic behaviour of mould growth. Nevertheless, also the VTT model has it's restrictions and therefore at present a project is pending in order to improve it. (Lähdesmäki et.al, 2008)

Generally, the models are based on measured data which is transformed to numerical values by e.g. regression analysis and/or implementation of hygrothermal calculation principles on mould spores. The measured data is obtained from laboratory tests using different mould fungi and different growth medium at regulated humidity and temperature conditions. Typically, the experimental results are given as isopleths – i.e. as a mould growth rate for different combinations of temperature and humidity.

2.1 VTT model for mould growth index

A mould growth model for pine and spruce sapwood material and it's applications has been presented in several papers (Hukka & Viitanen 1999), (Viitanen et.al 2000), (Ojanen & Salonvaara 2000), (Viitanen et.al 2003). The model is based on the laboratory work and comprehensive regression models for mould growth in constant and fluctuating humidity and temperature conditions are reported by Viitanen and Ritschkoff (Viitanen & Ritschkoff 1991). The mould growth model is based on, and describes, the mathematical relations for growth rate of mould index in different conditions including the effects of exposure time, temperature, relative humidity and dry periods. The model is purely mathematical in nature. Quantification and evaluation of mould growth in the model is based on the mould index (TABLE 1) used in the experiments for visual inspection for pine and spruce sapwood material (Viitanen & Ritschkoff 1991).

TABLE 1: Mould growth index for the experiments and modelling

Index	Growth rate	Description
0	No growth	Spores not activated
1	Small amounts of mould on surface (microscope)	Initial stages of growth
2	<10% coverage of mould on surface (microscope)	
3	10-30% coverage mould on surface (visual)	New spores produced
4	30-70% coverage mould on surface (visual)	Moderate growth
5	> 70% coverage mould on surface (visual)	Plenty of growth
6	Very heavy and tight growth	Coverage around 100%

In the simulation of mould growth, it is crucial to know the lowest (threshold) conditions where fungal growth is possible in different material. Also the duration of these conditions is significant. There are certain minimum and maximum levels for moisture content of material (or water activity) or temperature between which fungi can grow in wood. Under these favourable conditions mould growth may start and proceed at different rates depending upon the interrelationship between humidity and temperature and upon other factors such as the organisms and the properties of the materials. There may exist different mould species but the mould index used is based on the growth activity of different mixed mould species. Different mould species depending on the conditions were found in the studies which were used as a data source for the modelling.

Time period needed for the initiation of mould growth and growth intensity are mainly regulated by water activity, temperature, exposure time and surface quality of the substrate. The experiments on pine sapwood material supported this theory and based on the results, a mathematical model was developed. The favourable temperature range for mould growth is 0-50 °C, and the critical relative humidity required for initiation and development of mould growth (mould index) is a function of temperature and exposure time (FIG. 3).

Based on experiments on pine and spruce sapwood, the critical humidity, temperature and exposure conditions for mould growth can be described using a polynomial function, Eq.(1) (Hukka & Viitanen 1999), (Viitanen et.al 2000)

$$RH_{crit} = \begin{cases} -0.00267T^3 + 0.160T^2 - 3.13T + 100.0, \text{ when } T <= 20 \\ 80\ \%, \text{ when } T > 20 \end{cases} \quad (1)$$

The Equation (2) for mould growth intensity is a function of temperature and relative humidity values.

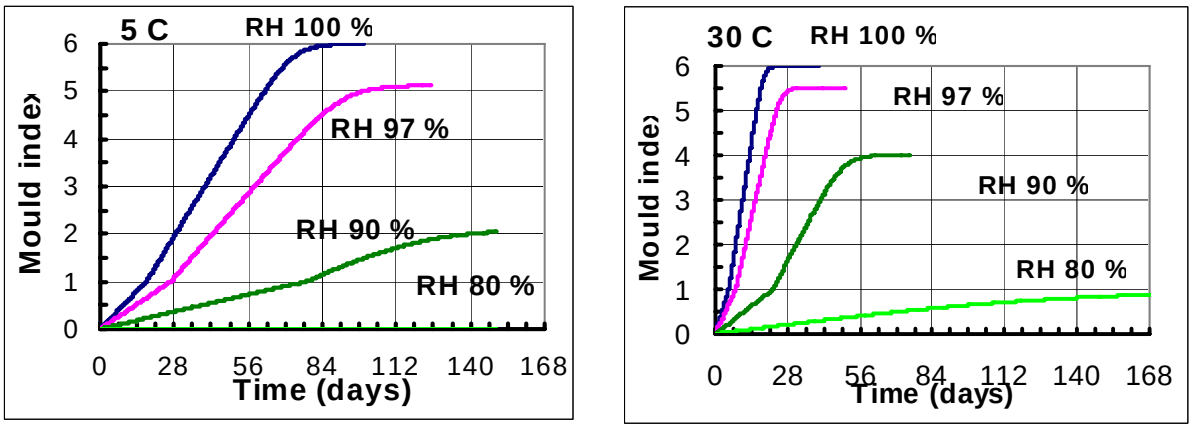

FIG. 3. The critical humidity, temperature and exposure time periods at varied constant conditions for initiation of mould growth on pine sapwood based on a mathematical model 1 (Viitanen et.al 2000).

$$\frac{dM}{dt} = \frac{1}{7 \cdot \exp(-0.68 \ln T - 13.9 \ln RH + 0.14W - 0.33SQ + 66.02)} k_1 k_2 \qquad (2)$$

where M is the mould growth index, t is time (weeks), W is the wood species (0 = pine and 1 = spruce), SQ is the surface quality (0 is for kiln dried timber and 1 for timber dried under normal kiln drying process), and

$$k_1 = \begin{cases} 1, \text{ when } M < 1 \\ \dfrac{2}{t_v / t_m - 1}, \text{ when } M > 1 \end{cases} \qquad (3)$$

Taking into account the upper limit for mould growth defined by regression equations, the use of a correction coefficient is needed. The retardation of the growth in the later stages is defined by coefficient k_2, Eq.(4). This means, that when the mould index will approach the level 4 - to 6 or the maximum growth level, the response curve will be bended. Assuming the delay to affect the growth rate by 10 % at 1 unit below the maximum value of the index gives this coefficient a form

$$k_2 = \max[1 - \exp[2.3 \cdot (M + M_{\max})], 0] \qquad (4)$$

A mathematical description of the delay of mould growth when conditions become unfavourable (RH drops below critical RH) can be written by using the time passed from the beginning of the dry period (t-t_1) Eq.(5):

$$\frac{dM}{dt} = \begin{cases} -0.032, \text{ when } t - t_1 \le 6 \text{ h} \\ 0, \text{ when } 6 \text{ h} \le t - t_1 \le 24 \text{ h} \\ -0.016, \text{ when } t - t_1 > 24 \text{ h} \end{cases} \qquad (5)$$

The numerical values of the parameters included in the model are fitted for pine and spruce sapwood using large set of data from various constant and short term dynamic experiments carried out using wooden test samples. Special features have been included in the model to simulate the effect of the dynamically changing conditions on the delay of initiation of mould growth. These relatively short term cycles (hours, some days or weeks) represent the delay of mould growth on pine sapwood surface. The effect of long periods (months), seasonal cycles (effect of frost) are not taken into account.

The mould growth model can be used to study the risks for mould growth on (wooden) material surface when the surface conditions (temperature and relative humidity) are known. Typically the conditions vary dynamically

and their hourly values should be known to be able to study the mould growth. Long period (daily, weekly. etc.) time averaged values may not show the risks of the actual conditions, i.e. the peak humidity levels etc. on the mould growth. The same kind of error may be caused when the adjacent climate conditions are used as critical conditions instead of the actual surface conditions. Therefore the effect of the structure and material should always be taken into account when solving the critical conditions for the mould growth.

The VTT model has been implemented in a hygrothermal simulation model TCCC2D (Ojanen et.al 1994), (Ojanen 1996). This 2D model solves the transient heat, air and moisture transport fields of a structure that can consist of several material layers. The boundary conditions for the analysed structure can be, for example, hourly changing climate conditions and indoor conditions that have a set increase in humidity compared to outdoor conditions. Measured data can also be used as boundary conditions. The model solves the temperature and moisture content / relative humidity value for every time step of the solution and for each node of the mesh representing the structure section. The mould growth index values can be solved for each node and the risk for mould growth in wood based or other organic (or soiled) material surface can be predicted.

2.2 Development of an improved VTT model for mould growth

At the moment, the VTT model only predicts the mould growth for wood. The wooden materials are among the most sensitive materials for mould growth and therefore the model can be used as a worst-case-scenario. Nevertheless, a research project to improve the model is going on as collaboration between VTT and Tampere University of Technology (TUT). The aim is to formulate a more diversified and improved application of the existing VTT model for mould growth. Some of the improvement aspects are:

- to increase reliability of the existing mathematical model in fluctuating conditions
- to increase the number of material choices for the model
- to test usage of the model by doing experiments for structures and materials in laboratory and in field conditions, including the effects of adjacent material layers in a construction

An important part of this model improvement work is a large experimental study on 8 different building materials (edge glued spruce board, polyurethane (paper coated and grounded), glass wool, expanded polystyrene, polyester wool, concrete, autoclaved cellular concrete and expanded light aggregate concrete) going on in collaboration with TUT and VTT, Finland. These materials are tested as pure materials and as a part of building envelope constructions both in laboratory and outdoors. The laboratory tests are made partly under constant, but different conditions and partly under varying conditions to simulate real exposure. Outdoors the materials and constructions are tested under real conditions. (Lähdesmäki et.al 2008)

2.3 Other models predicting mould growth

(Adan 1994) used a non-linear regression technique to model sigmoidal curves describing vegetative fungal growth of *Penicillium chrysogenum* on gypsum board material. He used the time-of-wetness (TOW) as an overall measure of water availability for fungal growth under fluctuating humidity conditions. The TOW is defined by the ratio of the cyclic wet period (RH>= 80 %) and the cyclic dry period. The mould growth is a function of the effect of lowest humidity, time of wetness and high relative humidity frequency, and finally of periods of wet and dry conditions. He used LTSEM to analyse the growth and studied the effect of coatings and surface quality on the mould growth. He also evaluated the effect of distribution of growth density on test results.

(Sedlbauer 2001) has studied different models to evaluate spore germination and growth of different mould species on different type of materials. He found, that the isopleths based on artificial medium can be used to evaluate the growth rate of different fungi. He used a biohygrothermal model based on the relative humidity, temperature and exposure time needed for the spore germination of mould fungi based on the osmotic potential of spores. He analysed the effect of different climatic conditions on the spore moisture content and germination. He also evaluated the spore moisture content and germination time based calculated time courses of temperature and relative humidity in various positions of the exterior plaster of an external wall using WUFI program (Wufi). The idea and relationship between the different parameters in the biohygrothermal model are shown in FIG. 4, i.e. a mould spore is given hygrothermal material parameters. This enables dynamic calculations, which again give the length and intensity of the conditions for mould growth based on critical limits for different type of materials (e.g. LIM I and LIM II in FIG. 5b). The calculation tool with the biohygrothermal model is called Wufi-Bio.

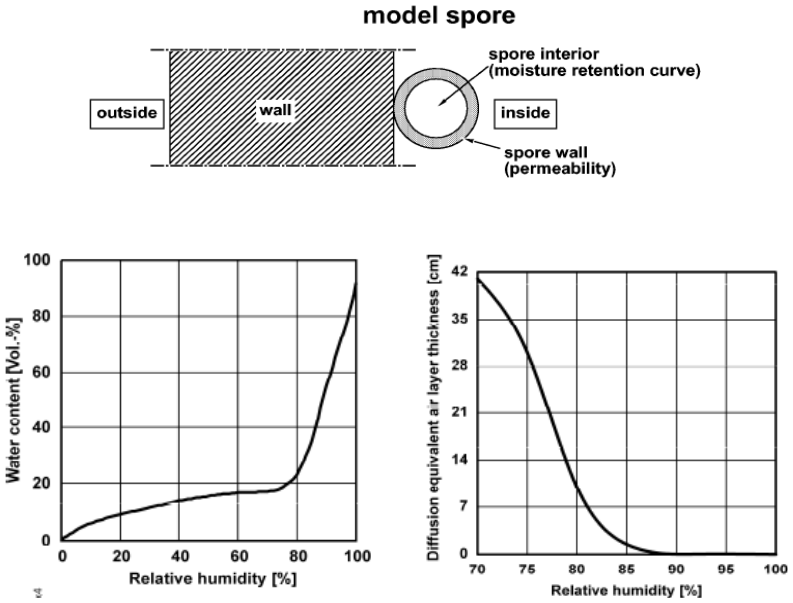

FIG. 4: The biohygrothermal model in Wufi-Bio: the principle idea and relationship between humidity and water content and diffusion resistance of the mould spore (Sedlbauer 2001)

The outcome of the dynamic calculations with Wufi-Bio is the mould growth in mm's during the simulated time, while it is the mould index from the VTT model. Also, the time periods in the biohygrothermal model for spore germination are shorter than that of start of the growth (mould index 1) used in the VTT model (Viitanen et.al 2000). There are also different types of material categories to be chosen and they affect on the time periods needed for the spore germination. (Hens 1999) has shown a performance related model of mould growth in buildings. (Moon 2005) has critically evaluated the problems of assessing of mould risk in building. Clarke et al (Clarke et.al 1998) have developed a simulation model and tool for mould growth prediction in buildings based on analysis of published data, growth limit curves for six generic mould categories in terms of minimum combination of temperature and relative humidity required to sustain growth on indoor building surfaces, FIG. 5a.

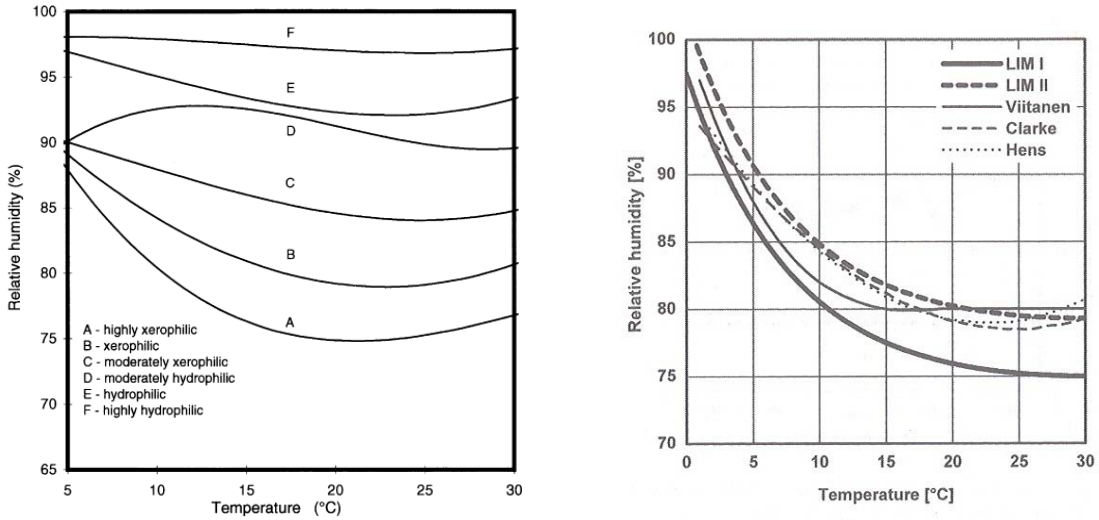

FIG. 5: a) Growth limit curves for six generic mould categories by (Clarke et.al 1998). b) Comparison of the LIM's of substrate class 1 (LIM I, biodegradable materials) and substrate class 2 (LIM II, porous materials) after (Sedlbauer 2001) with data from (Viitanen et.al 2000), (Clarke et.al 1998) and (Hens 1999).

These limits have been then incorporated within the ESP-r system for use in conjunction within combined heat and moisture flow simulation. The result is found by plotting the simulated temperature and humidity conditions on the graph of the growth limit curves and the risk and possible mould funghi species are found in the graph. Obviously, the time dependence of the exposure to the critical conditions is not taken into account in this model. However, the mould growth model is implemented in a whole building/system simulation tool, which enables a risk analysis of many different choices in a whole building and its systems. In FIG. 5b, comparison of the critical conditions for mould growth for some of these different models is shown. It is evident that these limits based on different experimental results agree fairly well.

3. Sensitivity analysis – modelled vs. measured mould growth

The following case study shows an example on how to use a mathematical model for predicting mould growth. The emphasis is on studying the effect of different assumptions on the resulting calculation result – the sensitivity analysis. The above described hygrothermal simulation tool TCCC2D with the mould index calculation according to VTTmodel is used together with field measurements. Also the biohygrothermal model implemented in Wufi-Bio is used for some of the analysis for comparison.

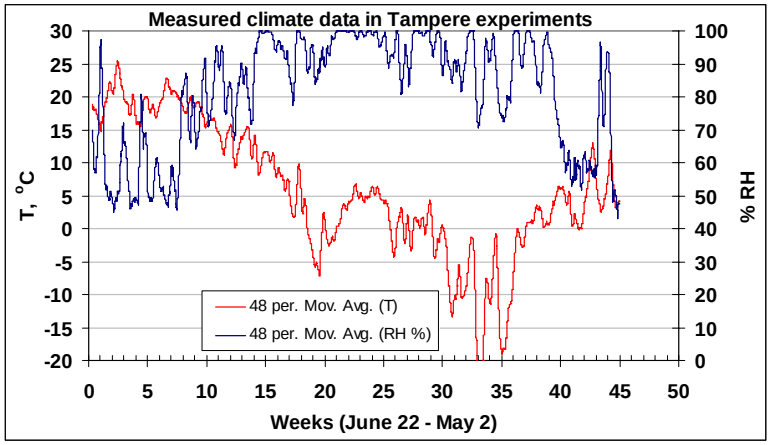

FIG. 6: Measured climate data presented using 48 hour moving average values. The simulations use the original hourly measured data.

The monitored temperature and humidity conditions from a field test of different building materials were used as boundary conditions for simulations when solving the mould growth for pine. These tests are part of the TUT and VTT collaboration project, still on-going and presented in (Lähdesmäki et al. 2008). The 48-hour-average values are shown in Figure 4. The detected mould growth level of pine samples were compared to those solved using different approaches for the mould index calculations. The period in focus is almost a year, starting in a summer time.

3.1 Study of capacity, decline of mould, convection and initial moisture

The results of any simulation model are a function of the model itself and the input parameters. Therefore, when assessing the quality of a model, the influence of any other parameters must be taken into account. The following example shows the effect of following different assumptions on the resulting calculation result:

- modeling heat and moisture capacity of materials or not
- modeling of decline of mould growth when unfavorable conditions
- size of convection
- initial moisture content

The first approach was to solve mould growth index for pine assuming that there is no heat or moisture capacity in the material (i.e. the conditions on the surface are equal to outdoor climate). The results are seen in FIG. 7 together with 2 different assumptions for decline of the mould growth within the model: No decline of mould index or normal decline: If the conditions are not favourable for mould growth – they are too dry or too cold – the mould index will decline. Also the moisture transport coefficient of the surface has an effect on the surface conditions and thus also to the mould growth. The case was studied using two different mass transfer coefficient

levels: normal convection and low convection (having convective heat transfer coefficient 4.0 W/Km2 and1.5 W/Km^2 , respectively). The results are seen in FIG. 8.

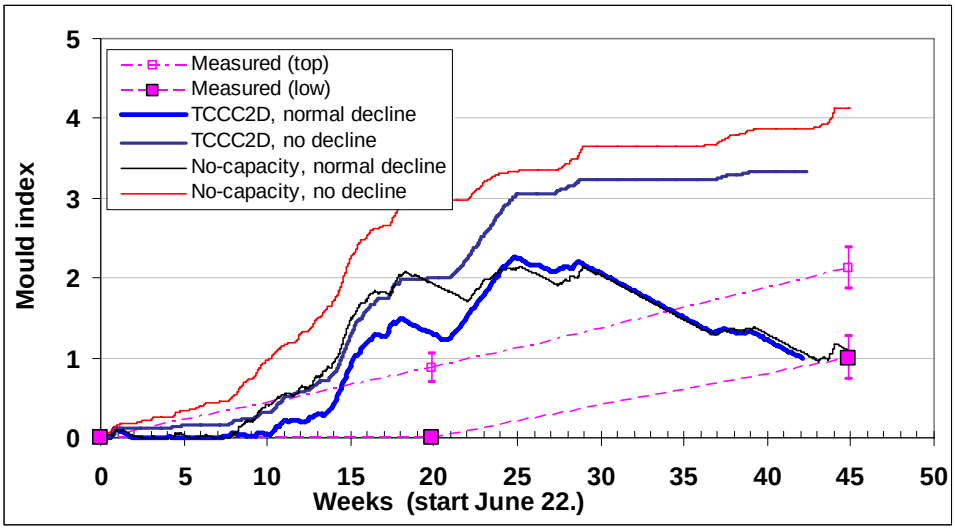

FIG. 7: Prediction of mould growth index of the wooden test board using measured climate data.Mould index was calculated using non-capacity and dynamic simulations (TCCC2D) with two different assumptions for decline of the mould growth. Measured (top) and (low) mould indexes stand for detected growth on the upper side and lower side of the sample. The upper side is exposed for soiling.

The difference between the no capacity – simulations and dynamic structure level simulations was significant during the first 20 – 22 weeks of simulation. For the final result after a year, the assumptions for decline – no decline vs. decline – seemed more remarkable. The detected mould index corresponds best with a result which is between the no-decline and normal decline approaches. The used model for decline is based on the measurements under relatively short period (days rather than weeks) dynamic condition cycles and it is meant to represent the delay in the starting of mould growth after a period of unfavourable conditions for the growth. It is obvious that this assumption cannot be totally correct for varying cases, especially for seasonal changes.

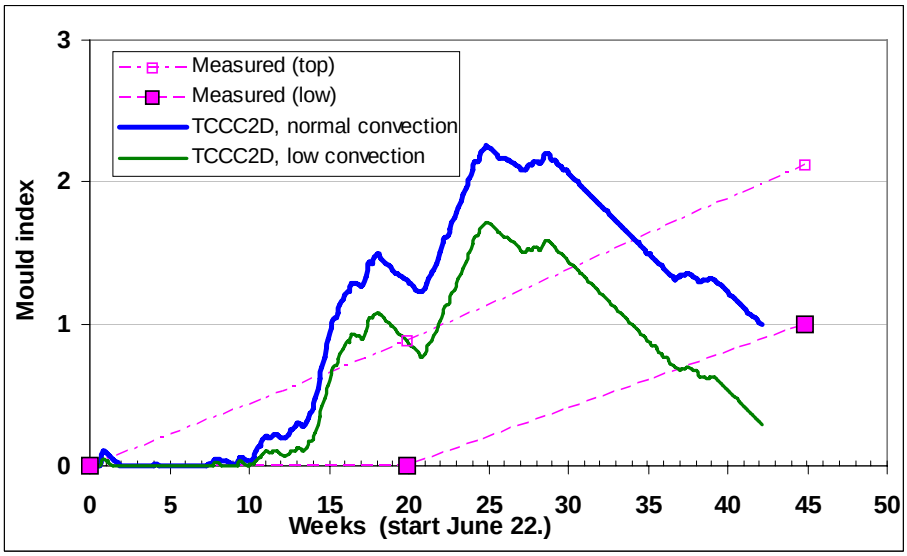

FIG. 8: Effect of convective moisture transfer of the surface on the mould growth index. Measured vs. simulated (TCCC2D) mould index assuming normal decline of the growth in the VTT model.

The size of convection showed a clear effect on the mould growth of the material surface. With low convection the surface conditions are more stabile under dynamic conditions than with high convection. This leads to lower

mould index, in this case. The situation is opposite in a drying situation: If the convection is low, the conditions for mould growth will stay favourable for a longer period and the mould growth index will be higher.

The effect of initial moisture content of the material (80 % RH or 65 % RH) was also studied. It did not have any effect on the mould growth. If the conditions had been suitable for mould growth already in the beginning of the simulation the initial moisture content level could have had some effect on the mould growth.

3.2 Comparison of models predicting mould growth

Above presented sensitivity analysis has already shown the great sensibility of the mould modelling results on different assumptions. Therefore even more care has to be taken when comparing totally different models. However, in FIG. 9 is shown comparison of the VTT and the biohygrothermal model. These simulation results are compared to the same measured results as before.

In the calculations, following assumptions for the parameter choices were taken:

- climate data from the experimental site in Tampere
- moisture capacity of the material is taken into account with the dynamic calculations with TCCC2D
- normal convection on surface corresponding to 4 W/m²K convection heat transfer coefficient
- VTT model with and without decline when conditions are unfavourable for mould growth
- material class for prediction of mould growth: pine sapwood (VTT model) and LIM I (Wufi-Bio)
- initial moisture content of materials at 80 % RH equilibrium

The comparison of the results in FIG. 9 shows that VTT model without decline corresponds relatively well with the biohygrothermal model. This is logical, as the assumption also in the biohygrothermal model is that there is no decline, when the conditions are unfavourable for mould growth. However, there is a difference in the growth rate, especially during longer periods of very high RH: The VTT model predicts here higher growth rate than the biohygrothermal model. The temperature in these periods varies roughly from +10ºC to 0ºC. In contrary, when the temperature stays below zero, the mould growth rate according to biohygrothermal model is still active, while it is practically stopped according to VTT model. Nevertheless, this is a very simplified approach for an explanation as the models include several parameters that have effects in various directions.

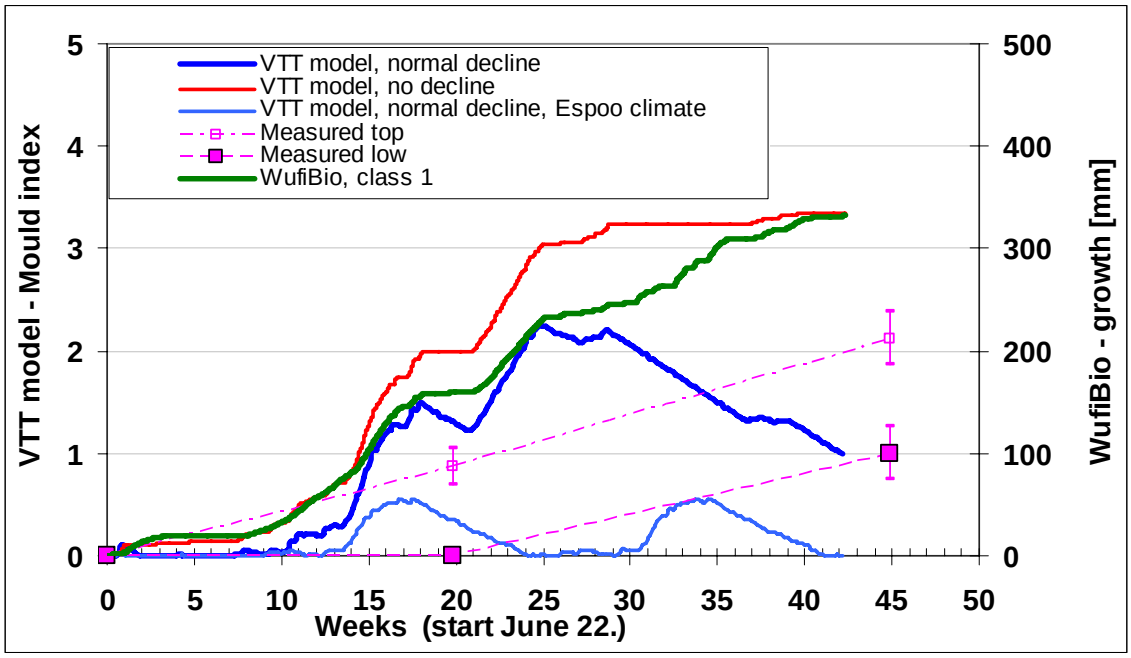

FIG. 9: Comparison between numerically predicted mould growth with VTT model and Wufi-Bio growth prediction with Biohygrothermal model using measured conditions. Comparison also to predicted mould growth under Espoo climate. Espoo results are calculated for normal assumption of mould decline under too dry or cold conditions.

3.3 Study of climatic data

As the mould growth predicting models in focus have the climatic conditions as criteria for the mould growth intensity, the results might be very sensitive to the given climatic data. This was investigated by predicting the mould growth also under Espoo climate data for the corresponding period. These results are also seen in FIG. 9. The difference between the predicted mould growth in Tampere and Espoo conditions (with decline) is significant. Under Tampere conditions the maximum mould growth index exceeds level 2 already in the first year and most probably the index would grow higher during each similar year. In Espoo climate the index remains in level 0.5 or less, which means that there should be no mould growth in the material.

These two cities lie about 160 km apart, so the climates are not identical. In addition, the air in the test storage hut was humidified always when T > 0ºC. When assessing the climatic data and the modelling results, it was observed that during a period with high mould growth conditions, between August 27 and December 31, the Tampere measurements showed 5.8 %RH higher average relative humidity level than that measured in VTT weather station in Espoo. The average temperature in Tampere measurements was 1.3ºC lower during this period.

Even though this case with the great deviation for using different weather data for predicting mould growth is a result of artificial humidification of the air, it also points out the sensibility of the results for the given boundary conditions. These again may relay on measurement with a given inaccuracy. On the other hand, it also illustrates the use of modelling in creating mould safe environments.

3.4 Study of the substrate class

Yet another source for uncertainty and deviation for the results when predicting mould growth with any model is the choice of the critical level of e.g. temperature and humidity conditions. These conditions vary a lot depending on the material itself. In addition, any soiling during the time will change the sensibility of the surface for mould growth. The limiting isoplets for three different substrate classes from (Sedlbauer 2001) are shown in FIG. 10a in order to illustrate the wide range of critical conditions depending on the subsrate material. Lim 0 stands for the optimal growth substrate.

A sensitivity analysis using the 3 substrate classes in FIG. 10a with WufiBio gave the result in FIG. 10b. The same measured climatic data as before is used and the results are given together with the observed mould growth index for pine sap wood. However, the choice of scale between these two measures is totally arbitrary and gives no quantitative idea of the connection between these parameters. These simulated results showed that the choice of material group to be analysed has a huge impact on the simulated results.

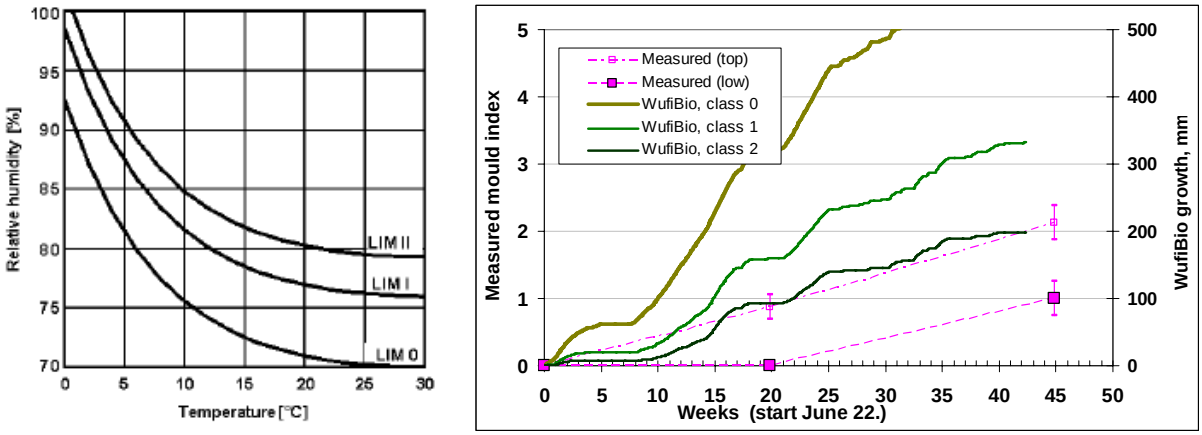

FIG. 10: a) The limiting isopleths (LIMs) for substrate classes 0, I and II that are used in WufiBio. From (Sedlbauer 2001). b) Effect of material classes on predicted mould growth solved using Wufi-Bio. The measured mould index for pine sap wood is given on the left hand axis.

4. Discussion

Prediction of mould growth, however, is always only predicting the risk and not the exact growth. The influence of the uncertainties, whether it is the model itself or e.g. the weather data, is significant. Yet another source for uncertainty and deviation for the results when predicting mould growth with any model is the choice of the critical level of e.g. temperature and humidity conditions. These conditions vary a lot depending on the material itself. In addition, any soiling during the time will change the sensibility of the surface for mould growth. Therefore, prediction of mould growth with calculations must always be assessed with expert knowledge on the nature of mould growth.

There are several aspects that have to be taken into account in the interpretation of the experiments and analysis of the mould growth levels: Under **dynamic tests** the conditions at the interface of the air and test sample are typically different than the air conditions adjacent to the test sample. Therefore it may cause errors if the measured dynamic climate conditions are used as the critical surface conditions. Even in constant conditions the **initial moisture content** of the test material should be known and reduced from the measured data. Under dynamic conditions the thermal and moisture **capacity** of material and the heat and mass **transfer coefficients** on the surface may cause a severe delay in the change of surface conditions, differences in the humidity level and in the mould growth when compared to the adjacent conditions. Dynamic simulation that solves the surface conditions should be used both in the analysis of dynamic mould experiments and when predicting the mould growth in structures under real climate conditions. The use of full simulation enables to separate the delay in the actual mould growth from the delay in the surface conditions.

The existing VTT model has **decline of mould** index when the conditions are not suitable for growth. The origin was to model the delay of mould growth during the short period dynamic conditions (some days). This decline seems to be artificially too effective and probably not proper to adopt in seasonal conditions. New seasonal experiments should provide information about the mould growth during and after too dry or cold conditions, which enables the improved modelling of the phenomena.

5. Conclusion

This paper has taken up the issue of modelling mould growth in building envelopes. There exist some model developments in different research institutions. Among them, there exists some kind of consensus about the overall criteria for mould growth as a function of temperature, relative humidity and time. Nevertheless, there is very little knowledge on mould growth on different kind of materials and effects of the aging of materials, coatings and dust accumulation on the mould growth. To understand the biological, chemical and physical phenomenon of the mould in building structures and modelling of it is challenging. Therefore, approaches to model this kind of complex problem have been done and are still going on.

The mould growth model can be used to study the risks for mould growth on (wooden) material surface when the surface conditions (temperature and relative humidity) are known. Typically the conditions vary dynamically and their hourly values should be known to be able to study the mould growth. Long period (daily, weekly. etc.) time averaged values may not show the risks of the actual conditions, i.e. the peak humidity levels etc. on the mould growth. The same kind of error may be caused when the adjacent climate conditions are used as critical conditions instead of the actual surface conditions. Therefore the effect of the structure and material should always be taken into account when solving the critical conditions for the mould growth.

6. References

Adan, O.C.G. (1994). On the fungal defacement of interior finishes. Eindhoven University of Technology. Thesis. Eindhoven.pp 83 – 185.

Ayerst, G. (1969). The effects of moisture and temperature on growth and spore germination in some fungi. J. Stored Prod. Res. 5:127-141.

Block, S.S. (1953). Humidity requirements for mould growth. Applied Microbiology 1(6):287-293.

Clarke, J.A. Johnstone, C.M. Kelly, N.J. Mclean, R.C. Anderson, J.A., Rowan N.J. and Smith, J.E. (1998). A technicque for prediction of the conditions leading to mould growth in buildings. Building and Environment 34 pp 515-521.

Grant, C., Hunter, C.A., Flannigan, B. and Bravery, A.F. (1989). The moisture requirements of moulds isolated from domestic dwellings. Internat. Biodet. 25:259-284.Hukka A. & Viitanen H. (1999). A mathematical model of mould growth on wooden material. Wood Science and Technology 33(6): 475-485.

Hens, H.L.S.C. (1999). Fungal defacement in buildings: A performance related approach. International Journal of Heating, Ventilation, Air-Conditioning and Refrigerating Research Vol 5 H 3, p. 256 – 280.

Künzel, H.M. (1995). Simultaneous Heat and Moistur Transport in Building Components – One- and Two-dimensional calculations using simple parameters. IRP Verlag, Stuttgart

Lähdesmäki K., Vinha J., Viitanen H., Salminen K., Peuhkuri R., Ojanen T., Paajanen L., Iitti H. & Strander T. (2008). Development of an improved model for mould growth: Laboratory and field experiments. Proceedings of 8th Nordic Symposium on Building Physics, Copenhagen.

Moon, H.J. (2005). Assessing mould risk in buildings under uncertainty. Doctoral thesis Georgia institute of Technology, USA.

Ojanen, T and Salonvaara, M. (2000). Numerical simulation of mould growth in timber frame walls. Healthy Buildings. Espoo, 6 - 10 Aug. 2000. Seppänen, O. & Säteri, J. (ed). Vol. 1. FiSIAQ.

Ojanen T., Kohonen R. & Kumaran M. (1994). Modeling HAM transport through building materials and components. Moisture Control in Buildings. Ed. H.R. Trechsel. ASTM. Philadelphia , pp. 18-34.

Ojanen T. (1996). Evaluation of simulation model TCCC2D using simplified weather data and material properties. IEA/Annex 24 Closing Seminar. Espoo 1996. Katholieke Universiteit Leuven. 22 p.

Sedlbauer K. (2001). Prediction of mould fungus formation on the surface of/and inside building components. University of Stuttgart, Fraunhofer Institute for building Physics, Doctoral thesis. Stuttgart. Germany.

Sedlbauer K. & Krus, M. (2003). A new model for mould prediction and its application in practice. In Research in Building Physics. Ed. by Carmelit et al. Proc. of 2nd International conference on Building Physics.

Smith, S.L. and Hill, S.T. (1982). Influence of temperature and water activity on germination and growth of *Aspergillus restrictus* and *Aspergillus versicolor*. Transactions of the British Mycological Society Vol 79. H 3 p. 558 – 560.

Viitanen H. (1996). Factors affecting the development of mould and brown rot decay in wooden material and wooden structures. Effect of humidity, temperature and exposure time. Doctoral thesis. Uppsala. The Swedish University of Agricultural Sciences, Department of Forest Products. 58 p.

Viitanen, H., Ritschkoff, A-C, Ojanen, T., Salonvaara, M. (2003). Moisture conditions and biodeterioration risk of building materials and structure. Proceedings of the 2nd International Symbosium ILCDES 2003. Integrated Lifetime Engineering of Buildings and Civil Infrastructures, Kuopio, 1-3 Dec. 2003 RIL, VTT, RILEM, IABSE, ECCE, ASCE. Espoo (2003), pp. 151 – 156.

Viitanen H., Hanhijärvi A., Hukka A. & Koskela K. (2000). Modelling mould growth and decay damages Healthy Buildings. Espoo, 6 - 10 August 2000. Vol. 3. FISIAQ, 2000, p. 341–346.

Viitanen H. & Bjurman J. (1995). Mould growth on wood under fluctuating humidity conditions. Mat. und Org. 29(1): 27-46.

Viitanen H. & Ritschkoff A. (1991). Mould growth in pine and spruce sapwood in relation to air humidity and temperature. Uppsala. The Swedish University of Agricultural Scienses, Department of Forest Products. Report no 221. 40 p + app 9 p.

Vinha J. (2007). Hygrothermal performance of timber-framed external wall in finnish climatic conditions: A method for determinig the sufficient water vapour resistance of the interior lining of a wall assembly. Doctoral thesis. Tampere. Tampere University of Technology. Publication 658. 338 p. + app. 10 p.

WUFI (Wärme und Feuchte instationär - Transient Heat and Moisture) 4.0 Pro software, The Fraunhofer Institute for Building Physics IBP.

Application of hygroscopic materials in HVAC systems

Melanie T. Fauchoux, PhD student,
Department of Mechanical Engineering, University of Saskatchewan, Saskatoon, CANADA;
mts919@mail.usask.ca

Carey J. Simonson, Professor,
Department of Mechanical Engineering, University of Saskatchewan, Saskatoon, CANADA;
carey.simonson@usask.ca

David A. Torvi, Associate Professor,
Department of Mechanical Engineering, University of Saskatchewan, Saskatoon, CANADA;
david.torvi@usask.ca

KEYWORDS: *hygroscopic desiccant, air-to-air energy wheel, ventilation, indoor humidity, perceived air quality, energy consumption, HVAC equipment capacities, life cycle costs.*

SUMMARY:
This paper presents the effect of a desiccant coated energy wheel on the air relative humidity (RH), perceived air quality (PAQ), energy consumption and life cycle costs in an office building. TRNSYS is used to model a 15 storey office building in Saskatoon, Saskatchewan; Vancouver, British Columbia; Tampa, Florida and Phoenix, Arizona. The hygroscopic energy wheel reduces the peak RH and percent dissatisfied with PAQ in Tampa, Phoenix and Saskatoon. The hygroscopic energy wheel also reduces the total energy consumption of the HVAC system in these three cities. There is a significant reduction in the size of the heating equipment in Saskatoon and in the size of the cooling equipment in Phoenix and Tampa. The HVAC system including a hygroscopic energy wheel has the least life-cycle costs in these three cities. In Vancouver, the hygroscopic energy wheel has a negligible impact on the indoor RH, PAQ, energy consumption and life-cycle costs.

1. Introduction

Well designed heating, ventilating and air-conditioning (HVAC) systems add or remove heat and moisture from occupied spaces of buildings to control the indoor temperature and humidity. The importance of temperature control is well known [1-3], but humidity control in buildings is also important because indoor humidity affects many parameters including:

(i) thermal comfort [4],

(ii) perceived air quality (PAQ) [5,6],

(iii) occupant health [7],

(iv) the durability of building materials [8,9],

(v) material emissions [10] and

(vi) energy consumption [11,12].

There are several methods that are typically applied to control the RH levels in buildings, such as using mechanical cooling equipment and desiccant dryers in humid climates and humidifiers and outdoor ventilation in dry climates to humidify or dehumidify the space [13,14]. Some disadvantages of these methods include the initial costs of purchasing and installing the equipment, as well as the large operational costs associated with the equipment. In addition, if the outdoor air is too dry or too humid it can actually make the indoor RH levels worse.

Hygroscopic materials in the indoor space can also be used to moderate RH levels and improve comfort, PAQ and energy consumption [15-18]. The purpose of this paper is to determine if similar results can be achieved by using hygroscopic materials in the HVAC system, in the form of a desiccant coated energy wheel.

Hygroscopic energy wheels are used in many buildings to reduce the energy required to condition outdoor ventilation air, which constitutes a large fraction of the total energy consumption of a building [19]. This paper will determine if a rotary air-to-air energy wheel that transfers both sensible and latent heat can help moderate the indoor RH levels and improve comfort conditions as well as reduce energy consumption and cost.

2. Weather data and office building model

The TRNSYS computer program [20] is used in this paper to calculate the hourly indoor temperature and relative humidity in the model office building. Most of the office building consists of open cubicle work space and it is assumed that the temperature and relative humidity are uniform throughout this work space. This paper will only report the conditions in the open work space. With the calculated temperature and humidity (or enthalpy) in the open work space, the percent dissatisfied with general thermal comfort [1] or perceived air quality can be calculated. The general thermal comfort equations are not repeated here, but the correlation for facial exposure to clean air [5] is used to calculate percent dissatisfied with perceived air quality (PD_{PAQ}) based on the enthalpy of the air (kJ/kg):

$$PD_{PAQ} = \frac{\exp(-0.18 - 5.28(-0.0333H + 1.662))}{1 + \exp(-0.18 - 5.28(-0.0333H + 1.662))} \qquad (1)$$

Hourly TMY2 weather data for 4 North American cities are used in this paper. Figure 1 presents the outdoor design conditions for each city and shows that: Saskatoon, Saskatchewan, Canada has a cold and dry climate; Vancouver, British Columbia, Canada has a mild climate; Tampa, Florida, USA has a hot and humid climate; and Phoenix, Arizona, USA has a hot and dry climate.

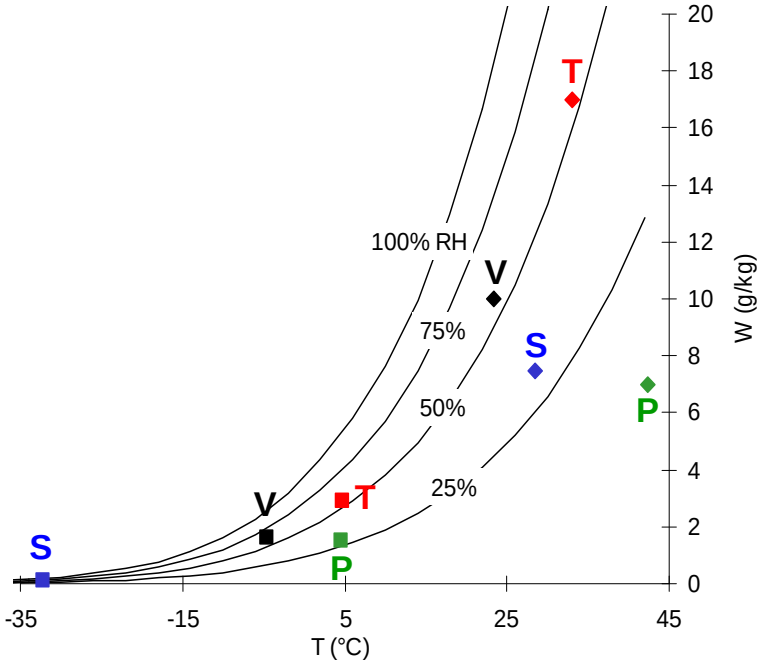

FIG. 1: Winter and summer design conditions for Saskatoon (S) [cold and dry], Vancouver (V) [mild], Tampa (T) [hot and humid] and Phoenix (P) [hot and dry].

The modelled office building is described in references [21,22] and only a brief overview is included here. The building is a 15 storey office building with a floor area of 23,000 m^2. The building has a curtain wall

construction where the opaque section has a U-value of 0.21 W/(m^2·K) and the windows, which make up 40% of the wall, have a U-value of 2.7 W/(m^2·K). The infiltration rate of the building is 0.8 L/(s·m^2) or 0.3 ach. The office is occupied by 1,600 people from 8:00 to 18:00 and by 160 people from 18:00 to 21:00. The office workers generate 75W of sensible and 75 W of latent energy. The outdoor ventilation rate is 16,000 L/s [23] and is provided 2 hours prior to occupation and 2 hours after occupation. The constant volume all-air HVAC system (Figure 2) normally provides 20% outdoor air to the conditioned space, but when the outdoor conditions are favourable the fraction of outdoor air is increased (economizer cycle). The natural gas boiler is assumed to have an efficiency of 79% and the electrical driven cooling unit has a COP of 2.7 [24]. The office building is simulated with and without a hygroscopic energy wheel with sensible, latent and total energy transfer effectivenesses of 70%. The base case is the case when there is no energy wheel in the HVAC system.

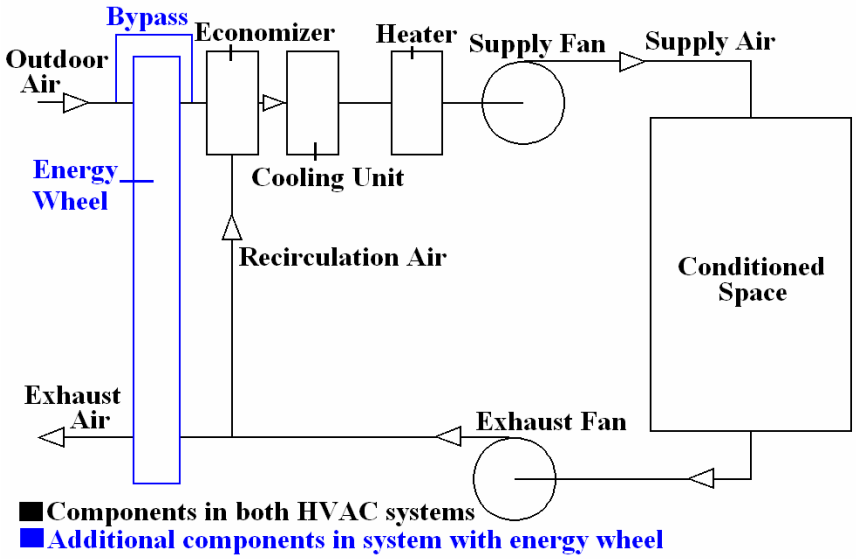

FIG. 2: Schematic of the constant volume all-air HVAC system used to condition the office building.

3. Numerical results

3.1 Hourly data

To see how the hygroscopic energy wheel affects the relative humidity during a typical day, an hourly comparison is shown in Figure 3(a) along with the cooling energy for both the base and energy wheel cases. The outdoor temperature, relative humidity and humidity ratio are shown for the same day in Figure 3(b).

In the base case simulation, the indoor humidity initially decreases from 55% RH to 50% RH between 0:00 and 2:00 due to moisture removed by the cooling coil. At 6:00, the relative humidity begins to increase considerably. This is because the ventilation system turns on at 6:00 and brings outdoor air, which is at a higher humidity ratio than the indoor air, into the building. At 8:00 when the people enter the building and other heat sources begin generating heat, the cooling required increases, causing a decrease in the relative humidity. Another RH increase is seen at 18:00 when some of the people leave and the demand for sensible cooling reduces. The cooling demand continues to drop through the evening and the indoor relative humidity continues to increase slowly. These results show the coupling between the sensible and latent performance of the cooling coil.

The case with the hygroscopic energy wheel shows a similar humidity profile as the base case, but with a humidity level that is about 10% RH lower. The impact of the energy wheel is first noticed at 6:00 when the outdoor ventilation system is activated. The energy wheel removes some of the moisture from the outdoor air before it is delivered to the cooling coil and space, reducing the amount of moisture that the supply air adds to the space. The relative humidity profile then continues the same as the base case during the day, but at this lower relative humidity level. During the night, the cooling unit is able to reduce the indoor relative humidity in the

base case so that it is similar to the indoor relative humidity in the energy wheel case by 6:00 the next morning. It can be seen in Figure 3 that the energy wheel lowers the energy consumption at most hours and the peak energy demand. The effect of the energy wheel on energy consumption and demand will be presented in sections 3.3 and 3.4.

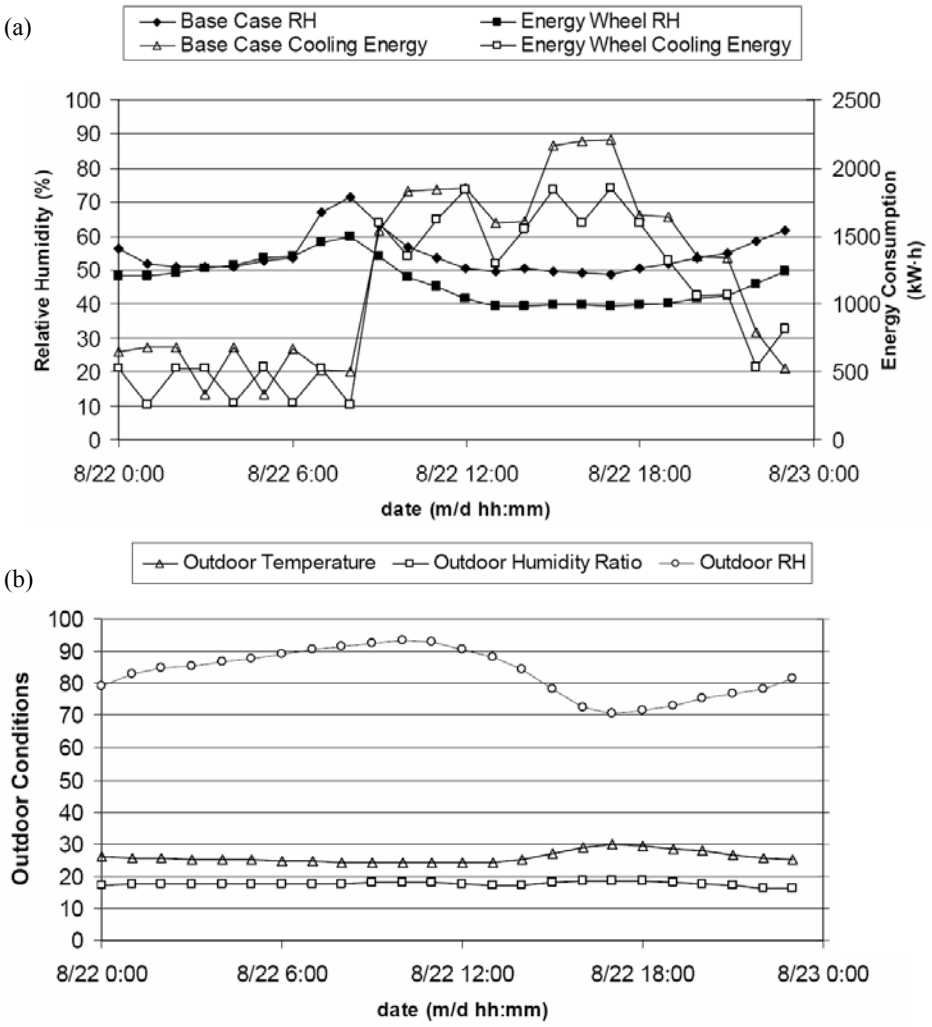

FIG. 3: Calculated (a) indoor relative humidity and cooling energy consumption with and without an energy wheel and (b) outdoor weather conditions on August 22 in Tampa.

The percentage of people dissatisfied with general thermal comfort during occupied hours in Tampa is shown in Figure 4(a). For the base case, the percent dissatisfied with thermal comfort fluctuates between 16% and 19%. There is a consistent decrease of about 2% at every occupied hour when the energy wheel is used. This is not a large change, but still shows that the energy wheel has a positive effect on the conditions in the building during occupation. The energy wheel is not expected to have a large impact on general thermal comfort because general thermal comfort is mostly based on the temperature in the space and the temperature is essentially the same in the two cases.

Figure 4(b) shows the percentage of people that are dissatisfied with perceived air quality (PD_{PAQ}) during occupied hours in Tampa. There is a large decrease in the PD_{PAQ} when the energy wheel is added to the system as compared to the base case. The peak decrease is 22% at 8:00 and the average decrease is about 17%. From these results it can be seen that the addition of an energy wheel into the HVAC system can have a significant

impact on the PAQ of a space. This will likely affect the productivity of the office workers and should be considered when conducting a life cycle cost analysis of buildings because the salary costs of workers often exceed the owning and operating costs (energy, maintenance, construction and rental) by a factor of 100 [25]. This analysis will be left for future work.

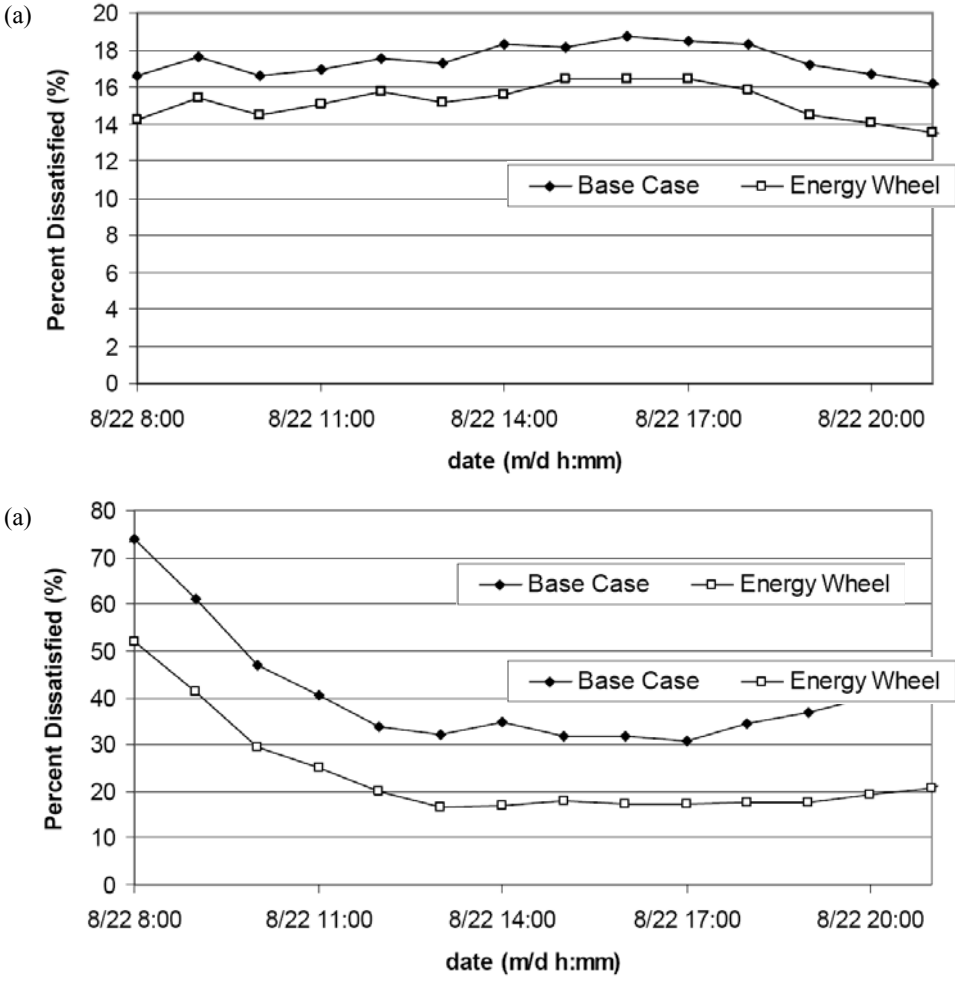

FIG. 4: Calculated percent dissatisfied with (a) general thermal comfort and (b) perceived air quality in the office building during occupied hours on August 22 in Tampa.

3.2 Yearly frequency distributions

The difference between the indoor RH with and without a hygroscopic energy wheel (ΔRH) is shown as a frequency distribution in Figure 5, where ΔRH is:

$$\Delta RH = RH_{\text{without energy wheel}} - RH_{\text{with energy wheel}} \qquad (2)$$

ΔRH is plotted over intervals of 1% RH, so a value of ΔRH = 0 is actually ΔRH = 0 ± 0.5% RH. The largest impact of the hygroscopic energy wheel on the indoor RH is seen in Tampa where a majority of the hours (61%) have a $|\Delta RH| > 2\%$. There are approximately 1100 hours (34%) where the hygroscopic energy wheel decreases

the indoor RH by more than 10% RH. The maximum reduction in Tampa is 14% RH. The effect of the hygroscopic energy wheel in Phoenix is not as large as in Tampa, but there are still about 1300 occupied hours (37%) where the hygroscopic energy wheel reduces the indoor RH by more than 2% RH in Phoenix. The maximum reduction in Phoenix is 11% RH.

The indoor RH during occupied hours is considerably lower in Saskatoon than in Tampa and Phoenix, due to the dry climate. Since the RH is quite low in Saskatoon during the winter months, it is favourable to not only decrease the RH in the summer months, but also to increase the RH in the winter months. There are about 3000 hours (86% of occupied hours) where $|\Delta RH|$ is less than 0.5% RH, indicating that the hygroscopic energy wheel does not have a large effect on the indoor conditions in Saskatoon. The maximum difference is about 10% RH and the minimum difference is about -5% RH. In Vancouver, the hygroscopic energy wheel changes the indoor RH by less than 1% RH.

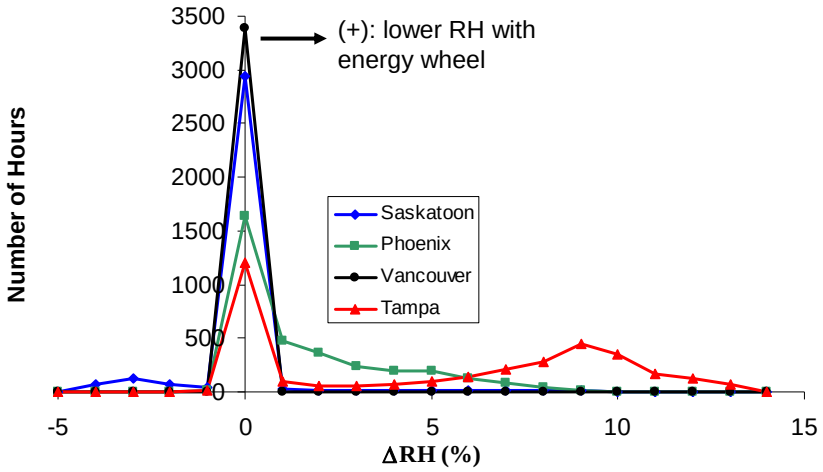

FIG. 5: Comparison of the indoor RH calculated with and without a hygroscopic energy wheel for all cities during occupied hours.

Figure 6 shows the difference in PD_{PAQ} with and without a hygroscopic energy wheel ($\Delta PD_{PAQ,}$) in each of the four cities, as a frequency plot. ΔPD_{PAQ} is calculated in the same manner as ΔRH (equation (2)) and the frequency is plotted with intervals of 2%. The addition of a hygroscopic energy wheel has the largest effect in Tampa where the PD_{PAQ} is reduced by up to 25% compared to the system with no hygroscopic energy wheel. The maximum reduction in the PD_{PAQ} is 19% in Phoenix and 10% in Saskatoon. There is no significant effect in Vancouver.

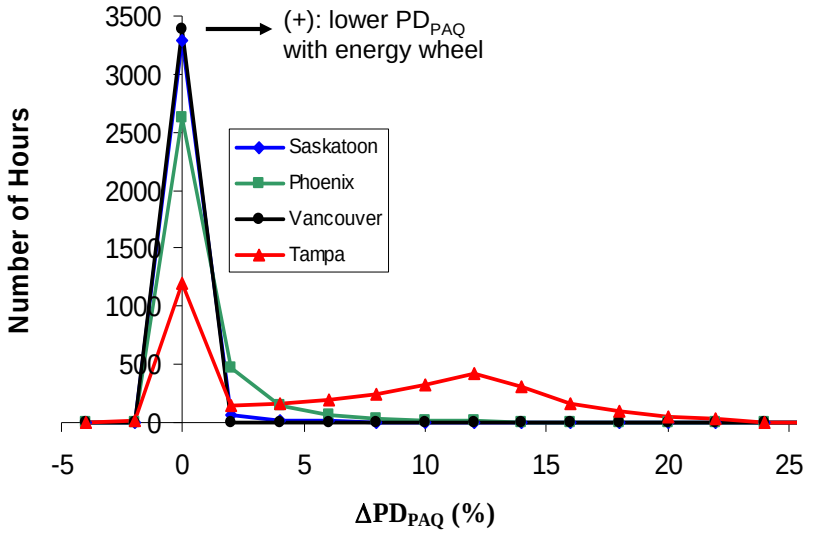

FIG. 6: Comparison of the PD_{PAQ} calculated with and without a hygroscopic energy wheel for all cities during occupied hours.

3.3 Energy consumption

The total amount of natural gas and electricity (cooling, heating and fans) consumed annually by the HVAC system with and without a hygroscopic energy wheel is shown in Figure 7 for each city. The natural gas consumption in Saskatoon decreases by 10% with the addition of the hygroscopic energy wheel as compared to the case with no hygroscopic energy wheel. The electrical energy consumed for cooling and fans is reduced by 8% in both Phoenix and Tampa with the addition of a hygroscopic energy wheel. The total amount of energy consumed by the building will be larger due to the lighting and equipment in the building that also consume electricity. The energy consumed by the HVAC system makes up approximately 60-70% of the total building energy [21].

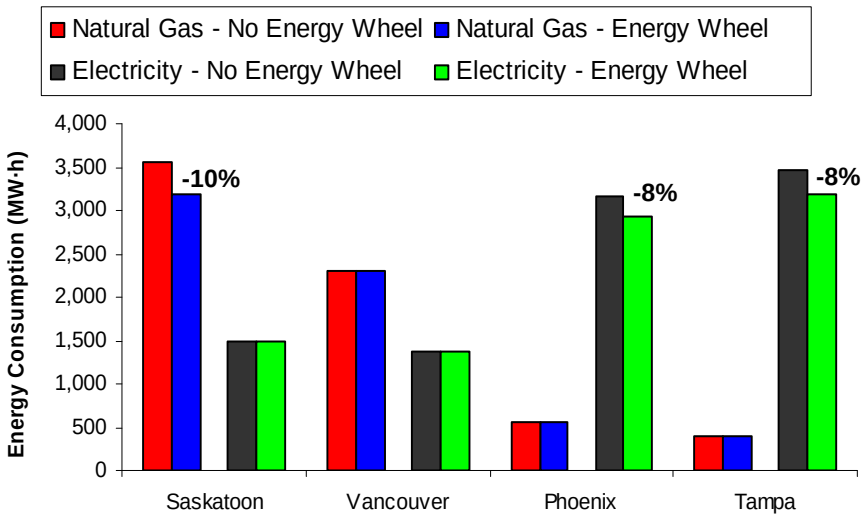

FIG. 7: Annual energy consumption of the HVAC system with and without an energy wheel.

3.4 HVAC equipment capacities

The required boiler and cooling unit capacities with and without a hygroscopic energy wheel can be seen in Figure 8. The hygroscopic energy wheel reduces the required boiler capacity by 26% in Saskatoon. With the hygroscopic energy wheel, there is a small reduction in the capacity of the cooling unit in Saskatoon (4%) and a large reduction in both Phoenix (18%) and Tampa (17%). There is no significant change in the capacity of the heating or cooling units in Vancouver when the hygroscopic energy wheel is added to the HVAC system.

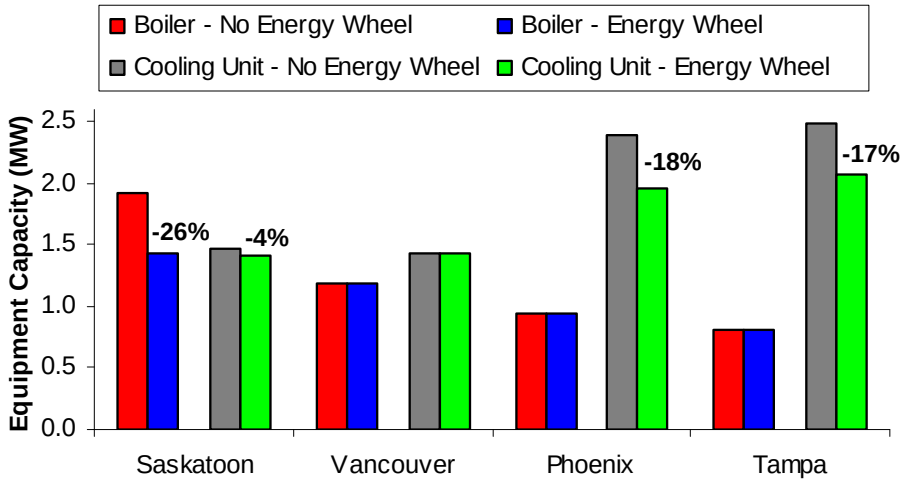

FIG. 8: Required boiler and cooling unit capacities with and without a hygroscopic energy wheel.

3.5 Economics

The life-cycle cost (LCC) and payback period (PB) of the HVAC system are [26]:

$$LCC = C_{ex} + C_{eq} + C_{fan} + C_{aux} \tag{3}$$

and

$$PB = \frac{C_{ex} - C_{aux,N} + C_{aux,ex}}{(C_{rec} - \Delta C_{fan})/P_{wef}} \tag{4}$$

where:

C_{ex} is the cost of the hygroscopic energy wheel,

C_{eq} is the cost of auxiliary heating and cooling equipment,

C_{fan} is the cost of fan power (present worth),

C_{aux} is the cost of auxiliary heating and cooling power (present worth),

C_{rec} is the savings due to heating and cooling recovered by the hygroscopic energy wheel,

ΔC_{fan} is the increase in the cost of running the fans due to the increased energy consumption created by the pressure drop across the hygroscopic energy wheel,

$C_{aux,N}$ is the cost of auxiliary heating and cooling equipment if there is no energy wheel,

$C_{aux,ex}$ is the cost of auxiliary heating and cooling equipment with a hygroscopic energy wheel, and

P_{wef} is the present worth escalation factor (8.61 for a system life of 10 years, an interest rate of 6% and an inflation rate of 3%).

The cost of heating and cooling equipment is assumed to be $200/kW and the cost of the hygroscopic energy wheel is assumed to be $6/(L/s). The cost of heating and cooling power is based on the amount of heating or cooling required as well as the cost of natural gas or electricity. The cost of fan power is calculated from the total electrical energy required by the fans as well as the cost of electricity. The monthly cost of natural gas and electricity for commercial customers in the four cities can be found in references [21,22].

Figure 9 presents the LCC of the system with and without a hygroscopic energy wheel over a 10 year life cycle in the four cities. LCC savings are realized in Saskatoon (4%), Phoenix (6%) and Tampa (6%) with the addition of the hygroscopic energy wheel. If the benefits of possible productivity improvements were included [3], the LCC savings would be even greater. In Vancouver, adding a hygroscopic energy wheel to the HVAC system will increase the LCC by about 5%, which is nearly equal to the capital cost of the hygroscopic energy wheel.

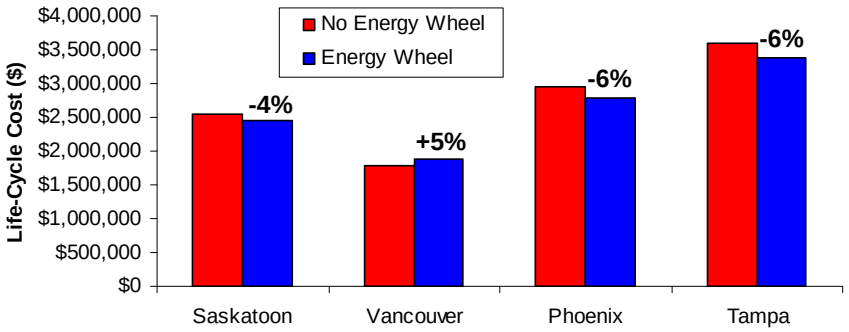

FIG. 9: Life cycle costs of the HVAC system with and without a hygroscopic energy wheel.

The PB periods are shown in Table 1. Saskatoon shows a negative PB because the capital cost of the HVAC equipment is actually smaller when the hygroscopic energy wheel is included due to the reduced heating and cooling equipment capacities required when a hygroscopic energy wheel is included in the HVAC system. Therefore, the PB in Saskatoon is immediate and any future benefits (energy savings and improved thermal comfort and PAQ) result from essentially no investment. Phoenix and Tampa show very good PB periods, each less than one year. No PB period is shown for Vancouver because it is very large, many times larger than the 10 year life cycle of the system.

TABLE. 1: Payback periods for the hygroscopic energy wheel in each city.

City	PB Period (years)
Saskatoon, Saskatchewan, Canada	-1.2
Vancouver, British Columbia, Canada	—
Phoenix, Arizona, USA	0.4
Tampa, Florida, USA	0.5

4. Conclusions

In this paper, the TRNSYS computer program is used to perform simulations on an office building in four North American cities. These simulations are performed with and without a hygroscopic energy wheel to determine the effect of hygroscopic materials in the HVAC system on the indoor RH, PAQ, thermal comfort, energy consumption and LCC. The results show that hygroscopic materials in the HVAC system can improve the indoor climate, energy consumption and economics in Tampa (hot and humid climate), Phoenix (hot and dry climate) and Saskatoon (cold and dry climate). However in Vancouver (mild climate), the HVAC system with hygroscopic material has a higher LCC and minimal impact on RH and PD_{PAQ}.

5. Acknowledgements

Financial support from the Natural Science and Engineering Research Council of Canada (NSERC) Special Research Opportunity and Discovery Grant Programs are greatly appreciated.

6. Nomenclature

ach	air changes per hour
C_{aux}	cost of auxiliary heating and cooling power ($)
$C_{aux,ex}$	cost of auxiliary heating and cooling equipment with a hygroscopic energy wheel ($)
$C_{aux,N}$	cost of auxiliary heating and cooling equipment with no energy wheel ($)
C_{ex}	cost of hygroscopic energy wheel ($)
C_{eq}	cost of auxiliary heating and cooling equipment ($)
C_{fan}	cost of fan power ($)
C_{rec}	savings due to energy recovered by the hygroscopic energy wheel ($)
COP	coefficient of performance
H	enthalpy of air (kJ/kg)
HVAC	Heating, Ventilating and Air-Conditioning
LCC	life-cycle cost ($)
P_{wef}	present worth escalation factor
PAQ	perceived air quality
PB	payback period (years)
PD	percent dissatisfied (%)
PD_{PAQ}	percent dissatisfied with perceived air quality (%)
RH	relative humidity (%)
U-value	overall heat transfer coefficient ($W/(m^2 \cdot K)$)
ΔC_{fan}	the increase in the cost of running the fans due to the increased energy consumption created by the pressure drop across the hygroscopic energy wheel
ΔRH	difference between the RH calculated with and without a hygroscopic energy wheel (a postive value means RH is lower with the hygroscopic energy wheel).
ΔPD_{PAQ}	difference between the PD_{PAQ} calculated with and without a hygroscopic energy wheel (a postive value means PD_{PAQ} is lower with the hygroscopic energy wheel).

7. References

[1] ISO Standard 7730-1994, *Moderate thermal environments - Determination of the PMV and PPD indices and specification of the conditions for thermal comfort*, International Standards Organization, Geneva, Switzerland, 1994.

[2] ANSI/ASHRAE Standard 55-2004. *Thermal environmental conditions for human occupancy*, ASHRAE, Atlanta, Georgia.

[3] Kosonen, R. and F. Tan, 2004. Assessment of productivity loss in air-conditioned buildings using PMV index, *Energy and Buildings*, **36**, 987–993.

[4] Toftum J., Jorgensen, A.S. and Fanger, P.O., 1998. Upper limits of air humidity for preventing warm respiratory discomfort, *Energy and Buildings*, **28**, 15-23.

[5] Fang, L., G. Clausen and P.O. Fanger, 1998. Impact of temperature and humidity on the perception of indoor air quality, *Indoor Air*, **8**, 80-90.

[6] Fang, L., G. Clausen and P.O. Fanger, 1998. Impact of temperature and humidity on perception of indoor air quality during immediate and longer whole-body exposures, *Indoor Air*, **8**, 276-284.

[7] Bornehag, C.-G., Blomquist, G., Gyntelberg, F., Jarvholm, B., Malmberg, P., Nordvall, L., Nielsen, A., Pershagen, G. and Sundell, J., 2001. Dampness in buildings and health, *Indoor Air*, **11**, 72-86.

[8] ASTM, 1994. *Moisture control in buildings*, (edited by H. R. Trechsel), Philadelphia, ASTM.

[9] Simonson, C.J., Ojanen, T. and Salonvaara, M., 2005. Moisture performance of an airtight, vapor permeable building envelope in a cold climate, *Journal of Thermal Envelope and Building Science*, **28**(3), 205-226.

[10] Haghighat, F., and Bellis, L.D., 1998. Material emission rates: literature review, and the impact of indoor air temperature and relative humidity, *Building and Environment*, **33**(5), 261-277.

[11] Rengarajan, K., Shirey, D. B. III and Raustad, R. A., 1996. Cost-effective HVAC technologies to meet ASHRAE Standard 62-1989 in hot and humid climates, *ASHRAE Transactions*, **102**(1), 166-182.

[12] Osanyintola, O.F. and Simonson, C.J., 2006. Moisture buffering capacity of hygroscopic building materials: Experimental facilities and energy impact, *Energy and Buildings*, **38**, 1270-1282.

[13] Harriman, L.G., Witte, M.J., Czachorski, M. and Kosar, D.R., 1999, Evaluating active desiccant systems for ventilating commercial buildings, *ASHRAE Journal*, **41**(10), 28–37.

[14] Pavlovas, V., 2004. Demand controlled ventilation A case study for existing Swedish multifamily buildings, *Energy and Buildings*, **36**, 1029–1034

[15] Simonson, C.J., Salonvaara, M. and Ojanen, T., 2002. The effect of structures on indoor humidity - possibility to improve comfort and perceived air quality, *Indoor Air*, **12**, 243-251.

[16] Simonson, C.J., Salonvaara, M. and Ojanen, T., 2004. Moderating indoor conditions with hygroscopic building materials and outdoor ventilation, *ASHRAE Transactions*, **110** (2), 804-819.

[17] Holm, A.H., Kuenzel, H.M. and Sedlbauer, K., 2004. Predicting indoor temperature and humidity conditions including hygrothermal interactions with the building envelope, *ASHRAE Transactions*, **110**(2), 820-826.

[18] Areemit, N. and Sakamoto, Y., 2007. Numerical and experimental analysis of a passive room-dehumidifying system using the sorption property of a wooden attic space, *Energy and Buildings*, **39**, 317–327.

[19] Simonson, C.J., 2007. Heat and energy wheels, *Encyclopedia of Energy Engineering and Technology*, Volume 2, Edited by Barney Capehart, CRC Press, Boca Raton, FL, 794-800.

[20] Solar Energy Laboratory, 2005. *A TRaNsient SYstems Simulation Program*, University of Wisconsin Madison, http://sel.me.wisc.edu/trnsys.

[21] Fauchoux, M., 2006. The Effect of Energy Recovery on Indoor Climate, Air Quality and Energy Consumption Using Computer Simulations, M.Sc. Thesis, Department of Mechanical Engineering, University of Saskatchewan, Saskatoon, SK. http://library2.usask.ca/theses/available/etd-06222006-162448/

[22] Fauchoux, M., Simonson, C.J. and Torvi, D.A., 2007. The effect of energy recovery on perceived air quality, energy consumption and economics of an office building, *ASHRAE Transactions*, **113**(2), 437-449.

[23] ASHRAE Standard 62.1-2001. *Ventilation for acceptable indoor air quality*, ASHRAE, Atlanta, Georgia.

[24] ASHRAE Standard 90.1-2004. *Energy standard for buildings except low-rise residential buildings*, ASHRAE, Atlanta, Georgia.

[25] Wood, J.E., 1989. Cost avoidance and productivity in owning and operating buildings, *Occupational Medicine*, **4**(4), 753–770.

[26] Asiedu, Y., R.W. Besant and C.J. Simonson, 2005. Cost-effective design of dual heat and energy recovery exchangers for 100% ventilation air in HVAC cabinet units, *ASHRAE Transactions*, **111**(1), 857-872.